UNIVERSITA' DEGLI STUDI DI VERONA

DIPARTIMENTO DI SCIENZE DELLA VITA E DELLA RIPRODUZIONE

SCUOLA DI DOTTORATO DI SCIENZE DELLA VITA E DELLA SALUTE

DOTTORATO DI RICERCA IN BIOSCIENZE, *curriculum* BIOCHIMICA

XXV ciclo

Molecular and cellular insights into defects of human alanine:glyoxylate aminotransferase variants associated with Primary Hyperoxaluria Type I

Coordinatore: Prof.ssa Marta Palmieri

Tutor: Dott.ssa Barbara Cellini

Dottoranda: Dott.ssa Elisa Oppici

INDEX

ABBREVIATIONS

PH1, primary hyperoxaluria type 1;
AGT, alanine:glyoxylate aminotransferase;
PLP, pyridoxal 5'-phosphate;
PMP, pyridoxamine 5'-phosphate
CHO, chinese hamster ovary;
FBS, fetal bovine serum;
GO, glycolate oxidase;
LDH, L-lactic dehydrogenase;
PTS1, peroxisomal targeting sequence;
MTS, mitochondria targeting sequence;
AGT-Mi, minor allele of AGT;
AGT-Ma, major allele of AGT;
$K_{D(PLP),}$ equilibrium dissociation constant for PLP;
SEC, size exclusion chromatography;
DLS, dynamic light scattering;
HPLC, high pressure liquid chromatography;
IEM immunoelectron microscopy;
IFM, immunofluorescence microscopy;
SEM, standard error mean

ABSTRACT

Primary hyperoxaluria type 1 (PH1) is a rare autosomal recessive disorder characterized by the deposition of insoluble calcium oxalate crystals at first in the kidneys and urinary tract and then, in the absence of appropriate treatments, in the whole body. PH1 is caused by the deficiency of human liver specific peroxisomal enzyme alanine:glyoxylate aminotransferase (AGT). AGT is a pyridoxal 5'-phosphate (PLP)-dependent enzyme, which converts glyoxylate to glycine, thus preventing glyoxylate oxidation to oxalate and calcium oxalate formation. Only two curative therapeutic approaches are currently available for PH1: the administration of pyridoxine, a precursor of PLP, which is only effective in a minority of patients (10-30%), and liver transplantation, a very invasive procedure. AGT is encoded by the gene *AGXT* for which two main polymorphisms can be found: the major allele (AGT-Ma) and the minor allele (AGT-Mi). Up to now, more than 150 mutations have been identified that lead to PH1 and several studies have tried to clarify the genotype/phenotype correlations. However, the mechanisms by which each mutation causes AGT deficiency at the protein level are still poorly understood. Therefore, we performed a side-by-side comparison between normal AGT and nine purified pathogenic variants in terms of catalytic activity, coenzyme binding mode and affinity, spectroscopic features, oligomerization and thermal stability of both the holo- and apo-form. Moreover a detailed analysis of the structural properties of the S187F-Ma variant and of the molecular and cellular properties of Gly161 variants has been undertaken. Altogether, the data obtained has allowed us (i) to provide evidence for the structural and/or functional effects caused by each mutation on the protein, (ii) to reassess previous data obtained with crude cellular extracts, and (iii) to indicate a suitable therapy among those already available, and to suggest new treatments strategies for patients bearing the mutations analysed.

THESIS EVALUATIONS

DEPARTMENT OF CELL & DEVELOPMENTAL BIOLOGY
DIVISION OF BIOSCIENCES
FACULTY OF LIFE SCIENCES

4th March 2013

Elisa Oppici,
Section of Biological Chemistry,
Department of Life Sciences & Reproduction,
University of Verona,
Strada Le Grazie 8,
37134 Verona,
Italy.

"Molecular and cellular insights into defects of human alanine:glyoxylate aminotransferase variants associated with primary hyperoxaluria type 1"

Dear Elisa,

Thank you for sending me your PhD thesis and giving me the opportunity to read and comment upon it.

I found your thesis fascinating and it was a joy to read. The interdisciplinary approach you have taken, in which you have amalgamated the complementary approaches of classic biochemistry, enzymology, biophysics, structural biology and cell biology, has provided exciting new insights into the molecular aetiology and pathogenesis of PH1. In particular, I liked your fine dissection of the detailed molecular basis for the phenotypic effects of the S187F and the G161 group of mutations. These studies, together with the enzymic and biophysical analysis of a number of other mutations, provide the essential starting point for the development of rational treatment strategies. The categorization of the effects of mutations on apo- and/or holo-AGT and the delineation of their effects on AGT catalytic activity and/or stability is very exciting. Little did I realise when my laboratory discovered the basic AGT deficiency in PH1 28 years ago, and identified the first mutation 23 years ago, that we could now dissect the relationship between mutation and disease phenotype, both proximal and distal, in such detail. I commend you on the efforts of you and your colleagues.

Of course, I am familiar with most of your co-authored papers bound within your thesis, all of which are published in high quality journals and are of a very high standard. I look forward to many more in the future.

Once again, congratulations.

With best wishes,

Christopher J. Danpure BSc PhD FHEA FSB FMedSci
Emeritus Professor of Molecular Cell Biology
Department of Cell and Developmental Biology, Division of Biosciences, University College London, Gower Street, London, WC1E 6BT, United Kingdom. Tel: +44 (0)20 7679 7036. Email: c.danpure@ucl.ac.uk

universitäts klinikum bonn

Statement on the doctoral thesis of Mrs. Elisa Oppici

Molecular and cellular insights into the defects of human alanine:glyoxylate aminotransferase (AGT) variants associated with primary hyperoxaluria type 1

Primary hyperoxaluria type I is a very heterogeneous disease, which is not always explainable by its genetic basis. More than a 100 mutations of the encoding gene (AGXT) of this disease specific enzyme alanine:glyoxylate aminotransferase are known, but multiple studies so far have failed to clearly demonstrate a genotype/phenotype correlation, with the exception of the vitamin B6 sensitiveness of the c.508G>A and other missense mutations.
Mrs. Oppici was now interested in finding out the mechanisms by which each mutation causes AGT deficiency at the protein level. For this purpose, she performed side by side comparisons of normal AGT and nine purified pathogenic variants in terms of catalytic activity, coenzyme binding and affinity, spectroscopic features, oligomerization and thermal stability. Next to that a more detailed analysis of the G167A Ala variant and the Gly183 variants were done. With the obtained data, she was able to provide evidence of structural and functional effects caused by mutations and to define which form, which part and which domain of the AGT enzyme is affected. Also, she was able to reevaluate previous data of experiments with cellular extracts regarding all analyzed mutations leading to either loss of immunoreactivity and catalytic activity. Most importantly, for the clinician, she was able to comment on suitable therapeutic options, if available and to suggest new treatment options based on the analyzed mutations.

This thesis is eloquently structured with one chapter based on the other and hence good to understand not only for the experienced, but also for the interested reader. She presents an extensive reference list, again indicating her profound involvement with the analyzed topics. This all evidently shows her ability for scientific work, as do the attached papers already published on this topic in peer review journals with a high impact factor.

In conclusion, the thesis presented is a fascinating work. Given the fact that Mrs. Oppici leads way to further research efforts both on a protein and a cellular level to better understand the

universitäts klinikum bonn

molecular defect of pathogenic variants causing PHI type I, she will hopefully stay on track focussing on this extremely interesting and important work in hypercoagulopathy research.

Hence and according to the grading system I am used to I would score the work presented with:

„magna cum laude"

and I hope, that the faculty of medicine of the University of Vienna can follow this grading.

Prof. Dr. Bernd Kopp

Bonn, 5.3.2013

INTRODUCTION

1.1 Primary Hyperoxaluria Type I (PH1)

Primary Hyperoxaluria Type I is a human metabolic autosomal recessive disease whose principal hallmark is the formation of calcium oxalate stones, forming at first in the kidneys and then in the whole body [1]. Although the first clinical manifestations of this disorder are related to renal dysfunction, the cause is the deficiency of a liver peroxisomal enzyme, alanine:glyoxylate aminotransferase (AGT)[2]. AGT is a pyridoxal 5'-phosphate (PLP)-dependent enzyme, encoded by the AGTX gene located on chromosome 2q37.3. AGT catalyzes an essentially irreversible transamination reaction in which the amino group of L-alanine is transferred to glyoxylate, leading to the formation of pyruvate and glycine. In the absence of functional AGT, glyoxylate accumulates in the peroxisomes and is transported to the cytosol were it is oxidized to oxalate by lactate dehydrogenase. Oxalate is an end product of metabolism and is excreted from the body, mainly by the kidneys[3] (Fig. 1).

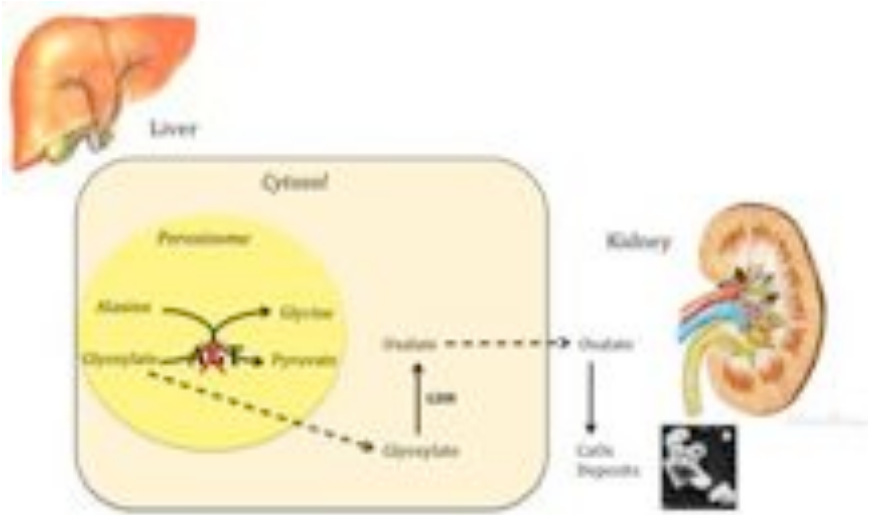

Fig. 1: Metabolic consequences of AGT deficiency. Sites and mechanisms of oxalate formation are shown.

In PH1 patients the over-production of glyoxylate and consequent oxalate accumulation allows the formation and deposition of calcium oxalate crystals (CaOx) in the kidneys and urinary tract. The progressive urolithiasis and nephrocalcinosis that follow finally lead to renal failure[4]. In these conditions the increased oxalate production is compounded by the decreased ability to eliminate it, thus leading to CaOx deposition at numerous sites within the body, a potentially fatal condition named systemic oxalosis and associated with various symptoms depending on the tissue involved (Table 1).

Table 1: Tissue involved in PH1 and related symptoms

TISSUE	CLINICAL SYMPTOM
Kidney and urinary tract	Urolithiasis, nephrocalcinosis, renal failure
Bone	Bone pain, multiple fractures, and osteosclerosis
Eye	Retinopathy and optic atrophy
Heart	Heart block, myocarditis, and cardioembolic stroke
Nerves	Peripheral neuropathy
Deep vasculature	Vasospasm

PH1 is difficult to treat. Classical treatments have the main objective of either preventing kidney failure, by decreasing the amount of oxalate and increasing the ability to eliminate it from the body, or restoring kidney function. They are aimed at [5]:

- Reducing the exogenous oxalate intake. Dietary restriction is aimed at decreasing the total body's intake of oxalate. Since several studies have shown that oxalate is only poorly absorbed from the diet [6-9] this strategy is not regarded as being very helpful.
- Reducing the endogenous oxalate synthesis. About 40% of the oxalate production appears to be derived from the glycine/glyoxylate metabolism[10, 11] thus, attempts to develop a therapeutic strategy to normalize endogenous oxalate synthesis in PH1 have been centered around glyoxylate metabolism and can be

divided into two main areas: 1) the inhibition of glyoxylate oxidation to oxalate, by inhibiting xanthine oxidase[12], glycolate oxidase (GO)[13], and lactic dehydrogenase (LDH)[14]; 2) the inhibition of glyoxylate synthesis by the administration of competitive inhibitors of D-aminoacid oxidase, or the reduction of the available glycine pool.

- Preventing CaOx crystallization, by the administration of crystallization inhibitors (i.e. magnesium and potassium citrate), hyperhydratation, and, the removal of CaOx stones by lithotripsy, which is the main treatment for PH1 patients.
- Treating renal failure and associated uremia by dialysis or kidney transplantation.

All these approaches address the more distal aspects of PH1, i.e. the symptoms rather than the causes. Thus, they do not represent a real cure for the disease because they only slow down disease progression.
Only two therapeutic approaches directed to the causes of the disease are currently available for PH1 patients. The first one is the administration of pharmacological doses of pyridoxine (Vitamin B6). It is known that pyridoxine can be converted in the body to PLP, the essential cofactor of AGT, but the molecular mechanism of action of this molecule has not been clarified. Moreover, only a minority (10−30%) of patients is responsive to pyridoxine therapy and clinical studies seem to indicate that responsiveness is confined to mutations that result in AGT mistargeting[15]. The only curative approach available for PH1 patients unresponsive to pyridoxine, is liver transplantation, which has the main objective of reintroducing most of the body's requirements of AGT. However, it represents a very wasteful intervention because an entire organ is employed to replace only one defective gene[5]. For these reasons it would be necessary to engage in new strategies to develop innovative and non-invasive treatments directed to the causes of the disease, which are

expected to provide long−term benefits, thus improving the treatment of PH1 patients.

1.2 AGT structure, function and intracellular localization

AGT is present in human hepatocytes as an 86 KDa homodimeric protein and each subunit comprises 392 aminoacids. The structure of the enzyme in complex with the inhibitor amino-oxyacetic acid solved in 2003[16] has revealed that it belongs to the Fold Type I class of PLP-dependent enzymes. Each subunit is composed of (Fig. 2):

- an N-terminal extension (residues 1-21) wrapping over the surface of the neighboring subunit,
- a large domain (residues 22-282) containing most of the active site and the dimerization interface,
- a C-terminal domain (residues 283-392) containing the peroxisomal targeting information.

The PLP coenzyme is covalently bound to the apoprotein by a Schiff base linkage with the ε-amino group of Lys209 forming a complex called internal aldimine.

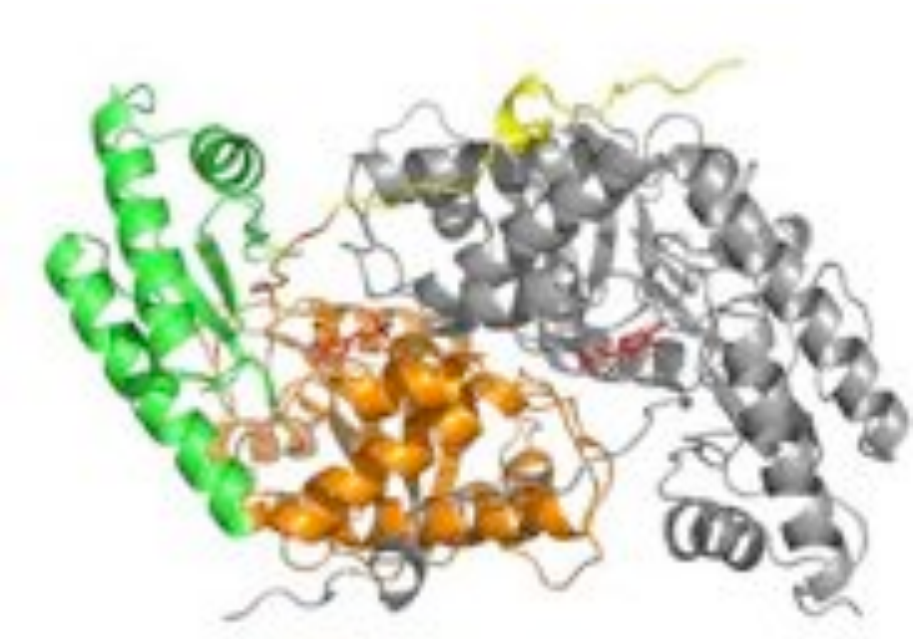

Figure 2. Dimeric structure of AGT (PDB file 1H0C). One monomer is colored gray, while the other one is colored yellow (N-terminal arm), green (C-terminal domain) and orange (large domain). PLP is represented as red sticks. The figure was rendered by using PyMol[17].

Other weak interactions at the active site stabilize the apoprotein-coenzyme interaction (Fig. 3). These are: (i) a ring stacking interaction between the pyridine ring of PLP and Trp108, (ii) a salt bridge between the protonated pyridine nitrogen and Asp183 and (iii) hydrogen bonds between the hydroxyl group of PLP and Ser158 as well as between the phosphate group of PLP and the residues His83 and Gly82, Tyr260* and Thr263* (* stands for residues belonging to the adjacent subunit) [16].

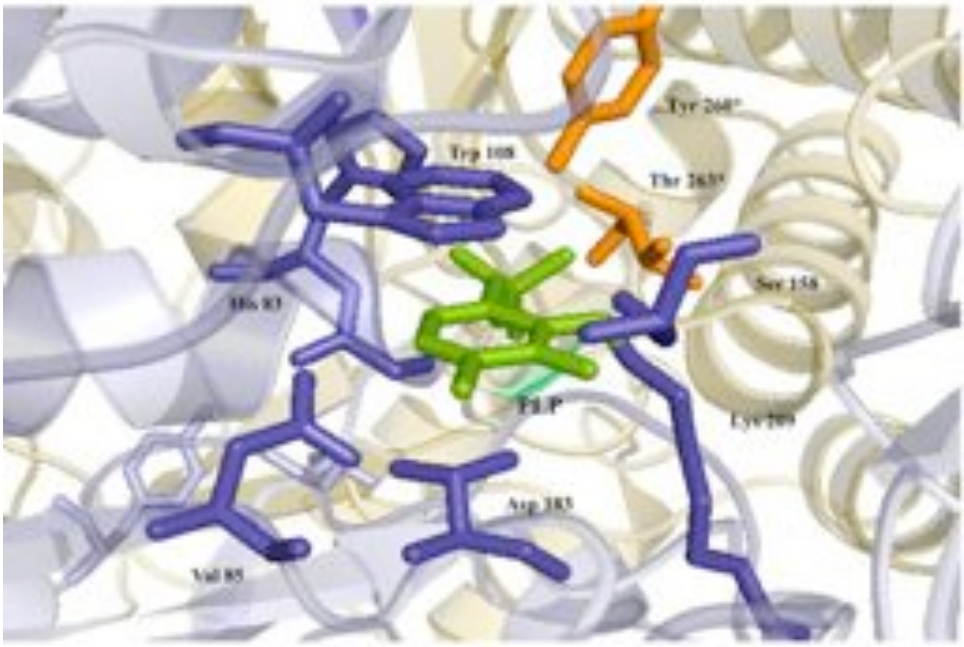

Figure 3: AGT active site (PDB file 1H0C). PLP is colored green. The residues that interact with the coenzyme are shown blue. The two orange residues interact with PLP but belong to the other monomer. The figure was rendered using PyMol[17]

The AGT spectroscopic features are those typical of PLP-dependent enzymes (Fig. 4A and B). The enzyme displays an absorption maximum at 420 nm, associated with a positive dichroic band at 429 nm, and a shoulder at about 340 nm, associated with a small negative dichroic signal at 335 nm probably corresponding to the ketoenamine and enolimine tautomers of the internal aldimine, respectively. Moreover, the enzyme shows positive dichroic bands in the 285-290 nm region and a negative dichroic band in the 256-266 region, which would indicate the asymmetry of some aromatic amino acids most probably located in the proximity of the active site[18].

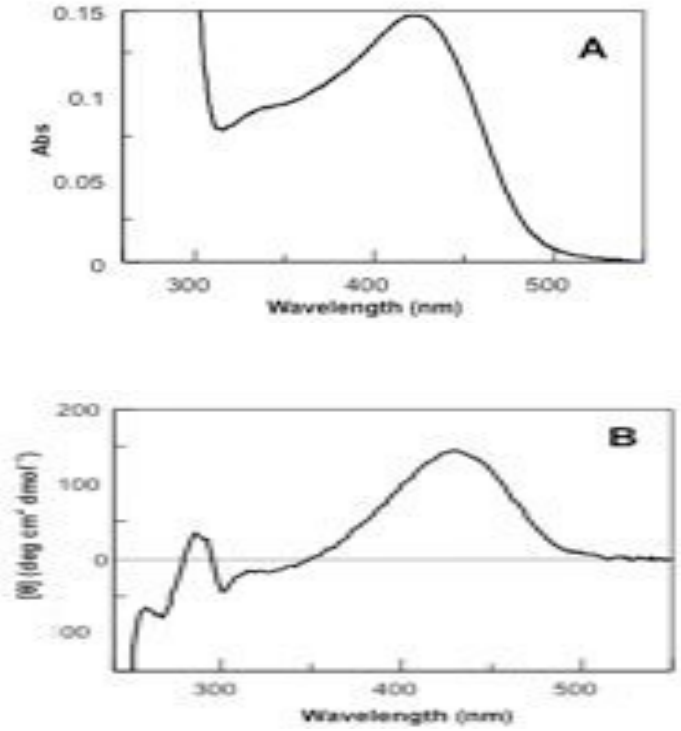

Figure 4: Absorbance **(A)** and CD-Visible **(B)** spectra of holo-AGT in 0.1M potassium phosphate buffer, pH7.4

AGT catalyzes the reversible transamination of L-alanine and glyoxylate to pyruvate and glycine by a classical ping-pong mechanism (Scheme 1). In the first half-reaction, after the binding of the substrate to the catalytic site of the enzyme in the internal aldimine form (AGT-PLP) and the formation of the Michaelis complex, the ε-amino group of Lys209 is replaced by the α-amino group of L-alanine, thus generating the external aldimine. The extraction of the C_{α}-proton from the external aldimine yields a quinonoid intermediate, which is reprotonated at the $C_{4'}$ of the coenzyme to give the

ketimine intermediate. The latter is then hydrolyzed to pyridoxamine 5'-phosphate (PMP) and pyruvate. In the second half transamination, following the same steps of the first half-reaction but in reverse order, glyoxylate reacts with the AGT-PMP complex and is converted to glycine, thus regenerating AGT-PLP [18].

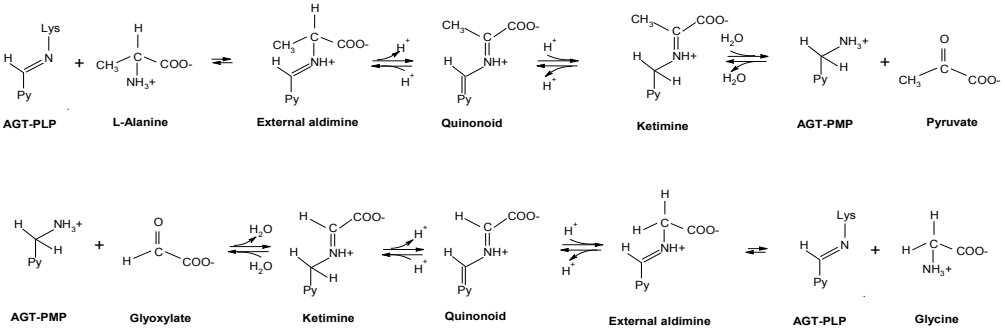

Scheme 1 Mechanism of the reaction catalyzed by AGT[18].

Kinetic studies have indicated that AGT is highly specific for the glyoxylate-to-glycine conversion, in agreement with the proposed physiological role of the enzyme in glyoxylate detoxification. In fact, the equilibrium constant of the overall transamination is about 9400 and the k_{cat} for the overall transamination reaction of the alanine/glyoxylate pair is around 100-fold higher than that of the glycine/pyruvate pair (45 s^{-1} vs 0.3 s^{-1}). Moreover, it has been shown that the enzyme has an higher affinity for PMP than for PLP, and that PMP remains tightly bound to the apoprotein during the catalytic cycle, thus making the enzyme more reactive toward oxo acids[18].
The study of the spectral changes occurring on AGT during the two half-transamination reactions have suggested that both the external aldimine formation and the interconversion between AGT-PLP and AGT-PMP are accompanied by conformational changes at the active site of the enzyme [18]. By means of computational analyses, it has been suggested that subtle

rearrangements of aromatic residues at the active site and a tilting of the coenzyme could occur and that these structural rearrangements could be determinant in the tight PMP binding and subsequent catalysis [18].

The localization of AGT inside the cell can vary from one species to another. During the evolution the targeting of AGT has been under the influence of strong dietary selection pressure, so that AGT tends to be mitochondrial in carnivores, peroxisomal in herbivores, and both peroxisomal and mitochondrial in omnivores. In many species, including the rat and marmoset, AGT is localized both in peroxisomes and in mitochondria. In some species, such as human, rabbit, guinea pig, and saki monkey, AGT is exclusively peroxisomal. In other species, such as the domestic cat, AGT is exclusively mitochondrial[19]

In human hepatocytes, like the large majority of peroxisomal proteins, AGT is synthetized in the cytosol and then transported inside the peroxisome trough the Pex5p carrier protein. The interaction between the AGT and the carrier occurs through a non-canonical type I peroxisomal targeting sequence (PTS1), i.e. a C-terminal KKL sequence instead of the SKL sequence normally found in the vast majority of peroxisomal proteins. This led to the hypothesis that AGT could possess an ancillary targeting sequence (PTS1A), which could work properly by interacting with Pex5p with the aid of an unidentified specific adaptor molecule[20]. Immunofluorescence and two-hybrid system studies had allowed the identification a putative ancillary peroxisomal targeting information (PTS1A) within the small C-terminal domain, in the region Val324-Ile345[20, 21]. Recently Fodor K. et al have solved the crystal structure of the complex of AGT and Pex5p[22]. This study has demonstrated that the two proteins are able to interact without the presence of an adaptor molecule and that the AGT-Pex5p interface consists of three regions: (i) the C-terminal PTS1 (residues 389-392) (ii) an “extended PTS1”, that includes the C-terminal part of the α helix 13 (residues 381-388) and the loop connecting the β strand 9 and the α helix 12 (residues 327-330), and (iii) a region topologically separate from the PTS1 formed by residues 303-307 [22].

1.3 Polymorphic mutations of AGT, the minor allele

As mentioned earlier, AGT is encoded by *AGXT* gene, located on chromosome 2q37.3. The *AGXT* gene is present in human population as two polymorphic variants, namely the “major allele” and the less common “minor allele”. The frequency of the minor allele varies among different populations, ranging from 2% in the Japanese population, to the 20% of Europeans and North Americans to 28% in the Saami population[23, 24]. The minor allele differs from the major allele by a 74-bp duplication in intron 1 and two point mutations (32C-T and 1020 A-G) leading to the Pro11Leu and Ile340Met amino acid substitutions[25]. Although the presence of the minor allele polymorphism is not pathogenic “per se”, it makes AGT more susceptible to the effect of several missense mutations, which are predicted to be non-pathogenic when associated with the major allele[26]. For this reason many investigations have been carried out to understand the differences between the two allelic forms of AGT at cellular and molecular level.

Studies performed on human hepatocytes [24, 26] indicate that the protein encoded by the minor allele (AGT-Mi) has a specific activity of about 70% compared with that encoded by the major allele (AGT-Ma) [26] Moreover, while AGT-Ma is entirely located in peroxisomes, AGT-Mi is localized in peroxisomes for about 95% and in mitochondria for 5% [24]. It has been demonstrated that the mislocalization is due to the P11L mutation, which creates a putative mitochondrial targeting sequence (MTS) at the N-terminus of AGT [27, 28]. However, the large part of AGT-Mi is not imported to mitochondria, probably because the protein quickly dimerizes, thus preventing the interaction with the mitochondrial import machinery that only acts on partly unfolded monomeric proteins.

The biochemical properties distinguishing the two allelic forms of AGT have been thoroughly analysed in vitro with purified recombinant AGT-Ma and AGT-Mi[29]. These studies have indicated that the P11L/I340M mutations do not affect either the UV-visible absorbance, dichroic and fluorescence

features of AGT or the equilibrium dissociation constant for PLP ($K_{D(PLP)}$) value, thus suggesting that no gross conformational changes have occurred and that the two species share a similar active site architecture. However, in agreement with the results obtained on human hepatocytes, the mutations induce a slight decrease (about 30%) of the k_{cat} value for the overall transamination of L-alanine and glyoxylate.
Yeast complementation assays[30], along with pulse-chase and cross-linking experiments performed on cell-free transcription/translation products [31] have indicated that AGT-Mi is less stable in vivo and is more susceptible to proteolytic degradation and aggregation with respect to AGT-Ma. In agreement with these results, thermal and chemical unfolding studies have provided evidence that both holo- and apoAGT-Mi show a decreased overall stability and a more unstable dimeric structure compared with the corresponding forms of AGT-Ma. The destabilization can be imputed to the P11L mutation [29]. It has been suggested that the substitution of Pro11 with a leucine residue would loosen the interaction of the N-terminal arm of one subunit of AGT with the large domain of the opposite subunit, thus facilitating dimer dissociation. This perturbation could also be transmitted to the AGT active site through a loop (residues 24-32), which contributes to the PLP binding site. These analyses, besides elucidating the differences between AGT-Ma and AGT-Mi, have represented the starting point to investigate the effect of pathogenic mutations associated with the major or the minor allele.

1.4 Pathogenic mutations of AGT

PH1 is considered a very heterogeneous disease from a genetic, enzymatic and clinical point of view. Up to now, more than 150 different pathogenic mutations on the *AGXT* gene have been identified, including nonsense, frameshift and the most common missense mutations. The latter

group, comprises mutations associated with the major allele, mutations that cosegregate and functionally interact with the minor allele, and mutations that can be found associated with the major or the minor allele (Table 2).
While nonsense and frameshift are null mutations that lead to a complete loss of the gene product, missense point mutations lead to single amino acid substitutions that cause the synthesis of an aberrant gene product.
A wide variety of enzymatic phenotypes, i.e. of mechanisms by which a missense pathogenic mutation leads to AGT deficiency, have been identified. Up to now, the mutations have been classified on the basis of western-blot and enzymatic activity analyses of either patient liver samples or crude lysates of eukaryotic and/or prokaryotic cells expressing the AGT variants[5, 26, 31-38]. The classes of mutations are defined as:

- ENZ^-/CRM^+: mutations that lead to the loss of the AGT catalytic activity without loss of immunoreactivity, and represent about 20% of the total;
- ENZ^-/CRM^-: mutations that lead to the absence of both AGT catalytic activity and immunoreactivity , and are the large majority of PH1-causing mutations;
- ENZ^+/CRM^+: mutations that cause the mistargeting of AGT from peroxisomes to mitochondria without negatively influencing either the catalytic activity or the immunoreactivity of the protein. This group includes the G170R substitution associated with the minor allele, the most frequent PH1-causing mutation that affects about one third of all the patients.

Table 2: Some of the most common PH1 mutations in the *AGXT* gene.

MUTATION	EXON	AMINO ACID SUBSTITUTION	FREQUENCE	ALLELE
367G>A	2	G82E	?%*	major
549G>A	3	D183N	?%*	major
444T>C	2	W108R	?%*	minor
630G>A	4	G170R	30%	minor
576T>A	4	F152I	1%	minor
735T>C	6	S205P	<1%	major
853T>C	7	I244T	9%	minor
243G>A	1	G41R	1%	minor
243G>A	1	G41R	?%*	major
244G>T	1	G41V	?%*	major

The resolution of the AGT crystal structure[16] has allowed to rationalize the impact of some pathogenic mutations, at least in terms of their likely effects on AGT tertiary and quaternary conformation. Moreover, in the last few years, more detailed studies on the pathogenic variants either in the recombinant purified form, or expressed in mammalian cells or in cell-free expression systems, have been performed to define how a particular amino

acid substitution could alter the AGT structural and/or functional properties. These analyses have made it possible to identify the following molecular mechanism leading to AGT deficiency in PH1 (Figure 5):

- The loss of catalytic activity and/or the reduction of coenzyme binding affinity, such as the G82E mutation associated with the major allele and the F152I associated with the minor allele. The biochemical characterization of the G82E-Ma variant in the purified form has shown that the mutation leads to a perturbation of the active site microenvironment, which causes a strong reduction of the PLP binding affinity and of the catalytic efficiency for the overall transamination reaction [18]. In the case of the F152I-Mi variant, a strongly reduced affinity for the PMP coenzyme has been reported, leading to a release of PMP during the overall transamination reaction[39].

- The loss of immunoreactivity of the protein, such as the G41R, G170R, F152I and I244T mutations, associated with the minor allele as well as the G41R and G41V mutations associated with the major allele. It has been demonstrated that various mechanisms can lead to a reduced immunoreactivity:
    1. a reduced dimer stability. Cross-linking studies on the G41R-Ma, G41R-Mi and G41V-Ma variants expressed either in mammalian cells or in cell-free expression systems have indicated a higher population of the monomer form of these variants with respect to AGT-Ma or AGT-Mi[31]. Moreover, size exclusion chromatography (SEC) and thermal and chemical denaturation studies of the G170R-Mi, F152I-Mi, G41R-Mi, G41R-Ma and G41V-Ma variants in the purified form have demonstrated that the mutations reduce the stability of the dimeric structure of the protein in the apo-form[29, 39-42].

2. a higher susceptibility to proteolytic degradation, such as can be found for the G41R and I244T mutations associated with the minor allele as well as the G41R and G41V mutations associated with the major allele. Analyses on the pathogenic variants both in the purified form and expressed in cell-free transcription-translation systems have shown that the mutation of Gly41 increases the sensibility to degradation of AGT, while the I244T mutation strongly sensitizes AGT to trypsin treatment. [31, 43, 44].
3. an increased aggregation propensity of the protein, as found for the G41R, I244T and F152I mutations associated with the minor allele as well as the G41R and G41V mutations associated with the major allele. A propensity to aggregate has been shown for these variants expressed in cell-free [31] and cellular systems[44, 45]. Moreover dynamic light scattering (DLS) and SEC studies of these variants in their purified form have confirmed that the G41V, G41R and F152I mutations lead to protein aggregation[26, 39, 40]. However, while the aggregation of the F152I-Mi variant is due to protein monomerization, the aggregation of G141R-Ma, G41V-Ma and G41R-Mi is driven by electrostatic interactions between dimers.

- The mislocalization of the protein, such as that found for F152I, G170R and I244T mutations on the background of the minor allele. Studies performed on patient liver biopsies or in mammalian cells expressing the G170R-Mi, F152I-Mi and the I244T-Mi variants, have led to the conclusion that the molecular defect of these variants is the mislocalization of the protein to mitochondria instead of peroxisomes[35, 36, 45]. In the last few years, the biochemical characterization of the G170R-Mi and F152I-Mi variants in their purified form[29, 39], has allowed to conclude that the variants display

a lower stability of the dimer structure in the apo-form, leading to the hypothesis that these mutations could affect the conversion of the partially unfolded monomer or of the folded monomer to the apodimer. The consequent accumulation of a partially unfolded monomer would synergize with the presence of the putative MTS, thus making the protein compatible with the interaction with the mitochondrial import machinery.

Figure 5: Molecular mechanisms leading to AGT deficiency

All together these results, besides demonstrating that the mechanisms leading to AGT deficiency are more complicated than previously thought, have highlighted that in order to have a more complete picture of the molecular defect of a pathogenic variant one should integrate data from (i) the inspection of the AGT crystal structure, (ii) the biochemical

characterization of the purified variant in both the holoenzymatic and the apoenzymatic form, and (iii) the study of variants expressed in mammalian cell lines.

Moreover, results from published studies have allowed to understand the basis for the therapeutic response and to suggest new therapeutic approaches for patients bearing the examined mutations. In particular, it has been suggested that the responsiveness to pyridoxine therapy in patients bearing the G170R or F512I mutations is due not only to a prosthetic role of PLP, which shifts the equilibrium from the apo to the more stable holo-form of the protein, but also to a conformational role of PLP, which could bind to the unfolded or partially unfolded monomer leading to the formation of a folded dimer that can be imported in peroxisomes. Moreover, it has been suggested that an approach with pharmacological chaperones would be useful for patients bearing the G41R, G41V and I244T mutations. Pharmacological chaperones are small drug−like molecules that diffuse into the cell and bind site−specifically to folding intermediates during the biosynthesis of a mutated protein, thereby improving its folding efficiency. Pharmacological chaperones could possibly rescue for the protein instability of the G41R-Ma, G41R-Mi, G41V-Ma and I244T-Mi AGT mutants.

AIM OF THE RESEARCH

Primary Hyperoxaluria Type I (PH1) is a rare disease caused by mutations in the gene encoding hepatic alanine:glyoxylate aminotransferase (AGT). AGT deficiency causes the formation and deposition of calcium oxalate crystals at first in the urinary tract and then in the whole body. PH1 is a heterogeneous disease in respect to the clinical manifestations, the response to treatment and the pathogenic mechanisms. In fact, more than 150 pathogenic mutations have been identified so far and the molecular mechanisms by which missense mutations cause AGT deficiency include functional, structural and subcellular localization defects. The only two curative treatments available for PH1 are pyridoxine therapy, which is effective only in a minority of patients, and liver transplantation, which is a very invasive and problematic procedure. Thus, approaches aimed at a deeper knowledge of genotype/phenotype correlations as the base to develop new treatment strategies appear to be desirable. Although in the last few years several efforts have been done to better understand the molecular defects of PH1-associated mutations, knowledge of the defect of the AGT variants at a protein level is still poor. Thus, we performed a side-by-side comparison between normal AGT and several purified pathogenic variants in terms of catalytic activity, coenzyme binding mode and affinity, spectroscopic features, oligomerization and thermal stability of both the holo- and apo-form. On the basis of the obtained results, a more detailed analysis of the S187F-Ma variant, by crystallographic, spectroscopic and kinetic analyses, as well as of the Gly161 variants, by biochemical studies on the purified proteins paired with cell biology studies, has been undertaken.

MATERIALS AND METHODS

3.1 Materials

PLP, pyridoxine, L-alanine, sodium glyoxylate, rabbit muscle L-lactic dehydrogenase, isopropyl-β-D-thiogalactoside (IPTG), EDTA and imidazole were all purchased from Sigma. Ham's F12 Glutamax medium was purchased from Invitrogen. All other chemicals were of the highest purity available. The rabbit polyclonal anti-AGT human and guinea-pig anti–peroxisomal proteins antibodies were kindly provided by Prof. C.J. Danpure of University College London (UK); the anti-rabbit HRP antibody was purchased from GE Healthcare. Oligonucleotides for site directed mutagenesis were purchased from MWG Biotech AG (Anzinger, Germany)

3.2 Site directed mutagenesis

The constructs encoding for the polymorphic and pathogenic variants of AGT were constructed starting from the pAGT-His construct, kindly provided by Prof. Christopher J. Danpure of the University College London (UK). This vector contains the complete open reading frame of AGT together with a C-terminal histidine-tag (AVDHHHHHH), cloned in a pTrcHis2A expression plasmid (Invitrogen)[26]. This vector allows to express recombinant AGT in E. coli under the lactose operon controller by adding IPTG to the culture broth. Moreover, the presence of a C-terminal 6-Histidine tag allows a one step purification of the protein by Immobilized Metal Affinity Chromatography.
For cell biology studies, the cDNA encoding human AGT was cloned in the mammalian expression vector pcDNA3.1/V5-His-TOPO, by means of the TOPO cloning kit (Invitrogen). This expression vector contains the human cytomegalovirus enhancer-promoter sequences upstream of the multicloning site, the transcription-termination sequence of the bovine growth hormone gene (bGH) downstream of the multicloning site and the gene for neomycine resistance.

The desired mutations were introduced on the desired vector by the QuikChange site-directed mutagenesis kit (Stratagene), which employs double-stranded DNA as a template, two complementary oligonucleotide primers containing the desired mutation, and DpnI endonuclease to digest the parental DNA template. The oligonucleotides used for mutagenesis are reported in Table 3.

Table 3: DNA sequence of the primers used for site-directed mutagenesis (5'-3'). The underlined codons indicate the mutated aminoacid.

AGT variant	DNA sequence of the mutagenic primers (5'-3 ')
W108R-Mi	GGGGCCAATGGCATTAGGGGGCAGCGAGCCGTG CACGGCTCGCTGCCCCCTAATGCCATTGGCCCC
S158L-Ma	CCACGGGGAGTTGTCCACCGGCG CGCCGGTGGACAACTCCCCGTG
G161C-Mi	GAGTCGTCCAACCTGCGTGCTGCAGC GCTGCAGCACGCAGGTGGACGACTC
G161S-Mi	GAGTCGTCCAACCAGCGTGCTGCAGC GCTGCAGCACGCTGGTGGACGACTC
D183N-Ma	CCTGCTCCTGGTGAATTCGGTGGCATCCC GGGATGCCACCGAATTCACCAGGAGCAGG
S187F-Ma	GGATTCGGTGGCATTCCTGGGCGGGAC GTCCCGCCCAGGAATGCCACCGAATCC
S218L-Ma	CCCCTCCAGGGACCTTGCTCATCTCCTTC GAAGGAGATGAGCAAGGTCCCTGGAGGGG
P319L-Ma	GCGCTCCGGCTTCTCACAGTCACCACT AGTGTGACTGTGAGAAGCCGGAGCGC
G350D-Mi	GAGATCATGGGTGACCTTGGGCCCTCC GGAGGGCCCAAGGTCACCCATGATCTC

3.3 Expression and purification of the AGT variants

E. coli JM109 cells transformed with the constructs encoding the AGT variants were grown in 750 ml of Luria broth at 37°C to an absorbance at 600 nm of 0.4-0.6. Expression was induced with 0.1 mM IPTG for 15 h at 30°C. Cells were harvested and resuspended in 20 mM sodium phosphate buffer, pH 7.4 containing 0.5 M NaCl, 20 mM imidazole and 100 μM PLP. Lysozyme was added to a concentration of 0.2 μg/ml and the culture was incubated for 15 min at room temperature. After a freeze-thaw, leupetin (0.5 μg/ml) and pepstatin (0.7 μg/ml) were added and the suspension was centrifuged at 30,000 *g* for 30 min at 4°C. The lysate was loaded on a HisPrep FF 16/10 (GE Healthcare) equilibrated with 20 mM sodium phosphate buffer pH 7.4 containing 0.5 M NaCl and 20 mM imidazole. A linear gradient was then inserted (0-100% in 200 ml) with the same buffer containing 500 mM imidazole. Soluble AGT elutes from the Ni^{2+} resin between 300 and 400 mM imidazole. After addition of 100 μM PLP, the protein solution was concentrated; imidazole and unbound coenzyme were removed by extensive washing with 100 mM potassium phosphate buffer, pH 7.4, using Amicon Ultra 10 concentrators (Amicon)[18]. AGT can be stored at -20 °C without loss of activity for more than 6 months. Protein concentration was determined by using the apparent molar absorption coefficient of 95400 M^{-1} cm^{-1} at 280 nm. The PLP content was determined by releasing the coenzyme in 0.1 M NaOH and by using the apparent molar absorption coefficient of 6600 M^{-1} cm^{-1} at 388 nm [18, 46].

3.4 Preparation of the apoenzyme

AGT in the apo form was prepared by incubating AGT-Ma, AGT-Mi or the variants (10–20 μM) in the holo-form with 500 mM L-alanine for 5-120 min, on the basis of the $k_{cat,}$ at 25 °C of the enzymatic species, in a final volume of 2 ml. The reaction mixture was concentrated to 0.2 ml by a Amicon Ultra 4 device (Millipore), washed twice with 2 ml of 1 M potassium phosphate

buffer, pH 6 and then 4–5 times with 100 mM potassium phosphate buffer, pH 7.4.

3.5 Determination of the equilibrium dissociation constants of the variants for PLP

The equilibrium dissociation constant for PLP ($K_{D(PLP)}$) of G161C-Mi, G161S-Mi, P319L-Ma and G350D-Mi variants was determined by measuring the quenching of the intrinsic fluorescence of the apo-enzymes (0.1 μM) in the presence of PLP at a concentration range of 0.01–10 μM. In the case of W108R-Mi, S158L-Ma, D183N-Ma and S81L-Ma variants the $K_{D(PLP)}$, was determined by measuring the CD signal at 430 nm of the apo forms at a concentration of 10 μM in the presence of PLP at concentrations ranging from 5 to 300 μM. All the experiments were carried out in 100 mM potassium phosphate buffer, pH 7.4.
The $K_{D(PLP)}$ values for the mutant-coenzyme complexes were obtained by fitting the data to the following equation:

$$Y = Y_{\max} \frac{[E]_t + [PLP]_t + K_{D(PLP)} - \sqrt{([E]_t + [PLP] + K_{D(PLP)})^2 - 4[E]_t[PLP]_t}}{2[E]_t} \quad (1)$$

where $[E]_t$ and $[PLP]_t$ represent the total concentrations of the mutant and PLP, Y refers to either the intrinsic fluorescence quenching or the 430 nm dichroic signal changes at a PLP_t concentration, [PLP], and Y_{max} refers to the aforementioned changes when all enzyme molecules are complexed with coenzyme.
The $K_{D(PLP)}$ for the S187F-Ma variant has been estimated as the upper limit value by the following procedure: samples of holo- and apo-S187F-Ma at

various protein concentrations (from 0.01 to 1 μM, being 0.01μM the detection limit) were incubated overnight at 25 °C in 100 mM potassium phosphate buffer, pH 7.4. The intrinsic fluorescence emission at 336 nm of each sample was registered and the percentage of fluorescence quenching at each protein concentration was then calculated.

3.6 Kinetic studies

The kinetic parameters for the overall transamination reaction for the pair alanine/glyoxylate of the AGT variants (0.1–10 μM) were determined in the presence of saturating PLP concentrations by varying the substrate concentration at a fixed saturating co-substrate concentration. At different times, the reactions were stopped by adding TCA 10% (v/v). In the case of the G161C-Mi, G161S-Mi, S218L-Ma, P319L-Ma and G350D-Mi variants the produced pyruvate was measured by a spectrophotometric assay using the coupled lactate dehydrogenase system[18]. In the case of the W108R-Mi, S158L-Ma, D183N-Ma and S187F-Ma variants, pyruvate production or glyoxylate consumption was measured by an HPLC assay based on the derivatization with 2,4-dinitrophenylhydrazine [47]. The mixture was injected onto a Supelco™ Discovery C18 column connected with a Jasco HPLC system and run with 25 mM sodium phosphate, 25mM sodium acetate, 20% acetonitrile. A Jasco UV-1570 detector set at 340 nm was employed and the flow rate was 0.9 ml/min.
Data of initial velocity (v) as a function of substrate concentration were fitted to the Michaelis-Menten equation:

$$\frac{v}{\mathrm{Et}} = \frac{k_{cat}[S]}{Km + [S]} \quad (2)$$

where E_t is the total enzyme concentration, S is the substrate concentration, k_{cat} is the turnover number, and K_m is the Michaelis-Menten constant.
The AGT enzymatic activity of CHO cell lysates expressing AGT-Ma, AGT-Mi, G161R-Ma, G161S-Mi and G161C-Mi, was determined by incubating 90 µg of lysate with 0.5 M L-alanine and 10 mM glyoxylate for 30-150 min in 100 mM phosphate buffer pH 7.4. The reactions were stopped by adding TCA 10% (v/v) and the pyruvate production was measured using the spectrophotometric assay coupled with lactate dehydrogenase described above.
The kinetic parameters for the overall transamination of the alanine/glyoxylate pair of the S187F mutant in the presence of 5 mM pyruvate were determined by measuring the amount of glyoxylate consumed by HPLC after derivatization with 2,4-dinitrophenylhydrazine as described above. Substrate saturation curves were fitted using equation 3, and dead-end inhibition data were fitted using equation 4 for competitive inhibition:

$$v = VA/(K_a + A) \qquad (3)$$

$$v = VA/K_a[1 + I/K_{is}] + [A] \qquad (4)$$

where v is the initial velocity, V is the maximum velocity, A is substrate concentration, K_α is the K_m for substrate A, and K_{is} is the slope constant.
The half-transamination reaction of holoS187F (15 µM) with L-alanine (5–500 mM) was performed in 100 mM potassium phosphate buffer, pH 7.4, at 25°C in a total volume of 250 µl. The decrease in the 413 nm absorbance signal was measured as a function of time and fitted to the equation:

$$A_t = A_\infty + \Delta A_1 \exp(-k_{obs1}t) + \Delta A_2 \exp(-k_{obs2}t) \qquad (5)$$

where A_t is the absorbance at time t, ΔA_1 is the amplitude of the fast phase,

ΔA_2 is the amplitude of the slow phase, k_{obs1} is the observed rate constant of the fast phase, k_{obs2} is the observed rate constant of the slow phase and A_∞ is the final absorbance.

The k_{max} and apparent K_m^{app} values for each phase of the L-alanine half-reaction were determined by plotting the observed rate constants versus L-alanine concentrations and fitting the data to equation 6:

$$k_{obs} = \frac{k_{\max}[S]}{K_m^{app} + [S]} \qquad (6)$$

The detection and quantification of PLP and PMP during the L-alanine half-transamination was performed by HPLC upon sample denaturation with 10% trichloroacetic acid (v/v). A Supelco™ Discovery C18 column connected with a Jasco HPLC system equipped with a Jasco UV-2075 detector set at 295 nm was used. The eluent was 50 mM potassium phosphate buffer, pH 2.35, at a flow rate of 1 ml/min. PLP elutes as a single peak at ~ 6.5 min, while PMP elutes as a single peak at ~ 5.3 min.

3.7 Spectroscopic measurements

Absorption measurements were made with a Jasco V-550 spectrophotometer with 1 cm path length quartz cuvettes at a protein concentration of 1-10 µM in 100 mM potassium phosphate buffer pH 7.4. The aggregation kinetics of Gly161 variants in both the holo- and the apo-form at 2 µM concentration was monitored by following the absorbance at 600 nm as a function of time under physiological conditions (150 mM ionic strength, pH 7.4, 37°C).

Intrinsic fluorescence emission spectra were recorded on a Jasco FP-750 spectrofluorimeter equipped with a thermostatically controlled cell holder by using a 1 cm path length quartz cuvette. Protein emission spectra were taken from 300 to 500 nm (excitation at 280 nm) with both the excitation and the emission slits set to 5 nm. The protein concentration was 1 or 5 µM.

Spectra of blanks, i.e. of samples containing all components except the enzyme, were taken immediately before the measurements of samples containing protein.
Visible and far-UV CD spectra were recorded on a Jasco J-710 spectropolarimeter equipped with a Peltier temperature controlled compartment, by using 1 cm and 1 mm path length cells, respectively. The enzyme concentration was 1-10 μM. Routinely, three spectra were recorded at a scan speed of 50 nm/min^{-1} with a bandwidth of 2 nm and averaged automatically, except where indicated.
DLS analyses were performed on filtered stock solutions of the AGT variants either in the holo or the apo-form at 10 μM concentration in 100 mM potassium phosphate buffer, pH 7.4 at 25°C. PLP at saturating concentrations was added to the holoenzyme solutions and each sample was incubated for 10 min at 25°C. The aggregation kinetics of AGT-Ma, AGT-Mi, G161S-Mi and G161C-Mi under physiological conditions was studied by incubating each enzymatic species at 1 μM concentration in 60 mM phosphate buffer pH 7.4 at 37°C. All DLS measurements have been performed on a Zetasizer Nano S device (Malvern Instruments) equipped with a Peltier temperature controller by using disposable 12.5 x 45-mm cells with stopper.

3.8 Thermostability studies

Thermostability studies on purified AGT variants in the holo- (in the presence of saturating PLP) or in the apo-form were performed by both CD-monitored thermal unfolding and differential scanning fluorimetry (DSF). In the first method, the CD signal at 222 nm of AGT variants at 10 μM concentration in 100 mM potassium phosphate buffer, pH 7.4, was registered with temperature increasing from 25 to 90 °C at a heating rate of 1.5 °C/min. PLP dissociation during thermal unfolding of the holoenzymes was monitored by measuring the CD signal at 430 nm under the same experimental conditions reported above. Calculation of the melting temperature (Tm) was carried out by fitting the CD signal either to a two or

a three state unfolding model using the Origin Pro7 software according to the method of Pace [48]. The rates of PLP dissociation and loss of secondary structure at the melting temperature for both AGT-Ma and AGT-Mi were measured by monitoring the CD signal at 430 and 222 nm with time and fitting the data to a single exponential curve. DSF experiments were performed with purified AGT variants at 1 µM concentration in 100 mM potassium phosphate buffer pH 7.4 containing 5X SYPRO orange, according to the method of Niessen et al.[49]. Considering the high background fluorescence of the holo- and apo-forms of W108R-Mi at 25 °C, the SYPRO orange final concentration was kept to 2.5X. Proteins were subjected to a ramp of 2.15° C/min in a Mastercicle EP Realplex 4 device (Eppendorf) at a temperature gradient from 25°C–90°C. Graph generation and calculation of Tm were carried out by using the Realplex software.

3.9 Crystallographic studies on the S187F variant

The crystal structure of the S187F-Ma variant was determined in collaboration with the group of Prof. Wilmanns at the European Molecular Biology Laboratory (EMBL) in Hamburg. Crystals of the S187F-Ma variant were obtained by mixing 1 µl of protein at 5 mg/ml concentration with 1 µl of a reservoir solution, composed of 0.1 M HEPES, pH 7.5, 0.1 M $LiSO_4$, 23% (w/w) PEG4000 and by submitting the mixture to hanging drop vapor diffusion at 20^0C. X-ray data were collected at X13 at DORIS III (Doppel-Ring Speicher) synchrotron radiation storage ring, Hamburg, Germany. Data were processed with XDS [50] and scaled with SCALA [51]. 5 % of the reflections were randomly selected for cross-validation. The structure of the S187F variant was solved by molecular replacement with Phaser [52] using normal AGT as starting model (PDB entry: 1H0C) [16]. REFMAC [53] was used to refine the initial structural model, applying translation/libration/srew parameterization, and including restraints from the non-crystallographic symmetry (NCS) between the AGT chains. Manual building and structure analysis were carried out in COOT [54]. The structure quality was assessed

with MOLPROBITY [55]. Programs of the CCP4 package [56] were used for average B-factor calculation, structure manipulation, analysis and validation.

3.10 Molecular modelling studies

Molecular modelling studies were perfomed in collaboration with Dr. Alessandro Paiardini from the University of Rome "La Sapienza". The three-dimensional coordinates of the S187F-Ma mutant in the internal aldimine form were used as a starting point to generate the external aldimine and the PMP bound forms of the enzyme by energy minimization means using the BIOPOLYMER package from InsightII (V.2000, MSI, Los Angeles, USA). PMP and external aldimine were positioned into the active site of S187F-Ma, initially following the binding mode of PLP. Atomic potentials, partial and formal charges were defined using the Cff91 forcefield, and it was verified that the proper values had been assigned. Each complex was then subjected to further energy minimization. The minimization protocol adopted was based on a multi-step approach: first, all atoms except added hydrogens were fixed to allow hydrogens to adjust to the atomic environment. To this purpose, 1000 steepest descents steps were performed, a distance-dependent dielectric constant and a cut-off distance of 40 Å were used during each simulation, until the maximum energy derivative was less than 41.8 $kJ \cdot mol^{-1}Å^{-1}$. Then main-chain atoms were fixed and side-chains of every residue comprised in a sphere of 5 Å from the coenzyme were subjected to a gradually decreasing tethering force (from 4180 $kJ \cdot Å^{-2}$ to 418 $kJ \cdot Å^{-2}$) using conjugated gradients, until maximum derivative was less than 4.18 $kJ \cdot mol^{-1}Å^{-1}$. Finally, a decreasing tethering force (until the system was totally relaxed) was applied on PMP, external aldimine and ketimine, and every side-chain atom comprised in a sphere of 5 Å from PLP, using conjugated gradients until the maximum derivative was less than 0.0004 $kJ \cdot mol^{-1}Å^{-1}$. Discover 2.9 and Analysis package of InsightII were used for minimization.

3.11 Cell culture and lysis

CHO cells were cultured at 37°C under O_2/CO_2 (19:1) in Ham's F12 Glutamax medium (Invitrogen) supplemented with fetal bovine serum (10%, v/v), penicillin (100 units/ml) and streptomycin (100 µg/ml). When the cells were 70–80 % confluent they were trypsinized, counted and re-seeded into 6-well plates or 60 mm dishes at a density of 0.3-0.6 × 10^6 cells/well respectively. After over night incubation at 37°C, cells were transfected with Turbofect™ Transfection Reagent (Fermentas) according to the manufacturer's instructions. After 4 hours from transfection cell were washed in phosphate buffered saline (PBS) and the medium was changed with complete Ham's F12. Where indicated, 100 µM pyridoxine was added to the medium. Transfection experiments were designed to minimize the variability introduced by transfection efficiency, which was controlled by co-transfection with pmaxGFP (Lonza), and only transfections with variability ≈ 10% were used. Except where indicated, cells were harvested after 24 hours and lysed in phosphate saline buffer (PBS), pH 7.2, plus protease inhibitor cocktail (Complete Mini, Roche), by five freeze/thaw cycles followed by treatment with DNAse (1 unit) at RT for 45 min. The whole cell extract was separated by centrifugation (29200 *g*, 10 min, 4°C) to obtain the soluble fraction. The pellets were then resuspended in an equal volume of denaturing gel loading buffer to obtain the insoluble fraction. The total protein concentrations in the cell lysate and/or in the soluble fraction, was measured using the Bradford protein assay.

3.12 Transcript expression analysis

CHO cells were grown in a 6-well plate and transfected using Turbofect (Fermentas) as described above. Cells were harvested, washed with PBS, and RNA was extracted using RNeasy mini kit (Qiagen). The cDNA was synthetized from 1 µg of mRNA using the Supersctipt VILO cDNA synthesis kit (Invitrogen, Carlsbad, CA) according to manufacturer's instructions. Real-time PCR was performed using 3 µl of a 1:10 cDNA dilution in a 25 µl reaction volume using SYBR Premix Ex Taq master mix (TaKaRa) on a Corbett RotorGene 6000 thermocycler. The reaction conditions were initial denaturation at 95°C for 15 min followed by 45 cycles of PCR which included 15 sec melting at 95°C, 30 sec annealing at 55°C and 30 sec extension at 72°C. The samples were examined for the expression of human AGT using the forward primer 5'-AGCCCAGGATGTACCATCAC-3' and the reverse primer 5'-GCCACCCATGATCTCAATGTC-3'. The amount of the AGT-Ma, AGT-Mi and G161 variants mRNA was calculated in relation to the glyceraldehyde 3'-phosphate dehydrogenase (GAPDH) mRNA in the same sample. Quantitation of individual transcripts was performed using the 'Comparative Quantitation' software supplied by Corbett Research for the RotorGene. The mean efficiency of a group of cycling curves is calculated at the point that the cycling curves take off and used to calculate a fold change according to the formula: fold change = efficiency Ct1–Ct2, where Ct1 and Ct2 are the take off values of the cycling curves being compared. All reactions were performed in duplicate.

3.13 Western blotting analysis and chemical cross-linking

10 µg of cell lysate were loaded per lane on a Mini Protean TGX™ pre-cast gel (Biorad) along with Precision plus protein Kaleidoscope™ (Bio-Rad) as

molecular mass markers. Following transfer on a nitrocellulose membrane by the iBlot device (Invitrogen) the membrane was blocked in 5% bovine serum albumin (BSA) for 1 h at 37°C. For AGT detection the membrane was incubated with polyclonal rabbit anti AGT serum (dilution 1:2000), washed three times in TBST (50 mM Tris-HCl pH 7.5, 150 mM NaCl, 0.1% Tween 20) and then incubated with peroxidase-conjugated anti rabbit IgG (dilution 1:1000). Blotted proteins were detected and quantified with ECL® (Millipore), using the ChemiDoc XRS Imaging System (Bio-Rad, Hercules, CA).

Cross-linking was performed with bis-N-succinimidyl-(pentaethylene glycol)ester, $BS(PEG)_5$ (Pierce). Cells were lysed as described above, then 25 µl of the whole lysate at 1 mg/ml total protein concentration was cross-linked with $BS(PEG)_5$ at fifty molar excess (1.25 mM final concentration), and quenched in 50 mM Tris–HCl after 30 min. 10 µg of each samplewere analysed by western blotting as above.

3.14 Pulse-chase experiments

Two million cells were seeded in a 10 cm dish and transfected with the pcDNA3.1 vectors encoding AGT-Ma, AGT-Mi, G161R-Ma, G161S-Mi or G161C-Mi. After 24 hours cells were incubated for 1 hour in Dulbecco's Modified Eagle Medium (DMEM) without methionine and cysteine (Gibco) and pulse labelled with 50 µCi of 35S methionine/cysteine (EasyTag™ EXPRESS 35S Protein Labeling Mix, [35S], Perkin Elmer). After 30 min an excess of unlabelled aminoacids was added and cells were split and incubated in Ham's F12 medium for chase periods from 4 to 48 hours. The soluble fraction of each cell lysate (50 µg) was incubated over night with 2 µg of guinea-pig anti-AGT antibody on a rotator at 4°C. Thereafter, the immunoprecipitation reaction was performed at room temperature by adding 30 µl of agarose-protein A (GE, Healthcare) to the mixture and by

incubating the solution for 1 h on a rotator at room temperature. The immunoprecipitated complex was pelleted by centrifugation at 29200 g at 4 °C for 5 min, washed three times with IP wash/lysis buffer (Thermo Scientific), and resuspended in 20 µl of denaturing gel loading buffer. Proteins were separated by SDS-PAGE and radiolabelled AGT was detected by autoradiography.

3.15 Gel filtration analyses

9 x 10^6 of CHO cells were transfected with the vector encoding AGT-Ma or the G161R-Ma variant. 24 hours after transfection cells were harvested and lysed in 500 µl of PBS as previously described. Lysates were than loaded onto a Superdex S200 H10/30 column (GE Healtcare) equilibrated in PBS plus 1mM EDTA, 1 mM EGTA and 1 mM DTT. 20 % (v/v) trichloroacetic acid (TCA) was added to each eluted fraction and the samples were incubated overnight at 4°C. After centrifugation at 16000 *g* for 30 min, the precipitated protein was washed twice in PBS and resuspendend in 20 µl of denaturing gel loading buffer 1X. 10 µl of each sample were separated by SDS-PAGE and immunoblotted against anti-AGT.

3.16 Immunoflurescence studies

CHO cells were grown and transfected in a 24-well plate on glass coverslips. 24 hours after transfection CHO cells were fixed in 4% (w/v) paraformaldehyde, permeabilized with 0.3% Triton X-100 in phosphate buffer saline (PBS), and blocked in 3% bovine serum albumin (BSA). For the immunolabelling, rabbit polyclonal anti-human AGT and anti-peroxisomal protein form guine-pig were used as primary antibodies, and Alexa Fluor conjugated antibodies (AF488 and AF555, Life technologies) were used as secondary antibodies. Mitochondria were stained with

Mitotracker Red (CMXRos version, Molecular Probes, Invitrogen) and nuclei with DAPI. The coverslips were mounted over slides in AF1 medium (Dako). The images were captured using a confocal laser-scanning fluorescence microscope (Leica Microsystem, Manheim, Germany) at 63× magnification and processed using Adobe Photoshop and ImageJ software (Rasband, W.S., ImageJ, U. S. National Insti- tutes of Health, Bethesda, Maryland, USA, http://rsb.info.nih.gov/ij/, 1997–2008).

3.17 Immunoelectron microscopy

Immunoelectron microscopy (IEM) analysis of AGT distribution were perfotmed in collaboration with Dr. Polishchuck of the Telethon Institute of Genetics and Medicine (TIGEM), Naples. The cells were fixed for 2 h in a mixture of 4% paraformaldehyde and 0.4% glutaraldehyde in 0.2 M PHEM buffer (60 mM Pipes, 25 mM Hepes, 10 mM EGTA, 2 mM $MgCl_2$ pH 6) and washed with a PBS-glycine solution. After washing, cells were detached from the dishes, pelleted and embedded in 10% gelatin, cooled in ice and cut into 1-mm^3 blocks. The blocks were infused with 2.3 M sucrose at 4°C overnight and frozen in liquid nitrogen. Ultrathin cryosections were cut using a Leica EM FC7 cryoultratome and picked up using a 1:1 mix of 2% methylcellulose and 2.3 M sucrose. Sections were mounted on formvar carbon-coated copper grids, and the localization of AGT in the cryosections was analyzed using the rabbit polyclonal anti-human AGT followed by protein A conjugated with 10 nm gold particles. After labeling, the cryosections were embedded in methylcellulose–uranyl acetate mixture. Cryosections were further investigated using a FEI Tecnai-12 electron microscope (FEI, Einhoven, The Netherlands) equipped with an Veletta CCD camera for digital image acquisition.

3.18 Statistical analysis

Experiments have been performed in triplicate and in any case the standard error mean (SEM) was less than 10%. Statistic analysis was performed with Origin® 7.03 (Origin Lab) or GraphPad Prism Version 5.0 (GraphPad software, San Diego, CA, USA).

RESULTS AND DISCUSSION

Impact of nine mutations associated with PH1 on the biochemical properties of AGT

Up to now, the effects of most missense mutations on the AGXT gene leading to PH1 have been defined by measuring the AGT transaminase activity (expressed as specific activity) and/or the protein expression level in patient liver samples, crude cellular extract or cell-free expression systems [26, 32-35, 43, 57]. However, in the case of mutations that reduce both the specific activity and the expression level of AGT, this approach does not allow to assess if the mutation exerts a structural and/or a functional effect on the protein. In the last years, our research group has carried out a detailed biochemical and bioinformatics characterization of several pathogenic variants in the recombinant purified form[18, 29, 39, 40, 46]. These studies have allowed not only to define the molecular defect associated with each pathogenic mutation, but also to predict the responsiveness to the pyridoxine therapy of the patients bearing the examined mutations. Thus, the definition of the defect of as many as possible AGT variants at molecular level would be highly desirable. To this aim, we decided to elucidate the molecular basis underlying AGT loss of function in a subset of nine pathogenic variant spread over the structure of AGT. We chose four pathogenic variants in which the mutated residues are located in the large domain of AGT either within the active site and interacting with the coenzyme or in its proximity (W108R-Mi, S158L-Ma, D183N-Ma and S218L-Ma) (Fig.6A), and five pathogenic variants in which the mutated residues are far from the active site either in the large or in the small domain (G161S-Mi, G161C-Mi, S187F-Ma, P319L-Ma and G350D-Mi)(Fig.6B).

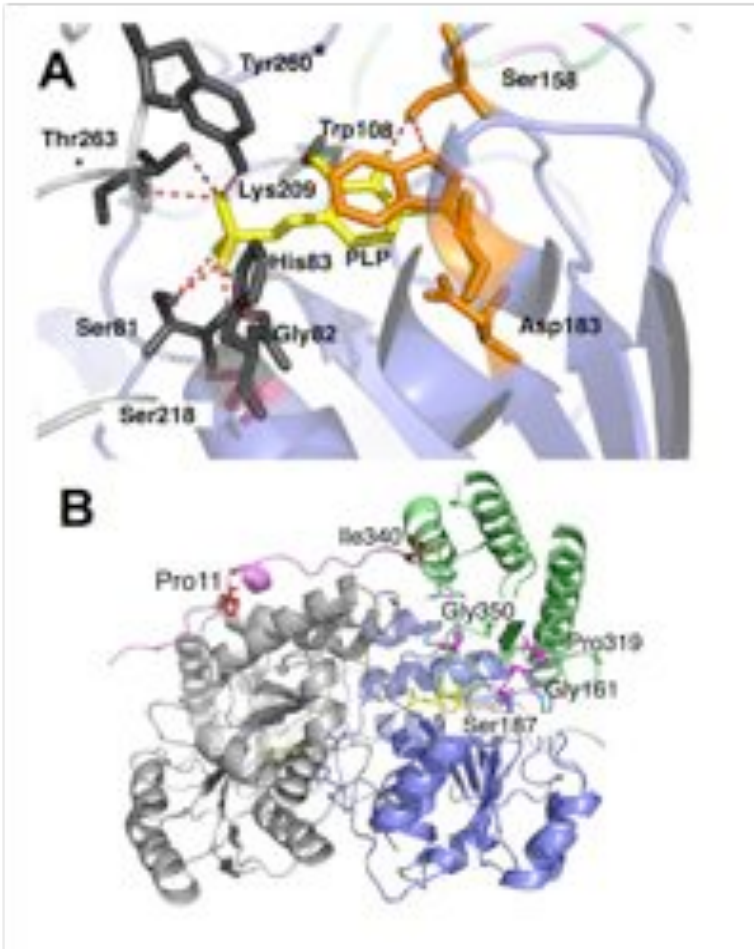

Figure 6: 3D representations of the AGT structure (PDB file 1H0C). **(A)** The AGT active site. PLP is represented as yellow sticks. Residues directly interacting with PLP are represented as dark grey sticks or, if their mutation is analyzed in this study, as orange sticks. Ser218 is represented as magenta sticks. The dotted lines indicate possible hydrogen bond interactions. **(B)** Overall structure of the AGT dimer. One monomer is coloured grey, while in the opposite monomer the N-terminus, the large domain and the small domain are coloured magenta, blue and green, respectively. PLP is represented as yellow sticks. Pro11 and Ile340 are represented as red sticks, while Gly161, Ser187, Pro319 and Gly350 are represented as magenta sticks. The figure was rendered using PyMol[17].

4.1 *In silico* analyses

In order to predict the possible local effect of each pathogenic mutation on the structure of AGT, we carried out a first inspection of the AGT-Ma crystal structure and performed *in silico* mutagenesis studies using the software PyMol[17]. The results of these analyses indicate that:

- the W108R, S158L and D183N mutations affect residues directly interacting with the coenzyme. Thus, they could have a functional effect on AGT by possibly altering the binding of the coenzyme and/or the catalytic activity of the enzyme.

- the S218L mutation involves an active site residue that does not directly interact with the coenzyme, but might be involved in the proper positioning of helix 4 that also comprises Gly82, a residue hydrogen-bonded to the PLP phosphate. Thus, the Ser218-to-Leu mutation is predicted to have a local structural effect on the large domain, possibly resulting in the distortion of the coenzyme binding cleft.

- the G161S, G161C and S187F mutations involve residues located in the large domain far from the active site. Gly161 is located between the large and the small domain and its substitution is supposed to alter intradomain contacts. Ser187 is located in a random coil region on the re side of the coenzyme and its mutation is supposed to indirectly affect the large domain/small domain contacts by possibly changing the positioning of the loop 154-169.

- the P319L and G350D mutations involve residues located in two random coil regions of the small domain. Both mutations are supposed to cause a structural effect limited to the small domain. In the case of the P319L mutation, the effect is due to the mispositioning of helix 11 on the surface of the protein, while in the case of the G350D mutation, it is due to the induction of steric

clashes in the small domain. In particular, the G350D mutation changes the conformation of the loop 343–357 at the entrance of the AGT active site, thus possibly affecting substrate binding.

4.2 Expression and purification of the AGT variants

Bacterial expression vectors encoding for the selected pathogenic variants were constructed by site-directed mutagenesis starting from the minor or the major allele of AGT according to the actual genotype of PH1 patients in whom each mutation was identified. The nine variants were expressed E. coli and purified to homogeneity, as indicated by a single band on SDS-PAGE at an apparent molecular weight of about 45 kDa (data not shown), by a previously developed protocol[18]. As compared with AGT-Ma and AGT-Mi, all the variants were present in good amounts in the soluble extract with the exception of Gly161 variants whose yield is about 10% that of AGT-Ma or AGT-Mi.

4.3 Impact of the mutations on the AGT secondary and quaternary structure

To study the impact of the examined pathogenic mutations on the secondary structure of AGT we registered the far-UV CD spectrum of the variants in their apo-form. Since no significant differences were observed between the spectra of the variants and that of apoAGT-Ma or apoAGT-Mi, it can be concluded that the mutations do not change the secondary structure composition of AGT. Moreover, in order to investigate the effect of each mutation on the dimeric structure of the enzyme, the molecular dimensions of the variants in both their holo- and the apo-form have been determined by DLS. For each protein, a peak with a size ranging from 9.2 to 10.8 nm, corresponding to that of a dimer, could be seen. Considering

that the intensity of the DLS signal is a function of the sixth power of a particle diameter, the dimer must be the most abundant species in solution, thus indicating that the mutations do no exert any major effect on the quaternary structure of AGT. However, the presence of low amounts of small aggregates (100-400 nm) could be noticed for W108R-Mi, S218L-Ma, S187F-Ma, G161S-Mi, G161C-Mi and G350D-Mi in both holo- and apo-forms as well as for G350D-Mi in the apo-form (data not shown).
Altogether, these data indicate that the nine examined mutation do not alter the gross conformation of AGT and do not prevent the formation of a dimeric structure.

4.4 Impact of the mutations on PLP binding

To study the impact of the analysed PH1-causing mutations on the coenzyme binding affinity of AGT, the $K_{D(PLP)}$ of each variant has been determined and compared with those previously determined for AGT-Ma and AGT-Mi[18, 39] .
From the results reported in Table 4 it can be observed that while G161C-Mi, G161S-Mi, P319L-Ma and G350D-Mi display an unaltered or even increased affinity for PLP, W108R-Mi, S158L-Ma, D183N-Ma and S218L-Ma, even if to a different extent, show a significantly reduced affinity for the coenzyme. This could be explained by considering that the residues Trp108, Ser158, Asp183 and Ser218 directly interact with the cofactor. In the case of the S187F-Ma variant, we could only estimate an upper limit value for the $K_{D(PLP)}$ of 0.01 μM, because the lowest protein concentration required for fluorescence experiments far exceeds the $K_{D(PLP)}$ value. However, it is possible to conclude that the S187F mutation causes an at least 27-fold increment of the affinity for PLP.

Table 4: Equilibrium dissociation constants for PLP ($K_{D(PLP)}$) and optical activity values of AGT-Ma, AGT-Mi and the pathogenic variants.

Enzymatic species	$K_{D(PLP)}$ (μM)	Optical activity
AGT-Ma	0.27 ± 0.03[a]	97 mdeg/Abs 420nm[a]
AGT-Mi	0.26 ± 0.02[b]	97 mdeg/Abs 420nm[b]
W108R-Mi	96 ± 19	4.73 mdeg/Abs 434nm
S158L-Ma	272 ± 47	45 mdeg/Abs 430nm
G161S-Mi	0.46 ± 0.07	66 medeg/Abs 430nm
G161C-Mi	0.56 ± 0.09	57 mdeg/Abs 414nm
D183N-Ma	2.1 ± 0.1	84 mdeg/Abs 430nm
S187F-Ma	< 0.01	103 mdeg/Abs 414nm
S218L-Ma	24.2 ± 0.1	31 mdeg/Abs 428nm
P319L-Ma	0.19 ±0.04	88 mdeg/Abs 420nm
G350D-Mi	0.031 ± 0.005	88 mdeg/Abs 420nm

[a]from ref [18]
[b]from ref[39]

In all the PLP-dependent enzymes, the binding of the coenzyme to the apoenzyme gives rise to both absorbance and CD signals in the visible region of the spectra. In particular, as previously described, the binding of PLP to AGT gives rise to a 420 nm absorbance band, associated with a positive CD signal, and a 340 nm band, associated with a negative dichroic signal, attributed to the ketoenamine and enolimine tautomers of the internal aldimine, respectively. The optical activity, which is the ratio between the millidegrees and the absorbance values at 420 nm and gives

information about the coenzyme microenviroment, is 97 mdeg/Abs 420 nm[18] for both AGT-Ma and AGT-Mi. Figure 7 shows the UV-visible CD spectra of the variants at 10 μM protein concentration in the presence of saturating coenzyme. The optical activity values (expressed as millidegrees/absorbance at 410-430 nm) are reported in Table 4.

It can be observed that only the W108R, G161S, G161C, S158L and S218L mutations change the microenvironment of the internal aldimine. In the case of the W108R, S158L and S218L mutations, this result is in line with the increased $K_{D(PLP)}$ value and it can be understood considering that the mutated residues are located at or near the AGT active site. More difficult is to explain the change of the active site microenvironment caused by the Gly161 mutations. One could argue that the mutation of Gly161 could cause some structural perturbations that indirectly affect the active site. Moreover, it is worth noting that the absorbance and dichroic band of the ketoenamine tautomer of the internal aldimine of the S187F-Ma variant is 6 nm blue shifted as compared to that of AGT-Ma. This finding, together with the increment of at least 27-fold in the coenzyme binding affinity, suggests that, although the mutation does not alter the optical activity value, it may induce some local structural changes at the AGT active site (chapter 5.1).

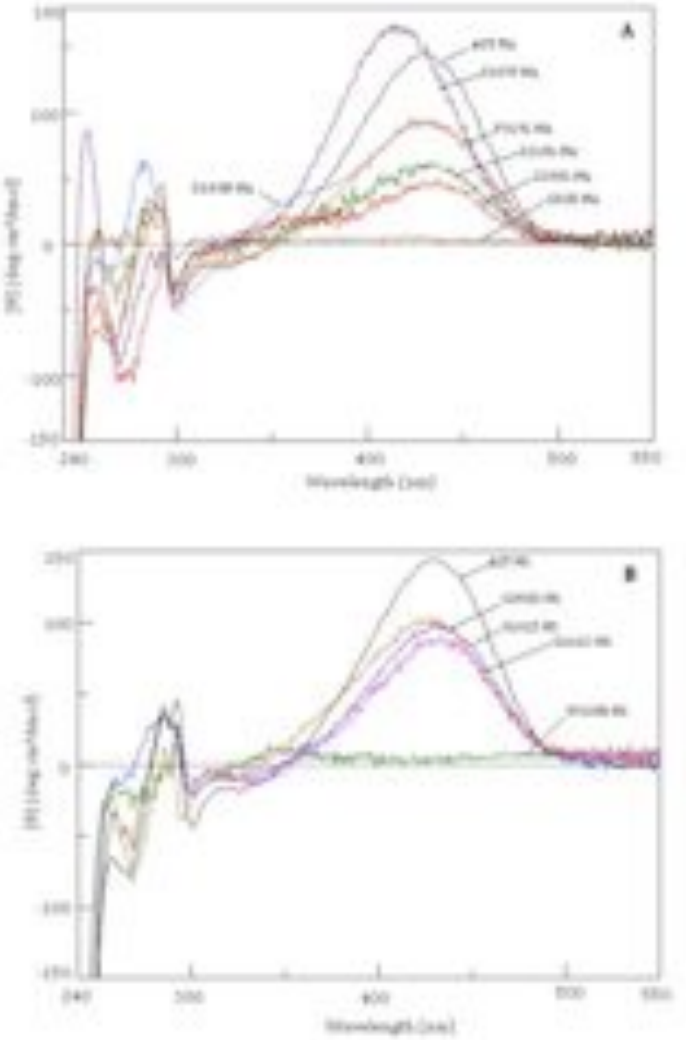

Figure 7: CD spectra of AGT-Ma, AGT-Mi and pathogenic variants. (A) CD spectra of AGT-Ma (black), S158L-Ma (red), D183N-Ma (blue), S187F-Ma (violet), S218L-Ma (green) and P319L-Ma (orange).(B) CD spectra of AGT-Mi (black), W108R-Mi (green), G161C-Mi (fucsia), G161S-Mi (blue) and G350D-Mi (orange). All CD spectra are registered in the presence of saturating PLP concentrations in 100 mM potassium phosphate buffer, pH 7.4, at an enzyme concentration of 9 μM.

4.5 Impact of the mutations on the enzymatic activity for the overall transamination of the alanine-glyoxylate pair

In order to define if and how each mutation affects the AGT catalytic activity, the steady-state kinetics parameter for the overall transamination of the alanine/glyoxylate pair were measured for each variant (Table 5).
Comparing the catalytic efficiency of the variants with those of AGT-Ma or AGT-Mi is possible to observe that, [33, 43, 58]: (i) the W108R-Mi, S158L-Ma, D183N-Ma, S187F-Ma, S218L-Ma and G350D-Mi variants display a reduced catalytic activity, (ii) the G161C-Mi, G161S-Mi and P319L-Ma variants display an enzymatic activity comparable to that of AGT-Ma or AGT-Mi. While in most cases the reduced specific activity is due to a decreased k_{cat} value, in the G350D-Mi variant it is due to an increased K_m value for L-alanine. It is reasonable to suggest that, the reduced catalytic efficiency of the D183N-Ma variant is due to the role of Asp183 in AGT in stabilizing the positive charge at N(1) of PLP, in analogy with what observed for Asp222 in E. coli aspartate aminotransferase[59]. The finding that the mutation of Trp108, Ser158, or Ser218 causes a reduction of the AGT catalytic activity can be understood by considering that these residues are part of the active site of the enzyme or are located nearby, and that the spectroscopic studies reported below (chapter 4.4) have indicated the presence of alterations of the active site microenvironment for the W108R-Mi, S158L-Ma and S218L-Ma variants.

Table 5: Steady-state kinetic parameters of AGT-Ma, AGT-Mi and pathogenic variants for the alanine-glyoxylate pair.

Enzymatic species	Substrate	Co-substrate	k_{cat} (s^{-1})	$K_{m\ L\text{-}alanine}$ (mM)	$K_{m\ Glyoxylate}$ (mM)	k_{cat}/K_m (s^{-1}/mM^{-1})
AGT-Ma[a]	A	G	45 ± 2[a]	31 ± 4[a]		1.4 ± 0.2[a]
	G	A	45 ± 2[a]		0.23 ± 0.05[a]	196 ± 4[a]
AGT-Mi[a]	A	G	33 ± 5[b]	28 ± 2[b]		1.2 ± 0.2[b]
	G	A	37 ± 1		0.22 ± 0.01[b]	168 ± 8[b]
W108R-Mi	A	G	0.0013±0.0003	36 ± 3		0.00004±0.00001
	G	A	n.d.		n.d.	n.d..
S158L-Ma	A	G	0.41 ± 0.03	25 ± 6		0.016 ± 0.001
	G	A	0.41 ± 0.04		0.35 ± 0.09	1.2± 0.3
G161S-Mi	A	G	55 ± 2	70 ± 9		0.8 ±0.1
	G	A	58 ± 2		0.63 ± 0.07	92 ± 2
G161C-Mi	A	G	36.1 ± 0.7	103 ± 6		0.35 ± 0.02
	G	A	36.6 ± 0.7		0.21 ± 0.02	174 ± 1
D183N-Ma	A	G	0.008 ± 0.003	140 ± 17		0.00006 ± 0.00001
	G	A	n.d.		n.d.	n.d.
S187F-Ma	A	G	0.13 ± 0.01	12 ± 2		0.0108 ±0.0002
	G	A	0.12 ± 0.01		0.13 ± 0.04	0.92 ± 0.09
S218L-Ma	A	G	2.7 ± 0.1	29 ± 6		0.09 ± 0.02
	G	A	2.95 ± 0.08		0.19± 0.02	15 ± 2
P319L-Ma	A	G	27.5 ± 0.8	44 ± 5		0.63 ± 0.01
	G	A	26.2 ± 0.7		0.11 ± 0.02	238 ± 44
G350D-Mi	A	G	15.0 ± 0.7	328 ± 51		0.046 ± 0.007
	G	A	15 ± 1		0.29 ± 0.04	52 ± 7

A, L-alanine; G, glyoxylate; n.d., not determined because the rate of glyoxylate half-transamination is comparable to that of PMP dissociation/PLP association at sub-saturating glyoxylate concentrations; [a] from ref [18], [b] from ref [39].

More difficult is to explain the effect on the AGT catalytic activity of the mutation of Ser187 or Gly350, two residues located far from the active site. The fact that the S187F-Ma variant displays a higher affinity for PLP and a different coenzyme binding, as compared with AGT-Ma, make it possible to hypothesize that this mutation causes some structural rearrangements that affect the active site topology. In the case of the G350D-Mi variant, the *in silico* mutagenesis studies have shown that the G350D mutation changes the conformation of the loop 343-357 at the entrance of AGT active site, thus possibly affecting substrate binding.

4.6 Impact of the mutations on the thermal stability of the variants in the holo-form.

Protein thermal unfolding, is widely used to study the stability of a protein. To investigate whether the analysed PH1-associated mutations could affect the stability of AGT, the thermal denaturation process of each variant in the holo-form has been studied by monitoring both the decrease of the dichroic signal at 222 nm and 430 nm, which are indicative of the loss of the protein secondary structure and of the PLP-bound content, respectively, and the signal on different scanning fluorimetry (DSF), a technique that allows to measure the exposure of hydrophobic groups during unfolding. In Table 6 have been reported the T_{mholo} values, derived from the loss of the 222 nm CD signal and DSF measurements, and the T_{mPLP}, derived from the loss of the 430 nm CD signal, for AGT-Ma, AGT-Mi and the pathogenic variants in the holo-form.
By analyzing the AGT-Ma and AGT-Mi thermal unfolding process (Fig. 8), it can be observed that both species are denatured and release PLP in a single-step process with melting temperatures of 78°C and 74°C,

respectively. Moreover, the rate of PLP release is higher than that of global unfolding, as shown by the kinetics of the 222 nm and 430 nm signal changes at the melting temperature. In fact, while the rate constants of the loss of the 430 nm dichroic signal are 0.0042 ± 0.0001 s^{-1} and 0.0057 ± 0.003 s^{-1}, those of the loss of the 222 nm dichroic band are 0.0024 ± 0.0001 s^{-1} and 0.0021 ± 0.001 s^{-1}, for AGT-Ma and AGT-Mi, respectively. Additionally, the irreversible binding of the coenzyme, by $NaBH_4$-reduction of the Schiff base linkage, increases the thermal stability of both enzymatic species, as shown by the increase in the T_{mholo} of 7°C and 5°C for AGT-Ma and AGT-Mi, respectively.

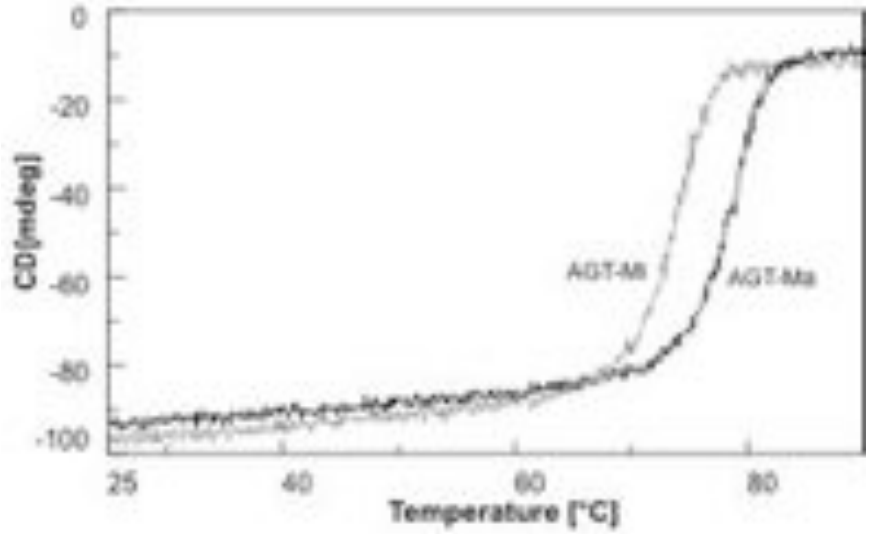

Figure 8: Far-UV CD-monitored heating scans of holoAGT-Ma and holoAGT-Mi. Far-UV CD changes of holoAGT-Ma (black curve, straight line) and holoAGT-Mi (grey curve, straight line) in the presence of 10 μM exogenous PLP. The enzyme concentration was 10 μM, and the buffer was 100 mM potassium phosphate, pH 7.4.

Altogether, these data indicate that: (i) the two amino acid substitutions typical of the minor allele (P11L and I340M) reduce the AGT thermal stability, in agreement with the results previously obtained by differential scanning calorimetry[40] and thermal inactivation[29] experiments, (ii) AGT-Mi displays a lower local stability of the PLP binding site with respect to AGT-Ma, in line with the higher sensitivity to urea stress of the PLP-bound state of AGT-Mi previously reported[29], and (iii) a conversion from the holo- to the apo-form occurs during the AGT thermal unfolding, thus suggesting that the T_{mholo} values are affected by the sensitivity of the AGT active site to thermal stress.

Table 6: T_{mholo} and T_{mPLP} values of AGT-Ma, AGT-Mi and pathogenic variants

Enzymatic species	T_{mholo}[a](°C) CD $_{222\ nm}$	T_{mPLP}[a](°C) CD $_{420nm}$	T_{mholo}[a](°C) DSF
AGT-Ma	77.5	78	78.6
AGT-Mi	73.6	73.6	74.1
W108R-Mi	54.1	53.4	53.9
S158L-Ma	67	64	64.7
G161S-Mi	62.5	62.8	61.8
G161C-Mi	64	64.2	63.8
D183N-Ma	80.8	79.6	80.1
S187F-Ma	76.7	74.4	73.6
S218L-Ma	57.8	57.9	56
P319L-Ma	77.9	76.3	77.5
G350D-Mi	73.5	73.7	72.6

[a] they represent apparent T_m values and are the mean of two independent experiments. The error is within $\pm$ 0.3 °C.

On these bases, it is possible to conclude that only the W108R-Mi, S158L-Ma, G161C-Mi, G161S-Mi and S218L-Ma variants show a reduced sensibility of the active site to the thermal stress. In this regard, it is worth

noting that the variants W108R-Mi and S218L-Ma show the most pronounced alteration with T_{mholo} of 54° and 57°C, respectively. However, it has been shown that the W108R-Mi variant displays a considerably high (~10-fold) ground state fluorescence signal at 25°C in comparison with AGT-Mi, thus suggesting that the variant is characterized by an increased hydrophobicity even in the absence of a thermal stress. More difficult is to explain the great destabilization induced by the S218L mutation on holoAGT-Ma. Although it can be speculated that the mutation could induce a conformational change that makes the protein more susceptible to unfolding at high temperature, further studies on the folding/unfolding pathway of the S218L-Ma variant would be required.

4.7 Impact of the mutations on the thermal stability of the variants in the apo-form

To define the impact of the examined pathogenic mutations on the intrinsic stability of AGT we investigated the thermal stability of the apo-forms of AGT-Ma, AGT-Mi and the variants through far-UV CD and DSF experiments.

Fig. 9 shows the thermal unfolding profiles of apoAGT-Ma and apoAGT-Mi. Both species display a two-phases unfolding profile, in which the first phase is characterized by a melting temperature (T_{m1apo}) of 61°C and 53°C for AGT-Ma and AGT-Mi, respectively, and the second phase is characterized by a melting temperature (T_{m2apo}) of 66°C for both AGT-Ma and AGT-Mi.

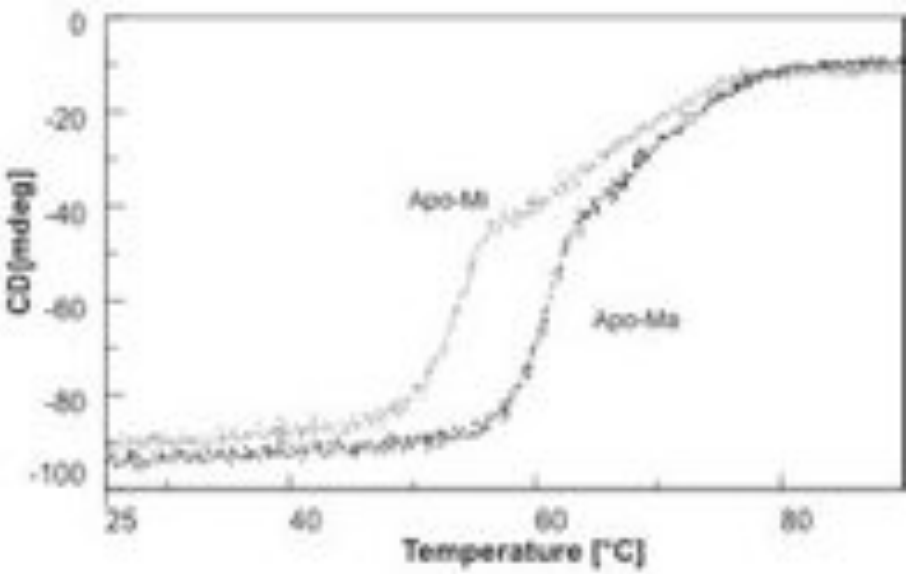

Figure 9: Far-UV CD-monitored heating scans of apoAGT-Ma and apoAGT-Mi. Far-UV CD changes of apoAGT-Ma (black curve, straight line) and apoAGT-Mi (grey curve, straight line). The enzyme concentration was 10 μM, and the buffer was 100 mM potassium phosphate, pH 7.4.

On the basis of these data, several considerations can be drawn. First, the fact that both T_{m1apo} and T_{m2apo} are lower than the corresponding T_{mholo} indicate that, in agreement with previous data[29, 30], AGT-Ma and AGT-Mi in the apo-form are significantly less stable than the corresponding holo-forms. It can be suggested that the coenzyme PLP, located at the interface between the two subunits of AGT, could increase the thermal stability of the protein by stabilizing its dimeric structure. Second, the presence of two transitions in the apoenzymes, as opposed to the single transition of the holoenzymes, suggests that the large and the small domain unfold in a concerted and cooperative way in the holo-forms, while they appear to be differentially stabilized in the apo-forms. Considering that PLP makes

several contacts only with the large domain, it can be speculated that in the apoenzymes the large domain could be less stable than the small one. Following this view, it is possible to describe the three state model of thermal denaturation of apoAGT as a process in which the low-temperature transition represents the unfolding of the large domain while the high-temperature transition represents the unfolding of the small domain. Third, the apo-form of the minor allele is less stable than the apo-form of the major allele probably as a consequence of a lower stability of the large domain, as shown by the ~8°C reduction of the T_{m1apo}. Previous reports have suggested that the reduced stability of AGT-Mi might depend on a distortion of the N-terminal arm of the protein caused by the P11L substitution[16]. Since the N-terminal arm wraps over the surface of the opposite subunit that interacts with the large domain, the distortion of the N-terminus caused by the P11L polymorphic mutation could specifically destabilize the large domain of AGT, thus explaining why the effect of the polymorphic mutations is limited to the T_{m1apo}.

Table 7 shows the melting temperatures of each of the examined pathogenic variants in the apo-form. ApoS158L-Ma and apoD183N-Ma variants unfold in a single step process with a T_{mapo} value similar to or higher than that of the high-temperature transition of AGT-Ma, thus indicating that the large domain mutations S158L and D183N do not decrease the AGT stability. ApoG161S-Mi, apoG161C-Mi and apoS187F-Ma are characterized by a single thermal transition with a mid-point temperature lower than the T_{m1apo} of apoAGT-Ma and apoAGT-Mi, thus allowing to conclude that these large domain mutations cause a destabilizing effect not limited to the large domain but extended to the small domain.

Table 7: T_{mapo} values of AGT-Ma, AGT-Mi and pathogenic variant

Enzymatic species	T_{m1apo}[a] (°C) CD $_{222\ nm}$	T_{m2apo}[a] (°C) CD $_{222\ nm}$	T_{m1apo}[a] (°C) DSF	T_{m2apo}[a] (°C) DSF
AGT-Ma	61.1	66.4	61.9	67.3
AGT-Mi	53.1	66	54.2	66.5
W108R-Mi	48.9	54		53.3
S158L-Ma	65.9		64.3	
G161S-Mi	46.8		46.5	
G161C-Mi	51.1		51.3	
D183N-Ma	70.2		70.3	
S187F-Ma	48.2		45.3	
S218L-Ma	50.9	57.8	47.2	55.7
P319L-Ma	61.6		60.1	
G350D-Mi	53.6		52.5	

[a] they represent T_m values and are the mean of two independent experiments. The error is within $\pm$ 0.3 °C.

These findings are consistent with in silico analyses indicating that Gly161 is located at the interface between the large and the small domain, and that the bulky hindrance of the side chain of phenylalanine at position 187 could cause a mispositioning of the loop 154-168 involved in interdomain interactions. ApoW108R-Mi and apoS218L-Ma unfold in a two steps process in which both transitions are left shifted and T_{mapo} values are lower than those of AGT-Ma and AGT-Mi. These data suggest that the mutations not only exert destabilizing effects of the large domain, in which they are located, but also influence the structural stability of small domain. The finding that apoW108R-Mi shows a single T_m similar to the T_{m2apo} of AGT-Mi on DSF analyses could be explained considering that this apovariant has a ground state fluorescence 100-fold higher than that of apoAGT-Mi, due to an increased hydrophobicity of the protein possibly caused by a partial

unfolding, which could cover the signal of the first transition in DSF experiments. Finally, the P319L and the G350D mutations in the small domain cause a complete loss of the T_{m2apo} without affecting the T_{m1apo}, thus indicating that these mutations affect only the stability of the domain in which they are located.

4.8 Identification of the major defect of the AGT pathogenic variants

On the basis of previous analyses performed on crude lysates[26, 32-35, 37, 43, 57, 60], all the examined pathogenic mutations causing PH1 were classified in the group comprising mutations leading to a reduction of both enzymatic activity and expression level. The biochemical characterization of the AGT pathogenic variants in their recombinant purified holo- and apo-form, by clarifying the various effects caused by each mutation on the protein, and allow us to define the major defect of each pathogenic variant (Table 8). In particular:

1. The D183N-Ma variant is characterized only by a functional defect that consists in a reduced catalytic activity and PLP binding affinity.

2. The G161S-Mi, G161C-Mi and P319L-Ma variants are characterized only by a structural defect. While the mutations associated to Gly161 cause the destabilization of both the holo- and the apo-form of the protein, the P319L mutation appears to cause the structural defect only on the apoenzyme.

3. The W108R-Mi, S158L-Ma, S187F-Ma, S218L-Ma and G350D-Mi variants are characterized by both a structural and a functional defect.

Table 8: Major defect(s) of AGT pathogenic variants analysed on recombinant purified proteins

AGT variants	PLP binding affinity	PLP binding mode	Specific activity	T_{mholo} and T_{mPLP}	T_{mapo}	Defect
W108R-Mi	- - -	A	- - -	- - -	- - -	functional and structural
S158L-Ma	- - -	A	- - -	- - -	+	functional and structural
G161S-Mi	-	A	-	- - -	- - -	structural
G161C-Mi	-	A	-	- - -	- - -	structural
D183N-Ma	- - -	S A	- - -	+	-	functional
S187F-Ma	+ + +	U	- - -	U	+ + +	functional and structural
S218L-Ma	- - -	A	- - -	- - -	- - -	functional and structural
P319L-Ma	+	S A	-	U	-	structural
G350D-Mi	+ + +	S A	- - -	U	- - -	functional and structural

--- decreased, - slightly decrease, +++ increased, + slightly increased, U unaltered, A altered and S slightly altered.

On the basis of these results, possible therapeutic approaches for patients bearing the examined mutations can be suggested. In particular, B6 supplementation is expected to be beneficial for patients carrying the G161C and G161S mutations on the minor allele as well as the P319L on the major allele. Since the major impact of these mutations is on the thermostability of the apo-form of AGT, the coenzyme is expected to shift the equilibrium toward the holo-form. In the case of patients bearing the G350D mutation on the minor allele, a combination of L-alanine and pyridoxine could be suggested to overcome the reduced affinity for the substrate and the reduced thermal stability of the apo form.
Again, the administration of molecules acting as chemical chaperones could be effective for patients harbouring the S218L mutation on the major allele, considering that the S218L-Ma variant has a reduced thermal stability in both the holo and the apo form and retains a significant specific activity. On the other hand, no suggestions can be advanced for a pharmacological treatment of patients carrying the W108R mutation on the minor allele or the S158L, D183N and S187F mutations on the major allele.

The biochemical characterization of the AGT variants in their purified form has indicated that the S187F-Ma and the Gly161 variants display a peculiar behaviour. In fact, although Ser187 is far from the active site, it's mutation to Phe affects the AGT functional properties. On the other and, the mutation of Gly161 does not affect the enzyme catalytic activity and the PLP binding but strongly reduces the protein thermal stability. Thus to shed light on the molecular defect of S187F-Ma, G161R-Ma, G161S-Mi and G161C-Mi, a more detailed characterization of the effects of the Ser187 and Gly161 mutation has been undertaken.

Impact of the S187F mutation on the structural properties of AGT

The C→T mutation at position 682 in the major allele of the *AGXT* gene, leading to the S187F amino acid substitution, has been initially found in a PH1 patient showing less than 1% AGT catalytic activity with respect to normal subjects as well as the nearly complete loss of AGT immunoreactive protein in liver biopsy. The genetic analysis revealed that the patient was heterozygous for the mutation, with the allele bearing the C682→T mutation producing an mRNA of normal size and abundance, while the other allele did not produce detectable amounts of mRNA[34].
Ser187 is a large-domain residue conserved in the mammalian AGTs and belongs to a random-coil region far from the active site [16]. Cell-free expression studies have revealed that the S187F variant has reduced dimer stability and increased sensitivity to proteasomal degradation and that PLP is able to increase the stability of the protein [31, 43]. As reported above, the S187F variant in the recombinant purified form displays a reduced thermal stability in the apo-form with respect to normal AGT and the presence of bound PLP is able to relieve the protein instability [61]. Nevertheless, we found that, although Ser187 is located far from the active site, its Ser-to-Phe substitution also affects the AGT functional properties.

In fact, the purified recombinant S187F-Ma variant has a remarkable reduced catalytic efficiency, an affinity for PLP increased of at least 27-fold, and a different coenzyme binding mode with respect to normal AGT [61]. This implies that the variant might be characterized by structural changes remote from the mutation site with effects on the topography of the active site.

5.1 The S187F crystal structure reveals that the mutation affects the enzyme active site topology

In collaboration with the group of Prof. Matthias Willmans at the EMBL (Hamburg), we have determined the crystal structure of the S187F-Ma variant at 2.9 Å resolution (PDB entry: 4I8A). The asymmetric unit contains two AGT dimers, of which the complete polypeptide chain is visible in the final electron density, except for the N-terminal residues 1-5 (molecules A and C) or 1-4 (molecules B and D), and the C-terminal residues 391-392 of molecules B, C and D. Interestingly, the complete C-terminus, known as a peroxisomal targeting signal type 1 (PTS1), is visible in chain A, possibly due to the proximity of the N-terminal domain of molecule C that stabilizes the C-terminal loop (data not shown).
The S187F structure superimposes well onto the normal AGT counterpart, with a root-mean-square deviation (RMSD) of 0.48 Å. Although the overall conformation of the two proteins is virtually identical, significant structural changes can be observed near the mutated amino acid (Fig. 10) as well as at the active site of the protein (Fig. 11).

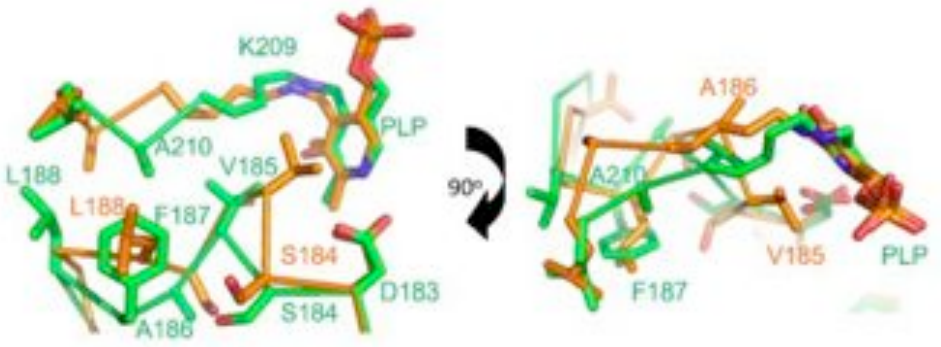

Figure 10. Superposition of the structure of the S187F variant (green) with that of normal AGT (orange) in the area of the cofactor binding site. Residues are labelled with the respective colors. The hydrophobic cleft that is formed by residues 185-188 triggers a conformational change in the loop where the PLP-binding lysine is located.

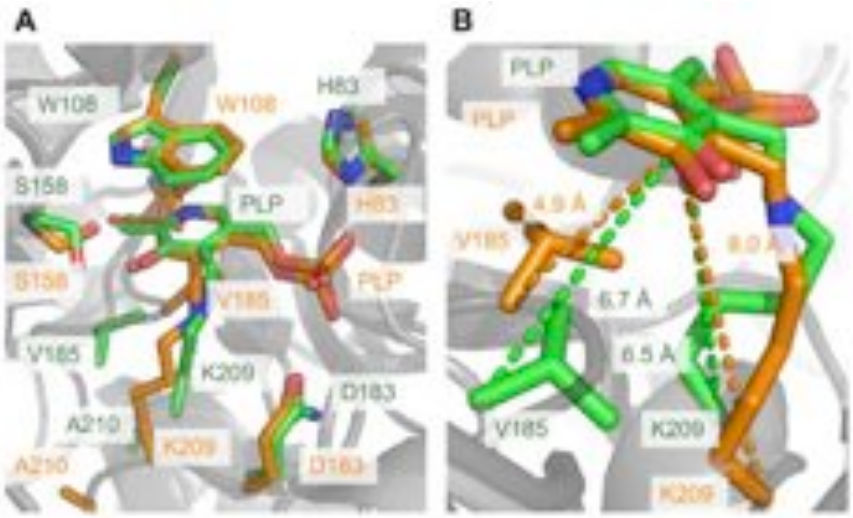

Figure 11. **(A)** Stick representation of the active site in the S187F variant (green) and normal AGT (orange). Due to the mutation, the main chain atoms of Lys209 in the mutant enzyme move closer to the PLP, which results in a shortened side chain conformation of Lys209. Other active site residues are only slightly affected by the mutation induced structural changes. **(B)** Changes in the PLP-Lys209 and PLP-Val185 distances are represented by dashed lines in the respective colors.

As a result of the mutation, the loop that contains Phe187 substantially changes its conformation, and moves Phe187 into the position of Leu188 of normal AGT. Due to this displacement, Val185 of the mutant protein also changes position, and its side chain moves away from the PLP. The small hydrophobic pocket that is formed by Phe187 and Leu188 can accommodate Ala210, which eventually causes a shift of Ala210 and Lys209 towards Phe187 (Fig. 10). While these conformational changes slightly alter the position of the PLP cofactor and of some active site residues (Trp108, Ser158, His83, and Asp183), they result in a significant displacement of Lys209 and the loop 183-188 (Fig. 10). In fact, the distance between the C_α of Lys209 and the $C_{3'}$ of the PLP methylpyridine ring decreases from 8.0 Å in the normal AGT enzyme to 6.5 Å in the mutant enzyme (Fig. 11), and the distance between the C_α of Val185 and the $C_{3'}$ of the PLP methylpyridine ring increases from 4.9 Å in the normal AGT enzyme to 6.7 Å in the mutant. Moreover, as calculated by Pocket Finder [62], in S187F the PLP cavity has a volume of 1073 $Å^3$, while in normal AGT it has a volume of 949 $Å^3$. These structural data allow us to explain why the mutation of a residue whose C_α is located at 10.5 Å from the $C_{4'}$ of the coenzyme, strongly affects the AGT functional properties. In particular, the observed shortened conformation of the lysine side chain could account for the reduced catalytic activity of the S187F variant, since Lys209 is a key residue taking part in the AGT catalytic mechanism, while the slightly altered position of several active site residues could account for the different PLP binding mode of S187F. Moreover, although it is difficult to understand the increased PLP binding affinity of the variant with respect to normal AGT [61], it can be speculated that it is ascribable to the increased volume of the PLP-binding pocket that could allow a better coenzyme accommodation.

5.2 The S187F mutation affects the PMP binding mode and affinity and the external aldimine microenvironment: spectroscopic and computational analyses

We investigated if the active site conformational changes of the S187F-Ma variant revealed by its crystal structure could affect the binding of other reaction intermediates besides the PLP coenzyme [61]. We found that even a prolonged incubation time of apoS187F with PMP (up to 350 μM) does not result in the appearance of the positive dichroic signal at 340 nm, typical of the AGT-PMP complex formation [18]. However, a 1 h incubation of the apo form of the mutant (10 μM) with 350 μM PMP in 100 mM potassium phosphate buffer, pH 7.4 (final volume of 500 μl) followed by concentration to about 10 μl by a Microcon device and four washing with 500 μl of the above buffer, results in a retentate that contains about 8 μM PMP. Thus, since only 40% of the variant is in the PMP bound form, the $K_{(D(PMP))}$ should be of ~ 10 μM, at least 100-fold higher than that of normal AGT (data not shown) [18]. We have also monitored the spectral changes occurring in the S187F variant upon addition of D-alanine, an unproductive substrate analogue that mimics the formation of the external aldimine intermediate. The CD spectrum of S187F in the presence of a saturating concentration of D-alanine displays a positive band at 415 nm, 10-nm blue-shifted with respect to that of normal AGT. Altogether, these data indicate that the variant is characterized by an altered PMP binding mode and affinity as well as by a different microenvironment of the external aldimine.
To have insights about the possible impact of the S187F mutation on the active site topography of these reaction intermediates, we compared docking models indicative of the putative binding mode of PMP and of the external aldimine with L-alanine (Figure 12A and B), obtained in collaboration with Prof. Alessandro Paiardini from University of Rome “La Sapienza”, with those of normal AGT [18].

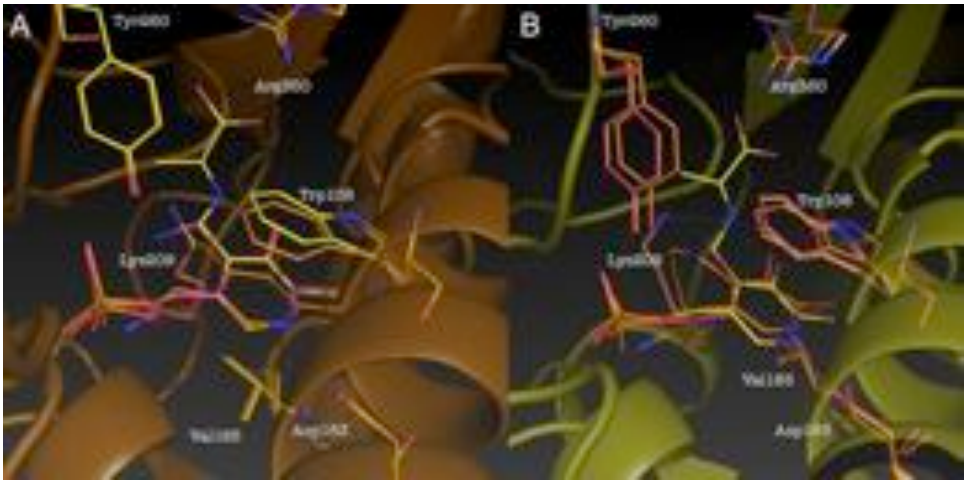

Figure 12. Modelling of the active site of the PMP- (pink) and of the L-alanine external aldimine (yellow) bound forms of normal **(A)** and S187F **(B)** AGT. The internal aldimine (orange) is also shown for reference. Oxygen, nitrogen and phosphorous atoms are coloured red, blue, and orange, respectively.

The putative position of the manually docked molecules and their neighbouring residues was relaxed by energy minimization means. Besides small changes related to the position of Tyr260*, the most striking feature that distinguishes the S187F variant from normal AGT is the relative positioning of the coenzyme moiety and of Trp108. In fact, in S187F both the AGT–PMP complex and the external aldimine are tilted by approx. 25° with respect to PLP towards Trp108 and Asp183 and the Trp108 side-chain (on the re side of PLP) undergoes a remarkable conformational change, flipping by approx. 45° around the Cα–Cβ bond. This predicted movement, probably due to the need to accommodate the amino group of PMP or the substrate's moiety and to avoid steric clashes with Lys209, is energetically impaired in normal AGT by the location of Val185 on the si side of the coenzyme[18]. Although these represent simulated conformations, the predicted changes would result in loss of stabilization of PMP and the

external aldimine on both re and si side of the pyridine ring. This is consistent with our experimental data and could account for the changes in both PMP binding mode and affinity and in the microenvironment of the external aldimine with D-alanine with respect to normal AGT.

5.3 The S187F mutation decreases the catalytic efficiency of the L-alanine half-transamination

We have previously reported (section 4.5) that the S187F variant in the absence of exogenous coenzyme has k_{cat} for the alanine/glyoxylate pair, $K_{mL\text{-}alanine}$ and $K_{mGlyoxylate}$ values equal to 0.147 ± 0.009 s^{-1}, 52 ± 2 mM and 0.038 ± 0.008 mM, respectively. In order to investigate if the decrease in the catalytic efficiency was due to an impact of the mutation on the first and/or the second half-transamination reaction, we compared the kinetics of the L-alanine half-transamination of the variant (15 μM) with that of normal AGT. Similar to what already observed in normal AGT [18], we couldn't detect the external aldimine with L-alanine and the quinonoid intermediates of the S187F variant. Nevertheless, while both the decrease of the 429 nm absorbance band and the concomitant PLP → PMP conversion are single exponential processes in normal AGT [18], they display a biphasic behaviour in the variant (Fig. 13). Both the apparent first-order rate constants, k_{obs}, of the fast and the slow phases show a hyperbolic dependence on L-alanine concentration, with k_{max} and K_{mapp} values of 0.15 ± 0.02 s^{-1} and 64 ± 15 mM and of 0.015 ± 0.002 s^{-1} and 132 ± 38 mM for the fast and the slow phase, respectively. Thus, the S187F mutation strongly affects the first half-reaction by causing a ~550-fold decrease of its catalytic efficiency with respect to normal AGT [18]. This is not unexpected, considering the mispositioning of Lys209, as revealed by the crystal structure of the S187F mutant, and the role of the PLP-binding lysine in aminotransferases on C_α proton abstraction and $C_{4'}$ reprotonation [63].

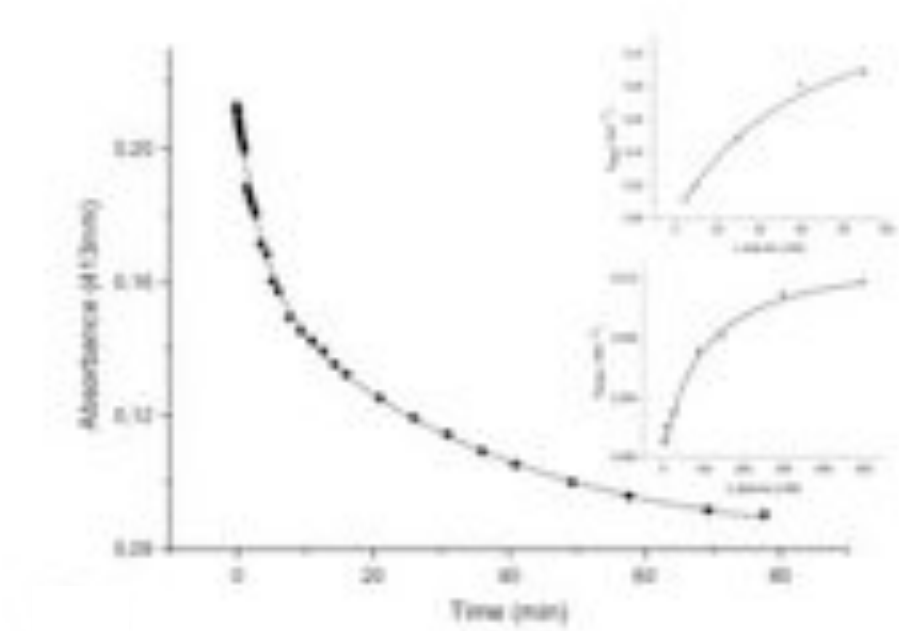

Figure 13. Time-dependent L-alanine half-transamination of the S187F variant. Plot of the 413 nm absorbance with time for the reaction of 15 μM S187F with 5 mM L-alanine. The line represents a two exponential fit. Insets: dependence of the rate constants (k_{fast} and k_{slow}) as a function of L-alanine concentration. The lines represent the data fitted to eq.5.

According to this view, replacement of Lys209 with Arg completely abolishes the AGT catalytic activity [26]. Since Lys209 is supposed to act as an acid/base catalyst in both half-reactions of AGT, an effect of the S187F mutation on the ketoacid half-transamination would also be expected. Unfortunately, this reaction cannot be monitored because the apoenzyme of the S187F variant is unstable and prone to aggregation at the high enzyme concentration required to obtain an apo-PMP complex (at least 100 μM).

How can be explained the biphasic kinetics of the L-alanine half-transamination of the S187F mutant? The finding that the PLP binding kinetics is a monophasic process and that the kinetics of the L-alanine half-

transamination does not change upon addition of D-alanine, allows to exclude that the S187F variant could exist in solution as a mixture of a fast and a slow reacting form. Moreover, since about 10 μM pyruvate is formed at the end of the fast phase and the variant exhibits a K_i value for the competitive inhibition of pyruvate against glyoxylate identical to that of normal AGT [18] (2.2 ± 1.3 mM), the slow phase of the half-transamination is not due to pyruvate inhibition. Nevertheless, we found that (i) the L-alanine half-transamination becomes a single exponential process (with a k_{obs} value comparable to that of the fast phase) when it is coupled to the LDH/NADH reaction system, (ii) 100% of the PMP formed during the fast phase is bound at the AGT active site, and (iii) a 40% of bound PMP is present at the end of the slow phase. These results indicate that pyruvate is not released in solution in two kinetically-distinguishable processes and that the slow phase is due to the accumulation of bound PMP that, in the presence of pyruvate, leads to an equilibrium between the forward and the reverse reaction. Consistent with this idea, a gradual recovery of the 413 nm absorbance is clearly detected at the end of the slow phase, indicative of the occurrence of the reversal transamination reaction.

5.4 The molecular defect of the S187F-Ma variant and its implications for the treatment of patients bearing the S187F mutation

Being PH1 a disease characterized by a remarkable heterogeneity in terms of enzymatic phenotype, the choice of the treatment strategy suitable for each patient strongly depends on the elucidation of the molecular mechanism leading from each specific mutation to AGT deficiency. Until now, the effect of many PH1-causing missense mutations has been rationalized in terms of the position of the mutated residue in the crystal structure of normal AGT [16]. However, this approach does not always guarantee the elucidation of the molecular defect of each variant. An example is herein presented for the S187F variant. As previously mentioned, the liver biopsy of a patient bearing the S187F mutation shows

a very low AGT catalytic activity and expression level [34]. This result along with the fact that, basing on the AGT-Ma crystal structure, the Ser187 is not part of the active site, might lead to hypothesize that the variant only has a structural defect and that a treatment with pharmacological chaperones, able to stabilize the folded conformation of the variant, would be the best therapeutic strategy for patients bearing the S187F mutation. However, we previously found that replacement of Ser187 by Phe in the recombinant protein causes both structural (reduced thermostability of the apo form) and functional (reduced catalytic efficiency and altered PLP binding mode and affinity) defects [61]. In this study, the crystal structure of the variant paired with bioinformatics analysis, has shown that the mutation causes a remarkable perturbation of the active site resulting in a mispositioning of (i) the PLP-binding lysine, (ii) the AGT-PMP complex, and (iii) the external aldimine. These data are consistent with biochemical analyses indicating a reduced rate of L-alanine half-transamination, a different PMP binding mode and affinity as well as an altered microenvironment of the external aldimine with D-alanine in comparison with normal AGT. On the basis of these data showing that even the folded variant exhibits structural defects at the active site responsible for a low transaminase activity, we can conclude that a therapy with pharmacological chaperones will likely have only limited effects for patients bearing the S187F mutation. Instead gene therapy or enzyme administration approaches most likely represent the preferred therapeutic strategies.

Impact of the Gly161 mutation on the molecular and cellular proprieties of AGT

Gly161 is a highly conserved residue and represents a hot-spot mutation site within the AGT sequence. In fact, three pathogenic mutations that affect the GCC triplet in exon 4 of the AGXT gene have been reported: the G161R mutation, co-segregating with the major allele, and the G161S and G161C mutations, both co-segregating with the minor allele. The AGT crystal structure reveals that Gly161 is far from the active site and is part of the loop 154-168 located in the large domain in close contact with the small domain (Fig.14)[37].

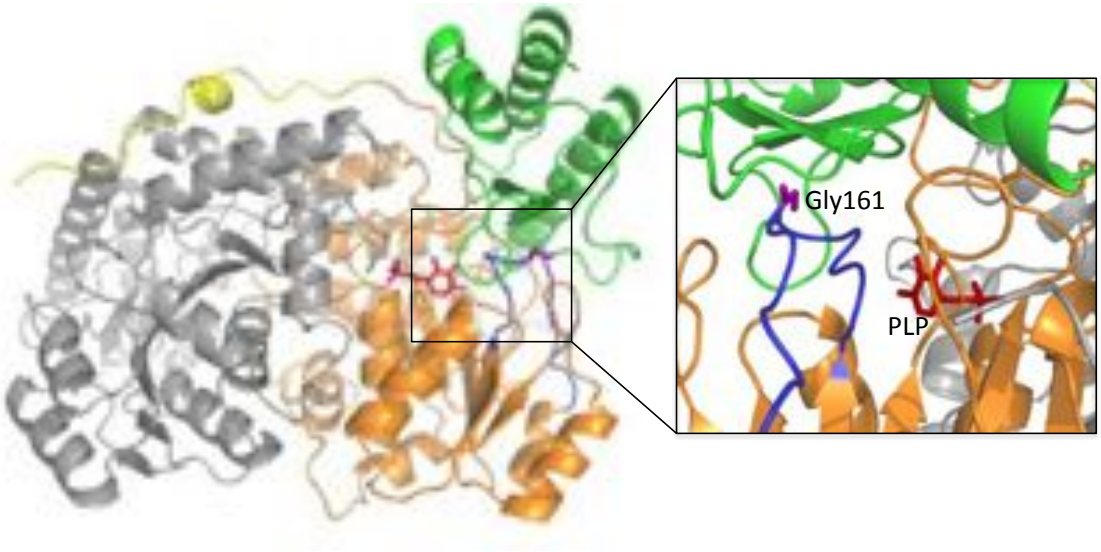

Fig. 14: Position of Gly161 residue in the AGT structure. The figure represents the crystal structure of AGT (PDB code 1H0C) in which one monomer is colored gray, while in the other monomer the large domain, the small domain and the N-terminal extension are represented orange, green and yellow respectively. The cofactor PLP is represented as red sticks, while Gly161 is represented as magenta sticks and the loop 154-168 is colored blue. The inset shows the position and the microenvironment of Gly161.

The substitution of the small side chain of glycine with the larger side chains of arginine, serine or cysteine is predicted to perturb the folding of both domains of the protein. We have shown (chapters 4.4, 4.5) that the G161S and G161C mutations do not significantly alter the catalytic activity and the PLP binding of AGT, but remarkably reduce the thermal stability of the protein in both the holo- and the apo-form. Moreover, crude *E.coli* lysates expressing the G161C-Mi, G161S-Mi and G161R-Ma variants display very low specific activity and AGT expression level [33, 60]. Finally, Coulter-Mackie M.B. et al [43] have reported cell-free expression experiments indicating that the G161R-Ma variant is prone to proteasomal and tryptic degradation. Although these data confirm that the mutation of Gly161 could induce structural perturbations in AGT, a detailed investigation of the mechanism by which it exerts its pathogenic effect is still lacking.

6.1 Gly161 variants show strongly reduced expression level in *E. coli*

As previously mentioned (chapter 4.2), when the G161S-Mi and G161C-Mi variants are overexpressed in *E. coli*, a large portion of the protein is present in the insoluble fraction and the purification yield drops to about 10% when compared to that of AGT-Ma. Unfortunately, when the G161R-Ma variant is expressed using the same procedure, the expression level is less than 5% with respect to AGT-Ma and the mutant protein is insoluble in crude extracts. Any attempt to reduce protein aggregation by lowering the expression temperature, by adding exogenous PLP and small osmolytes to the culture, or by using *E.coli* strains overexpressing molecular chaperones, have been unsuccessful. This has prevented us to obtain and characterize the G161R-Ma variant in the pure form.

6.2 Recombinant purified G161S-Mi and G161C-Mi variants in the apo-form are unstable and prone to aggregation under physiological conditions

Thermal denaturation studies have shown that both G161S-Mi and G161C-Mi are characterized by a melting temperature (Tm) considerably lower than AGT-Mi and that the effect of the mutations on stability is exacerbated in the apo-form. In order to investigate if the lower Tm could reflect an instability of the variants under physiological conditions, the catalytic activity of AGT-Mi, G161S-Mi and G161C-Mi at 2 μM concentration in the holo- and in the apo-form has been monitored at 37°C, pH 7.4 and 150 mM ionic strength. No time-dependent inactivation can be observed for AGT-Mi in the holo- and apo-form nor for the Gly161 variants in the holo-form. On the contrary, the residual catalytic activity of the apo-forms of Gly161 variants sharply decreases over time reaching at 180 min a value of ~25% and of ~5% for G161C-Mi and G161S-Mi, respectively (data not shown). Moreover, since the inactivation extent does not decrease with enzyme concentration, it can be affirmed that monomerization is not caused by the loss of activity.

To test if protein aggregation is the cause of the thermal inactivation, we incubated G161C-Mi and G161S-Mi under physiological conditions monitoring turbidity changes of the solution over a 60 min time interval. As shown in Fig. 15A and B, the absorbance at 600 nm does not change for the variants in the holo-form, whereas a significant change in turbidity is observed for apoG161S-Mi and apoG161C-Mi, thus indicating an ongoing aggregation process. The aggregation extent is similar for the two proteins, even if in the case of the G161C-Mi variant a decrease in turbidity is observed after 40 min of reaction due to aggregates precipitation. Notably, the addition of excess exogenous PLP (100 μM) decreases the extent of aggregation of both G161S-Mi and G161C-Mi (Fig. 15). This result indicates that the binding of the coenzyme competes with the aggregation

process and is able to shift the equilibrium versus the non-aggregating holoenzymatic form.

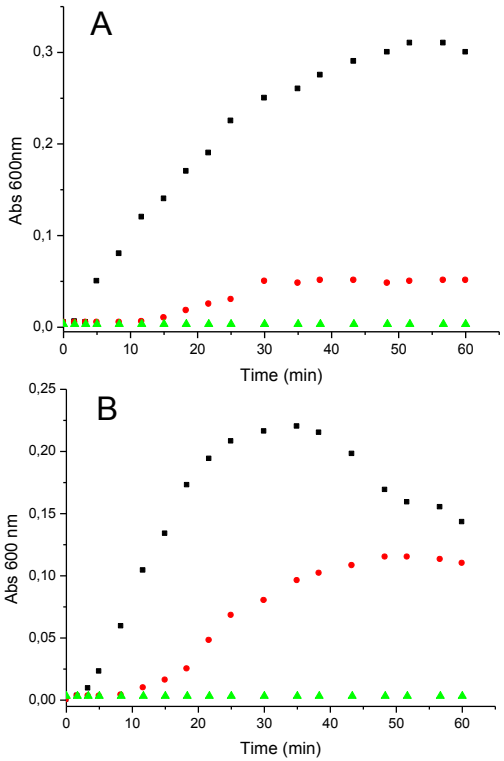

Fig. 15 : Time-dependent turbidity changes of G161S-Mi and G161C-Mi variants. Absorbance changes at 600 nm as function of time of the variants at 2μM in the apo-forms (▪), holo-forms (▲) and apo-forms + 100 μM PLP (▪) of Gly161 variants were monitored in 60 mM potassium phosphate buffer, pH 7.4, at 37 °C.

In order to characterize the species present in solution during incubation of G161S-Mi, G161C-Mi and AGT-Mi under physiological conditions, dynamic light scattering (DLS) studies were undertaken. Fig. 16A shows the time-

dependence of the total count rate, a parameter that depends on both the size and the quantity of the particles, for the three enzymatic species in the holo- and apo-form. While the increase in the count rate is very slow for the holoenzymes and for apoAGT-Mi, a fast aggregation process can be seen for apoGly161 variants, with the count rate levelling off after ~20 and ~30 min for apoG161S-Mi and apoG161C-Mi, respectively.

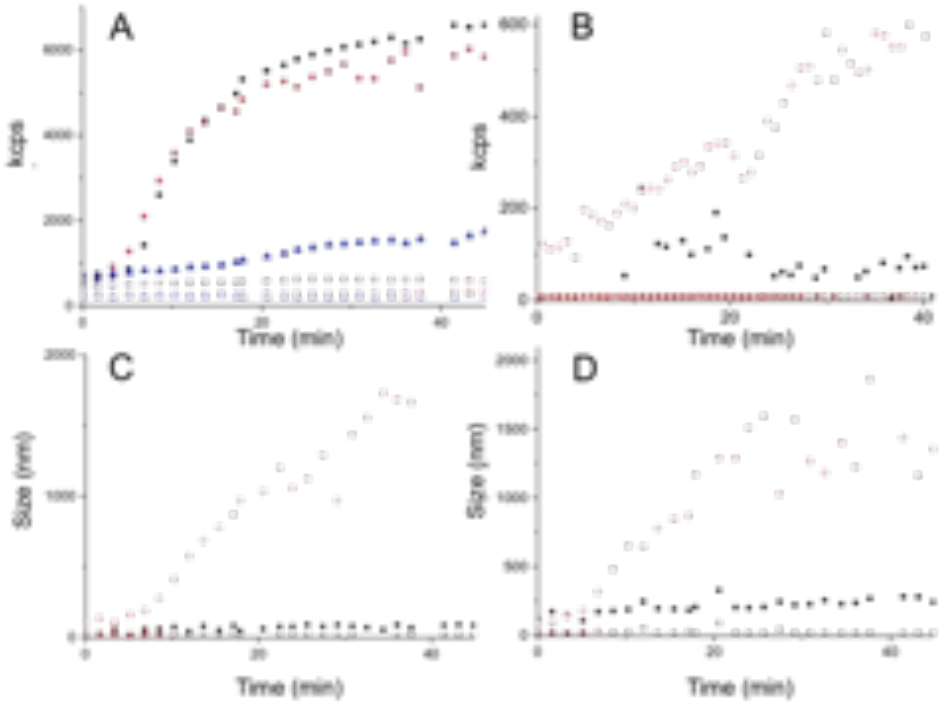

Fig. 16: Time-dependent aggregation of AGT-Mi and Gly161 variants: **(A)** total count rate (measured as kilo counts per second) of AGT-Mi and G161 variants as function of time. Color code: blue AGT-Mi; black G161S-Mi; red G161C-Mi. Open and closed symbols represent holo- and apo-form respectively. The other panels shown the time-dependent changes of the apparent diameter of **(B)** holo and apo-AGT-Mi, **(C)** holo and apo-G161S-Mi and **(D)** holo and apo-G161C-Mi. Symbol code: □ holo dimer; ■ apo dimer; ■ holo aggregates; O apo aggregates. All measurements have been performed at 1 µM enzyme concentration, 37 °C, in 60 mM potassium phosphate buffer pH 7.4

The plots of the particle size against time reported in Fig. 16B, C and D show that, although small aggregates (from 200 to 600 nm) are formed upon incubation of holo- and apoAGT-Mi, holoG161S-Mi and holoG161C-Mi, the signal of the dimer is continuously present. This means that the dimer is the most abundant species in solution, since the contribution to scattering from larger particles dominates the DLS signal being the scattering intensity proportional to the sixth power of a particle diameter. On the contrary, the signal of the dimer of apoG161S-Mi and apoG161C-Mi disappears after 5-10 min and aggregates of ~1500 nm are formed. Moreover, after ~40 min apoG161C-Mi forms a distinct population of high-order aggregates (~5000 nm) that could explain the precipitation phenomenon seen in turbidimetry experiments (Fig. 15A). Finally, the aggregation extent increases as the protein concentration increases, thus indicating that the aggregation does not depend on protein monomerization.
In order to define the aggregation mechanism of Gly161 variants and its possible correlation with the inactivation at physiological temperature, we followed the aggregation process by DLS and we measured the residual activity upon 1 h incubation at different ionic strengths (from 0.15 to 1.25 M). We found that the aggregation extent and the loss of activity of apoGly161 variants increases as the ionic strength decreases (Fig. 17), thus indicating that electrostatic forces mediate the interaction between dimers of apoG161S-Mi and apoG161C-Mi and that the inactivation and aggregation processes are probably linked.
The effect of Gly161 mutation on the stability of the dimeric structure of AGT in the apo-form was analysed by SEC under conditions in which no significant aggregation occurs, i.e. 0.1 M potassium phosphate buffer, pH 7.4, 25°C. No peaks corresponding to monomeric species were detected down to 100 nM concentration for apoG161S-Mi and apoG161C-Mi, thus suggesting that the apovariants are not characterized by a dimeric structure significantly less stable with respect to apoAGT-Mi. However, the comparison of the spectral properties of apoG161C-Mi and apoG161S-Mi with those of apoAGT-Mi revealed that the variants in the dimeric form

display (i) a different near-UV dichroic spectrum, characterized by a decreased ellipticity at 288 nm and an increased ellipticity at 265 nm, and (ii) a 5 nm red-shift of the intrinsic fluorescence emission maximum(data not shown). Moreover, we found that the rate constant of association of 100 μM PLP is equal to 0.28 ± 0.02 min^{-1}, 0.18 ± 0.03 min^{-1} and 0.14 ± 0.01 min^{-1}, for apoAGT-Mi, apoG161S-Mi and apoG161C-Mi, respectively.

Altogether, the obtained results indicate that the mutation of Gly161 to Ser or Cys on the background of the minor allele (i) makes AGT in the apo-form prone to a time-dependent inactivation and aggregation under physiological conditions, which is prevented by the binding of PLP, and (ii) changes the tertiary structure of apoAGT in the dimeric form and slows down PLP binding.

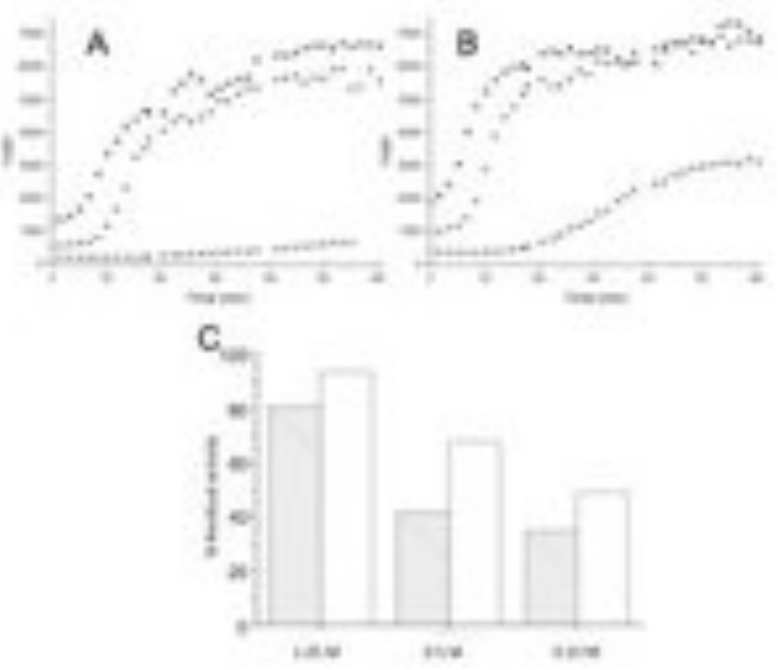

Fig. 17: Analyses of the aggregation and enzymatic activity of Gly161 variants at different ionic strength. Changes in the total count rate (measured as kilo counts per second) of G161S-Mi **(A)** and G161C-Mi **(B)** variants as function of time. Measurements performed at 1

μM enzyme concentration, 37 °C, in potassium phosphate buffer pH7.4 1.25 M (■), 0.5 M (•) and 0.15 M (▲)ionic strength. **(C)** Histogram representative of the residual activity of G161S-Mi (filled bars) and G161C-Mi (empty bars) after 1h incubation at the indicated ionic strength.

6.3 Gly161 variants show a reduced expression level and enzymatic activity in mammalian cells

In order to investigate how the mutation of Gly161 could alter the expression and the activity of AGT in a cell environment, the G161R-Ma, G161S-Mi and G161C-Mi variants have been expressed in chinese hamster ovary (CHO) cells. We didn't succeed in the generation of stable clones expressing the three Gly161 variants, as a consequence of the high mortality of the transfected cells probably caused by the accumulation of insoluble protein due to the expression of aggregation prone variants (see below). Thus, CHO cells transiently expressing AGT-Ma, AGT-Mi and the Gly161 variants were analysed for AGT enzymatic activity and expression level after 24h. While the transaminase activity of AGT-Mi is slightly lower with respect to AGT-Ma (310 ± 22 nmol pyruvate/min/mg lysate for AGT-Ma and 267 ± 60 nmol pyruvate/min/mg lysate for AGT-Mi), that of Gly161 variants is 0.6 ± 0.1, 1.2 ± 0.3 and 1.1 ± 0.2 nmol pyruvate/min/mg lysate for G161R-Ma, G161S-Mi and G161C-Mi, respectively. Moreover, Gly161 variants have a reduced expression level as shown by the intensity of the specific band of immunoreactive AGT that is equal to 4% for G161R-Ma as compared with AGT-Ma, and to 12 % and 5% for G161S-Mi and G161C-Mi, respectively, as compared with AGT-Mi (Fig. 18). Thus, considering that the catalytic efficiency of the G161S-Mi and G161C-Mi variants in the purified form is similar to that of AGT-Mi, the very low AGT enzymatic activity of CHO cells expressing the variants can be attributed to their very low expression level.

RT-PCR experiments have been conducted to rule out possible influences of the mutations at transcriptional level. No significant differences were observed in the levels of the mRNA transcripts for cells expressing AGT-Ma, AGT-Mi, G161R-Ma, G161S-Mi or G161C-Mi (data not shown).

Therefore, the reduced expression of Gly161 variants originates at the protein level.

6.4 Gly161 variants form cytosolic aggregates in mammalian cells

Considering the aggregation propensity of G161S-Mi and G161C-Mi in the recombinant purified form, we investigated if aggregates of Gly161 variants are also formed inside the cell. For this purpose determined the amount of AGT present in the soluble and insoluble fraction of lysates of CHO cells expressing AGT-Ma, AGT-Mi and the Gly161 variants.

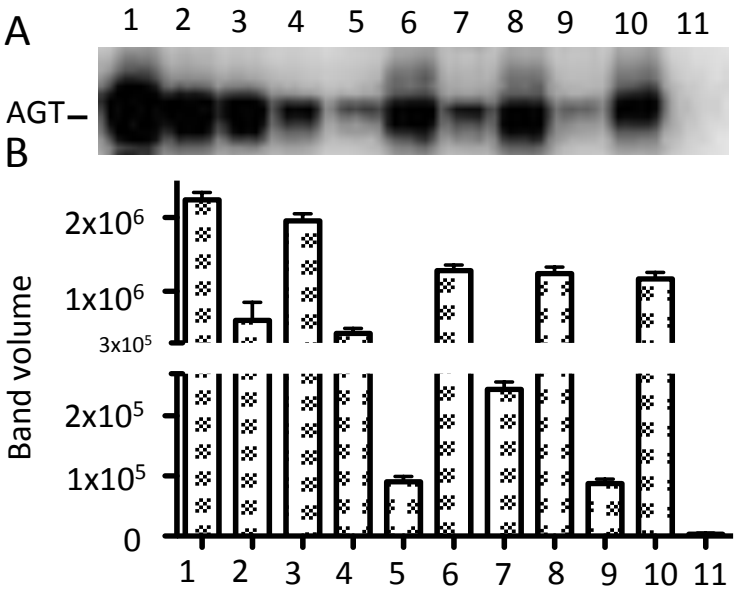

Fig. 18: Analysis of AGT expression in CHO cells expressing AGT-Ma, AGT-Mi and Gly161 variants. 24 h after transfection CHO cells were harvested and lysed; 10 µg of cell lysate was subjected to SDS/PAGE, immunoblotted whit anti-AGT from rabbit (1:2000) and than detected with a chemiluminescent substrate. (A) Immunoblot; (B) Histogram representative of the immunoblot bands volume. The immunoblot lanes and histogram bars are coded as follow: 1. soluble and 2. insoluble fraction of CHO cell lysate expressing AGT-Ma, 3. soluble and 4. insoluble fraction of CHO cell lysate expressing AGT-Mi, 5. soluble and 6. insoluble

fraction of CHO cell lysate expressing G161R-Ma, 7. soluble and 8. insoluble fraction of CHO cell lysate expressing G161S-Mi, 9. soluble and 10. insoluble fraction of CHO cell lysate expressing G161C-Mi, 11. whole cell lysate of untransfected CHO cells. Bar graphs represent the mean ± SEM. Data come from the mean of three different experiments.

While in the case of AGT-Ma and AGT-Mi about 75-80% of the protein was present in the soluble fraction, in the case of G161R-Ma, G161S-Mi and G161C-Mi variants 93%, 84% and 91% of the protein, respectively, was present in the insoluble fraction (Fig. 18). Although it should be noted that the total amount of protein (soluble plus insoluble fraction) present in the Gly161 variants is lower with respect to that of AGT-Ma or AGT-Mi, these data would suggest that the low expression level of the variants is mainly due to protein aggregation. In agreement with these results, two strong bands at 80-90 kDa, corresponding to the two structural isoforms of dimeric AGT [45], can be seen after cross-linking of lysates of cells expressing AGT-Ma or AGT-Mi. On the other hand, cross-linking of lysates of cells expressing Gly161 variants lead to the appearance of a faint band at a molecular weight higher than 200 kDa, and to the almost complete loss of immunoreactive AGT, probably due to the formation of high-molecular weight aggregates that are unable to enter the gel (Fig. 19). In order to confirm the aggregation propensity of AGT induced by Gly161 mutation in the cellular system, lysates of CHO cells expressing AGT-Ma or the G161R-Ma variant were subjected to SEC and the fractions collected were analysed by western-blot to detect the presence of immunoreactive AGT (Fig. 20 A and B). As expected, AGT-Ma eluted between 15 and 16 ml, an elution volume identical to that of the active dimeric protein in the purified form, whereas the G161R-Ma variant mainly eluted in a broad peak from 7 to 11 ml, consistent with the formation of a mixture of aggregates with apparent molecular weight from ~350 to more than 1000 kDa.

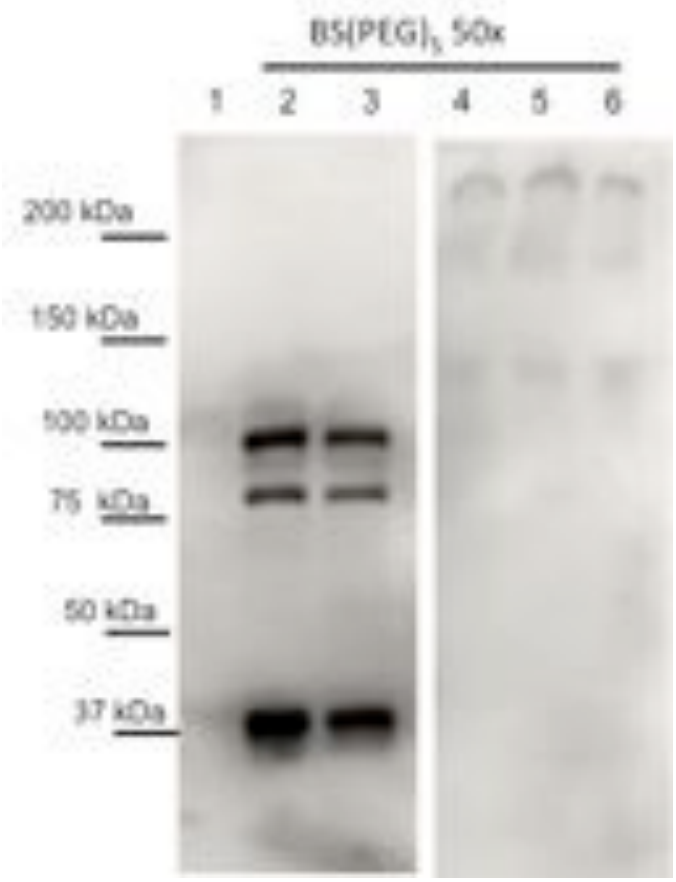

Fig. 19: Cross-linking analyses of CHO cells expressing AGT-Ma, AGT-Mi and Gly161 variants. 24 h after transfection CHO cells were harvested lysed and cross-linked with $BS(PEG)_5$ at 50X molar excess; 10 µg of each mixture was subjected to SDS/PAGE, immunoblotted whit anti-AGT from rabbit (1:2000) and then detected with a chemiluminescent substrate. The immunoblot lanes are coded as follow: 1. untransfected CHO cells, 2. CHO cells expressing AGT-Ma, 3. CHO cells expressing AGT-Mi, 4. CHO cells expressing G161R-Ma, 5. CHO cells expressing G161S-Mi, 6. CHO cells expressing G161C-Mi.

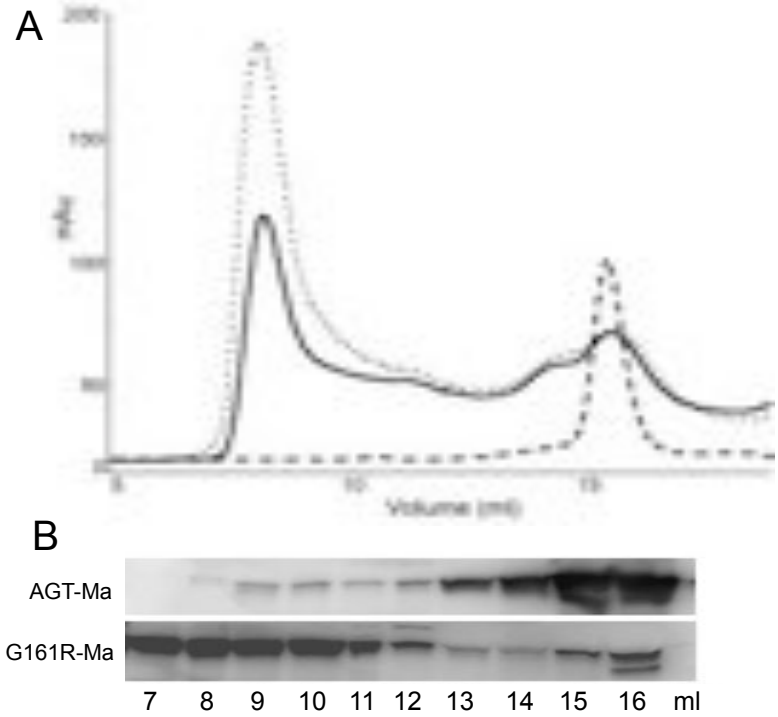

Fig. 20: Gel filtration analyses of CHO cells expressing AGT-Ma and the G161R-Ma variant. 24 h after transfection CHO cells were harvested and lysed. (A) Size exclusion chromatography (SEC) elution profile of CHO cells expressing AGT-Ma (-), CHO cells expressing G161R-Ma(····) and recombinant purified AGT-Ma (--). (B) Western blot analyses of SEC fractions of CHO cells expressing AGT-Ma and G161R-Ma.

Immunofluorescence microscopy studies were performed to define if the mutation of Gly161 could also affect the subcellular localization of AGT. Intracellular spots staining for AGT that do not colocalize neither with the peroxisomal nor with the mitochondrial marker were present in CHO cells transiently expressing G161R-Ma, G161S-Mi or G161C-Mi (Fig. 21). Only in the case of the G161S-Mi and G161C-Mi variants a qualitative analysis of the confocal images indicated a partial peroxisomal localization of AGT. On the other hand, as expected, a clear peroxisomal localization can be observed in CHO cells transiently expressing AGT-Ma or AGT-Mi (Fig. 22).

Notably, under these experimental conditions, no significant mitochondrial import of AGT-Mi, G161S-Mi and G161C-Mi can be seen (Fig. 21B).

A

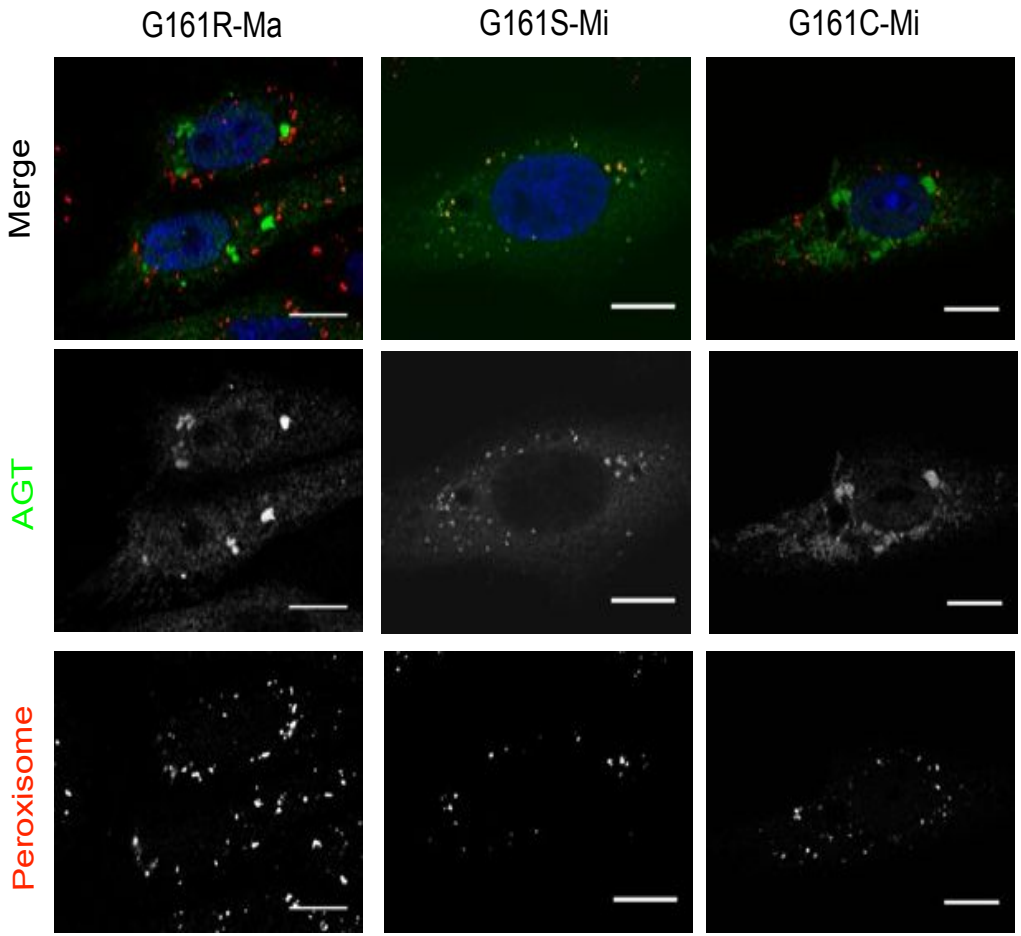

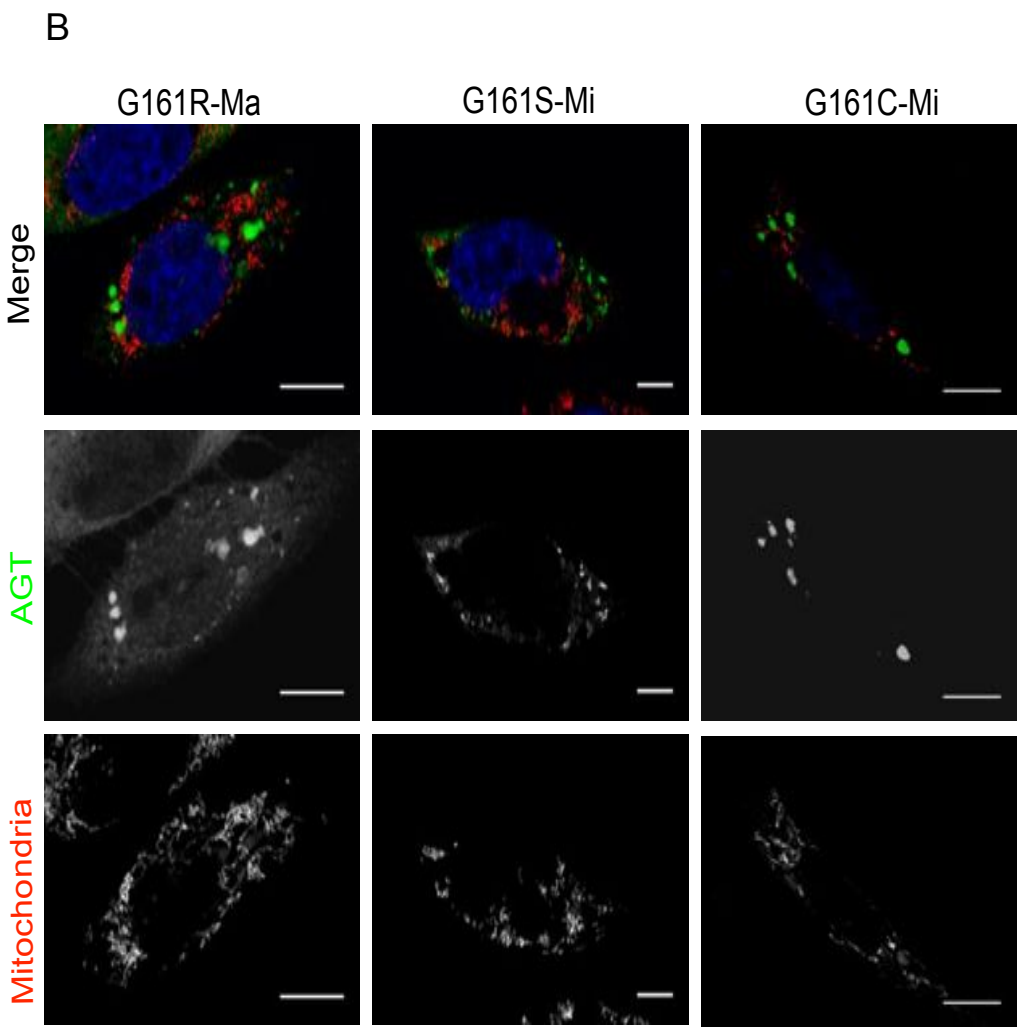

Fig. 21: Subcellular distribution of Gly161 variants in CHO cells. 24 h after transfection cells were fixed and coloured as follow: **(A)** anti-AGT (green), anti-peroxisomal proteins (red); **(B)** anti-AGT (green), Mito Tracker (red). Nuclei were stained with Dapi (blue). Merge and single channel images come from a single z-plane. Scale bar: 10 µm.

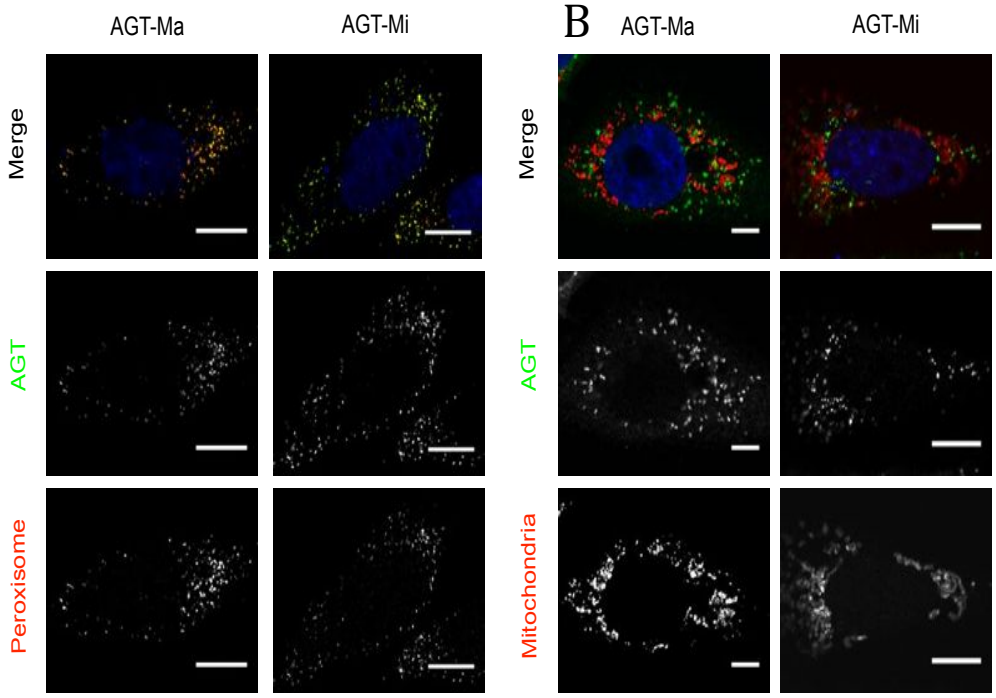

Fig. 22: Subcellular distribution of AGT-Ma and AGT-Mi in CHO cells. 24 h after transfection cells were fixed and coloured as follow: **(A)** anti-AGT (green), anti-peroxisomal proteins (red); **(B)** anti-AGT (green), Mito Tracker (red). Nuclei were stained with Dapi (blue). Merge and single channel images come from a single z-plane. Scale bar: 10 µm.

In agreement with immunofluorescence studies, IEM analyses revealed that AGT-Ma expressed in CHO cells is present in round or ovoid membrane organelles with electrone-dense interior whose shape, size and ultrastructural features were consistent with those of peroxisomes (Fig. 23A). In contrast, the G161R-Ma signal was detected mainly in structures with irregular shape varying from 200-300 nm to several microns in size

(Fig. 23B). Importantly, these G161R-Ma positive structures lack external membrane, a feature consistent with the hypothesis of protein aggregates in the cytosol.

Altogether, these data indicate that the mutation of Gly161 strongly induces the aggregation of AGT inside the cell, leading to the formation of high-molecular weight cytosolic aggregates.

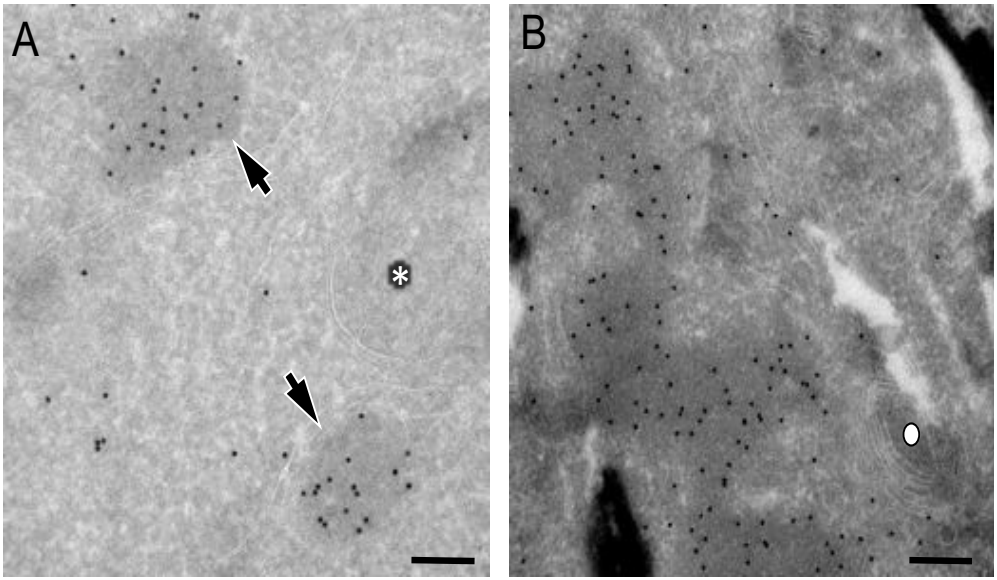

Fig. 23: IEM analyses CHO cells expressing AGT-Ma or G161R-Ma. 24 h after transfection CHO cells expressing AGT-Ma **(A)** and the G161R-Ma **(B)** variant were stained with the anti-AGT antibody followed by protein A conjugated with 10 nm gold particles. Asterisks indicate mitochondria, arrows indicate peroxisomes and the circle indicates Golgi. Scale bar: 150 nm.

6.5 Gly161 variants show a reduced half-life in mammalian cells

Although protein aggregation is one of the features that distinguish Gly161 variants, it does not completely account for their reduced expression level. Thus, we investigated if the mutation of Gly161 could affect the intracellular stability of AGT by determining the kinetics of expression of the protein (Fig. 24). We found that while the expression of AGT-Ma and AGT-Mi is maximal at 24 h and remains stable up to 48 h, the expression level of Gly161 variants shows its maximum level at about 8 h and then decreases with time, thus suggesting that the variants could be susceptible to intracellular degradation. Following this result, we determined the half-life of AGT-Ma, AGT-Mi and Gly161 variants expressed in CHO cells. The data reported in Fig. 25 clearly show that: (i) AGT-Ma and AGT-Mi are very stable, displaying half-lives of 29 ± 2 h and 27 ± 3 h, respectively, and (ii) the G161R-Ma, G161S-Mi and G161C-Mi variants show a lower intracellular stability with respect to AGT-Ma or AGT-Mi, displaying half-lives of <4 h, 13 ± 2 h, and 10 ± 1 h, respectively. Thus, the reduced expression level of the variants can be attributed not only to their aggregation propensity, but also to their greater susceptibility to intracellular degradation.

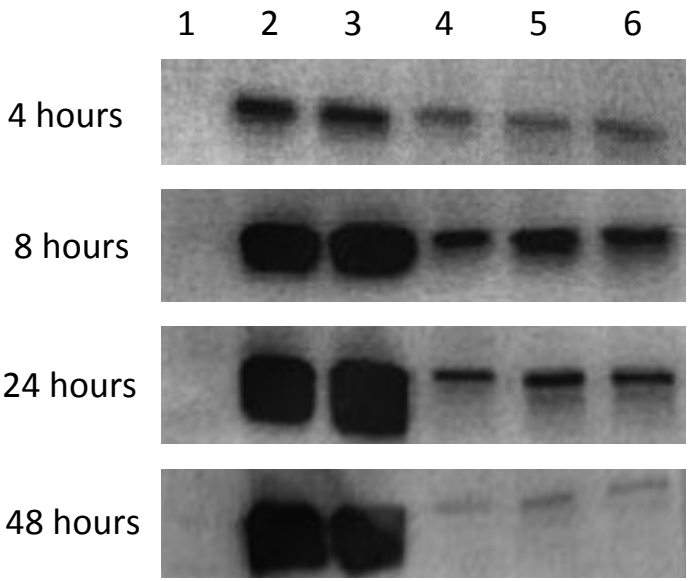

Fig. 24: Time course of AGT-Ma, AGT-Mi and Gly161 variants expression in transiently transformed CHO cells. After transfection CHO cells were harvested at various times and lysed; 10 µg of cell lysate was subjected to SDS/PAGE, immunoblotted whit anti-AGT from rabbit (1:2000) and then detected with a chemiluminescent substrate. The immunoblot lanes are coded as follow: 1. untransfected CHO cells, 2. CHO cells expressing AGT-Ma, 3. CHO cells expressing AGT-Mi, 4. CHO cells expressing G161R-Ma, 5. CHO cells expressing G161S-Mi, 6. CHO cells expressing G161C-Mi.

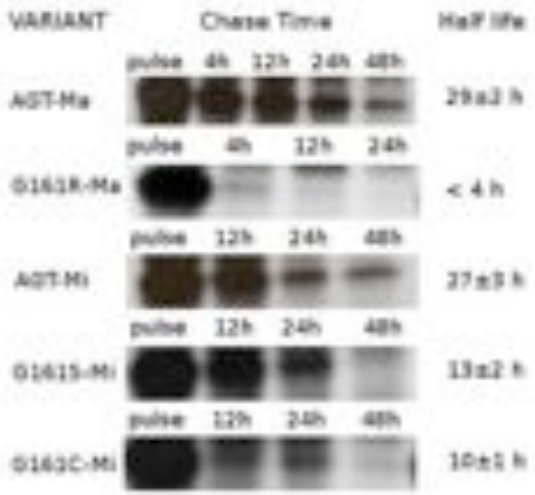

Fig. 25: Measurement of the half-life of AGT-Ma, AGT-Mi, and Gly161 variants in CHO cells. Transiently transfected CHO cells were pulse labeled with ^{35}S Cys-Met Mix and then incubated in complete DMEM for a chase time from 0 to 48 hrs. Cell lysates were immunoprecipitated with anti-AGT antibody and loaded on SDS-PAGE; signal of radiolabelled AGT was detected by autoradiography.

6.6 Exogenous pyridoxine is able to partly rescue for the effect of Gly161 mutation

100 μM pyridoxine, a vitamer of vitamin B6 known to be converted to PLP inside the cell [64], was added to the culture medium of CHO cells expressing AGT-Ma, AGT-Mi or the Gly161 variants. The specific activity of AGT-Ma and AGT-Mi drops to about 70% in the presence of exogenous coenzyme in the culture medium, a result very difficult to explain at present. On the other hand, the specific activity of G161R-Ma, G161S-Mi and G161C-Mi increases of 2.8, 3.1 and 2.1 fold, respectively, in the presence

of 100 μM pyridoxine (Fig. 26). Pyridoxine treatment does not change the total amount of protein of any of the analysed enzymatic species, but increases of 2.5, 3 and 2.8 fold the amount of protein present in the soluble fraction for G161R-Ma, G161S-Mi and G161C-Mi, respectively (Fig. 26). These results suggest that the action of the coenzyme is not due to an increased expression or to a decreased degradation of the variants, rather to a shift of the equilibrium from the apo to the holo-form of the variants, which partly prevented protein aggregation.

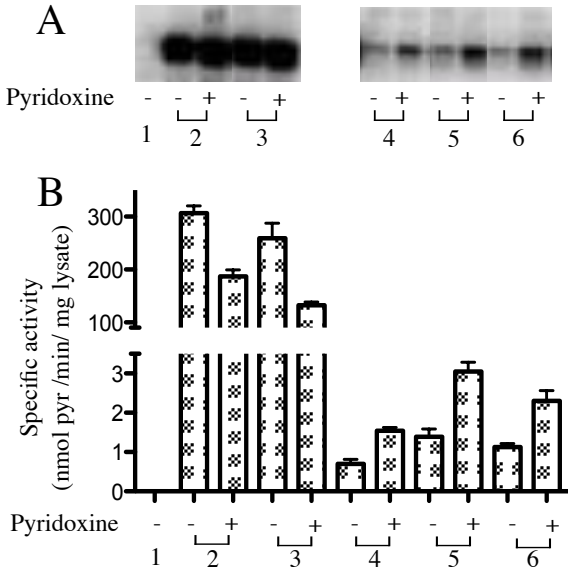

Fig. 26: Effect of pyridoxine on the expression level and specific activity of AGT-Ma, AGT-Mi and Gly161 variants. Where indicated, CHO cells were treated with 100 μM pyridoxine 4h after transfection and, after 24h, were harvested and lysed. (A) 15 μg of cell lysate was subjected to SDS/PAGE, immunoblotted with anti-AGT from rabbit (1: 2000) and detected by chemiluminescence. (B) 100 μg of cell lysate was incubated with 0.5 M L-alanine and 10 mM glyoxylate, and the amount of pyruvate produced after 30 min was determined .The immunoblot lanes and histogram bars are coded as follow: 1. untransfected CHO cells 2. CHO cells expressing AGT-Ma, 3. CHO cells expressing AGT-Mi, 4. CHO cells expressing G161R-Ma, 5. CHO cells expressing G161S-Mi, 6. CHO cells expressing G161C-Mi. Data are representative of three different experiments. Bar graphs represent the mean ± SEM.

6.7 Gly161 mutation causes a folding defect of AGT

Previous data indicate that the mutation of Gly161 to either Ser or Cys does not compromise the enzymatic activity but strongly reduces the thermal stability of both the holo- and, to a higher extent, the apo-form of AGT[61]. Here, we show that: (i) the mutation of Gly161 strongly reduces the AGT expression level, both in *E.coli* and in a mammalian cellular model, and the reduction is not produced by differences at the level of transcription, (ii) under physiological conditions of temperature, ionic strength and pH, purified G161S-Mi and G161C-Mi variants in the apodimeric form are prone to inactivation and electrostatically-driven aggregation, (iii) when expressed in CHO cells, Gly161 variants form insoluble aggregates that localize in the cytosol, and (iv) the substitution of Gly161 strongly reduces the AGT intracellular half-life in the order G161R>G161C>G161S, in agreement with previous cell-free expression system studies indicating that the G161R-Ma variant is prone to proteasomal degradation [31]. All in all, these results indicate that Gly161 variants, although at different extents, are mainly characterized by a folding defect such that it is the inability of the mutated peptide chain to achieve or maintain a fully functional conformation, rather than the loss of protein function per se, that causes the disease. Therefore, the mutation is expected to induce a conformational change ultimately responsible for the propensity of the protein to both degradation and aggregation.

In the absence of the crystal structure of Gly161 variants, it is unclear how the substitution of Gly161 with Arg, Ser or Cys could accelerate the degradation and the aggregation of AGT and whether the two processes are mutually related. Nevertheless, our data suggest that the defects of Gly161 variants are not due to a reduced stability of the dimeric structure. In fact, in line with Gly161 not being an interfacial residue, the purified G161S-Mi and G161C-Mi variants do not display an increased monomer-dimer dissociation constant. Additionally, SEC analyses of lysates of CHO cells expressing G161R-Ma do not reveal the presence of monomeric AGT. Rather, DLS experiments show that the aggregation extent of the

apovariants is proportional to protein concentration and increases wiyh decreasing ionic strength.
These data indicate that the variants in the dimeric form are prone to a self-association process mediated by the electrostatic interaction between patches of opposite charge. AGT shows a highly positive charge distribution around its surface[40].
On these bases, whatever the conformational change caused by Gly161 mutation is, it can be hypothesized that it could lead to the exposure of negatively changed surfaces thus creating a dipole segregation of charges that leads to the electrostatic aggregation of the protein. A similar mechanism has been previously suggested for pathogenic variants of AGT bearing mutations at Gly41 [40]. Following this view, it is reasonable to think that the conformational change induced by Gly161 mutation could also cause the exposure of stretches susceptible to proteolytic degradation. Although this would explain the enhanced intracellular degradation of the variants, a direct evidence for this interpretation is lacking.

6.8 The aggregation of Gly161 variants originates from the apo-form of the protein

Our investigations on purified G161S-Mi and G161C-Mi variants suggest that (i) the mutation of Gly161 induce some structural changes in apoAGT that make it prone to aggregation under physiological conditions and (ii) the binding of PLP competes with protein aggregation by shifting the equilibrium toward the non-aggregating holo-form. A similar competition between aggregation and PLP binding is expected to occur also in the cell cytosol where the cytosolic aggregates formed by Gly161 variants primarily originate from the apo-form of the protein. Moreover, since the variants show a slower PLP binding than AGT-Mi, their apo-forms are expected to be more populated. On the basis of both this hypothesis and previous data on the response of AGT to chemical stress [29], a plausible model that explains the pathogenicity of Gly161 variants can be outlined. Figure 27A

and B compare the possible folding pathway of AGT-Ma and AGT-Mi in the cell cytosol with that of Gly161 variants. In both cases, the unfolded polypeptide chain (U) is expected to generate monomeric AGT (M) passing through a partly folded monomeric intermediate (M*). M can either bind PLP (M_{PLP}) and then dimerize (D_{PLP}), or dimerize (D) and then bind PLP (D_{PLP}). In the case of AGT-Ma and AGT-Mi, most of the protein is converted to D_{PLP}, which is readily imported to peroxisomes.

On the contrary, the conformational change affecting Gly161 variants makes their apodimeric form (D) susceptible to a self-assembly process that competes with PLP binding. Thus, the molecular defect of Gly161 variants seems to affect mostly the apo-form of the protein, similarly to other pathogenic AGT variants such as the more common G170R-Mi and the F152I-Mi [29, 39].

The increased propensity to aggregation, in both non-cellular and cellular systems, is not a novelty in the array of enzymatic phenotypes leading to AGT deficiency [39, 40, 44, 45]. However, one distinctive feature of Gly161 variants is that they form large aggregates in the cell cytosol, as revealed by immunofluorescence and electron microscopy analyses unlike, for instance G41R-Mi variant, which forms intraperoxisomal aggregates, as recently reported by Fargue S. et al[45].This different intracellular behaviour does not seem to depend on the inability of the variants to interact with the peroxisomal carrier Pex5p, as both G161S-Mi and G161C-Mi show a partial peroxisomal localization. It seems more likely that the aggregation of Gly161 variants occurs so rapidly that large aggregates unable to enter the peroxisome are formed before peroxisomal import can take place. In agreement with this view, the aggregation kinetics of purified apoG161S-Mi and apoG161C-Mi under physiological conditions is faster than that previously reported for the G41R-Mi variant[40]. This model can also explain the absence of a mitochondrial localization of G161S-Mi and G161C-Mi in our study. In fact, Fargue S. et al. [45] reported that some destabilizing mutations cosegregating with the minor allele polymorphism lead to a mitochondrial mistargeting of the protein stably expressed in CHO cells as

the result of a synergism between two different effects: the polymorphic P11L mutation unmasks a putative mitochondrial targeting sequence [27, 28], on the other hand the pathogenic mutations promote the accumulation of unfolded or partly folded monomeric species that are compatible with the mitochondrial import machinery. In the case of the G161S-Mi and G161C-Mi variants, the pathogenic mutation does not seem to cause the accumulation of monomeric species and the consequent mitochondrial import. However, it cannot be excluded that the mitochondrial localization is prevented by the short-term expression of the protein that favours a peroxisomal localization[45].

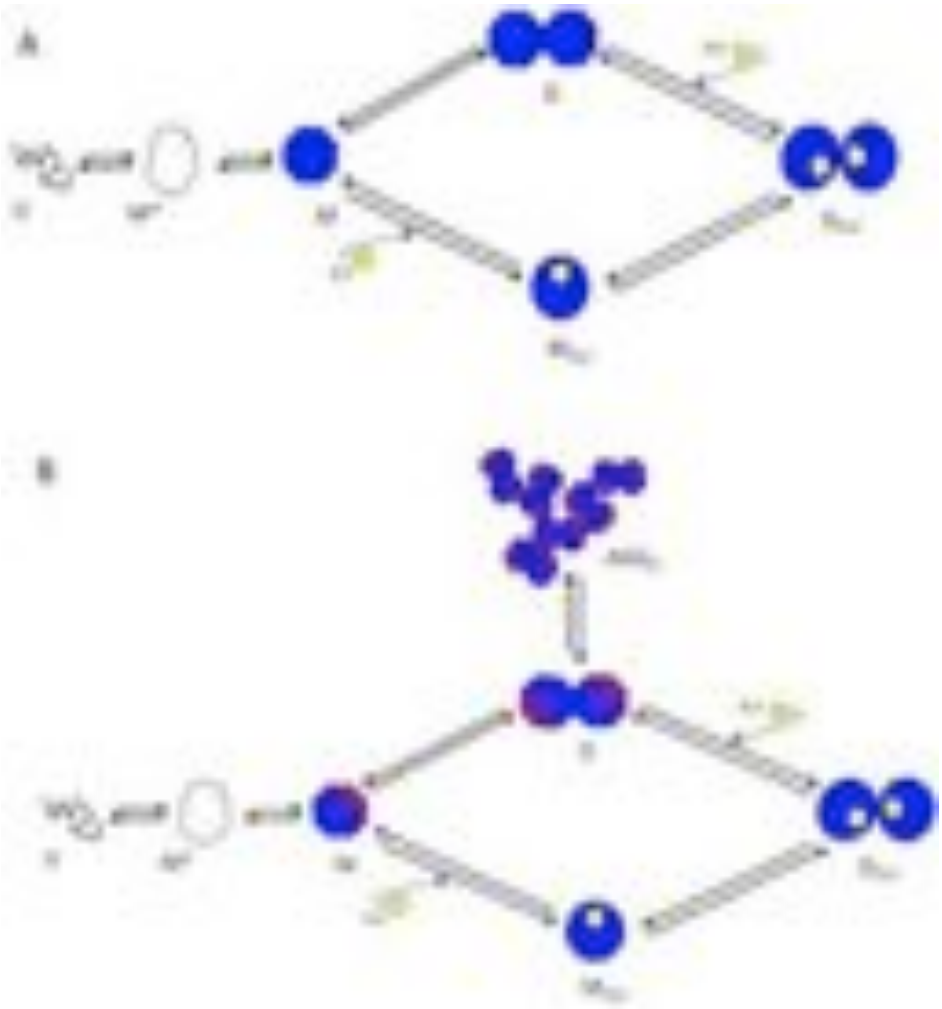

Fig. 27: Proposed folding pathways of (A) AGT-Ma, AGT-Mi and (B) Gly161 variants. U, unfolded monomer, M*, partially folded monomer, M, folded monomer, M_{PLP}, PLP-bound monomer, D, apodimer, D_{PLP}, holodimer and AGG_D aggregates of apodimer.

6.9 PLP is able to partly rescue for the effects of Gly161 mutation by reducing their aggregation extent

Treatment with B6 is a common strategy for the therapy of many metabolic diseases caused by PLP-dependent enzymes. However, the degree of responsiveness is extremely variable depending on both the disease and the genotype of the patients. In the case of PH1, pyridoxine administration is effective in about 10-30% of the patients and clinical data suggest that the responsive mutations are associated with AGT mistargeting. Moreover, although it is known that pyridoxine administration increases the intracellular concentration of PLP, the molecular bases of the effect of the coenzyme are not fully understood. The evidences reported in this study suggest that PLP (i) reduces the aggregation extent of purified G161S-Mi and G161C-Mi variants by shifting the equilibrium from the apo- to the more stable holo-form, (ii) increases the specific activity of the variants expressed in the CHO cellular model system, likely by preventing protein aggregation and (iii) does not increase the total expression level of the variants. Thus, the coenzyme seems to essentially play a prostetic role facilitating the conversion of D to D_{PLP} (Fig. 27). Although further studies will be required to establish the exact mechanism of action of exogenous coenzyme on Gly161 variants, our results suggest that pyridoxine administration should be regarded as a first line option for PH1 patients bearing mutations at Gly161. Considering the limited effect of pyridoxine on the specific activities of Gly161 variants, vitamin B6 administration should be associated with other molecules able to further stabilize Gly161 variants, such as compounds acting as pharmacological chaperones.

CONCLUSIONS

The molecular pathogenesis of PH1 is extremely varied, as several diverse enzymatic phenotypes, including loss of enzymatic activity, altered coenzyme binding affinity, folding defects, aggregation propensity, reduced intracellular stability and mislocalization can result in AGT deficiency. In this thesis is described the biochemical characterization of nine AGT variants (W108R-Mi, S158L-Ma, G161S-Mi, G161C-Mi, G161R-Ma, D183N-Ma, S187F-Ma, S218L-Ma, P319L-Ma and G350D-Mi) associated with PH1. Moreover a detailed analysis of the structural properties of the S187F-Ma variant and of the molecular and cellular properties of Gly161 variants is reported.

Altogether, the obtained data have allowed us:

1. to provide evidence for the structural and/or functional effects caused by each mutation on the protein and to define which form, holo- or apo-, and which part, active-site, large domain or small domain, of the enzyme is affected by the mutation.
2. to reassess previous data obtained with crude cellular extracts in which all the analysed mutations were referred as causing loss of both immunoreactivity and catalytic activity.
3. to indicate the suitable therapy, among those available, and to suggest new treatments strategies for patients bearing the analysed mutations.

Thus, a multi-disciplinary approach comprising both studies on purified proteins and cellular biochemistry analyses should be applied to shed light on the molecular defect of pathogenic variants causing PH1. This would improve our understanding of the molecular pathogenesis of the disease and pave the way to define suitable therapies on the basis of the patient genotype.

ADDENDUM

S250F variant associated with aromatic amino acid decarboxylase deficiency: molecular defects and intracellular rescue by pyridoxine

During the last year of my PhD I've been involved in the study of aromatic amino acid decarboxylase (AADC) deficiency, a rare neurometabolic disorder due to the absence of functional Dopa decarboxylase (DDC). DDC is a PLP-dependent enzyme responsible for the production of the neurotransmitters dopamine and serotonin. More than 50 patients with DDC deficiency have been tabulated on the BIOMDB database (http://www.biopku.org/biomdb/biomdb_start.asp), and 23 missense pathogenic mutations have been identified, half of which in homozygous patients. Although the clinical phenotype associated with the disease has been widely investigated [65, 66], the molecular effect(s) that each mutation induces on DDC is almost unknown. Nonsense and frameshifts mutations lead to the complete loss of the gene product, while missense point mutations cause the synthesis of an aberrant gene product which can be characterized by defects of enzymatic activity, PLP binding, protein stability and/or folding, protein half-life, etc. Current treatments for AADC deficiency include the administration of pyridoxine or PLP to increase the residual DDC activity, MAO-B inhibitors to minimize the dopamine degradation, or dopamine agonists to mime the action of the neurotransmitter [67]. The response to these therapies is variable, but the overall outcome is poor, probably reflecting the allelic heterogeneity. Moreover, since drugs are almost always given in combination, response is hardly ascribable to a single drug. In diseases related to protein malfunction it is diagnostically and therapeutically essential to understand the multiple mechanisms that relate the specific mutants with the pathology. Therefore, the knowledge of the structural and/or functional effect(s) that each amino acid substitution produces on DDC would be highly desirable. A first example of this approach is a recent study in which, by means of biochemical and bioinformatic analyses, the molecular defects of four recombinant purified

pathogenic variants whose mutations concern residues located at or near the active site have been identified. On these bases, a therapeutic treatment has also been proposed [68]. During my PhD the effects of the S250F mutation, the most frequent associated with AADC deficiency, have been defined by a combined analyses on the S250F variant both in the purified form and expressed in a cellular system. We found that Ser250 is not essential for the catalytic activity of DDC. However, its mutation to Phe causes a ~7-fold reduction of catalytic efficiency and a conformational change in the proximity of the mutated residue that is transmitted to the active site. In cellular extracts of *E. coli* and mammalian cells, both the specific activity and the protein level of the variant decrease with respect to the wild-type. The results with mammalian cells indicate that the mutation does not affect intracellular mRNA levels, and are consistent with a model where the S250F variant undergoes a degradation process via the proteasome, possibly through an ubiquitination process occurring faster than in the wild-type. Overall, biochemical and cell biology experiments show that loss of function of S250F occurs by two distinct but not exclusive mechanisms affecting activity and folding. Importantly, 4-phenylbutirric acid (4-PBA) or, to a major extent, pyridoxine increase the expression level and, in a dose-dependent manner, the decarboxylase specific activity of mutant-expressing cells. This strongly suggests that 4-PBA and/or pyridoxine administration may be of important value in therapy of patients bearing the S250F mutation.

BIBLIOGRAPHY

[1] Danpure, C. J.;Rumsby, G., Molecular aetiology of primary hyperoxaluria and its implications for clinical management. *Expert Rev Mol Med* **2004,** *6* (1), 1-16.
[2] Danpure, C. J.;Jennings, P. R., Peroxisomal alanine:glyoxylate aminotransferase deficiency in primary hyperoxaluria type I. *FEBS Lett* **1986,** *201* (1), 20-4.
[3] Osswald, H.;Hautmann, R., Renal elimination kinetics and plasma half-life of oxalate in man. *Urol Int* **1979,** *34* (6), 440-50.
[4] Morgan, S. H.;Purkiss, P.;Watts, R. W.;Mansell, M. A., Oxalate dynamics in chronic renal failure. Comparison with normal subjects and patients with primary hyperoxaluria. *Nephron* **1987,** *46* (3), 253-7.
[5] Danpure, C. J., Molecular etiology of primary hyperoxaluria type 1: new directions for treatment. *Am J Nephrol* **2005,** *25* (3), 303-10.
[6] Archer, H. E.;Dormer, A. E.;Scowen, E. F.;Watts, R. W., Studies on the urinary excretion of oxalate by normal subjects. *Clin Sci (Lond)* **1957,** *16* (3), 405-11.
[7] Zarembski, P. M.;Hodgkinson, A., Some factors influencing the urinary excretion of oxalic acid in man. *Clin Chim Acta* **1969,** *25* (1), 1-10.
[8] Marshall, R. W.;Cochran, M.;Hodgkinson, A., Relationships between calcium and oxalic acid intake in the diet and their excretion in the urine of normal and renal-stone-forming subjects. *Clin Sci* **1972,** *43* (1), 91-9.
[9] Chadwick, V. S.;Modha, K.;Dowling, R. H., Mechanism for hyperoxaluria in patients with ileal dysfunction. *N Engl J Med* **1973,** *289* (4), 172-6.
[10] Atkins, G. L.;Dean, B. M.;Griffin, W. J.;Scowen, E. F.;Watts, R. W., Primary Hyperoxaluria. The Relation between Ascorbic Acid and the Increased Urinary Excretion of Oxalate. *Lancet* **1963,** *2* (7317), 1096-7.
[11] Crawhall, J. C.;Scowen, E. F.;De Mowbray, R. R.;Watts, R. W., Conversion of glycine to oxalate in a normal subject. *Lancet* **1959,** *2* (7107), 810.

[12] Ratner S;Nocito V;DE, G., Glycine oxidase. *J Biol Chem* **1944,** *152*, 119.
[13] Richardson, K. E.;Tolbert, N. E., Oxidation of glyoxylic acid to oxalic acid by glycolic acid oxidase. *J Biol Chem* **1961,** *236*, 1280-4.
[14] Weinhouse, S.;Friedmann, B., Metabolism of labeled 2-carbon acids in the intact rat. *J Biol Chem* **1951,** *191* (2), 707-17.
[15] Monico, C. G.;Olson, J. B.;Milliner, D. S., Implications of genotype and enzyme phenotype in pyridoxine response of patients with type I primary hyperoxaluria. *Am J Nephrol* **2005,** *25* (2), 183-8.
[16] Zhang, X.;Roe, S. M.;Hou, Y.;Bartlam, M.;Rao, Z.;Pearl, L. H.;Danpure, C. J., Crystal structure of alanine:glyoxylate aminotransferase and the relationship between genotype and enzymatic phenotype in primary hyperoxaluria type 1. *J Mol Biol* **2003,** *331* (3), 643-52.
[17] DeLano, W. L., The pyMol Molecular Graphics system. *DeLano Scientifics, San Carlos, CA. In.* **2002**.
[18] Cellini, B.;Bertoldi, M.;Montioli, R.;Paiardini, A.;Borri Voltattorni, C., Human wild-type alanine:glyoxylate aminotransferase and its naturally occurring G82E variant: functional properties and physiological implications. *Biochem J* **2007,** *408* (1), 39-50.
[19] Danpure, C. J.;Fryer, P.;Jennings, P. R.;Allsop, J.;Griffiths, S.;Cunningham, A., Evolution of alanine:glyoxylate aminotransferase 1 peroxisomal and mitochondrial targeting. A survey of its subcellular distribution in the livers of various representatives of the classes Mammalia, Aves and Amphibia. *Eur J Cell Biol* **1994,** *64* (2), 295-313.
[20] Huber, P. A.;Birdsey, G. M.;Lumb, M. J.;Prowse, D. T.;Perkins, T. J.;Knight, D. R.;Danpure, C. J., Peroxisomal import of human alanine:glyoxylate aminotransferase requires ancillary targeting information remote from its C terminus. *J Biol Chem* **2005,** *280* (29), 27111-20.
[21] Knott, T. G.;Birdsey, G. M.;Sinclair, K. E.;Gallagher, I. M.;Purdue, P. E.;Danpure, C. J., The peroxisomal targeting sequence type 1 receptor, Pex5p, and the peroxisomal import efficiency of alanine:glyoxylate aminotransferase. *Biochem J* **2000,** *352 Pt 2*, 409-18.

[22] Fodor, K.;Wolf, J.;Erdmann, R.;Schliebs, W.;Wilmanns, M., Molecular requirements for peroxisomal targeting of alanine-glyoxylate aminotransferase as an essential determinant in primary hyperoxaluria type 1. *PLoS Biol* **2012,** *10* (4), e1001309.
[23] Purdue, P. E.;Lumb, M. J.;Fox, M.;Griffo, G.;Hamon-Benais, C.;Povey, S.;Danpure, C. J., Characterization and chromosomal mapping of a genomic clone encoding human alanine:glyoxylate aminotransferase. *Genomics* **1991,** *10* (1), 34-42.
[24] Purdue, P. E.;Takada, Y.;Danpure, C. J., Identification of mutations associated with peroxisome-to-mitochondrion mistargeting of alanine/glyoxylate aminotransferase in primary hyperoxaluria type 1. *J Cell Biol* **1990,** *111* (6 Pt 1), 2341-51.
[25] Purdue, P. E.;Lumb, M. J.;Allsop, J.;Danpure, C. J., An intronic duplication in the alanine: glyoxylate aminotransferase gene facilitates identification of mutations in compound heterozygote patients with primary hyperoxaluria type 1. *Hum Genet* **1991,** *87* (4), 394-6.
[26] Lumb, M. J.;Danpure, C. J., Functional synergism between the most common polymorphism in human alanine:glyoxylate aminotransferase and four of the most common disease-causing mutations. *J Biol Chem* **2000,** *275* (46), 36415-22.
[27] Purdue, P. E.;Allsop, J.;Isaya, G.;Rosenberg, L. E.;Danpure, C. J., Mistargeting of peroxisomal L-alanine:glyoxylate aminotransferase to mitochondria in primary hyperoxaluria patients depends upon activation of a cryptic mitochondrial targeting sequence by a point mutation. *Proc Natl Acad Sci U S A* **1991,** *88* (23), 10900-4.
[28] Lumb, M. J.;Drake, A. F.;Danpure, C. J., Effect of N-terminal alpha-helix formation on the dimerization and intracellular targeting of alanine:glyoxylate aminotransferase. *J Biol Chem* **1999,** *274* (29), 20587-96.
[29] Cellini, B.;Lorenzetto, A.;Montioli, R.;Oppici, E.;Voltattorni, C. B., Human liver peroxisomal alanine:glyoxylate aminotransferase: Different stability under chemical stress of the major allele, the minor

allele, and its pathogenic G170R variant. *Biochimie* **2010,** *92* (12), 1801-11.
[30] Hopper, E. D.;Pittman, A. M.;Fitzgerald, M. C.;Tucker, C. L., In vivo and in vitro examination of stability of primary hyperoxaluria-associated human alanine:glyoxylate aminotransferase. *J Biol Chem* **2008,** *283* (45), 30493-502.
[31] Coulter-Mackie, M. B.;Lian, Q., Consequences of missense mutations for dimerization and turnover of alanine:glyoxylate aminotransferase: study of a spectrum of mutations. *Mol Genet Metab* **2006,** *89* (4), 349-59.
[32] Purdue, P. E.;Lumb, M. J.;Allsop, J.;Minatogawa, Y.;Danpure, C. J., A glycine-to-glutamate substitution abolishes alanine:glyoxylate aminotransferase catalytic activity in a subset of patients with primary hyperoxaluria type 1. *Genomics* **1992,** *13* (1), 215-8.
[33] Williams, E.;Rumsby, G., Selected exonic sequencing of the AGXT gene provides a genetic diagnosis in 50% of patients with primary hyperoxaluria type 1. *Clin Chem* **2007,** *53* (7), 1216-21.
[34] Minatogawa, Y.;Tone, S.;Allsop, J.;Purdue, P. E.;Takada, Y.;Danpur, C. J.;Kido, R., A serine-to-phenylalanine substitution leads to loss of alanine:glyoxylate aminotransferase catalytic activity and immunoreactivity in a patient with primary hyperoxaluria type 1. *Hum Mol Genet* **1992,** *1* (8), 643-4.
[35] Danpure, C. J.;Purdue, P. E.;Fryer, P.;Griffiths, S.;Allsop, J.;Lumb, M. J.;Guttridge, K. M.;Jennings, P. R.;Scheinman, J. I.;Mauer, S. M.;et al., Enzymological and mutational analysis of a complex primary hyperoxaluria type 1 phenotype involving alanine:glyoxylate aminotransferase peroxisome-to-mitochondrion mistargeting and intraperoxisomal aggregation. *Am J Hum Genet* **1993,** *53* (2), 417-32.
[36] Danpure, C. J., Primary hyperoxaluria type 1: AGT mistargeting highlights the fundamental differences between the peroxisomal and mitochondrial protein import pathways. *Biochim Biophys Acta* **2006,** *1763* (12), 1776-84.

[37] Coulter-Mackie, M. B.;Applegarth, D.;Toone, J. R.;Henderson, H., The major allele of the alanine:glyoxylate aminotransferase gene: seven novel mutations causing primary hyperoxaluria type 1. *Mol Genet Metab* **2004,** *82* (1), 64-8.
[38] Salido, E. C.;Li, X. M.;Lu, Y.;Wang, X.;Santana, A.;Roy-Chowdhury, N.;Torres, A.;Shapiro, L. J.;Roy-Chowdhury, J., Alanine-glyoxylate aminotransferase-deficient mice, a model for primary hyperoxaluria that responds to adenoviral gene transfer. *Proc Natl Acad Sci U S A* **2006,** *103* (48), 18249-54.
[39] Cellini, B.;Montioli, R.;Paiardini, A.;Lorenzetto, A.;Voltattorni, C. B., Molecular Insight into the Synergism between the Minor Allele of Human Liver Peroxisomal Alanine:Glyoxylate Aminotransferase and the F152I Mutation. *J Biol Chem* **2009,** *284* (13), 8349-58.
[40] Cellini, B.;Montioli, R.;Paiardini, A.;Lorenzetto, A.;Maset, F.;Bellini, T.;Oppici, E.;Voltattorni, C. B., Molecular defects of the glycine 41 variants of alanine glyoxylate aminotransferase associated with primary hyperoxaluria type I. *Proc Natl Acad Sci U S A* **2010,** *107* (7), 2896-901.
[41] Pey, A. L.;Salido, E.;Sanchez-Ruiz, J. M., Role of low native state kinetic stability and interaction of partially unfolded states with molecular chaperones in the mitochondrial protein mistargeting associated with primary hyperoxaluria. *Amino Acids* **2011,** *41* (5), 1233-45.
[42] Pittman, A. M.;Lage, M. D.;Poltoratsky, V.;Vrana, J. D.;Paiardini, A.;Roncador, A.;Cellini, B.;Hughes, R. M.;Tucker, C. L., Rapid profiling of disease alleles using a tunable reporter of protein misfolding. *Genetics* **2012,** *192* (3), 831-42.
[43] Coulter-Mackie, M. B.;Lian, Q., Partial trypsin digestion as an indicator of mis-folding of mutant alanine:glyoxylate aminotransferase and chaperone effects of specific ligands. Study of a spectrum of missense mutants. *Mol Genet Metab* **2008,** *94* (3), 368-74.
[44] Santana, A.;Salido, E.;Torres, A.;Shapiro, L. J., Primary hyperoxaluria type 1 in the Canary Islands: a conformational disease

due to I244T mutation in the P11L-containing alanine:glyoxylate aminotransferase. *Proc Natl Acad Sci U S A* **2003,** *100* (12), 7277-82.
[45] Fargue, S.;Lewin, J.;Rumsby, G.;Danpure, C. J., Four of the most common mutations in primary hyperoxaluria type 1 unmask the cryptic mitochondrial targeting sequence of alanine:glyoxylate aminotransferase encoded by the polymorphic minor allele. *J Biol Chem* **2012**.
[46] Cellini, B.;Montioli, R.;Bianconi, S.;Lopez-Alonso, J. P.;Voltattorni, C. B., Construction, purification and characterization of untagged human liver alanine-glyoxylate aminotransferase expressed in Escherichia coli. *Protein Pept Lett* **2008,** *15* (2), 153-9.
[47] Cellini, B.;Bertoldi, M.;Borri Voltattorni, C., Treponema denticola cystalysin catalyzes beta-desulfination of L-cysteine sulfinic acid and beta-decarboxylation of L-aspartate and oxalacetate. *FEBS Lett* **2003,** *554* (3), 306-10.
[48]Pace, C. N., Shirley, B.A., Thompson, J.T., *Measuring the conformational stability of a protein*. IRL

Press, Oxford, England.: 1989; p 311-330.
[49] Niesen, F. H.;Berglund, H.;Vedadi, M., The use of differential scanning fluorimetry to detect ligand interactions that promote protein stability. *Nat Protoc* **2007,** *2* (9), 2212-21.
[50] Kabsch, W., Xds. *Acta Crystallogr D Biol Crystallogr* **2010,** *66* (Pt 2), 125-32.
[51] Evans, P. R., SCALA. *Joint CCP4 and ESF-EAMBC Newletter on Protein Crystallography* **1997,** *22*, 2.
[52] McCoy, A. J.;Grosse-Kunstleve, R. W.;Adams, P. D.;Winn, M. D.;Storoni, L. C.;Read, R. J., Phaser crystallographic software. *J Appl Crystallogr* **2007,** *40* (Pt 4), 658-674.
[53] Murshudov, G. N.;Vagin, A. A.;Dodson, E. J., Refinement of macromolecular structures by the maximum-likelihood method. *Acta Crystallogr D Biol Crystallogr* **1997,** *53* (Pt 3), 240-55.

[54] Emsley, P.;Cowtan, K., Coot: model-building tools for molecular graphics. *Acta Crystallogr D Biol Crystallogr* **2004,** *60* (Pt 12 Pt 1), 2126-32.
[55] Chen, V. B.;Arendall, W. B., 3rd;Headd, J. J.;Keedy, D. A.;Immormino, R. M.;Kapral, G. J.;Murray, L. W.;Richardson, J. S.;Richardson, D. C., MolProbity: all-atom structure validation for macromolecular crystallography. *Acta Crystallogr D Biol Crystallogr* **2010,** *66* (Pt 1), 12-21.
[56] Collaborative Computational Project, N., The CCP4 suite: programs for protein crystallography. *Acta Crystallogr D Biol Crystallogr* **1994,** *50* (Pt 5), 760-3.
[57] Coulter-Mackie, M. B.;Lian, Q.;Applegarth, D.;Toone, J., The major allele of the alanine:glyoxylate aminotransferase gene: nine novel mutations and polymorphisms associated with primary hyperoxaluria type 1. *Mol Genet Metab* **2005,** *86* (1-2), 172-8.
[58] von Schnakenburg, C.;Rumsby, G., Identification of new mutations in primary hyperoxaluria type 1 (PH1). *J Nephrol* **1998,** *11 Suppl 1*, 15-7.
[59] Yano, T.;Kuramitsu, S.;Tanase, S.;Morino, Y.;Kagamiyama, H., Role of Asp222 in the catalytic mechanism of Escherichia coli aspartate aminotransferase: the amino acid residue which enhances the function of the enzyme-bound coenzyme pyridoxal 5'-phosphate. *Biochemistry* **1992,** *31* (25), 5878-87.
[60] Coulter-Mackie, M. B.;Lian, Q.;Wong, S. G., Overexpression of human alanine:glyoxylate aminotransferase in Escherichia coli: renaturation from guanidine-HCl and affinity for pyridoxal phosphate co-factor. *Protein Expr Purif* **2005,** *41* (1), 18-26.
[61] Oppici, E.;Montioli, R.;Lorenzetto, A.;Bianconi, S.;Borri Voltattorni, C.;Cellini, B., Biochemical analyses are instrumental in identifying the impact of mutations on holo and/or apo-forms and on the region(s) of alanine:glyoxylate aminotransferase variants associated with primary hyperoxaluria type I. *Mol Genet Metab* **2012,** *105* (1), 132-40.

[62] Hendlich, M.;Rippmann, F.;Barnickel, G., LIGSITE: automatic and efficient detection of potential small molecule-binding sites in proteins. *J Mol Graph Model* **1997,** *15* (6), 359-63, 389.
[63] Eliot, A. C.;Kirsch, J. F., Pyridoxal phosphate enzymes: mechanistic, structural, and evolutionary considerations. *Annu Rev Biochem* **2004,** *73*, 383-415.
[64] Monico, C. G.;Rossetti, S.;Olson, J. B.;Milliner, D. S., Pyridoxine effect in type I primary hyperoxaluria is associated with the most common mutant allele. *Kidney Int* **2005,** *67* (5), 1704-9.
[65] Pons, R.;Ford, B.;Chiriboga, C. A.;Clayton, P. T.;Hinton, V.;Hyland, K.;Sharma, R.;De Vivo, D. C., Aromatic L-amino acid decarboxylase deficiency: clinical features, treatment, and prognosis. *Neurology* **2004,** *62* (7), 1058-65.
[66] Manegold, C.;Hoffmann, G. F.;Degen, I.;Ikonomidou, H.;Knust, A.;Laass, M. W.;Pritsch, M.;Wilichowski, E.;Horster, F., Aromatic L-amino acid decarboxylase deficiency: clinical features, drug therapy and follow-up. *J Inherit Metab Dis* **2009,** *32* (3), 371-80.
[67] Allen, G. F.;Land, J. M.;Heales, S. J., A new perspective on the treatment of aromatic L-amino acid decarboxylase deficiency. *Mol Genet Metab* **2009,** *97* (1), 6-14.
[68] Montioli, R.;Cellini, B.;Borri Voltattorni, C., Molecular insights into the pathogenicity of variants associated with the aromatic amino acid decarboxylase deficiency. *J Inherit Metab Dis* **2011,** *34* (6), 1213-24.

PUBLICATIONS

Molecular defects of the glycine 41 variants of alanine glyoxylate aminotransferase associated with primary hyperoxaluria type I

Barbara Cellini[a,1], Riccardo Montioli[a,1], Alessandro Paiardini[b], Antonio Lorenzetto[a], Fabio Maset[c], Tiziana Bellini[d], Elisa Oppici[a], and Carla Borri Voltattorni[a,2]

[a]Dipartimento di Scienze Morfologico-Biomediche, Sezione di Chimica Biologica, Facoltà di Medicina e Chirurgia, Università degli Studi di Verona, Strada Le Grazie, 8, 37134 Verona, Italy; [b]Dipartimento di Scienze Biochimiche "A. Rossi Fanelli" and Centro di Biologia Molecolare del Consiglio Nazionale delle Ricerche, Università "La Sapienza", 00185 Rome, Italy; [c]Dipartimento di Scienze Farmaceutiche, Università di Padua, via Marzolo 5, 35131 Padua, Italy; and [d]Dipartimento di Biochimica e Biologia Molecolare, Università di Ferrara, via Borsari 46, 44100 Ferrara, Italy

Edited by Gregory A. Petsko, Brandeis University, Waltham, MA, and approved December 31, 2009 (received for review July 31, 2009)

G41 is an interfacial residue located within the α-helix 34–42 of alanine:glyoxylate aminotransferase (AGT). Its mutations on the major (AGT-Ma) or the minor (AGT-Mi) allele give rise to the variants G41R-Ma, G41R-Mi, and G41V-Ma causing hyperoxaluria type 1. Impairment of dimerization in these variants has been suggested to be responsible for immunoreactivity deficiency, intraperoxisomal aggregation, and sensitivity to proteasomal degradation. However, no experimental evidence supports this view. Here we report that G41 mutations, besides increasing the dimer-monomer equilibrium dissociation constant, affect the protein conformation and stability, and perturb its active site. As compared to AGT-Ma or AGT-Mi, G41 variants display different near-UV CD and intrinsic emission fluorescence spectra, larger exposure of hydrophobic surfaces, sensitivity to Met53-Tyr54 peptide bond cleavage by proteinase *K*, decreased thermostability, reduced coenzyme binding affinity, and catalytic efficiency. Additionally, unlike AGT-Ma and AGT-Mi, G41 variants under physiological conditions form insoluble inactive high-order aggregates (~5,000 nm) through intermolecular electrostatic interactions. A comparative molecular dynamics study of the putative structures of AGT-Mi and G41R-Mi predicts that G41 → R mutation causes a partial unwinding of the 34–42 α-helix and a displacement of the first 44 N-terminal residues including the active site loop 24–32. These simulations help us to envisage the possible structural basis of AGT dysfunction associated with G41 mutations. The detailed insight into how G41 mutations act on the structure-function of AGT may contribute to achieve the ultimate goal of correcting the effects of these mutations.

dimer interface | pathogenic variant | protein aggregation | pyridoxal 5'-phosphate

Alanine:glyoxylate aminotransferase (AGT) is a homodimeric pyridoxal 5′-phosphate (PLP) dependent enzyme which catalyzes the interconversion of L-alanine and glyoxylate into pyruvate and glycine. Human AGT has been cloned, expressed in *E. coli* and purified. The enzyme crystal structure, complexed with the competitive inhibitor amino-oxyacetic acid, was determined at a resolution of 2.5 Å. Each subunit includes a N-terminal extension (residues 1–21), a large N-terminal domain (residues 22–282) containing the PLP-binding lysine (K209), and a smaller C-terminal domain (residues 283–392) (1). Steady-state and pre-steady-state kinetic studies featuring the AGT transamination revealed high specificity for glyoxylate to glycine processing, consistent with a key role of AGT in glyoxylate detoxification (2). The human liver-specific AGT is localized in the peroxisomal matrix (3). The enzyme has been the focus of extensive clinical research because its functional deficiency causes primary hyperoxaluria type 1 (PH1). PH1 is a rare autosomal recessive disorder characterized by excessive synthesis and excretion of oxalate and glycolate, and progressive accumulation of insoluble oxalate in the kidneys and urinary tract (4). The AGT gene (*AGXT*) occurs normally as one of the two allelic forms: the major (AGT-Ma) or minor (AGT-Mi) alleles. The latter, comprising two coding polymorphisms, P11L and I340M, and a noncoding duplication in intron 1 (5), has no dramatic effect on the properties of AGT. To date, well over 100 pathogenic mutations associated to AGT-Ma and/or AGT-Mi are known (6). Three categories of enzymatic phenotypes causing PH1 can be identified: deficiency of AGT catalytic activity but not AGT immunoreactivity, catalytic activity and immunoreactivity deficiency, and mistargeting to mitochondria (4, 7). Notably, clinical data for single PH1 AGT mutations are generally limited to a small number of individuals, which may interfere with identifying clear correlations between disease characteristics and properties of mutant proteins. Currently, the way of treatment of this progressive and potentially fatal disease is poor, as the molecular bases of the effects of the various disease-associated point mutations are unknown. In the last years, a biochemical characterization of the pathogenic variants G82E-Ma and F152I-Mi allowed us to correlate the clinical and enzymatic phenotypes with the structural and functional properties of the corresponding variants (2, 8).

The G41 series of pathogenic mutations, including the G41R encoded on the background of the major (G41R-Ma) and the minor (G41R-Mi) alleles, and the G41V, which only cosegregates with the major allele (G41V-Ma), is of special interest because (*i*) G41 is an interfacial residue making van der Waals contacts with the same residue of the other subunit and belongs to an α-helix connected with the active site loop 24–32 (Fig. S1), (*ii*) G41R mutation is more severe when it occurs on AGT-Mi than on AGT-Ma (4), and (*iii*) responsiveness to pyridoxine therapy for the patients bearing these mutations is so far unknown (9). Previous clinical and cell biochemical studies suggested that the weakening of the dimeric structure of AGT consequent to G41 replacements could be responsible for depletion of immunoreactive AGT, its intraperoxisomal aggregation (4, 10), and sensitivity to proteasomal degradation (11, 12). Because formal proves of the effect of these mutations at the molecular level are so far absent, we thought to provide insights into the molecular basis of the G41 mutation's pathogenicity. Biochemical data indicate that G41 mutations, besides causing a weakening of the intersubunit interaction, alter the conformational state of the AGT dimeric form, reduce its resistance to thermal inactivation

Author contributions: B.C., R.M., and C.B.V. designed research; B.C., R.M., A.P., A.L., F.M., T.B., and E.O. performed research; B.C., R.M., A.P., and C.B.V. analyzed data; C.B.V. wrote the paper.

The authors declare no conflict of interest.

This article is a PNAS Direct Submission.

[1]B.C. and R.M. contributed equally to this work.

[2]To whom correspondence should be addressed. E-mail: carla.borrivoltattorni@univr.it.

This article contains supporting information online at www.pnas.org/cgi/content/full/0908565107/DCSupplemental.

and unfolding, and induce susceptibility to proteolytic degradation and self-aggregation. Moreover, predictions of the structural effects caused by G41 mutation by means of molecular dynamics (MD) provide a possible interpretation and explanation of our in vitro results.

Results

G41 Mutations Affect the Spectral Features and the Coenzyme Binding Affinity. Like AGT-Ma and AGT-Mi, G41 variants bind 2 mol of PLP per dimer, and exhibit visible absorbance and CD spectra similar to those of AGT-Ma or AGT-Mi, even if their absorbance and dichroic maxima are about 10–12 nm blue shifted (Fig. S2 and *Inset*). The $K_{D(PLP)}$ values for G41R-Ma, G41V-Ma, and G41R-Mi were found to be 1.5 ± 0.4, 0.55 ± 0.1, and 6.0 ± 0.5 μM, respectively, that are ~6-, 2-, and 23-fold higher than that of AGT-Ma or AGT-Mi (2, 8). Both AGT-Ma and AGT-Mi bind pyridoxamine 5′-phosphate (PMP) with a $K_{D(PMP)}$ value $\ll 0.1$ μM, whereas even a prolonged time of incubation of the apo forms of G41 variants with PMP (up to 5 mM) does not result in a dichroic signal at 340 nm, typical of the AGT-PMP complex (2). Thus, G41 mutations exert a decrease in the PLP binding affinity and a dramatic reduction in the PMP binding affinity. The comparison of near-UV CD spectra as well as of intrinsic and 1-anilinonaphthalene sulfonic acid (ANS) fluorescence spectra of AGT-Ma, AGT-Mi, and G41 variants provides evidence that a different conformation exists between each apoenzymatic form and the corresponding holo form, and between the holo and apo forms of G41 variants and the corresponding forms of AGT-Ma or AGT-Mi (Fig. S3*A* and *B*). These data imply that (*i*) conformational changes seem to accompany the apo to holo transition for each enzymatic form, and (*ii*) G41 mutations affect the overall conformation of both holo and apo AGT.

The far-UV CD spectra of G41 variants have been compared with those of AGT-Ma and AGT-Mi. All spectra exhibit minima at 210 and 222 nm, typical of proteins containing appreciable amounts of α-helix. However, spectra deconvolution reveals that AGT-Ma, AGT-Mi, and G41V-Ma have an identical composition of the overall secondary structure, whereas both G41R-Ma and G41R-Mi display about 5% less α-helical content.

G41 Mutations Slightly Affect the Kinetic Parameters. The kinetic parameters of AGT-Ma, AGT-Mi, and G41 variants for the pair alanine-glyoxylate are reported in Table S1. The K_m values of G41 variants for L-alanine and glyoxylate are not significantly altered, whereas the k_{cat} values decrease by 1.5–3.5-fold as compared to those of the corresponding AGT-Ma and AGT-Mi. Altogether, these data indicate that the G41 mutations slightly affect the catalytic properties of AGT.

G41 mutations increase the dimer-monomer equilibrium dissociation constant (K_d). As a first step to investigate the impact of G41 mutations on the AGT dimeric structure, photo-induced cross-linking experiments with Tris(2,2′-bipyridyl) ruthenium(II) chloride (TBPR) have been carried out at 1 μM enzyme concentration. TBPR cross-linking is incomplete and also gives rise to the formation of aggregates and intramolecular cross-linked monomers. Nevertheless, it is possible to estimate the relative population of chemically cross-linked dimer to monomer with similar results for all the holo species, but lower for apo G41 variants than for apoAGT-Ma and apoAGT-Mi (Fig. S4). To validate these data we used the very accurate and sensitive size-exclusion chromatography (SEC) method. Holo and apo forms of AGT-Ma and AGT-Mi as well as the holo forms of the G41 variants from 5 to 0.1 μM concentration (the latter value being the detection limit), eluted as a single peak with a retention volume corresponding to a dimer. Thus, the K_d values of these species must be $\ll 0.1$ μM. On the other hand, the apo forms of G41 variants over the range $50 - 0.1$ μM enzyme concentration eluted as a single peak whose position varied between the dimeric and the monomeric forms of the enzyme, indicating a rapid equilibrium process. Plots of the percent dimer as a function of apoG41R-Ma and apoG41R-Mi concentrations give hyperbolic-like curves, the linear transformation of which yields the K_d values of 0.32 ± 0.05 and 1.8 ± 0.5 μM, respectively. In the case of apoG41V-Ma, a decrease of the integrated peak area starts at 1.5 μM reaching at 0.1 μM a value about 30% of the one expected, possibly because of monomerization followed by artefactual aggregation. A K_d value ranging from 1.5 to 0.1 μM can be estimated for this mutant. The SEC results, consistent with those of cross-linking analyses, do not allow to quantify the impact of G41 mutations on the K_d value of holoAGT, but clearly indicate that the mutations increase the K_d value of apoAGT.

G41 Mutations Induce Susceptibility to Proteinase *K* Digestion. Limited proteolysis was used to further probe that replacements of G41 change the overall conformation of AGT. AGT-Ma, AGT-Mi, and the G41 variants in the holo and apo forms were incubated in 100 mM potassium phosphate buffer, pH 7.4, at 25 °C with proteinase *K* at different AGT/protease weight ratios (from 5,000/1 to 100/1). When aliquots of these reaction mixtures were withdrawn at different times and subjected to SDS-PAGE, it was observed that, although the size of the band (~42.7 kDa) corresponding to the intact holo or apo forms of AGT-Ma and AGT-Mi remains unaltered even after a prolonged time of incubation (Fig. S5*A*), that of G41 variants gradually decreases and simultaneously a faster migrating band (~40.2 kDa) appears. Both the 42.7 and 40.2 kDa bands stain with antibody raised against the C-terminal hexahistidine tag, as revealed by Western blot analysis, indicating that the cleavage occurs within the N terminus. In fact, Maldi-mass spectrometry analysis yields a molecular weight difference for the N terminus truncated fragment of 5503 ± 15 atomic mass unit compared with the full-length G41R mutant, compatible with a cleavage site located at the peptide bond Met53-Tyr54. The effect of proteinase *K* on holo G41R-Mi is shown in Fig. 1, and that on holo G41V-Ma in Fig. S5*B*. The initial velocity values of the cleavage (expressed as μg enzyme/min/μg proteinase *K*) determined by measuring the decrease of the intensity of the band corresponding to the intact enzyme, are 4 ± 1, 530 ± 40, and 6 ± 1 for the holo forms of G41R-Ma, G41R-Mi, and G41V-Ma, respectively, and 130 ± 30, 870 ± 90, and 30 ± 6 for the corresponding apo forms. The proteolytic cleavage is accompanied by a time dependent loss of transaminase activity occurring for holoG41R-Mi with an initial velocity of 420 ± 50 μg mutant/min/μg proteinase *K*, a value that agrees with that of degradation. At a 10/1 AGT/proteinase *K* weight ratio, G41 variants are degraded in less than a half-hour to low molecular weight peptides, whereas AGT-Ma and AGT-Mi remain unaltered. Altogether these data indicate that, unlike

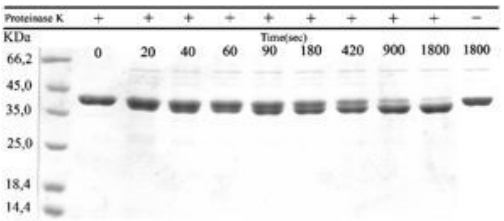

Fig. 1. Effect of proteinase *K* on holoG41R-Mi. HoloG41R-Mi (15 μM) was incubated at 25 °C in 100 mM potassium phosphate buffer, pH 7.4, at a 1,000/1 (wt/wt) mutant/proteinase *K* ratio. At times indicated, aliquots were removed, treated (see *Methods*), and subjected to 12% SDS-PAGE. Plus and minus signs indicate presence or absence of proteinase *K*.

AGT-Ma and AGT-Mi, G41 variants undergo digestion and concomitant inactivation more pronounced for their apo than for the corresponding holo forms.

G41 mutations induce formation of high order inactive aggregates. We noticed that, unlike AGT-Ma and AGT-Mi, holoG41 variants at an ionic strength (I) value lower than 260 mM and/or at an enzyme concentration higher than 10 μM form visible insoluble aggregates. When these solutions are centrifuged, a yellow pellet indicative of PLP-bound aggregates appears. The specific activity of the precipitates resuspended in the assay buffer is <5% than that of the supernatant containing the dimeric species. This observation, together with the documented presence of intraperoxisomal aggregates in patients bearing G41R mutation (10), led us to investigate in some detail this phenomenon by means of turbidimetry and dynamic light scattering (DLS) studies under physiological conditions, i.e., at 37 °C, pH 7.4 at I = 150 mM. As shown in Fig. 2, significant changes in turbidity began after a lag phase ranging from 50 to 120 min for both the holo and apo forms of G41R-Mi as well as for the apo forms of G41R-Ma and G41V-Ma. No turbidity could be detected for these enzymatic species at pH 7.4, and I = 260 mM at either 25 °C or 37 °C at least over a 5 h interval. Fig. 3*A* and *B* show plots of the total count rate as a function of time for holo and apoenzymes of AGT-Ma, AGT-Mi, and G41 variants. The increase in count rate for the holo and apo forms of AGT-Ma and AGT-Mi is very slow, whereas the more typical fast aggregation for G41 variants could be seen with the count rate leveling off after ~20–40 min. The decrease in the light scattering intensity occurring for holoG41R-Mi and for the apo forms of G41 variants is due to precipitation of the protein aggregates. Altogether, the turbidity and DLS data indicate that (*i*) replacements of G41 are responsible for the propensity of mutants to self-association, the extent of which is more pronounced for the apo forms than for the corresponding holo forms, and (*ii*) G41R-Mi results the variant most prone to aggregation. The molecular size of the species present in the enzymic solutions has been also evaluated. The particle size of the dimeric form of AGT-Ma, AGT-Mi, and G41 variants, measured at 25 °C, pH 7.4, at I = 260 mM, i.e., under conditions of no detectable association, is about 10 nm. This value is consistent either with that (9.32 nm) derived from the X-ray structure (1) or that (7 ± 2 nm) calculated by an appropriate empirical equation (13). When the aggregation process occurring under the physiological conditions mentioned above was followed by DLS,

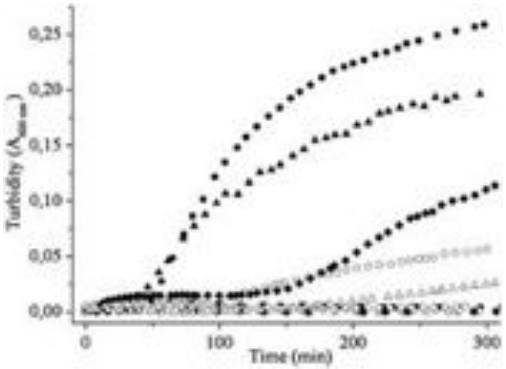

Fig. 2. Time dependence of turbidity of AGT-Ma, AGT-Mi, and G41 variants. Absorbance at 600 nm as a function of time of 4 μM apo forms of AGT-Ma (■), AGT-Mi (▼), G41R-Ma (▲), G41V-Ma (◆), and G41R-Mi (•) in potassium phosphate buffer, pH 7.4, I = 150 mM at 37 °C. Corresponding holoenzymes, open symbols.

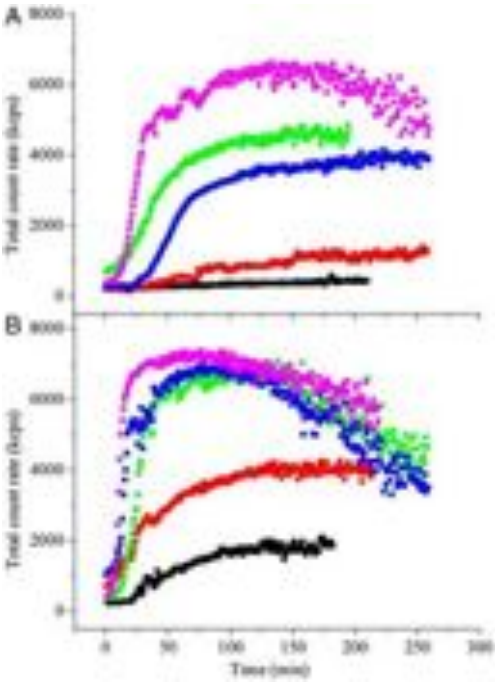

Fig. 3. Time-dependence of total count rate (measured as kilo counts per second) of AGT-Ma, AGT-Mi, and G41 variants in the holo (*A*) and apo (*B*) forms. Measurements performed at 4 μM enzyme concentration, 37 °C, I = 150 mM, pH 7.4. Color code: black, AGT-Ma; red, AGT-Mi; blue, G41R-Ma; green, G41V-Ma; fuchsia, G41R-Mi.

the time dependence of the apparent particle size indicates that the 10 nm species is always present for holo and apo AGT-Ma and holoAGT-Mi, although small aggregates (100–800 nm) appear after about 30 min (Fig. 4*A* and *B*). Considering that the scattering intensity is proportional to the sixth power of the particle diameter, the dimer must be in these species very abundant in number. In contrast, the dimer disappears over a 5–75 min time range, depending on the enzymatic species, for AGT-Mi in the apo form and for G41 variants in both the holo and apo forms. Moreover, whereas only small aggregates (100–800 nm) accumulate in apoAGT-Mi, in G41 variants a distinct population of higher-order aggregates (~5,000 nm), along with small aggregates, can be identified (Fig. 4*B–E*). From these data it can be also envisaged that (*i*) the turbidity is mainly associated to the presence of high-order aggregates, and (*ii*) the lack of detectable turbidity for G41R-Ma and G41V-Ma in the holo form could be ascribed to the very low fractional contribution of the larger particles to the total scattering intensity.

The effect of 200 mM trimethylamine-N-oxide (TMAO) or 100 mM betaine [two osmolytes known to suppress protein aggregation (14)] on the aggregation process of holoG41R-Mi has been followed by DLS. Either TMAO or betaine, although unable to decrease the amount of and size of the aggregates formed at equilibrium, as detected by the final count rate leveling off, cause a slight increase in the lag time duration (from 10 to 20 min) and in the persistence of the dimeric species (from 35 to 70 min) in the aggregation kinetics.

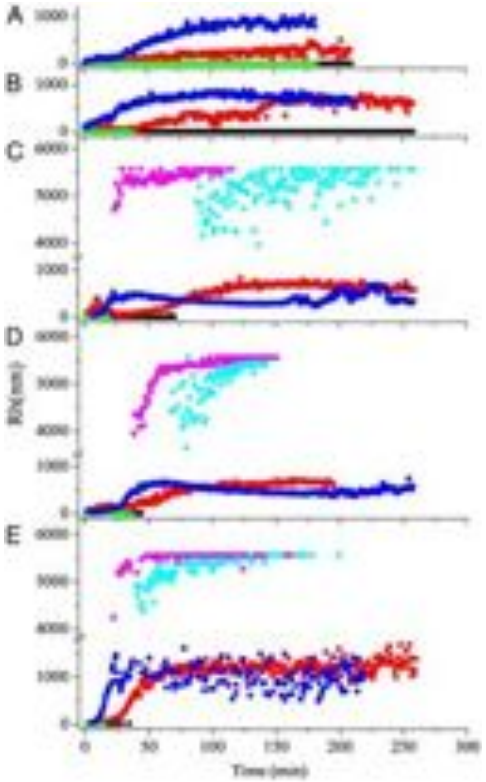

Fig. 4. Time dependence of the apparent diameters of AGT-Ma, AGT-Mi, and G41 variants. Experimental conditions (see legend to Fig. 3). (*A*) holo and apo AGT-Ma. (*B*) holo and apo AGT-Mi. (*C*) holo and apo G41R-Ma. (*D*) holo and apo G41V-Ma. (*E*) holo and apo G41R-Mi. Color code: black, holo dimer; green, apo dimer; red, holo small aggregates; blue, apo small aggregates; cyan, holo high aggregates; fuchsia, apo high aggregates.

G41 Mutations Decrease Resistance to Thermal Denaturation and Inactivation. A differential calorimetric study (DSC) was carried out to reveal the impact of G41 mutations against thermal denaturation. Thermal denaturation of holo and apo forms of AGT-Ma, AGT-Mi, G41R-Ma, and G41V-Ma as well as of holo form of G41R-Mi produces DSC profiles consisting of an endothermic transition due to the protein denaturation followed by a large exothermic transition due to the aggregation of the denaturated protein (Fig. S6), precluding the peaks deconvolution. Thus, the maxima of the endothermic transitions of these species represent apparent melting temperature (Tm) values. The Tm of apoG41R-Mi could not be determined because of the lack of an observable transition, possibly due to overlapping of the denaturation and aggregation processes (Table 1). The thermal effect on the catalytic function of AGT-Ma, AGT-Mi, and G41 variants was also measured, and the transition midpoints of thermal inactivation (Ti) are reported in Table 1. The results indicate that (*i*) holo AGT-Ma, AGT-Mi, and G41 variants display Tm and Ti values higher than those of the corresponding apoenzymes, which supports different conformational states of holo and apo forms, (*ii*) AGT-Ma is more resistant than AGT-Mi, and (*iii*) G41 mutations decrease the thermal stability, being G41R-Mi the most thermally instable variant.

Table 1. Transition midpoints of thermal denaturation (Tm) and inactivation (Ti) of AGT-Ma, AGT-Mi, and G41 variants

Enzyme	Holo form	Apo form	Holo form	Apo form
	Tm*, °C		Ti†, °C	
AGT-Ma	77.3	62.4	77.4	59.1
AGT-Mi	73.2	55.6	72.6	52.2
G41R-Ma	60.3	57.6	57.7	53.0
G41R-Mi	53.7	ND	51.8	46.0
G41V-Ma	61.0	58.3	62.3	54.5

ND, not detectable.

*They represent apparent Tm values and are the mean of two independent experiments. The error is within ±0.3 °C error.

†Data inactivation points were subjected to nonlinear regression analysis and Ti values were calculated. The data are the means of at least two independent experiments. The standard error of the mean was less than 5% of the mean value in every case.

MD studies. We examined in a comparative way the conformational space sampled by the putative structures of AGT-Mi and G41R-Mi by high-temperature (500 K) MD simulations with explicit water solvation. Both AGT-Mi and G41-Mi reach an equilibrated state after ~100 ps (Fig. S7*A*), thereafter their global architecture remaining stable, as confirmed by the indicators commonly used to analyze MD simulations (Fig. S7*A–C*). Unlike that observed for AGT-Mi, a marked fluctuation can be observed for the region spanning residues 1–44 of both monomers of G41R-Mi. This region comprises the active site loop (residues 24–32) and the α-helix 34–42 in which the G41R substitution takes place. In particular, the MD simulation of G41R-Mi reveals that the N-terminal α-helices (residues 34–42) undergo a progressive displacement (Fig. S8), and a partial unwinding of the first and second turns

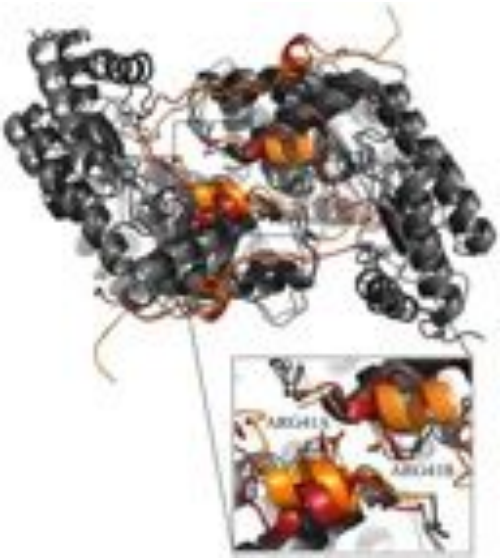

Fig. 5. Comparison of the initial 3D model of G41R-Mi (dark gray) with the averaged structure obtained from MD simulation (light gray). Residues 1–46, roughly corresponding to the N-terminal arm of G41R-Mi, are highlighted in orange for the initial 3D model and in red for the averaged structure. (*Inset*) Detail of the α-helix in which the G41R substitution takes place (residues 34–42).

of the helix (Fig. 5). It is likely that these events could be related to the accommodation of the long side chain of Arg41.

Discussion

G41, located at the end of the α-helix 34–42 of AGT, is an interfacial residue which makes van der Waals contacts with the same residue of the adjacent subunit (1). Thus, it is not surprising that (*i*) the conversion of the small, uncharged Gly41 to the bulky, charged Arg causes a ∼5% loss of α-helix content, while the conversion to Val, a larger uncharged residue, does not have a detectable effect on the overall secondary structure, and (*ii*) the apo forms of G41 variants undergo reversible dissociation of the subunits with K_d values from at least ∼3-fold to ∼20-fold higher than that of apoAGT-Ma or apoAGT-Mi. Actually, we found that G41 variants in the dimeric form differ from AGT-Ma or AGT-Mi under many respects. Their structural conformation and stability are altered, as detected by difference in the near-UV CD and intrinsic emission fluorescence spectra, larger exposure of hydrophobic surfaces, sensitivity to proteinase *K* cleavage, and decrease in Tm and Ti with respect to AGT-Ma and AGT-Mi. Additionally, G41 variants show slightly altered visible spectroscopic features, a reduced steady-state catalytic activity, and a decreased PLP binding affinity as well as a dramatic reduction in the PMP binding ability.

A comparative study of the putative structures of AGT-Mi and G41R-Mi by MD predicts that the G41R mutation would cause the partial unwinding of the α-helix 34–42 as well as the displacement of the N-terminal arm and its exposure to the environment. Although these predictions are of course not an experimental evidence of the structural effects caused by the mutation, they are consistent with the in vitro data of G41R-Mi, i.e., the 5% loss of the α-helix content and the susceptibility of the Met53-Tyr54 peptide bond to proteinase *K* cleavage. It is worth noting that, although G41 is far from the active site, it is located in the α-helix connected with the active site loop (residues 24–32) belonging to the N terminus (Fig. S1). Therefore, we might speculate that the alterations of the visible spectroscopic and catalytic features of G41 variants could be due to the rearrangements occurring around the mutated residue transmitted to the active site.

Another particularly interesting aspect is that, unlike AGT-Ma and AGT-Mi, G41 variants spontaneously form insoluble inactive high-order aggregates (∼5,000 nm) under physiological conditions of temperature, I and pH. The finding that the aggregation extent greatly decreases as I increases may be ascribed to the reduction in favorable attractive interactions due to screening effects. This behavior indicates that aggregation is not due to hydrophobic interactions, in which case the addition of salt would enhance aggregation and little effect would be seen at low I, but rather to electrostatic intermolecular interactions arising from protein charge heterogeneity. It is also worth noting that the aggregation occurs at a pH value lower than pI, thus excluding an isoelectric precipitation. Why are the G41 variants aggregation prone? In the absence of the crystal structure of these variants, the protein electrostatic potential distribution for AGT-Mi and the 1–44 N-terminus lacking form of AGT-Mi has been calculated by electrostatic computer modeling. The truncated form was chosen for comparison because it would mimic the structure of G41R-Mi upon the displacement of the N-terminal arm. As shown in Fig. 6*A* and *B*, AGT-Mi displays a highly positive charge distribution around its surface, whereas the truncated form exhibits a clear dipole segregation of charges. In fact, the depletion of the highly positively charged N-terminal arm of AGT-Mi leads to the exposure of several negatively charged residues (Asp51, Glu59, Glu62, Glu274, Glu281, Asp344, Glu346 of each monomer), i.e., to a condition of electrostatically driven self-aggregation of AGT. Thus, one can reason out that the fluctuation of the N terminus in G41R-Mi could cause the exposure of negative charged residues similar to that observed for the truncated AGT form. Although this could be a plausible explanation for the propensity of G41 variants to aggregate spontaneously, a conclusive evidence for this interpretation is lacking.

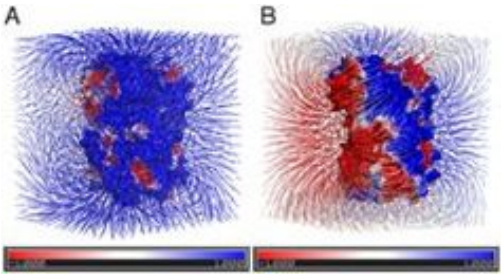

Fig. 6. Electrostatic potential surface maps of AGT-Mi and its truncated form. Electrostatic gradient and map (kT/e) of AGT-Mi (*A*), and 1–44 truncated form of AGT-Mi (*B*).

The finding that G41R-Mi displays structural and functional alterations more pronounced than G41R-Ma needs to be discussed. The thermal unfolding data indicate that the instability of G41R-Mi is due to the additive contribution of the polymorphic and pathogenic mutations. The effect of the polymorphic substitutions is possibly due to P11L in that Pro instead of Leu (*i*) contributes to the increase of structural rigidity, (*ii*) exerts additional constraints to the backbone, because the ring closure keeps its Φ angle value almost fixed, and (*iii*) makes hydrophobic interactions with a surface cavity surrounded by residues Leu14, Glu62, Gly63, Tyr66, and Ala280.

Altogether, our data assist in assessing a picture of the G41 variants enzymatic phenotype more exhaustive than that previously proposed. The pathogenicity of G41 variants has been until now related to a disruption of the interface and impairment of dimerization resulting in formation of monomers with reduced catalytic activity and prone to degradation and/or intraperoxisomal aggregation (1, 4, 15). Our in vitro results would indicate not only the impact of G41 mutations on the dimerization but also provide evidence that G41 variants in the dimeric form are prone to degradation and aggregation. The presence of aggregates only within the peroxisomal matrix in patients bearing G41R mutation (10) is consistent with this view in that the peroxisomal import machinery acts on folded dimeric proteins. In any case, it will be important to establish if the intraperoxisomal aggregates have ultrastructure similarities with the aggregates spontaneously formed in vitro. If this were the case, the electrostatically driven protein aggregation between folded dimers could represent a unique pathogenic mechanism by which G41 inherited mutations would cause protein aggregation. Indeed, many disease-related genetic mutations are known to alter the folding or stability of proteins leading to intermediates in which hydrophobic patches become exposed and prone to self-association.

Overall, our work improves the understanding of the correlation between the genotype and the enzymatic phenotype, thus allowing us to foresee the response to pyridoxine in patients carrying the G41 mutations. Administration of pyridoxine to these patients is not sufficient to counteract the disease because the molecular defects of these variants appear to be related to structural rearrangements yielding molecules that are both in the apo and the holo forms prone to degradation and aggregation. A promising therapeutic strategy could be the administration of small molecules able to stabilize the native state of the protein, thus preventing degradation and aggregation. In this regard, our preliminary results on the effects of osmolytes on the aggregation behavior of G41 variants could be an encouraging perspective.

Methods

Construction, Expression and Purification of G41 Variants. AGT-Ma and AGT-Mi were prepared as reported (2, 8). Site-directed mutagenesis, expression, and purification of G41 variants in the C-terminal His-tagged form were performed using standard procedures as described in *SI Text*.

Enzyme Activity Assays. Pyruvate formation was measured by the spectrophotometric assay already reported (2). Kinetic parameters for the pair alanine/glyoxylate of G41 variants were determined in the presence of 150 μM PLP by varying the substrate concentrations at a fixed saturating cosubstrate concentration. Data were fitted to the Michaelis–Menten equation. Thermal inactivation experiments were performed as follows: enzyme (10 μM) was incubated for 10 min in 100 mM potassium phosphate buffer, pH 7.4, at different temperatures, and then chilled on ice. Transaminase activity was measured as indicated above.

Binding Affinity for PLP. The $K_{D(PLP)}$ of G41 variants were determined by measuring the PLP-induced changes either on the intrinsic fluorescence or in the CD visible spectrum of the apoenzymes. The experimental conditions and the relative data analysis are given in *SI Text*.

Cross-Linking and SEC Experiments. Photo-induced cross-linking with TBPR was performed as previously described (7). SEC experiments were done on an Akta FPLC system (GE Healthcare) using a custom packed Sephacryl S-300 10/600 column. The data were analyzed according to the method of Manning et al. (16). Details are given in *SI Text*.

Proteinase *K* Digestion and Mass Spectrometry Analysis. Holo and apo AGT-Ma, AGT-Mi, and G41 variants (15 μM) were treated with proteinase *K* in 100 mM potassium phosphate buffer, pH 7.4, at 25 °C at various AGT/proteinase *K* (wt/wt) ratios. At various times, 15 μL-aliquots were withdrawn from the reaction mixtures and subjected to enzymatic activity assay, SDS-PAGE, and immunoblotting. The reaction was stopped by adding PMSF or EGTA to a final concentration of 2 mM to each aliquot. After staining with Coomassie blue, the band intensities were visualized and analyzed using ImageJ software (Wajne Rasband). Immunoblotting was made as described in *SI Text*. Liquid-chromatography/MS analyses of G41R-Mi were carried out with a model Mariner Esi-Tof spectrometer from PerSeptive Biosystems, connected to a C4 Grace-Vydac microbore column (1 × 50 mm). Column elution was carried out with a CH_3CN-1% HCOOH gradient from 1 to 80% in 30 min. Proteolysis reaction of G41R-Mi with proteinase *K* was analyzed with a model 4800 Plus Maldi-Tof-Tof instrument from Applied Biosystems. Samples were desalted on a P10 C4 Zip-Tip, eluted with a sinapinic acid (Sigma) saturated solution (2 μL) in CH_3CN:H_2O (60:40 by vol). Details are given in *SI Text*.

Turbidimetry Measurements. The aggregation experiments were carried out in potassium phosphate buffer, pH 7.4, at different I values and/or different enzyme concentrations. The turbidity was monitored by measuring the absorbance at 600 nm as already reported (17).

DLS Measurements. DLS measurements were made on a Zetasizer Nano S device from Malvern Instruments. The temperature of sample cell was controlled by a thermostating system within ±0.1 °C and 12.5 × 45-mm disposable cells with stopper were used. To study the aggregation kinetics, an aliquot of each enzymatic species was diluted to a final concentration of 4 μM in potassium phosphate buffer pH 7.4 at the desired I and temperature. PLP was added to the holoenzyme solutions to a final concentration of 60 μM. The buffer was filtered immediately before use to eliminate any impurities. TMAO or betaine were added to the buffer before the addition of G41R-Mi.

Spectroscopic Measurements. Absorption, fluorescence, and CD spectra were performed as described in *SI Text*.

DSC. DSC experiments were conducted with a VP-DSC microcalorimeter (Microcal) in the temperature interval from 20 to 90 °C, with a scan rate of 90 °C/h in 100 mM potassium phosphate buffer, pH 7.4, and at 5.5 μM protein concentration.

Computational Analyses. MD simulations of the molecular models of AGT-Mi and G41R-Mi, derived from the crystal structure of human AGT (1), downloaded from Brookhaven Protein Data Bank (18) were performed. A detailed description of the generation of these structures and MD simulations is given in *SI Text*. Electrostatic computations on AGT-Mi and its N terminus deleted form were carried out by solving the nonlinear Poisson–Boltzmann equation, one of the most popular continuum models for describing electrostatic interactions between molecular solutes in salty, aqueous media. Adaptive Poisson Boltzman Solver was used to this purpose (19), with a protein and solvent dielectric of 2.0 and 80.0, respectively, and I = 150 mM.

ACKNOWLEDGMENTS. We gratefully acknowledge experimental contribution and advice by V. De Filippis, O. Marin, G. Arrigoni, and F. Dallocchio. Work was supported by grants from the Oxalosis and Hyperoxaluria Foundation and M.I.U.R. (PRIN 2007) (to C.B.V.).

1. Zhang X, et al. (2003) Crystal structure of alanine:glyoxylate aminotransferase and the relationship between genotype and enzymatic phenotype in primary hyperoxaluria type 1. *J Mol Biol* 331(3):643–652.
2. Cellini B, Bertoldi M, Montioli R, Paiardini A, Borri Voltattorni C (2007) Human wild-type alanine:glyoxylate aminotransferase and its naturally occurring G82E variant: Functional properties and physiological implications. *Biochem J* 408(1): 39–50.
3. Motley A, et al. (1995) Mammalian alanine/glyoxylate aminotransferase 1 is imported into peroxisomes via the PTS1 translocation pathway. Increased degeneracy and context specificity of the mammalian PTS1 motif and implications for the peroxisome-to-mitochondrion mistargeting of AGT in primary hyperoxaluria type 1. *J Cell Biol* 131(1):95–109.
4. Danpure CJ (2005) Molecular etiology of primary hyperoxaluria type 1: New directions for treatment. *Am J Nephrol* 25(3):303–310.
5. Purdue PE, Takada Y, Danpure CJ (1990) Identification of mutations associated with peroxisome-to-mitochondrion mistargeting of alanine/glyoxylate aminotransferase in primary hyperoxaluria type 1. *J Cell Biol* 111(6 Pt 1):2341–2351.
6. Coulter-Mackie MB, Rumsby G (2004) Genetic heterogeneity in primary hyperoxaluria type 1: Impact on diagnosis. *Mol Genet Metab* 83(1–2):38–46.
7. Lumb MJ, Danpure CJ (2000) Functional synergism between the most common polymorphism in human alanine:glyoxylate aminotransferase and four of the most common disease-causing mutations. *J Biol Chem* 275(46):36415–36422.
8. Cellini B, Montioli R, Paiardini A, Lorenzetto A, Voltattorni CB (2009) Molecular insight into the synergism between the minor allele of human liver peroxisomal alanine:glyoxylate aminotransferase and the F152I mutation. *J Biol Chem* 284(13): 8349–8358.
9. Coulter-Mackie MB, Lian Q, Wong SG (2005) Overexpression of human alanine: glyoxylate aminotransferase in *Escherichia coli*: Renaturation from guanidine-HCl and affinity for pyridoxal phosphate co-factor. *Protein Expres Purif* 41(1):18–26.
10. Danpure CJ, et al. (1993) Enzymological and mutational analysis of a complex primary hyperoxaluria type 1 phenotype involving alanine:glyoxylate aminotransferase peroxisome-to-mitochondrion mistargeting and intraperoxisomal aggregation. *Am J Hum Genet* 53(2):417–432.
11. Coulter-Mackie MB, Lian Q (2008) Partial trypsin digestion as an indicator of mis-folding of mutant alanine:glyoxylate aminotransferase and chaperone effects of specific ligands. Study of a spectrum of missense mutants. *Mol Genet Metab* 94(3):368–374.
12. Coulter-Mackie MB, Lian Q (2006) Consequences of missense mutations for dimerization and turnover of alanine:glyoxylate aminotransferase: Study of a spectrum of mutations. *Mol Genet Metab* 89(4):349–359.
13. Wilkins DK, et al. (1999) Hydrodynamic radii of native and denatured proteins measured by pulse field gradient NMR techniques. *Biochemistry* 38(50):16424–16431.
14. Venkatesu P, Lee MJ, Lin HM (2007) Thermodynamic characterization of the osmolyte effect on protein stability and the effect of GdnHCl on the protein denatured state. *J Phys Chem B* 111(30):9045–9056.
15. Danpure CJ (2006) Primary hyperoxaluria type 1: AGT mistargeting highlights the fundamental differences between the peroxisomal and mitochondrial protein import pathways. *Biochim Biophys Acta* 1763(12):1776–1784.
16. Manning LR, Dumoulin A, Jenkins WT, Winslow RM, Manning JM (1999) Determining subunit dissociation constants in natural and recombinant proteins. *Methods Enzymol* 306:113–129.
17. Yong YH, Foegeding EA (2008) Effects of caseins on thermal stability of bovine beta-lactoglobulin. *J Agric Food Chem* 56(21):10352–10358.
18. Sussman JL, et al. (1998) Protein data bank (PDB): Database of three-dimensional structural information of biological macromolecules. *Acta Crystallogr D* 54(Pt 1, Pt 6): 1078–1084.
19. Baker NA, Sept D, Joseph S, Holst MJ, McCammon JA (2001) Electrostatics of nanosystems: Application to microtubules and the ribosome. *Proc Natl Acad Sci USA* 98(18):10037–10041.

Biochimie 92 (2010) 1801–1811

Contents lists available at ScienceDirect

Biochimie

journal homepage: www.elsevier.com/locate/biochi

Research paper

Human liver peroxisomal alanine:glyoxylate aminotransferase: Different stability under chemical stress of the major allele, the minor allele, and its pathogenic G170R variant

Barbara Cellini, Antonio Lorenzetto, Riccardo Montioli, Elisa Oppici, Carla Borri Voltattorni*

Dipartimento di Scienze della Vita e della Riproduzione, Sezione di Chimica Biologica, Facoltà di Medicina e Chirurgia, Università degli Studi di Verona, Strada Le Grazie, 8 37134 Verona, Italy

ARTICLE INFO

Article history:
Received 7 June 2010
Accepted 2 August 2010
Available online 14 August 2010

Keywords:
Alanine:glyoxylate aminotransferase
Pyridoxal 5′-phosphate
Urea-induced unfolding
Pathogenic variant
Primary hyperoxaluria type 1

ABSTRACT

The sensitivity to denaturant stress of the major (AGT-Ma) and the minor (AGT-Mi) allele of alanine:-glyoxylate aminotransferase and P11L mutant has been examined by studying their urea-induced equilibrium unfolding processes with various spectroscopic and analytical techniques. AGT-Ma loses pyridoxal 5′-phosphate (PLP) and unfolds completely without exposing significant hydrophobic clusters through a two-state model (C_m ~ 6.9 M urea). Instead, the unfolding of AGT-Mi and P11L variant proceeds in two steps. The first transition (C_m ~ 4.6 M urea) involves PLP release, dimer dissociation and exposure of hydrophobic patches leading to a self-associated intermediate which is converted to an unfolded monomer in the second step. The unfolding pathways of apoAGT-Mi and apoP11L are similar to each other, but different from that of apoAGT-Ma. Notably, the monomerization step in apoAGT-Mi and apoP11L occurs with a C_m value (~1.6 M urea) lower than in apoAGT-Ma (~2.4 M urea). These data indicate that Pro11 is relevant for the stability of both the dimeric structure and the PLP binding site of AGT. Moreover, to understand the pathogenic consequences of G170R mutation on AGT-Mi at the protein level, G170R-Mi has been characterized. HoloG170R-Mi exhibits spectroscopic and catalytic features and urea unfolding profiles comparable to those of AGT-Mi, while the apo form monomerizes with a C_m of ~1.1 M urea. These biochemical results are discussed in the light of the characteristics of the enzymatic phenotype of PH1 patients bearing G170R mutation in AGT-Mi and the positive response of these patients to pyridoxine treatment.

1. Introduction

Primary hyperoxaluria type 1 (PH1) is a rare autosomal recessive disorder caused by a deficiency of the liver peroxisomal pyridoxal 5′-phosphate (PLP)-dependent enzyme alanine:glyoxylate aminotransferase (AGT). AGT catalyzes the transamination of the intermediary metabolite glyoxylate to glycine, and its deficiency results in the oxidation of glyoxylate to oxalate. Excessive oxalate synthesis leads to the chronic deposition of insoluble calcium oxalate mainly in the kidney and urinary tract. Following renal failure, the problem of excessive oxalate synthesis is compounded by the inability to remove it from the body and in some cases oxalate can deposit almost anywhere in the body [1].

AGT is encoded by the *AGXT* gene which is located on chromosome 2q37.3, and comprises 11 exons spreading over 10 kB [2]. The atomic resolution of the AGT structure complexed with the competitive inhibitor aminooxyacetic acid has been reported [3]. The enzyme is a dimer, and each monomer consists of a N-terminal arm, a large N-terminal domain, and a small C-terminal domain. Two main polymorphic variants have been identified. The minor allele (AGT-Mi) differs from the major allele (AGT-Ma) by the presence of 32C → T and 1020A → G nucleotide substitutions, which lead to Pro11Leu and Ile340Met amino acids replacements, respectively. In addition, the minor *AGXT* allele contains a 74-bp duplication in intron 1 [4]. AGT-Mi is not a variant disease-causing, even if its presence enables a small amount (~5%) of AGT to be imported into the mitochondria [4] and causes several biochemical effects, including an ~15% decrease in catalytic efficiency and a ~5 °C reduction in the transition mid-points of denaturation and inactivation [5,6]. Nevertheless, AGT-Mi is deleterious when combined with certain additional mutations,

Abbreviations: AGT, alanine:glyoxylate aminotransferase; PLP, pyridoxal 5′-phosphate; PH1, primary hyperoxaluria type 1; SEC, size exclusion chromatography; ANS, 8-Anilino-1-naphtalenesulfonic acid; DLS, dynamic light scattering.

* Corresponding author. Tel.: +39 045 8027 175; fax: +39 045 8027 170.
E-mail address: carla.borrivoltattorni@univr.it (C.B. Voltattorni).

0300-9084/$ – see front matter © 2010 Elsevier Masson SAS. All rights reserved.
doi:10.1016/j.biochi.2010.08.005

leading to impairments of the stability, localization, and/or dimerization of the enzyme [7]. This is the case for G170R mutation, the most common mutation found so far, accounting for about 25 to 30 per cent of the mutant alleles in European and North American patients [4]. On the basis of the crystal structure of AGT and previous biophysical studies in which both Pro10 and Pro11 were replaced by Leu, it was suggested that the structural change occurring in the N-terminal extension of AGT-Mi is the main determinant of the decreased dimerization and mitochondrial mistargeting [8]. However, no reports providing experimental evidence for this hypothesis are available so far. The clarification of this issue is important in that it may help to understand why the P11L and I340M polymorphisms sensitize AGT to the untoward effects of many pathogenic mutations that are predicted to be innocuous in their absence.

Recent studies have demonstrated that AGT-Ma and AGT-Mi display the same overall conformation, spectroscopic features and equilibrium dissociation constant for PLP, $K_{D(PLP)}$ ($\sim$0.3 μM) [6], as well as a dimer–monomer equilibrium dissociation constant $<<$0.1 μM [5]. Thus, since these results do not allow the identification of the structural elements distinguishing AGT-Mi from AGT-Ma under native conditions, as a first step we decided to investigate and compare the stability of AGT-Mi with that of AGT-Ma under stressed conditions. The urea denaturation profiles of the two allelic forms of AGT indicate that they unfold through a different mechanism, and that the dimeric structure of AGT-Mi is less stable than that of AGT-Ma. In addition, the finding that the urea-induced unfolding pathway of the P11L artificial mutant is superimposable on that of AGT-Mi indicates that the P11L mutation might be responsible for the significant decrease in the stability of the dimeric structure of AGT. This could be caused by the selective destabilization of the interactions between the N-terminal arm of one subunit and the opposite subunit. Moreover, we performed urea and thermal denaturation experiments of the G170R pathogenic variant associated with the minor allele (G170R-Mi). The results obtained indicate that, unlike the holo dimer, the dimeric apo form of G170R-Mi is more susceptible to dimer dissociation than the corresponding apo form of AGT-Mi. These biochemical characteristics are discussed in the light of previous data of the enzymatic phenotype bearing G170R mutation on the minor allele.

2. Materials and methods

2.1. Materials

Urea, PLP, L-alanine, glyoxylate, isopropyl-β-D-thiogalactopyranoside, and rabbit muscle L-lactic dehydrogenase were obtained from Sigma. 8-Anilino-1-naphtalenesulfonic acid (ANS) was obtained from Molecular Probes. All other chemicals were of the highest purity available.

2.2. Production and purification of AGT-Ma, AGT-Mi, P11L and G170R-Mi variants

The vectors coding for the P11L variant, the double mutant P11L/I340M (AGT-Mi) and the triple mutant P11L/I340M/G170R (G170R-Mi) were obtained from the AGT-NoHis construct by using the QuikChange II site-directed mutagenesis kit (Stratagene). The oligonucleotides used for mutagenesis were as follows: P11L forward primer, 5′- GCTGCTGGTGACCCCCCTCAAGGCCCTGCTC AAGC and its complement; I340M forward primer, 5′- CATCGTCA GCTACGTCATGGACCACTTCGACATTG and its complement; G170R forward primer, 5′- CCCCTTGATGGCTTCCGGGAACTCTGCCACAGG -3′, and its complement. The underlined codons indicate mutated aminoacids. All mutations were confirmed by DNA sequencing. AGT-Ma and AGT-Mi as well as the P11L and G170R-Mi variants were expressed and purified by the same procedure previously described for AGT-NoHis [9,10]. The protein concentration was determined by absorbance spectroscopy using an extinction coefficient of $9.7 \times 10^4\ M^{-1}\ cm^{-1}$ at 280 nm [9,10]. The PLP content was determined by releasing the coenzyme in 0.1 M NaOH and by using $\varepsilon = 6600\ M^{-1}\ cm^{-1}$ at 388 nm.

2.3. Binding affinity for PLP of G170R-Mi

The apo form of G170R-Mi was prepared as previously described [9]. The $K_{D(PLP)}$ from G170R-Mi (0.1 μM) was determined by measuring the quenching of the intrinsic fluorescence of the apoenzyme in the presence of PLP at concentrations ranging from 0.02 to 10 μM.

2.4. Denaturant-induced unfolding experiments

To determine the stability of AGT-Ma, AGT-Mi, P11L and G170R-Mi variants toward denaturation by urea, stock solutions of enzyme and 10 M freshly prepared urea, dissolved in 100 mM potassium phosphate buffer, pH 7.4, were mixed to give the desired concentration of enzyme and denaturant. Holoenzymes incubation was performed in the presence of 10 μM exogenous PLP. Each mixture was allowed to equilibrate at 25 °C for 3 h, which was sufficient to reach the limiting values for all enzyme properties (catalytic activity, fluorescence, visible and far-UV CD, and molecular size) at each urea concentration used. The actual urea concentration was checked using refractive index data [11].

2.5. Activity measurements

During the purification of AGT enzymes, transaminase activity assays were performed as previously described [9]. In the experiments designed to determine the effect of various concentrations of denaturant on transaminase activity, pyruvate production was measured by an assay based on measuring the 2,4-dinitrophenylhydrazine derivative of pyruvate by HPLC as reported previously [12].

2.6. Size-exclusion chromatography (SEC)

The molecular dimensions of 1 μM AGT-Ma, AGT-Mi, P11L and G170R-Mi in the holo- and apo-form upon incubation for 3 h at 25 °C in the presence of varying urea concentrations, were determined by SEC. The mixtures were loaded on a custom packed Sephacryl S-300 10/600 column equilibrated and run with 100 mM potassium phosphate buffer pH 7.4 containing the desired urea concentration on an Akta FPLC system (GE Healthcare). The injection volume was 500 μl at a flow rate of 0.4 ml/min with detection at 280 nm. Three chromatography experiments were run per sample, and the software Unicorn 5.01 (GE Healthcare) was used to calculate the elution volume and the area of each peak. The apparent hydrodynamic radius of the eluting species was calculated by comparing their elution volume to that of a set of molecular weight standards under the same experimental conditions.

2.7. Fluorescence measurements

Fluorescence measurements were performed by using a 1 cm path length quartz cuvette in a Jasco FP-750 spectrofluorimeter equipped with a thermostatically controlled cell holder. Protein emission spectra were taken from 300 to 450 nm (excitation at 280 nm) with both the excitation and the emission slits set to 5 nm. The protein concentration was typically 1 μM. All the spectra were corrected by

subtracting the emission spectrum of the buffer. Phase-diagrams were obtained from the analysis of intrinsic fluorescence emission data by plotting fluorescence intensity values measured at 365 nm (I_{365nm}) against the corresponding intensity values at 320 nm (I_{320nm}) according to the method of Kuznetsova et al. [13]. The dependence $I_{365nm} = f(I_{320nm})$ is linear when changes in the protein environment lead to the all-or-none transition between two different conformations. On the contrary, the nonlinearity of this function reflects the sequential character of structural transformations, i.e., the population of one or more intermediates.

ANS fluorescence experiments were carried out as follows: AGT-Ma, AGT-Mi or variants at 1 μM concentration were equilibrated at the desired denaturant concentration for 3 h at 25 °C. Then, 5 μl from a stock solution of 3 mM ANS were added to each sample and incubated at 25 °C for 1 h. ANS excitation was done at 365 nm and the emission was monitored between 400 and 560 nm using excitation/emission slit widths of 5 nm. The values were normalized by subtracting the baseline recorded for the probe alone under identical conditions.

2.8. CD measurements

Visible and far-UV CD were recorded on a Jasco J-710 spectropolarimeter with 1 cm and 1 mm cell path length, respectively. The enzyme concentration was 1 μM. The values obtained were normalized by subtracting the baseline recorded of the buffer having the same denaturant concentration. The thermal unfolding of AGT-Mi and G170R-Mi was monitored by CD at 222 nm at a concentration of 1 μM in 100 mM potassium phosphate buffer, pH 7.4, with temperature increasing of 0.5 °C/min from 25 to 90 °C. CD signals were fitted either to two or three state unfolding mode using Origin Pro7 software according to the method of Pace [11].

2.9. Dynamic light scattering (DLS)

Filtered stock solutions of AGT-Ma, AGT-Mi or G170R-Mi either in the holo or in the apo-form, were diluted to 1 μM concentration with various filtered urea solutions in 100 mM potassium phosphate buffer pH 7.4. Each sample was incubated for 3 h at 25 °C and DLS analysis was performed on a Zetasizer Nano S device (Malvern Instruments) by using disposable 12.5 × 45-mm cells with stopper. The appropriate viscosity and refractive index for each solution was set and the temperature was kept at 25 ± 0.1 °C during the measurements.

2.10. Data analysis

The comparison of data collected with different methods was made by normalising the data to F_u, the apparent fraction of unfolded protein:

$$F_u = (Y_0 - Y_n)/(Y_u - Y_n) \quad (1)$$

where Y_0 is the signal at a given urea concentration and Y_n and Y_u are the observed values for the native and unfolded protein, respectively.

The analysis of the equilibrium unfolding curves corresponding to a two-state model (N⇔U) was performed according to the equation (2):

$$Y = \frac{Y_N + \alpha_N C + (Y_U + \alpha_U C)e^{-m(C_m - C)/RT}}{1 + e^{-m(C_m - C)/RT}} \quad (2)$$

where Y is the measured signal; Y_N and Y_U are the signal values characteristic of the native (N) and fully unfolded (U) conformations, respectively; C denotes the urea concentration; α_N and α_U represent the dependence on urea concentration of the signal of the native and unfolded conformation, respectively; C_m is the midpoint of urea required for unfolding and m stands for the slope of the unfolding curve at C_m.

The urea-unfolding curves corresponding to a three-state denaturation pathway (N ↔ I ↔ U, where I is the intermediate state) or a four-state denaturation pathway (N ↔ I_1 ↔ I_2 ↔ U) were analyzed using equations (3) or (4), respectively:

$$Y = \frac{Y_{N-I}[urea]^{n1}}{C_{m1}^{n1}[urea]^{n1}} + \frac{Y_{I-U}[urea]^{n2}}{C_{m2}^{n2} + [urea]^{n2}} \quad (3)$$

$$Y = \frac{Y_{N-I_1}[urea]^{n1}}{C_{m1}^{n1}[urea]^{n1}} + \frac{Y_{I_1-I_2}[urea]^{n2}}{C_{m2}^{n2} + [urea]^{n2}} + \frac{Y_{I_2-U}[urea]^{n3}}{C_{m3}^{n3} + [urea]^{n3}} \quad (4)$$

in which C_{m1}, C_{m2} and C_{m3} are the midpoint concentrations of urea, $Y_{N \leftrightarrow I}$ (or $Y_{N \leftrightarrow I1}$), $Y_{I1 \leftrightarrow I2}$ and $Y_{I \leftrightarrow U}$ (or $Y_{I2 \leftrightarrow U}$) represent the change in the signal for the N ↔ I (or N ↔ I_1), I_1 ↔ I_2 and I ↔ U (or I_2 ↔ U) transitions, respectively, and exponents n_1, n_2 and n_3 reflect the steepness of the transition between states as a function of urea concentration.

3. Results and discussion

3.1. AGT-Ma and AGT-Mi display a different sensitivity to chemical stress

Under native conditions, both AGT-Ma and AGT-Mi exhibit an emission spectrum (exc. at 280 nm) centered at 337 nm, which reflects the average microenvironment of 6 tryptophan residues. No gross differences in the secondary structure of AGT-Ma and AGT-Mi are seen on far-UV CD. Upon denaturation at 10 M urea, both proteins display a maximum fluorescence emission at 352 nm (Fig. 1 of SI) and a complete loss of far-UV CD signals. However, significant differences between AGT-Ma and AGT-Mi occur at intermediate levels of urea. Indeed, Fig. 1A and B show that (i) the transition curves for the urea-induced unfolding of AGT-Ma monitored by far-UV CD (which reflects α-helix content) and emission intensity as well as emission maximum tryptophan fluorescence (indicative of the microenvironment of the side chain aromatic ring) describe a two-state process with a mid-point transition of ~6.9 M urea (Table 1), and (ii) these curves for AGT-Mi appear biphasic, suggestive of a three-state model between the native dimeric state and the unfolded monomeric state. An intermediate state appears to be stable at ~5.5 M urea, and the transition midpoints were at about 4.6 M and 6.4 M for the first and the second transition, respectively (Table 1). While the first step of the unfolding profile of AGT-Mi shifts to a higher denaturant concentration and the intermediate appears to be more populated at 8 μM than at 1 μM (Fig. 1B), the second transition is independent, within the experimental error, on enzyme concentration. Thus, it is likely that the first transition includes the dimer to monomers dissociation, and that the significant increase in fluorescence intensity observed during the first transition may result from the loss of quenching due to the release of PLP. In order to examine the changes in fluorescence in greater detail, we applied the phase diagram analysis, which could illuminate populated intermediates and their properties, to the emission fluorescence spectra of AGT-Ma and AGT-Mi at various urea concentrations. To this end, we selected tryptophan fluorescence at 320 nm and 365 nm that reflect the amount of folded (blue-shifted) and unfolded (red-shifted) states, respectively. When these parameters are plotted in a x–y graph, a straight line, typical for a two-state process, can be observed in the diagram of AGT-Ma from 0 to 10 M urea. Two linear

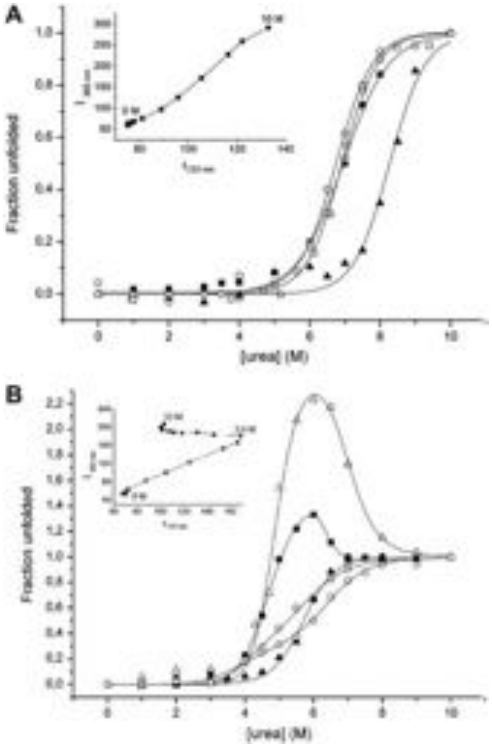

Fig. 1. Urea-induced unfolding equilibrium of holoAGT-Ma and holoAGT-Mi monitored by spectroscopic probes. Unfolding profiles of holoAGT-Ma (A) and holoAGT-Mi (B) monitored by intrinsic fluorescence intensity (■), emission maximum fluorescence (○), far-UV CD at 222 nm (□), and of $NaBH_4$ reduced holoAGT-Ma (A) and holoAGT-Mi (B) monitored by intrinsic fluorescence intensity (▲). In (B) is also reported the unfolding profile of 8 μM holoAGT-Mi monitored by intrinsic fluorescence intensity (△). The fraction unfolded, F_u, was calculated using the observed fluorescence or CD signals and eq. (1) as described under Materilas and methods. The solid lines represent the best fit obtained to a two-state (eq. (2)) or a three-state model (eq. (3)). Insets: phase diagrams representing urea-induced unfolding of holoAGT-Ma (A) and holoAGT-Mi (B). Each straight line represents an all-or none transition between two conformers. The denaturant concentration values are indicated in the vicinity of the corresponding symbol. Except where indicated, the enzyme concentration was 1 μM.

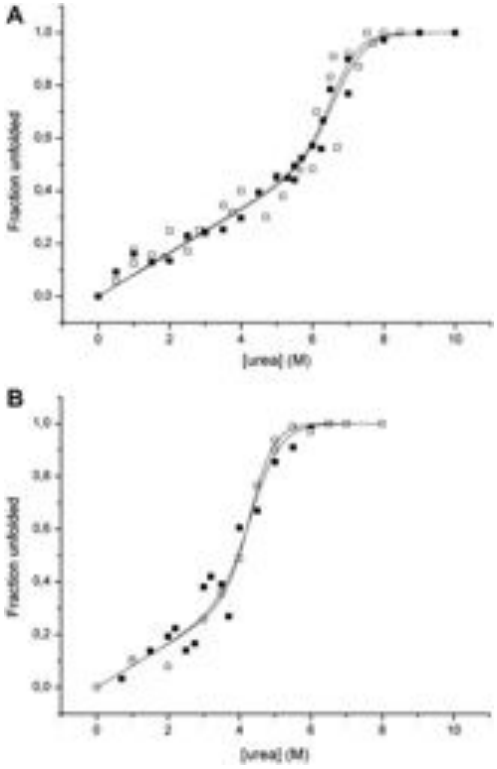

Fig. 2. Urea-induced unfolding equilibrium of holoAGT-Ma and holoAGT-Mi monitored by catalytic activity and visible CD. Unfolding profiles of holoAGT-Ma (A) and holoAGT-Mi (B) monitored by transaminase activity (■), and visible CD at 429 nm (□). The fraction unfolded, F_u, was calculated using the observed activity or visible CD data and eq. (1) as described under Materials and methods. The solid lines represent the best fit obtained to a two-state model (eq. (2)). The enzyme concentration was 1 μM.

segments, 0–5.5 and 5.5–8 M urea, characterize instead the phase diagram of AGT-Mi. They represent the existence of two independent transitions separating three conformational states (insets of Fig. 1A and B).

Table 1
C_m values for urea-induced unfolding of AGT-Ma, AGT-Mi, P11L and G170R-Mi in the holo and apo forms monitored by various parameters at an enzyme concentration of 1 μM.

Probe	HoloAGT-Ma	HoloAGT-MI	HoloP11L	HoloG170R-Mi	ApoAGT-Ma	ApoAGT-Mi	ApoP11L	ApoG170R-Mi
Transaminase activity	6.7 ± 0.2	4.4 ± 0.1	4.4 ± 0.2	4.4 ± 0.1	n.m.	n.m.	n.m.	n.m.
CD visible	6.7 ± 0.1	4.35 ± 0.06	4.65 ± 0.3	4.3 ± 0.1	–	–	–	–
Tryptophan fluorescence								
Emission maximum	6.5 ± 0.1	4.6 ± 0.1	4.6 ± 0.2	4.10 ± 0.15	6.6 ± 0.1	6.0 ± 0.1	6.2 ± 0.1	6.4 ± 0.1
		6.4 ± 0.1	6.2 ± 0.1	6.3 ± 0.1				
Relative intensity		4.7 ± 0.1	4.5 ± 0.1	4.56 ± 0.03	2.37 ± 0.03	1.74 ± 0.01	1.4 ± 0.1	1.17 ± 0.06
						3.0 ± 0.04	3.2 ± 0.1	3.0 ± 0.1
Far UV CD	6.9 ± 0.1	4.5 ± 0.1	4.3 ± 0.4	4.4 ± 0.1	2.4 ± 0.1	1.90± 0.03	1.66 ± 0.2	1.10 ± 0.03
		6.4 ± 0.1	6.6 ± 0.2	6.4 ± 0.2	6.4 ± 0.1	2.7 ± 0.1	2.9 ± 0.1	2.7 ± 0.04
						6.4 ± 0.2	6.2 ± 0.1	6.5 ± 0.1

Single, double and triple C_m values result from fitting data to a two-state (eq. (2)), three-state (eq. (3)), and four-state (eq. (4)) process, respectively. n.m., not measurable since one cannot distinguish between inactivation due to inhibitory or unfolding effects.

As shown in Fig. 2A and B, AGT-Ma and AGT-Mi also differ for the extent of PLP dissociation and loss of transaminase activity during their urea-induced unfolding processes. The internal aldimine of AGT-Ma and AGT-Mi exhibits an absorbance band at 423 nm, associated with a positive dichroic band at 429 nm [9]. For both AGT-Ma and AGT-Mi, the unfolding profiles monitored by CD visible and enzymatic activity are coincident, and the data fit a two-state model with transition midpoints of about 6.7 and 4.4 M urea, respectively (Table 1). From these data it can be concluded that (i) as expected, the loss of PLP from AGT-Ma and AGT-Mi results in the loss of enzymatic activity, and (ii) the loss of 429 nm dichroic band and enzymatic activity takes place at a lower denaturant concentration for AGT-Mi than for AGT-Ma. Moreover, the finding that the visible CD and enzymatic activity C_m values for AGT-Ma are coincident with those observed by fluorescence and far-UV CD measurements suggests that PLP release for AGT-Ma occurs at a high denaturant concentration, once the structure is sufficiently destabilized. On the other hand, the coincidence of the Cm values (~4.4 M urea) measured by visible CD and transaminase activity with those of the first transition of AGT-Mi observed by intrinsic fluorescence and far-UV CD indicates that PLP dissociation from AGT-Mi takes place at a low denaturant concentration with a partial loss of tertiary and secondary structures.

It should also be noted that there is a slight steady decrease in the CD visible signal and enzyme activity from 0 to 4 M for AGT-Ma and from 0 to 2 M urea for AGT-Mi, i.e., within denaturant ranges in which the intrinsic fluorescence and far-UV CD signals of the two enzymatic species remain unmodified. These pre-transition changes suggest that urea might bind and act as an enzyme inhibitor. In fact, experiments in which the kinetic parameters are determined in the absence or presence of 1, 2, 3 and 4 M urea clearly demonstrate that urea is responsible for a mixed-type inhibition. This behaviour has been also observed for other PLP-enzymes [14,15].

The difference of the effects that increasing levels of urea have on AGT-Ma and AGT-Mi is further supported by ANS binding studies. ANS is an anionic fluorescent probe that binds to apolar surfaces and exhibits a red shift in the emission maximum due to the changes in hydrophobic patches on protein unfolding [16]. As previously reported [17], upon the addition of native AGT-Ma or AGT-Mi in the holo form to ANS, the ANS fluorescence is characterized in both cases by an emission maximum at 515 nm and a slight increase of emission intensity. Fig. 3 shows the unfolding of AGT-Ma and AGT-Mi monitored by ANS fluorescence as a function of added urea. No remarkable changes of ANS fluorescence over the 0–8 M urea range have been observed for AGT-Ma. On the other hand, in the 0–5 M urea range there is a steady increase in ANS fluorescence for AGT-Mi, which reaches at 5 M urea a fluorescence intensity ~8-fold higher than that observed in the absence of urea, as well as a shift of the emission maximum from 515 to 489 nm. Further additions of urea resulted in a decrease in ANS fluorescence intensity and an increase in the λ_{max} consistent with dispersing the hydrophobic surface and unfolding of the protein. These binding studies indicate that (i) no significant hydrophobic patches become exposed during the urea-induced unfolding of holoAGT-Ma, and (ii) the unfolding intermediate observed by protein fluorescence and far-UV CD–monitored denaturation profiles of holo AGT-Mi is characterized by exposed hydrophobic patches that are accessible to ANS. Such a change in AGT-Mi structure may lead to its aggregation due to hydrophobic interactions. This indeed was supported by SEC and DLS experiments. As shown in Fig. 4A and B, and insets, both the native dimer of AGT-Ma and AGT-Mi in the holo form elute as a single peak from SEC column with a retention volume of 31.5 ml (corresponding to that of a dimer), and display a peak of about 10 nm on DLS consistent with the hydrodynamic diameter of the molecule determined by X-ray crystallography [17]. Analyses of the chromatograms indicate that (i) while AGT-Ma elutes as a peak whose total area does not significantly change over 0–8 M urea range, AGT-Mi elutes as a peak whose

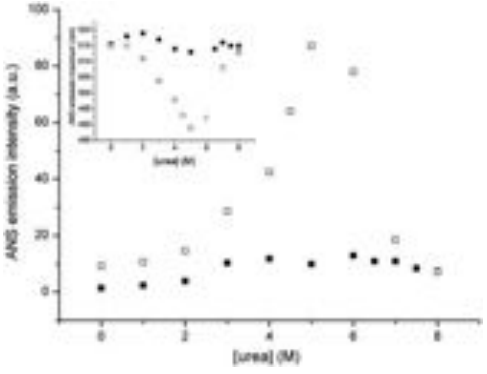

Fig. 3. ANS fluorescence of holoAGT-Ma and holoAGT-Mi at various urea concentrations. ANS emission fluorescence intensity at 515 nm in the presence of holoAGT-Ma (■) and holoAGT-Mi (□) as a function of urea concentrations (exc. at 365 nm). Inset, changes in emission maximum of holoAGT-Ma (■) and holoAGT-Mi (□) as a function of urea concentrations. The enzyme concentration was 1 μM.

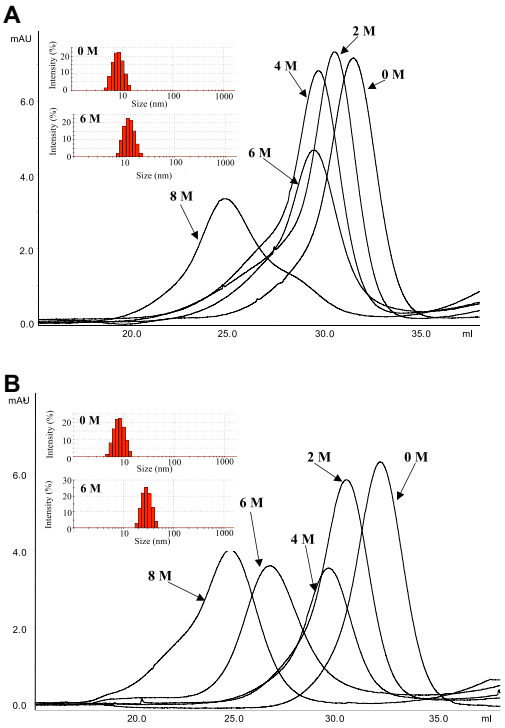

Fig. 4. Urea-induced changes in molecular dimension of holoAGT-Ma and holoAGT-Mi. Size distribution from chromatographic profiles on SEC of holoAGT-Ma (A) and holoAGT-Mi (B) at the indicated urea concentration. Insets, size distribution on DLS at 0 and 6 M urea of holoAGT-Ma (A) and holoAGT-Mi (B). The enzyme concentration was 1 μM.

integrated area begins to decrease at 2 M, reaches at 5 M urea a minimum value of about 40% relative to the native protein, and then gradually regains the total integrated area when the urea concentration is further increased, and (ii) both AGT-Ma and AGT-Mi elute with a decreased retention volume (up to 29 ml) between 0 and 5 M urea, and from 5 to 10 M urea are gradually converted into the unfolded monomer characterized by a further decrease in the retention volume of the peak. DLS measurements indicate that at 6 M urea AGT-Ma shows a peak at 14 nm, possibly due to an expanded dimeric structure, whereas AGT-Mi exhibits a peak at 25–30 nm, which suggests aggregate species (insets of Fig. 4A and B).

Altogether these data provide evidence that the unfolding of AGT-Ma occurs via a single transition in which only native and denaturated molecules are populated, while that of AGT-Mi proceeds through a three-state process (Scheme 1). The first step of AGT-Mi unfolding, associated with PLP release, concomitant inactivation and monomerization, yields an intermediate which lacks PLP. This intermediate is significantly populated at ~6 M urea. It retains ~40% of the native CD signal and ~60% of the native fluorescence, and consists of 25–30 nm aggregates, which are converted into a completely unfolded monomer during the second transition (Fig. 1B and inset of Fig. 4B). The kinetics of the changes of the 429 and 222 nm dichroic signals of AGT-Mi at 6 M urea reveals that they occur with similar rate constants ($0.0240 \pm 0.0001\ min^{-1}$), thus suggesting that PLP release and loss of secondary structure are concerted events. It is reasonable to hypothesize that the different unfolding mechanism of AGT-Ma and AGT-Mi in the holo form could be attributable to the fact that PLP release and monomerization take place in AGT-Mi at urea concentration lower than in AGT-Ma. Thus, to elucidate the stabilizing effect of the cofactor on AGT-Ma and AGT-Mi, the urea-mediated denaturation of the $NaBH_4$-reduced forms of AGT-Ma and AGT-Mi, in which the coenzyme is irreversibly bound to the proteins was studied. The tryptophan fluorescence data following urea denaturation indicate that both reduced AGT-Ma and AGT-Mi are unfolded in a single enzyme concentration independent step with urea concentration at mid-denaturation of ~8.1 and 5.9 M, respectively (Fig. 1A and B). Additionally, neither the presence of aggregates nor changes in ANS fluorescence can be seen during the urea-mediated unfolding of the $NaBH_4$ reduced forms of both the enzymatic species. Thus, the reductive trapping of the cofactor as a nondissociable derivative converts the unfolding profile of AGT-Mi from a three-state to a two-state model by preventing the formation of an aggregated intermediate. Moreover, the different resistance of the reduced forms of AGT-Ma and AGT-Mi to chemical stress strongly suggests that the difference in stability between holoAGT-Ma and holoAGT-Mi is an intrinsic structural feature of the two apoproteins. The results on the irreversibly bound PLP forms of AGT lead us to investigate the stability of the apo forms of AGT against urea denaturation. Their fluorescence and far-UV CD

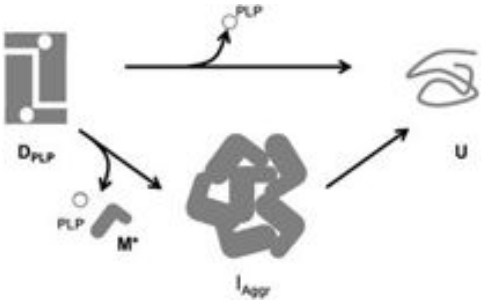

Scheme 1. Urea-induced equilibrium unfolding pathway of AGT-Ma ($D_{PLP} \rightarrow U$) and AGT-Mi ($D_{PLP} \rightarrow I_{Aggr} \rightarrow U$), where D_{PLP} and U indicate the native holodimer and the unfolded monomer, respectively, M* represents a transient partially unfolded monomeric species, and I_{Aggr} the insoluble PLP-unbound aggregates.

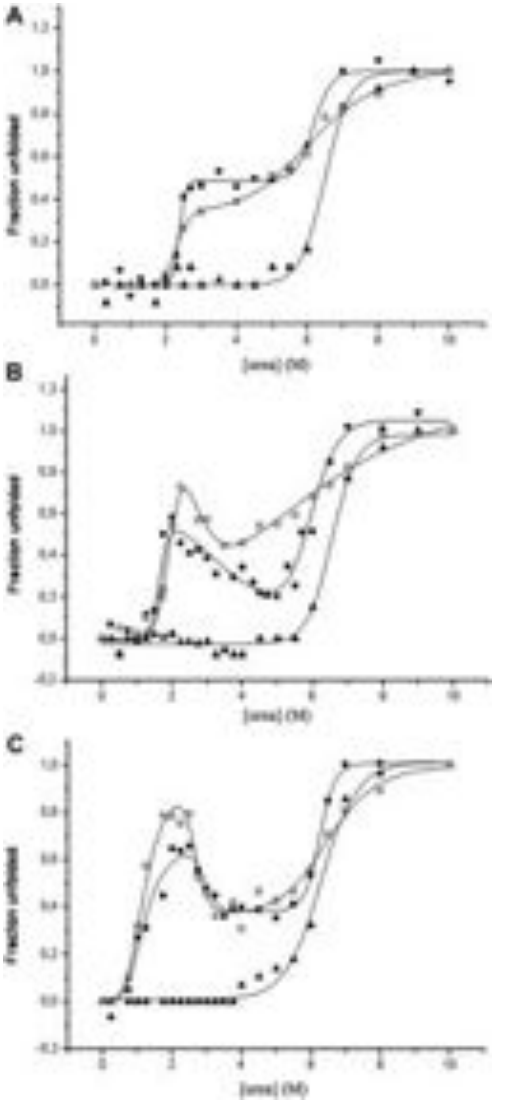

Fig. 5. Urea-induced unfolding equilibrium of apoAGT-Ma, apoAGT-Mi and apoG170R-Mi. Unfolding profiles of apoAGT-Ma (A), apoAGT-Mi (B) and apoG170R-Mi (C) monitored by intrinsic fluorescence intensity (■), emission maximum fluorescence (▲) and far-UV CD at 222 nm (□). The fraction unfolded, F_u, was calculated using the observed fluorescence or CD signals and eq. (1) as described under Materials and methods. The solid lines represent the best fit obtained to a two-state (eq. (2)) or a three-state (eq. (3)) or a four-state model (eq. (4)). The enzyme concentration was 1 μM.

properties under denaturation conditions are presented in Fig. 5A and B, and the C_m values are reported in Table 1. The denaturation curves of apoAGT-Ma monitored by intrinsic fluorescence and far-UV CD fit a biphasic model. The first transition, which is not associated with a λ_{max} shift, is enzyme concentration dependent with a midpoint of ~2.3 M urea, followed by a transition concentration independent with C_m value of ~6.3 M urea (Table 1). An inactive intermediate state appears to be stable from ~3 to 5.5 M urea in a conformation able to bind ANS, as revealed by the maximum emission wavelength at 482 nm and a 5-fold increase in the ANS fluorescence intensity relative to the native protein (Fig. 6). Evidence for the formation of aggregates over this urea range is provided by a significant decrease in the total peak area on SEC (Fig. 2A of SI), and confirmed by the presence of ~30 nm particles seen by DLS experiments (Fig. 7). At urea concentrations ≥5.5 M aggregates are gradually converted into soluble unfolded monomer, as revealed by a gradual shift of the peak on SEC toward lower retention volume (Fig. 2A of SI). The unfolding pathway of apo AGT-Mi is more complex than that of apo AGT-Ma. A look at the variations of intrinsic fluorescence and far-UV CD with urea concentrations reveals some interesting features. As presented in Fig. 5B, increasing urea concentration induces a decrease in both the fluorescence intensity and far-UV CD signal between 1 and 2 M. This transition (C_m ~ 1.7 M urea) (Table 1) is highly cooperative, characterized by a loss of about 70% and 50% of the secondary and tertiary structures, respectively, and leads to an inactive intermediate. Above 2 M urea, fluorescence intensity and ellipticity at 222 nm begin to rise, and they reach a maximum at ~3.5 M remaining unchanged up to 5.5 M. Obviously, this complex pattern needs further explanation. The first transition is not associated with a λ_{max} shift, as shown in Fig. 5B. Therefore, it is probably not caused by changes in the hydratation of tryptophans but rather by an increase in quenching of these residues, possibly due to conformational changes. This idea is supported by several observations. First, the findings that this transition is dependent on protein concentration and that the elution profile on SEC of 2 M-treated apoAGT-Mi (Fig. 2B of SI) reveals a mixture of a dimeric and a monomeric species strongly suggest that this step is linked to a dissociation event. Since the retention volume of the monomeric species is 33.1 ml (Fig. 2B of SI), a value slightly lower than the theoretical one of a folded monomer (33.3 ml), it is reasonable to think that the dissociation gives rise to a partially unfolded monomer. Second, the ANS fluorescence profile of apoAGT-Mi treated with increased urea concentrations reveals a ~13-fold increase in emission intensity and a blue shift in the emission maximum (from 507 to 481 nm) from 1 to 2 M urea (Fig. 6). This suggests that clusters of hydrophobic residues become exposed during this transition, and they are possibly susceptible to aggregation. This interpretation gains support from SEC and DLS experiments on apoAGT-Mi as a function of urea concentration: a consistent decrease of the peak area (Fig. 2B of SI) and the formation of approximately 3500 nm particles (Fig. 7) can be seen in the 1–2.5 M range. On the basis of this finding, the observed loss of the intensity fluorescence and far-UV CD signal over this range could be due to light scattering effects of these high-order aggregates. The second transition, characterized by a gradual decrease in the molecular dimensions of apoAGT-Mi (Fig. 7) and a concomitant increase in the fluorescence intensity and 222-nm ellipticity without any detectable change in emission maximum (Fig. 5B), describes a conversion from high-order to low-order aggregates. The latter populate the intermediate extending from 3.5 to 5.5 M urea, and are then converted to the completely unfolded monomer with a Cm transition of ~6.2 M urea.

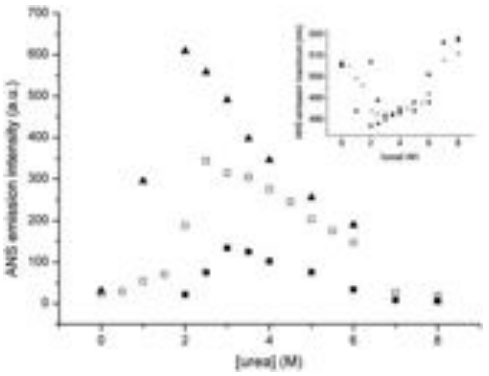

Fig. 6. ANS fluorescence of apoAGT-Ma, apoAGT-Mi and apoG170R-Mi at various urea concentrations. ANS emission fluorescence intensity at 507 nm in the presence of apoAGT-Ma (■), apoAGT-Mi (□) and apoG170R-Mi (▲) as a function of urea concentrations (exc. at 365 nm). Inset, changes in the emission maximum of apoAGT-Ma (■), apoAGT-Mi (□) and apoG170R-Mi (▲). The enzyme concentration was 1 μM.

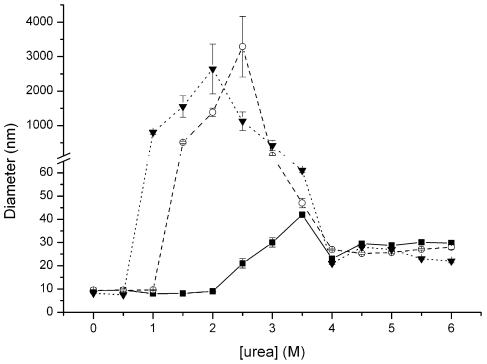

Fig. 7. DLS measurements of size of apoAGT-Ma, apoAGT-Mi and apoG170R-Mi at various urea concentrations. DLS measurements of apoAGT-Ma (■), apoAGT-Mi (○) and apoG170R-Mi (▼) as a function of urea concentration. The data points represent values averaged over 20 acquisitions, depending on the quality of the data; bars indicate standard deviations. The enzyme concentration was 1 μM.

On the basis of all the above data, it can be concluded that P11L and I340M substitutions characterizing AGT-Mi (i) result in a decreased stabilization of the dimeric form of apoAGT, and (ii) convert the overall process of urea unfolding of apoAGT from a three-state (native dimer → low order aggregates → unfolded monomer) into a four state (native dimer → high-order aggregates derived from a partially unfolded monomer → low-order aggregates → unfolded monomer).

3.2. P11L mutation is responsible for the urea sensitivity of AGT-Mi

The sensitivity of P11L mutant to urea stress has been evaluated by monitoring its urea unfolding in the holo and apo forms by visible, far-UV CD and intrinsic fluorescence as well as by ANS binding, activity, and SEC measurements under equilibrium conditions. The results (data not shown) obtained for all these probes are identical to the corresponding of AGT-Mi in the holo and apo forms (Table 1). Thus, the presence of a leucine residue at position 11 decreases the stability of the dimeric structure of AGT.

3.3. Unfolding of AGT-Ma and AGT-Mi in correlation with their structural features

We tried to explain all the above results by looking at the structure of the enzyme. The AGTase dimeric interface is very large (~23% of the solvent accessible area), and is composed of interactions across the two large domains as well as contacts between the N-terminus of one subunit and the large domain of the adjacent subunit. Thus, as already suggested [3], the N-terminal segments are probably relevant for dimer formation. Inspection of the crystal structure of AGT reveals that Pro11, belonging to the N-terminus, not only contributes to the increase in the structural rigidity, but also exerts additional constraints to the backbone, since the ring closure keeps its Φ angle value almost fixed. In addition, this residue makes hydrophobic interactions with a surface cavity surrounded by residues Glu62, Gly63, Tyr66 and Ala280 of the opposite subunit. Therefore, it is likely that replacement of Pro11 by Leu could destabilize the interactions between the N-terminus of one subunit with the large domain of the adjacent subunit. This observation provides an explanation for why the monomerization of holo and apo AGT-Mi occurs at lower urea concentration than the monomerization of AGT-Ma. However, it does not explain why the complete release of PLP in AGT-Ma requires a higher degree of structural destabilization than in AGT-Mi. The lower destabilization observed for AGT-Mi as compared with AGT-Ma suggests that the substitution of Pro11 by Leu could result in an altered sensitivity to urea stress of the PLP-bound state. In the native AGT-Ma dimer [3] PLP is located in a wide catalytic cleft that is assembled by residues from both subunits and its phosphate group entails two interactions with Tyr260 and Thr263 of the adjacent subunit. Moreover, Lys209, the PLP binding residue, is held in place by an active site loop (residues 24–32) directly connected with the N-terminal extension. In fact, as shown in the inset A of Fig. 8, the hydroxyl side chain of Ser31 is at an appropriate distance to make hydrogen bonds with the peptide carbonyl groups of Gln208 (3.34 Å) or Lys209 (3.27 Å) or with the $N_{\delta 2}$ of Asn212 (2.92 Å). In addition, the peptide NH of Ser31 might interact with the peptide carbonyl group of Gln208 (3.12 Å). Based on these observations, it seems reasonable to suggest that the perturbation at the N-terminus caused by P11L mutation could be transmitted through the active site loop to the PLP binding site. This could explain why PLP release takes place in AGT-Ma at urea concentrations higher than in AGT-Mi. All of this considered, it can be proposed that Pro11 in AGT may be conserved in order to optimize not only the global stability of the dimeric structure but also the local stability of the PLP binding site.

3.4. Refolding trials of AGT-Ma and AGT-Mi

AGT enzymatic activity can be restored after treatment with denaturant providing that the initial urea concentrations are <6 and <2 M for AGT-Ma and AGT-Mi, respectively, i.e., at denaturant concentrations lower than those at which monomerization occurs. At higher concentrations of denaturant, the refolding of these enzymatic species is largely irreversible. Neither quick or step dialysis, nor different initial (from 1 to 100 μM) or final (from 0.02 to 5 μM) concentration of the enzyme, had any effect on the degree of reactivation. The addition of non-ionic detergent, dithiothreitol, alanine, the use of different pH values in the reactivation mixture, or a variation of the time allowed for reactivation all failed to restore transaminase activity.

When fully denatured samples of AGT-Ma or AGT-Mi were brought by quick dilution (100-fold) in the absence or presence of PLP (from 0.01 to 1 mM) to an urea concentration that would be expected to support native enzyme, only about 20 and 5% of activity was recovered for AGT-Ma and AGT-Mi, respectively. These refolded species eluted on SEC as dimers but their integrated peaks area are

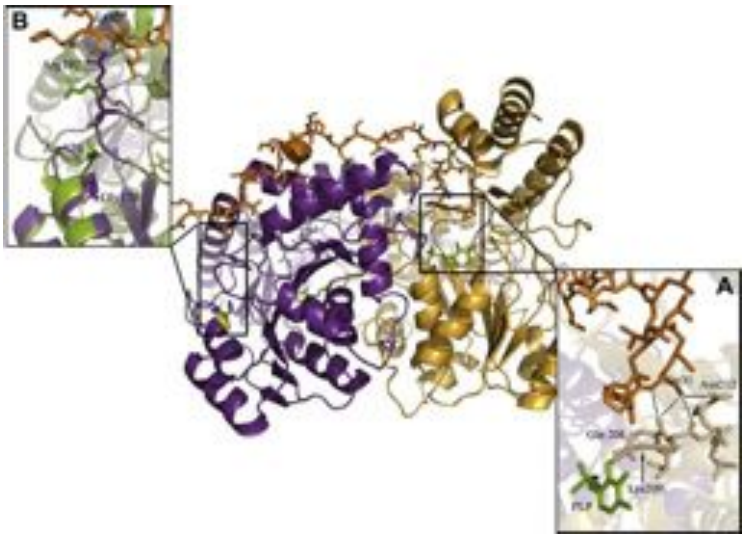

Fig. 8. Ribbon diagram of the crystal structure of AGT. Ribbon diagram of the crystal structure of AGT (PDB code 1H0C): the two subunits are coloured yellow and violet; the N-terminus (residues 1–40) of the yellow subunit, represented as ribbons/sticks, is orange; PLP, represented as sticks, is green; Gly170 of the violet subunit is yellow. Inset A: detail of the active site loop of the yellow subunit. The positions of the residues Ser31, Lys209, Gln208, and Asn212 are indicated. Black bars represent the possible hydrogen bonds involving Ser31. Inset B: detail of the region in which Gly170 is located (violet ribbons) compared with the same region in which the G170R mutation takes place (green ribbons) (PDB code 1J04). Gly170, Arg170, Arg197 and Lys5* are labelled. Black bars represent the possible hydrogen bonds involving Arg197.

about 20 and 5% of those expected, thus indicating that during the refolding the majority of the protein forms insoluble aggregates. All these data suggest that in both the allelic forms of AGT the bimolecular reaction corresponding to the monomer–dimer transition is impaired, at least under the experimental conditions tested. The refolding efficiency of AGT was also studied starting from fully denatured enzyme in 6 M guanidine hydrochloride. The recovery of enzyme activity was comparable to that obtained from 8 M-urea treated enzyme. This result is in apparent contrast with what previously reported by Coulter-Mackie et al. [18]. These authors stated that denaturation and refolding of the overexpressed AGT after guanidine hydrochloride treatment of the inclusion bodies produces high yield of biologically active protein and that successful folding of AGT was independent on the presence of PLP. This apparent contradiction can be understood by the following considerations. The finding that both soluble and insoluble fractions contain AGT enzymatically active, even if the specific activity in the untreated insoluble fraction is about 10% that in the soluble fraction, indicates that AGT is not completely unfolded in the inclusion bodies. In addition, since the unfolding has been carried out on the pellet of inclusion bodies in the presence of 6 M guanidine hydrochloride for 1 h at 4 °C, it can be hypotesized that these experimental conditions could be sufficient to extract AGT from the inclusion bodies but possibly not strong enough to completely unfold AGT.

Recently, Albert et al. [19] have solved the three-dimensional structure of a complex between the bacterial chaperonine GroEL and a folding intermediate of the I244T variant associated with the minor allele of AGT by cryo-electron microscopy. These results show that the assisted folding of this mutant is driven through the forced unfolding of a quasi-native state of the protein. Based on this finding, together with the very low refolding yield of AGT-Ma and AGT-Mi obtained in our "in vitro" refolding experiments, it can be suggested that a molecular chaperone system is vital for guiding AGT to its native state.

3.5. Sensitivity of G170R-Mi to urea and thermal stress

Cell biology studies have indicated that G170R mutation associated with the minor allele causes the aberrant localization of AGT to mitochondria instead of peroxisomes [20]. It has been hypothesized, but not proved, that an alteration of dimerization during the folding pathway could be the cause of the mistargeting of this variant [21]. In order to understand the biochemical effects of this mutation, G170R-Mi has been constructed, purified and characterized. The purified variant was homogenous as indicated by a single band on SDS-PAGE with a mobility identical to that of AGT-Ma and AGT-Mi. The yield of this variant after the standard purification was about 20% with respect to that of AGT-Mi. Like AGT-Ma and AGT-Mi, G170R-Mi variant binds 2 mol of PLP per dimer with a $K_{D(PLP)}$ of 0.4 ± 0.1 μM, a value comparable to that of AGT-Mi, and exhibits visible absorbance and CD spectra similar to those of AGT-Ma or AGT-Mi (data not shown). Again, the kinetic parameters of this variant for the pair alanine/glyoxylate ($k_{cat} = 34 \pm 3\ s^{-1}$, $K_{mL\text{-}ala} = 36 \pm 2$ mM, $K_{mglyox} = 0.4 \pm 0.1$ mM) do not significantly differ from the corresponding ones of AGT-Mi [6]. The urea unfolding profiles of holoG170R-Mi have been monitored by intrinsic fluorescence, far-UV CD and catalytic activity, and the C_m values are reported in Table 1. Data from these experiments as well as those from SEC and DLS studies are essentially equivalent to those of holoAGT-Mi (data not shown). Therefore, the G170R mutation on the minor allele of the holoform (i) does not affect either the spectroscopic or, in contrast with previous reports [22,23], the catalytic features, and (ii) does not alter the sensitivity to the urea stress. Moreover, since the unfolding profile of apoG170R-Mi monitored by far-UV CD, intrinsic (Fig. 5C) and ANS fluorescence (Fig. 6), and DLS experiments (Fig. 7) appears qualitatively comparable to that of apoAGT-Mi, it can be described by a four-state model in which the following transitions occur: native dimer → high-order aggregates → low-order aggregates → unfolded monomer. Since, like in apoAGT-Mi, the first transition of the unfolding pathway of apoG170R-Mi is protein concentration dependent, it is reasonable to suggest that monomerization gives rise to exposure of hydrophobic surfaces and aggregation. Nevertheless, it is of interest to point out that while the Cm values of the second and third transitions of apoG170R-Mi are similar to those of apo AGT-Mi, the C_m value of the first transition (∼1 M urea) is lower than that of apoAGT-Mi (C_m = ∼1.7 M urea) (Table 1). This could indicate an higher instability of the apo dimeric structure of G170R-Mi with respect to the corresponding of AGT-Mi, thus suggesting that G170R mutation alters the dimer–monomer dissociation of apoAGT-Mi.

The impact of the G170R mutation on the stability of AGT-Mi in the holo and apo forms was further investigated through monitoring the sensitivity of AGT-Mi and G170R-Mi to thermal denaturation. We performed far-UV CD-monitored heating scans of these proteins at a rate scan of 0.5 °C/min (Fig. 3 of SI). A single transition is observed for both holoenzymes with similar Tm values (72.4 ± 0.1 °C and 72.5 ± 0.1 °C for AGT-Mi and G170R-Mi, respectively). On the other hand, the thermal unfolding of the apoenzymes is a two-step process with two apparent Tm: 51. 1 ± 0.1 °C and 64 ± 1 °C for apoAGT-Mi, 48.2 ± 0.1 °C and 64 ± 1 °C for apoG170R-Mi. In both cases, the amplitude is of about 80% and 20% for the first and the second transition, respectively. Altogether these data indicate that G170R mutation only affects the stability of apoAGT-Mi, and are consistent with those obtained by urea unfolding experiments.

It is not easy to explain why G170R mutation decreases the stability of the dimeric structure of AGT-Mi in the apo form without any apparent effect on the holo form. Recently, Djordjevic et al. [24] solved the crystal structure of the major allelic form of human AGT containing the G170R mutation. The authors found that this variant has an overall structural architecture and a spatial configuration of the active site microenvironment similar to those of AGT-Ma. Thus, it is not surprising that holoG170R-Mi displays spectroscopic and catalytic properties indistinguishable from those of holoAGT-Mi. Nevertheless, significant local structural changes are seen in the vicinity of the G170R mutation (inset B of Fig. 8). Gly170 is located in the first turn of helix 168–175, and its replacement by an arginine side chain causes a conformational change leading to a 1 Å translation in the position of the Cα of residue Asp167 as well as an approximately 30° turn along the helical axis. The consequences of this helical displacement are (i) a 1.5 Å change in the Cα position of Gly170 and roughly a half peptide bond turn of the helix, and (ii) the breakdown of a salt bridge between His174 and Asp201 as well as the rotation of His174 toward solvent. It is also worth pointing out that in AGT-Ma Arg197 forms a hydrogen bond to the carbonyl O atom of Lys5 from the adjacent subunit, while the predominant rotamer of Arg197 in the G170R structure impairs the formation of this interaction. This is possibly due to change of the position of the α-helix 168–175 relative to that of the loop 184–201. On the basis of these crystallographic data, it can be speculated that the decreased stability under urea stress of the dimeric form of apoG170R-Mi compared to that of AGT-Mi could be due mainly to the loss of intersubunit hydrogen bond between Arg197 and Lys5*. The finding that the holo form of G170R-Mi exhibits dimer stability comparable to that of AGT-Mi is likely due to compensatory hydrogen bonds between PLP of one subunit and residues of the opposite subunit. However, the determination of the 3D structure of both the apo forms of AGT-Mi and G170R-Mi would be necessary to verify this interpretation.

We tried to correlate our "in vitro" results on the functional features of G170R-Mi variant with the observed enzymatic phenotype associated with this mutation. The possible folding pathway of AGT has been taken into consideration, even if we are aware that the partial reversibility of the unfolding process based on an equilibrium process does not allow a thermodynamic model to be defined. As shown in Scheme 2, the pathway a → b → c → d foresees the conversion of the unfolded monomer (U) to a partially unfolded monomer (M*), and then to a folded monomer (M) which dimerizes giving the apodimeric species (D). Upon PLP binding D is converted into the catalytically active dimer (D_{PLP}). In the alternative pathway a → b → e → f, after the conversion of U to M* and of M* to M, M would bind PLP leading to M_{PLP} which dimerizes generating D_{PLP}. On the basis of the different requirements of the protein for mitochondria or peroxisomes import, it can be postulated that unfolded (U) or loosely folded (M*) monomeric species are compatible with the mitochondrial import machinery, while folded monomeric (M and M_{PLP}) and dimeric (D and D_{PLP}) species are compatible with the peroxisomal import machinery. However, it cannot be excluded that the M* species could be also imported to the peroxisome. The route a → b → c → d should be the preferred one in that (i) the concentration of vitamin B6 in whole blood with normal dietary intake is expected to be 1.6–2 μM (with about 0.1 μM in plasma) [25], (ii) even if not yet measured, the $K_{D(PLP)}$ value of M is expected to be higher than that of D. Since G170R mutation associated with the minor allele is responsible for the mistargeting of 90–95% of AGT from its normal location in the peroxisomes to the mitochondrial matrix, the G170R-Mi variant should not follow the a → b → c → d route, and its dimeric structure should not form. This is supported by the following results and considerations. Our finding that the holodimeric form of G170R-Mi is catalytically equivalent to that of AGT-Mi indicates that, if it formed in the liver cytosol, it would be imported in the peroxisomes, and would not be pathogenic. Moreover, the G170R-Mi variant displays a PLP binding affinity comparable to that of AGT-Mi, thus implying that the responsiveness to vitamin B6 of PH1 patients carrying this mutation [26,27] could not be ascribed to the conversion of D to D_{PLP}. On this basis, and taking into account that the D species of G170R-Mi is more destabilized than the D species of AGT-Mi, it is reasonable to suggest that during the folding process of G170R-Mi the step c should be altered. As a consequence, since the formation of D is greatly impaired, the formation of monomeric forms (M* and M) could prevail. While M could undergo aggregation either in the peroxisome or in the cytosol, M* could be imported into mitochondria, possibly with a rate higher than that of its conversion to M. Following this view, and considering that the dimeric structure of AGT-Mi and P11L mutant is more destabilized than that of AGT-Ma, it can be suggested that P11L mutation itself could affect step c, even to a lower extent than when it is associated with G170R mutation. Indeed, only 5% of AGT-Mi is mistargeted to mitochondria. Thus, the functional synergism between the P11L polymorphism and the G170R mutation appears to be related to their combined effect on dimer stability. It has been previously proposed that the effect of G170R mutation on AGT-Mi consists in the retardation of dimerization in the cytosol [21]. In addition, it has been reported that treatments, known as being able to increase non-specifically the stability of proteins, correct the intracellular targeting of G170R-Mi in COS cells [26]. Although these data are in line with our results and interpretation, a thermodynamic and kinetic analysis of the monomer/dimer associative process of AGT-Ma, AGT-Mi and G170R-Mi would be necessary to clarify this issue. To this end, studies to engineer a folded monomer of AGT by site-directed mutagenesis are in progress.

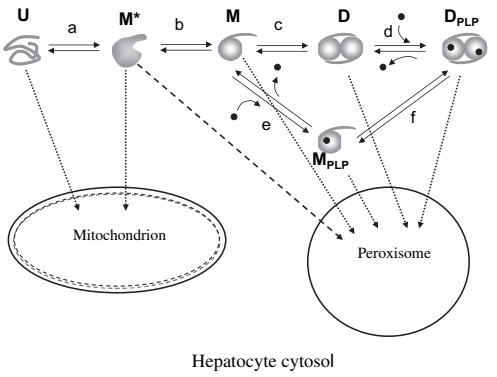

Scheme 2. Proposed pathways of AGT folding. U, unfolded monomer, M*, partially folded monomer, M, folded monomer, M_{PLP}, PLP-bound monomer, D, apodimer, D_{PLP}, holodimer and PLP (●). The arrows (…) indicate the import of different AGT species to mitochondrion or to peroxisome, the arrow (- - -) indicates the possible import of M* to peroxisome.

Nevertheless, the molecular mechanism by which the vitamin B6 therapy is able to counteract the effects caused by G170R mutation associated to the minor allele remains to be established. Based on our results, it can be argued that the effect of increasing PLP concentration (about 100–500-fold with respect to normal daily intake [23]) could result in binding of the coenzyme to the M species able to generate D_{PLP} through the route a → b → e → f. It is also possible that PLP could bind to M* leading to M_{PLP} and then to D_{PLP}. In the first case, PLP would play a prosthetic role, while in the second case it would play both conformational and prosthetic roles. The role of PLP as pharmacological chaperone in AGT folding has been already raised [22,27], even if it needs to be proved.

4. Conclusions

Our studies on the sensitivity to urea stress of AGT-Ma, AGT-Mi and P11L variant point out that the dimeric structure and the PLP binding site of AGT-Mi are destabilized with respect to AGT-Ma, and that these destabilizing effects are due to the P11L mutation. It has been proposed that this mutation is responsible for the loss of some intersubunit contacts between the N-terminus of one subunit and the large domain of the opposite subunit as well as for the perturbation transmitted from the N-terminus through the active site loop to bound-PLP. In addition, we attempted to identify the molecular basis of the impact of G170R mutation associated to the minor allele. This mutation, the most common in PH1, is responsible for a ∼90% of AGT mistargeting from its usual peroxisomal location to mitochondria [20]. Administration of vitamin B6 has a beneficial therapeutic effect in patients carrying this mutation [27,28]. The biochemical characterization of recombinant G170R-Mi has allowed us to establish that the holoform exhibits spectroscopic and catalytic features as well as sensitivity to urea and chemical stress indistinguishable from those of AGT-Mi. However, evidence is provided for a stability of its apodimer dimeric structure lower than that of apoAGT-Mi. These findings suggest that it is the dimer-monomer dissociative process to be affected in apoG170R-Mi, and that pharmacological doses of vitamin B6 allow binding of PLP to the monomeric species and rescue the variant from being targeted to mitochondria. To our knowledge, this study is the first report of the biochemical impact of G170R mutation on AGT-Mi, thus allowing to correlate the molecular defect with the pathogenic consequences of this variant.

Acknowledgments

Work was supported by grants from the Oxalosis and Hyperoxaluria Foundation and M.I.U.R. (Prin 2007) (to C.B.V.).

Appendix. Supplementary data

Supplementary data associated with this article can be found in the online version, at doi:10.1016/j.biochi.2010.08.005.

References

[1] B. Hoppe, B.B. Beck, D.S. Milliner, The primary hyperoxalurias, Kidney Int. 75 (2009) 1264–1271.
[2] E.L. Williams, C. Acquaviva, A. Amoroso, F. Chevalier, M. Coulter-Mackie, C.G. Monico, D. Giachino, T. Owen, A. Robbiano, E. Salido, H. Waterham, G. Rumsby, Primary hyperoxaluria type 1: update and additional mutation analysis of the AGXT gene, Hum. Mutat. 30 (2009) 910–917.
[3] X. Zhang, S.M. Roe, Y. Hou, M. Bartlam, Z. Rao, L.H. Pearl, C.J. Danpure, Crystal structure of alanine:glyoxylate aminotransferase and the relationship between genotype and enzymatic phenotype in primary hyperoxaluria type 1, J. Mol. Biol. 331 (2003) 643–652.
[4] P.E. Purdue, Y. Takada, C.J. Danpure, Identification of mutations associated with peroxisome-to-mitochondrion mistargeting of alanine/glyoxylate aminotransferase in primary hyperoxaluria type 1, J. Cell. Biol. 111 (1990) 2341–2351.
[5] B. Cellini, R. Montioli, A. Paiardini, A. Lorenzetto, F. Maset, T. Bellini, E. Oppici, C.B. Voltattorni, Molecular defects of the glycine 41 variants of alanine glyoxylate aminotransferase associated with primary hyperoxaluria type I, Proc. Natl. Acad. Sci. U S A 107 (2010) 2896–2901.
[6] B. Cellini, R. Montioli, A. Paiardini, A. Lorenzetto, C.B. Voltattorni, Molecular insight into the synergism between the minor allele of human liver peroxisomal alanine:glyoxylate aminotransferase and the F152I mutation, J. Biol. Chem. 284 (2009) 8349–8358.
[7] M.J. Lumb, C.J. Danpure, Functional synergism between the most common polymorphism in human alanine:glyoxylate aminotransferase and four of the most common disease-causing mutations, J. Biol. Chem. 275 (2000) 36415–36422.
[8] M.J. Lumb, A.F. Drake, C.J. Danpure, Effect of N-terminal alpha-helix formation on the dimerization and intracellular targeting of alanine:glyoxylate aminotransferase, J. Biol. Chem. 274 (1999) 20587–20596.
[9] B. Cellini, M. Bertoldi, R. Montioli, A. Paiardini, C. Borri Voltattorni, Human wild-type alanine:glyoxylate aminotransferase and its naturally occurring G82E variant: functional properties and physiological implications, Biochem. J. 408 (2007) 39–50.
[10] B. Cellini, R. Montioli, S. Bianconi, J.P. Lopez-Alonso, C.B. Voltattorni, Construction, purification and characterization of untagged human liver alanine-glyoxylate aminotransferase expressed in *Escherichia coli*, Protein Pept. Lett 15 (2008) 153–159.
[11] C.N. Pace, B.A. Shirley, J.T. Thompson (Eds.), Measuring the Conformational Stability of a Protein, IRL Press, Oxford, England, 1989, pp. 311–330.
[12] B. Cellini, M. Bertoldi, C. Borri Voltattorni, *Treponema denticola* cystalysin catalyzes beta-desulfination of L-cysteine sulfinic acid and beta-decarboxylation of L-aspartate and oxalacetate, FEBS Lett. 554 (2003) 306–310.
[13] I.M. Kuznetsova, K.K. Turoverov, V.N. Uversky, Use of the phase diagram method to analyze the protein unfolding-refolding reactions: fishing out the "invisible" intermediates, J. Proteome Res. 3 (2004) 485–494.
[14] R. Florio, R. Chiaraluce, V. Consalvi, A. Paiardini, B. Catacchio, F. Bossa, R. Contestabile, The role of evolutionarily conserved hydrophobic contacts in the quaternary structure stability of *Escherichia coli* serine hydroxymethyltransferase, FEBS J. 276 (2009) 132–143.
[15] G.B. Strambini, M. Gonnelli, Effects of urea and guanidine hydrochloride on the activity and dynamical structure of equine liver alcohol dehydrogenase, Biochemistry 25 (1986) 2471–2476.
[16] G.V. Semisotnov, N.A. Rodionova, O.I. Razgulyaev, V.N. Uversky, A.F. Gripas, R.I. Gilmanshin, Study of the "molten globule" intermediate state in protein folding by a hydrophobic fluorescent probe, Biopolymers 31 (1991) 119–128.
[17] M.R. Cellini, B. Paiardini, A. Lorenzetto, A. Maset, F. Bellini, T. Oppici, E. Borri Voltattorni, C Molecular bases of human liver peroxisomal alanine:glyoxylate aminotransferase dysfunction associated with mutations at Glycine 41, Proc. Natl. Acad. Sci. 107 (2010) 2896–2901.
[18] M.B. Coulter-Mackie, Q. Lian, S.G. Wong, Overexpression of human alanine:-glyoxylate aminotransferase in *Escherichia coli*: renaturation from guanidine-HCl and affinity for pyridoxal phosphate co-factor, Protein Expr. Purif. 41 (2005) 18–26.
[19] A. Albert, C. Yunta, R. Arranz, A. Pena, E. Salido, J.M. Valpuesta, J. Martin-Benito, Structure of GroEL in complex with an early folding intermediate of alanine glyoxylate aminotransferase, J. Biol. Chem. 285 (2010) 6371–6376.
[20] C.J. Danpure, P.J. Cooper, P.J. Wise, P.R. Jennings, An enzyme trafficking defect in two patients with primary hyperoxaluria type 1: peroxisomal alanine/glyoxylate aminotransferase rerouted to mitochondria, J. Cell. Biol. 108 (1989) 1345–1352.
[21] C.J. Danpure, Primary hyperoxaluria type 1: AGT mistargeting highlights the fundamental differences between the peroxisomal and mitochondrial protein import pathways, Biochim. Biophys. Acta 1763 (2006) 1776–1784.
[22] M.B. Coulter-Mackie, Q. Lian, Partial trypsin digestion as an indicator of misfolding of mutant alanine:glyoxylate aminotransferase and chaperone effects of specific ligands. Study of a spectrum of missense mutants, Mol. Genet. Metab. 94 (2008) 368–374.
[23] M.B. Coulter-Mackie, Q. Lian, D. Applegarth, J. Toone, The major allele of the alanine:glyoxylate aminotransferase gene: nine novel mutations and polymorphisms associated with primary hyperoxaluria type 1, Mol. Genet. Metab. 86 (2005) 172–178.
[24] S. Djordjevic, X. Zhang, M. Bartlam, S. Ye, Z. Rao, C.J. Danpure, Structural implications of a G170R mutation of alanine:glyoxylate aminotransferase that is associated with peroxisome-to-mitochondrion mistargeting, Acta Crystallogr. Sect. F Struct. Biol. Cryst. Commun. 66 (2010) 233–236.
[25] J. Leklem, Vitamin B6. in: L. Machlin (Ed.), Handbook of Vitamins. M. Dekker, Inc, New York, 1991, pp. 341–392.
[26] M.J. Lumb, G.M. Birdsey, C.J. Danpure, Correction of an enzyme trafficking defect in hereditary kidney stone disease in vitro, Biochem. J. 374 (2003) 79–87.
[27] C.G. Monico, J.B. Olson, D.S. Milliner, Implications of genotype and enzyme phenotype in pyridoxine response of patients with type I primary hyperoxaluria, Am. J. Nephrol. 25 (2005) 183–188.
[28] C.G. Monico, S. Rossetti, J.B. Olson, D.S. Milliner, Pyridoxine effect in type I primary hyperoxaluria is associated with the most common mutant allele, Kidney Int. 67 (2005) 1704–1709.

Molecular Genetics and Metabolism 105 (2012) 132–140

Contents lists available at SciVerse ScienceDirect

Molecular Genetics and Metabolism

journal homepage: www.elsevier.com/locate/ymgme

Biochemical analyses are instrumental in identifying the impact of mutations on holo and/or apo-forms and on the region(s) of alanine:glyoxylate aminotransferase variants associated with Primary Hyperoxaluria Type I ☆

Elisa Oppici, Riccardo Montioli, Antonio Lorenzetto, Silvia Bianconi, Carla Borri Voltattorni, Barbara Cellini *

Department of Life Sciences and Reproduction, Section of Biological Chemistry, Faculty of Medicine and Surgery, University of Verona, Strada Le Grazie 8 37134 Verona, Italy

ARTICLE INFO

Article history:
Received 3 August 2011
Received in revised form 28 September 2011
Accepted 28 September 2011
Available online 5 October 2011

Keywords:
Primary Hyperoxaluria Type I
Alanine:glyoxylate aminotransferase
Pyridoxal 5′-phosphate
Pathogenic mutations
Site-directed mutagenesis

ABSTRACT

Primary Hyperoxaluria Type I (PH1) is a disorder of glyoxylate metabolism caused by mutations in the human *AGXT* gene encoding liver peroxisomal alanine:glyoxylate aminotransferase (AGT), a pyridoxal 5′-phosphate (PLP) dependent enzyme. Previous investigations highlighted that, although PH1 is characterized by a significant variability in terms of enzymatic phenotype, the majority of the pathogenic variants are believed to share both structural and functional defects, as mainly revealed by data on AGT activity and expression level in crude cellular extracts. However, the knowledge of the defects of the AGT variants at a protein level is still poor. We therefore performed a side-by-side comparison between normal AGT and nine purified recombinant pathogenic variants in terms of catalytic activity, coenzyme binding mode and affinity, spectroscopic features, oligomerization, and thermal stability of both the holo- and apo-forms. Notably, we chose four variants in which the mutated residues are located in the large domain of AGT either within the active site and interacting with the coenzyme or in its proximity, and five variants in which the mutated residues are distant from the active site either in the large or in the small domain. Overall, this integrated analysis of enzymatic activity, spectroscopic and stability information is used to (i) reassess previous data obtained with crude cellular extracts, (ii) establish which form(s) (i.e. holoenzyme and/or apoenzyme) and region(s) (i.e. active site microenvironment, large and/or small domain) of the protein are affected by each mutation, and (iii) suggest the possible therapeutic approach for patients bearing the examined mutations.

1. Introduction

Primary Hyperoxaluria Type I (PH1) is a human metabolic disease whose principal hallmark is the formation of calcium oxalate stones at first in the kidneys and urinary tract and then, should renal failure occur, in the whole body [1]. Although the first clinical manifestations are related to renal dysfunction, the cause of the disease is the deficiency of an hepatic peroxisomal protein, namely alanine:glyoxylate aminotransferase (AGT) [2]. AGT is a pyridoxal 5′-phosphate (PLP)-dependent enzyme that converts L-alanine and glyoxylate into pyruvate and glycine. In the absence of AGT, the oxidation of glyoxylate by lactate dehydrogenase results in the synthesis of oxalate with the consequent formation and deposition of insoluble calcium oxalate crystals [1]. AGT is encoded by the *AGXT* gene [3], which is present in humans as two polymorphic variants, the "major allele" (AGT-Ma) and the less common "minor allele" (AGT-Mi). AGT-Mi differs from AGT-Ma by a 74-bp duplication in intron 1 and by two mutations leading to the P11L and I340M amino acid substitutions, respectively [4,5].

PH1 is characterized by a remarkable heterogeneity in terms of enzymatic phenotypes. Among the more than 150 pathogenic mutations in the *AGXT* gene identified so far [6], missense mutations are the most common type and lead to AGT deficiency by a variety of different mechanisms. Indeed, some mutations reduce AGT catalytic activity, others affect either protein folding, stability or localization inside the cell, while others, that represent the vast majority, influence at varying degrees both AGT catalytic activity and folding. Moreover, some mutations cosegregate and functionally interact with the minor allele polymorphism [7–9]. It should be pointed out that the effects of most pathogenic mutations have been identified by measuring the AGT transaminase activity (expressed as specific activity) and/or the protein expression level in crude cellular extracts or cell-free expression systems [9–16]. However, in cases of low specific activity and low expression level, this approach does not allow one to assess if a mutation exerts a structural and/or a functional impact. Since in diseases related to protein malfunction it is diagnostically and therapeutically essential to understand the multiple mechanisms that relate the specific mutants

Abbreviations: PH1, primary hyperoxaluria type I; AGT, alanine:glyoxylate aminotransferase; PLP, pyridoxal 5′-phosphate; DLS, dynamic light scattering; CD, circular dichroism; $K_{D(PLP)}$, equilibrium dissociation constant for PLP; DSF, differential scanning fluorimetry; T_m, melting temperature.

☆ This work was supported by Telethon Foundation (grant GGP10092 to C.B.V.).

* Corresponding author. Fax: +39 0458027170.
E-mail address: barbara.cellini@univr.it (B. Cellini).

1096-7192/$ – see front matter © 2011 Elsevier Inc. All rights reserved.
doi:10.1016/j.ymgme.2011.09.033

with the pathology, the knowledge of the structural and/or functional effect(s) that each amino acid substitution produces on AGT would be highly desirable. A relevant step in this direction has been the resolution of the crystal structure of AGT in complex with the inhibitor aminooxyacetic acid [17]. The structure revealed that AGT is dimeric and belongs to the aspartate aminotransferase family of PLP-dependent enzymes. Each subunit is comprised of an N-terminal extension (residues 1–21) that wraps over the surface of the other subunit, a large domain (residues 22–282) containing most of the active site and the dimerization interface, and a C-terminal domain (residues 283–392) containing the peroxisomal targeting information (Fig. 1A). As in all PLP-enzymes, the cofactor is covalently bound to the apoprotein by a Schiff base linkage with a lysyl residue which is at position 209 in AGT. The analysis of the crystal structure of AGT not only provided information on the active site topography and on the residues involved in binding of coenzyme and substrates but also allowed one to rationalize and interpret the impact of some disease-specific mutations in terms of their likely effects on AGT tertiary and quaternary conformation [17]. Indeed, in the last 5 years, biochemical and bioinformatic investigations on several pathogenic variants in the recombinant purified form have uncovered their molecular defects. In particular, it has been demonstrated that (i) the dramatic loss of catalytic activity of the G82E-Ma variant is related to its inability to undergo an efficient transaldimination [18] rather than to an impaired PLP binding, as previously suggested [9], and (ii) the decreased catalytic activity and immunoreactivity of Gly41 variants are not primarily due to the destabilization of the dimeric structure, as previously reported [9,17,19], but to the propensity of these variants in the dimeric form to undergo aggregation and degradation [20]. Additionally, evidence has been provided that the defect of G170R-Mi [21] and F152I-Mi [22] consists of a reduced dimer stability of their apo-forms. In this regard, it must be pointed out that, although the crystal structure of apoAGT is not available yet, near-UV CD and fluorescence spectra strongly suggest a different conformation between the apo- and holo-forms of AGT [20]. Importantly, the identification of the mechanism(s) leading to AGT loss of function in these variants has allowed to predict that patients carrying mutations at Gly82 or Gly41 will be unresponsive to pyridoxine treatment and to explain why patients bearing the G170R and F152I mutations have been found to be responsive to B6 therapy [23–25]. Following these considerations, it would be desirable to extend the analysis on the structural and functional properties to as many purified recombinant pathogenic variants as possible in both the holo- and apo-forms.

To this aim, we decided to elucidate the molecular basis underlying AGT loss of function in a subset of known pathogenic mutations spread over the structure of AGT. Specifically, we chose mutations affecting (i) residues at the active site directly interacting with the PLP coenzyme (Trp108, Ser158 and Asp183), (ii) a residue located in the large domain of AGT in the proximity of the active site (Ser218), and (iii) residues located far from the AGT active site either in the large (Gly161, Ser187) or in the small domain (Pro319 and Gly350) (Figs. 1A and B). Enzyme activity, PLP binding mode and affinity, oligomerization, and thermal unfolding were analyzed for each of these variants in its purified holo- and apo-forms. The integrative analysis of the kinetic, spectroscopic and thermostability data allows one to (i) establish that, in contrast with previous data obtained on crude lysates, not all the variants have both structural and functional defects, (ii) define if a mutation causes a structural defect limited to the active site or extended to the large and/or the small domain of AGT, and (iii) suggest the treatment that could be effective for patients carrying the examined mutations.

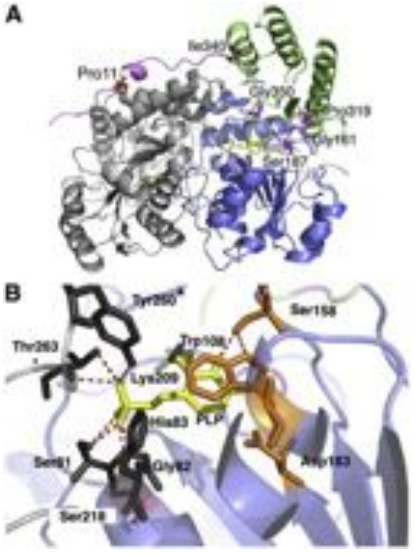

Fig. 1. 3D representation of the AGT structure (PDB file 1H0C). (A) Overall structure of the AGT dimer. One monomer is colored gray, while in the opposite monomer the N-terminus, the large domain and the small domain are colored magenta, blue and green, respectively. PLP is represented as yellow sticks. Pro11 and Ile 340 are represented as red sticks, while Gly161, Ser187, Pro319 and Gly350 are represented as magenta sticks. (B) The AGT active site is shown. PLP is represented as yellow sticks. Residues directly interacting with PLP are represented as dark gray sticks or, if their mutation is analyzed in this study, as orange sticks. Ser218 is represented as magenta sticks. The dotted lines indicate possible hydrogen bond interactions. The figure was rendered using PyMol [26].

2. Materials and methods

2.1. Materials

PLP, SYPRO orange, L-alanine, sodium glyoxylate, pyruvate, rabbit muscle L-lactic dehydrogenase, and isopropyl β-D-thiogalactopyranoside were all purchased from Sigma. All other chemicals were of the highest purity available.

2.2. In silico analyses

In silico mutagenesis analyses were performed by means of the software PyMol [26] (DeLano Scientific) starting from the three-dimensional structure of AGT (pdb files 1H0C_A and 1H0C_B).

2.3. Site-directed mutagenesis

The polymorphic and pathogenic variants of AGT were constructed starting from the pAGT-His construct that contains the complete open reading frame of AGT cloned in a pTrcHis2A expression plasmid [9]. The mutations were introduced by using the QuikChange site-directed mutagenesis kit (Stratagene) and the oligonucleotides used for mutagenesis are reported in Supplementary Table 1. All the mutations were confirmed by the entire DNA sequence analysis.

2.4. Protein expression and purification

Mutant enzymes in their histidine-tagged form were expressed in *E. coli* and purified with the procedure already described [18]. The apo-form of each variant was prepared as previously described [18]. The protein concentration in the AGT samples was determined by absorbance spectroscopy using an extinction coefficient of $9.54 \times 10^4\ M^{-1}\ cm^{-1}$ at 280 nm [18]. The PLP content of the holoenzymes was determined by releasing the coenzyme in 0.1 M NaOH and by using an $\varepsilon_M = 6600\ M^{-1}\ cm^{-1}$ at 388 nm.

2.5. Determination of the equilibrium dissociation constants of the variants for PLP

The equilibrium dissociation constant for PLP ($K_{D(PLP)}$) of G161C-Mi, G161S-Mi, P319L-Ma and G350D-Mi variants was determined by measuring the quenching of the intrinsic fluorescence of the apo-enzymes (0.1 μM) in the presence of PLP at a concentration range of 0.01–10 μM. In the case of W108R-Mi, S158L-Ma, D183N-Ma and S218L-Ma variants, the $K_{D(PLP)}$ was determined by measuring the CD signal at 430 nm of the apo forms at a concentration of 10 μM in the presence of PLP at concentrations ranging from 5 to 300 μM. All the experiments were carried out in 100 mM potassium phosphate buffer, pH 7.4. The $K_{D(PLP)}$ values for the mutant–coenzyme complexes were obtained by using the following equation:

$$Y = Y_{max}\frac{[E]_t + [PLP]_t + K_{D(PLP)} - \sqrt{\left[(E)_t + [PLP] + K_{D(PLP)}\right)^2 - 4[E]_t[PLP]_t}}{2[E]_t}$$

where $[E]_t$ and $[PLP]_t$ represent the total concentrations of the mutant and PLP, respectively, Y refers to either the intrinsic fluorescence quenching or the 430 nm dichroic signal changes at a PLP_t concentration, [PLP], and Y_{max} refers to the aforementioned changes when all enzyme molecules are complexed with coenzyme.

The $K_{D(PLP)}$ for the S187F-Ma variant has been estimated as the upper limit value by the following procedure: samples of holo- and apo-S187F-Ma at various protein concentrations (from 0.01 to 1 μM, being 0.01 μM the detection limit) were incubated overnight at 25 °C in 100 mM potassium phosphate buffer, pH 7.4. The intrinsic fluorescence emission at 336 nm of each sample was registered and the percentage of fluorescence quenching at each protein concentration was then calculated.

2.6. Enzyme activity measurements

The kinetic parameters for the overall transamination reaction for the pair alanine/glyoxylate of the AGT variants (0.1–10 μM) were determined in the presence of saturating PLP concentration by varying the substrate concentration at a fixed saturating co-substrate concentration. For the G161C-Mi, G161S-Mi, S218L-Ma, P319L-Ma and G350D-Mi variants pyruvate formation was measured by a spectrophotometric assay using the coupled lactate dehydrogenase system previously described [18], while for the W108R-Mi, S158L-Ma, D183N-Ma and S187F-Ma variants a more sensitive assay based on measuring the 2,4-dinitrophenylhydrazine derivative of pyruvate by HPLC analysis was used [27]. Data of initial velocity as a function of substrate concentration were fitted to the Michaelis–Menten equation.

2.7. Dynamic light scattering (DLS)

Stock solutions of all AGT variants, either in the holo- or the apo-form, were diluted to 10 μM concentration with 100 mM potassium phosphate buffer, pH 7.4. PLP at saturating concentrations was added to the holoenzyme solutions. Each sample was incubated for 10 min at 25 °C and DLS analysis was performed on a ZetasizerNano S device (Malvern Instruments) by using disposable 12.5 × 45-mm cells with stopper. The temperature was kept at 25 ± 0.1 °C during the measurements by a Peltier temperature controller.

2.8. Thermostability

The thermostability studies on purified AGT variants in the holo- (in the presence of saturating PLP) or the apo-form were performed by both CD-monitored thermal unfolding and differential scanning fluorimetry (DSF). In the first method, the CD signal at 222 nm of AGT variants at 10 μM concentration in 100 mM potassium phosphate buffer, pH 7.4, was registered with temperature increasing from 25 to 90 °C at a heating rate of 1.5 °C/min. For the holo-forms the PLP dissociation during thermal unfolding was also monitored by measuring the CD signal at 430 nm under the same experimental conditions reported above. Calculation of the melting temperatures (T_m) was carried out by fitting the CD signal either to a two or a three state unfolding model using the Origin Pro7 software according to the method of Pace [28]. The rates of PLP dissociation and loss of secondary structure at the melting temperature for both AGT-Ma and AGT-Mi were measured by monitoring the CD signal at 430 and 222 nm with time, and fitting the data to a single exponential curve.DSF experiments were performed with purified AGT variants at the concentration of 1 μM in 100 mM potassium phosphate buffer pH 7.4 containing 5× SYPRO orange, according to the method of Nielsen et al. [29]. Considering the high background fluorescence of the holo- and apo-forms of W108R-Mi at 25 °C, the SYPRO orange final concentration was 2.5×. Proteins were subjected to a ramp of 2.15 °C/min in a Mastercicle EP Realplex 4 (Eppendorf) at a temperature gradient from 25 °C–90 °C. Graph generation and calculation of T_m were carried out by using the Realplex software.

2.9. Spectroscopic measurements

Absorption measurements were made with a Jasco V-550 spectrophotometer with a 1 cm path length quartz cuvette at a protein concentration of 1–10 μM. Visible and far-UV CD spectra were recorded on a Jasco J-710 spectropolarimeter equipped with a thermostatically controlled compartment at 25 °C, by using 1 cm path-length quartz cuvettes. The enzyme concentration was 1–10 μM and the spectra of the holoenzymes were recorded in the presence of saturating PLP concentrations. Routinely, three spectra were recorded at a scan speed of 50 nm/min^{-1} with a bandwidth of 2 nm and averaged automatically. Intrinsic fluorescence emission spectra were recorded on a Jasco FP-750 spectrofluorometer equipped with a thermostatically controlled cell holder.

3. Results

3.1. In silico analyses

To investigate the possible local effect of each of the studied amino acid substitutions on AGT we mapped them onto the available crystal structure of the enzyme in its major allelic form [17] and performed in silico mutagenesis by the software PyMol [26]. The location of the residues whose mutation has been analyzed in this work is shown in Figs. 1A and B. Trp108, Ser158 and Asp183 are active site residues that directly interact with the coenzyme. The side chain of Ser158 is hydrogen-bonded to the 3′ hydroxyl group of PLP, the indolic ring of Trp108 forms a base-stacking interaction with the pyridine ring of the coenzyme, and the carboxylic group of Asp183 forms a salt-bridge with the positive pyridine nitrogen of PLP. Thus, it can be predicted that the W108R, S158L and D183N mutations could have a functional effect on AGT, by possibly altering the binding of the coenzyme and/or the catalytic properties of the enzyme. Ser218, a residue located near the active site, does not interact with the coenzyme, and is located at the end of the strand 6 of the β-barrel. Since its hydroxyl group could interact with the peptydic oxygens of Ser81, Gly80 and Ile78, this residue might be involved in the proper positioning of the helix 4 that also comprises Gly82, a residue hydrogen-bonded to the PLP phosphate. The S218L mutation is predicted to have a local structural effect on the large domain, possibly resulting in the distortion of the coenzyme binding cleft. Gly161 and Ser187 are two large domain residues located far from the active site. Gly161 is located at the interface between the large and the small domain and the in silico analysis predicts that both G161C and G161S mutations would alter

the inter-domain contacts of the AGT subunit. Ser187 is located in a random coil region on the *re* face of the coenzyme and its substitution with a phenylalanine residue would possibly change the positioning of the loop 154–169 comprising Gly161, thus indirectly affecting the large domain/small domain contacts. Finally, Pro319 and Gly350 belong to two random coil regions of the small domain. It can be predicted that the P319L mutation could have a structural effect on the small domain by leading to a mispositioning of the helix 11 located on the surface of the protein. Gly350 faces the active site on the *si* side of the coenzyme and the Gly350-to-Asp substitution could induce steric clashes of the small domain, in particular of the loop 343–357.

3.2. E. coli expression and purification

E. coli expression vectors encoding for the selected pathogenic variants were constructed by site-directed mutagenesis. Each mutation was inserted on the background of the major or the minor allele according to the genotype of the PH1 patients in whom the mutation was identified. Then, by a previously developed protocol [18], the nine AGT variants were expressed and purified to homogeneity, as indicated by a single band on SDS–PAGE at an apparent molecular weight of about 45 KDa (data not shown). The majority of the mutant proteins was present in good amounts in the soluble extract as compared to AGT-Ma or AGT-Mi, except Gly161 variants whose yield is ~10% that of AGT-Mi. The far-UV CD spectrum of each variant in the apo-form was registered and found to be identical to that of apoAGT-Ma or apoAGT-Mi, thus indicating that the mutations do not introduce major changes on the secondary structure of the protein. Moreover, the molecular dimensions of the variants in both the holo- and apo-forms have been determined by DLS. For each protein at 10 μM concentration in 100 mM potassium phosphate buffer pH 7.4, a peak with a size ranging from 9.2 to 10.8 nm, corresponding to that of a dimer, could be seen. This indicates that the dimer is the most abundant species in solution, given that the intensity of the signal on DLS varies with the sixth power of a particle diameter. However, the presence of low amounts of small aggregates (100–400 nm) could be noticed for W108R-Mi, S218L-Ma, S187F-Ma, G161C-Mi, G161S-Mi and P319L-Ma in both the holo- and apo-forms as well as for G350D-Mi in the apo-form (data not shown).

3.3. PLP binding mode and affinity

The equilibrium dissociation constants ($K_{D(PLP)}$) for the complexes between PLP and the variants were determined by titrating the apo-form of each enzymatic species with increasing concentrations of PLP and by fitting the data to the appropriate equation. The obtained $K_{D(PLP)}$ values are reported in Table 1 along with the previously determined $K_{D(PLP)}$ values for AGT-Ma and AGT-Mi [18,22]. Basing on these data, it can be observed that: (i) W108R-Mi, S158L-Ma, D183N-Ma and S218L-Ma, even if at different extents, show a significantly reduced affinity for the coenzyme while (ii) G161C-Mi, G161S-Mi, P319L-Ma and G350D-Mi display an unaltered or even increased affinity for PLP. In the case of S187F-Ma, the enzyme concentration required for fluorescence measurements far exceeds the $K_{D(PLP)}$, which precludes the determination of a precise value for $K_{D(PLP)}$. Thus, only an upper limit of 0.01 μM has been estimated for the $K_{D(PLP)}$ of the S187F-Ma variant.

Coenzyme binding to AGT gives rise to typical absorbance bands at 430 and 340 nm associated with positive and negative dichroic signals, respectively [18]. In order to define if the analyzed PH1-causing mutations could alter the AGT coenzyme binding mode, the UV–visible absorbance and CD spectrum of each enzymatic species at 10 μM concentration has been registered in the presence of saturating PLP concentrations (Fig. 2), and the corresponding optical activity (expressed as millidegrees/absorbance at 410–430 nm) has been calculated (Table 1). The results indicate that, at varying degrees, only the W108R,G161C, G161S, S158L and S218L mutations decrease the optical activity with respect to that of AGT-Ma or AGT-Mi, thus indicating that these mutations cause a change in the microenvironment of the internal aldimine. It is worth noting that, although the S187F-Ma variant does not show an altered value of the optical activity, its internal aldimine is characterized by about 6 nm-blue shifted absorbance and dichroic maxima (Fig. 2A). This finding, along with the increase of at least about 27-fold in the $K_{D(PLP)}$ value, suggests that the mutation should induce some local structural changes at the AGT active site.

Table 1
Equilibrium dissociation constants for PLP ($K_{D(PLP)}$) and optical activity of AGT-Ma, AGT-Mi and pathogenic variants.

Enzymatic species	$K_{D(PLP)}$ (μM)	Optical activity
AGT-Ma	0.27 ± 0.03[a]	97 mdeg/Abs 420 nm[a]
AGT-Mi	0.26 ± 0.02[b]	97 mdeg/Abs 420 nm[b]
W108R-Mi	96 ± 19	4.73 mdeg/Abs 434 nm
S158L-Ma	272 ± 47	45 mdeg/Abs 430 nm
G161S-Mi	0.46 ± 0.07	66 medeg/Abs 430 nm
G161C-Mi	0.56 ± 0.09	57 mdeg/Abs 414 nm
D183N-Ma	2.1 ± 0.1	84 mdeg/Abs 430 nm
S187F-Ma	<0.01	103 mdeg/Abs 414 nm
S218L-Ma	24.2 ± 0.1	31 mdeg/Abs 428 nm
P319L-Ma	0.19 ± 0.04	88 mdeg/Abs 420 nm
G350D-Mi	0.031 ± 0.005	88 mdeg/Abs 420 nm

[a] From Cellini B. et al. [18].
[b] From Cellini B. et al. [22].

3.4. Enzymatic activity

The steady-state kinetic parameters of the overall transamination of the alanine-glyoxylate pair were measured on the variants and compared with those of either AGT-Ma or AGT-Mi. A summary of the resulting steady-state parameters is listed in Table 2. The k_{cat}/K_m value of D183N-Ma vs AGT-Ma and W108R-Mi vs AGT-Mi is decreased by ~23,000- and 30,000-fold, respectively. The reduction in the catalytic efficiency is mainly driven by the decrease in the k_{cat} value, being about 0.02% and 0.04% that of AGT-Ma and AGT-Mi, respectively. Both S158L and S218L mutations do no significantly change the K_m values, but reduce the k_{cat} values of AGT-Ma by ~100-fold and ~16-fold, respectively, thus causing a reduction in the catalytic efficiency. As for S187F-Ma, the K_m and the k_{cat} values decrease by ~2- and 360-fold, respectively, as compared to AGT-Ma. Taken together, these results agree with those previously obtained on both purified proteins [13] and crude bacterial extracts [12]. On the other hand, a moderate, if any, reduction of the k_{cat} value (≥50% residual activity) has been observed for the P319L-Ma variant (vs AGT-Ma) and for the G161C-Mi, G161S-Mi, and G350D-Mi variants (vs AGT-Mi). This is in contrast with previous reports showing that the specific activity of Gly161 variants and G350D-Mi in crude cellular extracts was less than 1% [12] and 2.9% [30], respectively, that of AGT-Ma. However, the subsaturating substrate concentration used in these studies (150 mM L-alanine, by comparison see the K_m values for L-alanine listed in Table 2) coupled with the low expression level of these variants might explain this discrepancy.

3.5. Thermal stability studies

To investigate whether the analyzed PH1-associated mutations could affect the stability of AGT, which could give information about the steady-state amount of active enzyme, we compared the thermal unfolding profiles of the purified variants with those of AGT-Ma or AGT-Mi.

Thermal protein denaturation was studied either by monitoring the decrease of the dichroic signal at 222 nm and 430 nm, which are indicative of the loss of the protein secondary structure and of the PLP-bound

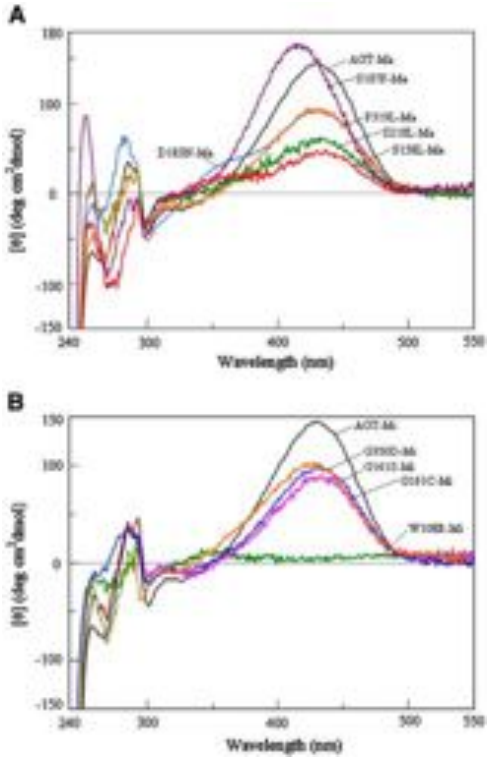

Fig. 2. CD spectra of AGT-Ma, AGT-Mi and pathogenic variants. (A) CD spectra of AGT-Ma (black), S158L-Ma (red), D183N-Ma (blue), S187F-Ma (violet), S218L-Ma (green) and P319L-Ma (orange).(B) CD spectra of AGT-Mi (black), W108R-Mi (green), G161C-Mi (fucsia), G161S-Mi (blue) and G350D-Mi (orange). All CD spectra are registered in the presence of saturating PLP concentrations in 100 mM potassium phosphate buffer, pH 7.4, at an enzyme concentration of 9 μM.

content, respectively, or by differential scanning fluorimetry (DSF), that allows one to monitor unfolding events by measuring the exposure of hydrophobic groups of the denaturing protein [29]. This analysis was performed both in the holo- and apo-forms of each enzymatic species and the obtained results are listed in Tables 3 and 4, respectively. The far-UV (222 nm) (Fig. 3) and the visible (430 nm) CD-monitored heating scans as well as the DSF experiments reveal that the holo-forms of AGT-Ma and AGT-Mi are denatured and release PLP in a single-step process with melting temperatures at about 78 °C and 74 °C, respectively. This is in agreement with previous results obtained by differential scanning calorimetry [20] and thermal inactivation experiments [22]. In order to assess whether the loss of secondary structure and the PLP release are concerted events in these enzymatic species, the kinetics of changes of the 430 nm and 222 nm have been measured at their T_m values. We found that while the rate constant of the loss of the 430 nm dichroic signal is $0.0042 \pm 0.0001\ s^{-1}$ and $0.0057 \pm 0.003\ s^{-1}$ for AGT-Ma and AGT-Mi, respectively, that of the loss of the 222 nm dichroic band is $0.0024 \pm 0.0001\ s^{-1}$ and $0.0021 \pm 0.001\ s^{-1}$. These data provide evidence for a higher local stability of the PLP binding site in AGT-Ma than in AGT-Mi, in line with the higher sensitivity to urea stress of the PLP-bound state of the latter form [21]. They also indicate that both the allelic forms of AGT release the coenzyme before losing their secondary structure, as corroborated by the finding that, when the coenzyme is covalently bound to the protein by $NaBH_4$-reduction, the mid-point transition of AGT-Ma and AGT-Mi is at 85.6 °C and 79.1 °C, respectively.

Like holoAGT-Ma and holoAGT-Mi, the nine pathogenic variants in the holo-form display a single thermal transition with the T_{mholo} values, derived from the 222 nm CD and DSF measurements, comparable to the corresponding resulting from the 430 nm CD measurements (T_{mPLP}). The D183N mutation appears to exert a stabilizing effect, while the S187F, G350D and P319L mutations do not exert any effect on protein stability. For all the remaining variants the transition from the native state to the unfolded state occurs at temperatures lower than the corresponding wild-type, i.e. AGT-Ma or AGT-Mi. The variants W108R-Mi and S218L-Ma show the most pronounced alteration with T_{mholo} of 54° and 57 °C, respectively. However, it should be noted that W108R-Mi displays a considerably (~10-fold) elevated ground state fluorescence signal at 25 °C in comparison with AGT-Mi, thus suggesting an increased hydrophobicity due to partial protein unfolding even without the application of the thermal stress.

Interestingly, the apo-forms of AGT-Ma and AGT-Mi display a first unfolding phase with a mid-denaturation at 61 °C and 53 °C for AGT-Ma and AGT-Mi, respectively, and then a second unfolding transition with a mid-denaturation at 66 °C for both AGT-Ma and AGT-Mi (Fig. 3). In order to define the impact of the nine pathogenic mutations on the intrinsic stability of AGT, the thermal unfolding of the apo-form of each variant has been measured by far-UV CD (Supplementary Fig. 1) and DSF experiments. Apo-S158L-Ma unfolds in a single-step process with a T_{mapo} value identical to that of the high-temperature transition (T_{m2apo}) of apoAGT-Ma, thus suggesting that this large domain mutation does not significantly affect the T_{m2apo} value. On the other hand, the small domain mutations G350D and P319L, associated with the major and the minor alleles, respectively, cause the complete loss of the high-temperature transition (T_{m2apo}) without affecting the low-temperature transition (T_{m1apo}). All together, these findings indicate that the mutations of residues located in the large or in the small domain only affect the T_{m1apo} or the T_{m2apo} values, respectively.

Distinct alterations of thermal unfolding parameters were observed for the variants S187F-Ma, G161C-Mi and G161S-Mi in the apo-form. These residue replacements in the large domain give rise to a single thermal transition with a mid-point at temperatures lower than those of the T_{m1apo} of AGT-Ma or AGT-Mi. On the other hand, a two step process was observed for apo-S218L-Ma and apo-W108R-Mi with both transition left-shifted, and T_{mapo} values lower than those of apoAGT-Ma and apoAGT-Mi, respectively. These data suggest that these large domain mutations not only exert destabilizing effects of the domain in which they are located but also influence the structural stability of the region responsible for the high-temperature transition.

It should be noted that the analysis of apo-W108R-Mi performed using DSF, unlike that performed using CD, reveals a single T_{mapo} value similar to the T_{m2apo} measured by CD. This could be explained by the fact that this apovariant has a ground state fluorescence 100-fold higher than that of apoAGT-Mi, reflecting an increased hydrophobicity due to partial protein unfolding of the native apoprotein.

4. Discussion

To date, about 150 point mutations leading to PH1 have been identified that span throughout all the 11 exons of the *AGXT* gene and about half of them are missense mutations [6]. While prediction of the effect of splice-site mutations, premature stop-codon insertion and major deletions is straightforward, missense point mutations or small insertions/deletions are more dubious and suitable instruments should be available to evaluate their consequences on the AGT structural and/or functional properties. Until now, the effect of many PH1-causing mutations has been evaluated by either the analysis of patient liver samples or by eukaryotic and/or prokaryotic cell expression

Table 2
Steady-state kinetic parameters of AGT-Ma, AGT-Mi and pathogenic variants for the pair alanine-glyoxylate.

Enzymatic species	Substrate	Cosubstrate	k_{cat} (s^{-1})	$K_{m\ L\text{-alanine}}$(mM)	$K_{m\ Glyoxylate}$ (mM)	k_{cat}/K_m (s^{-1}/mM^{-1})
AGT-Ma[a]	L-Alanine	Glyoxylate	45 ± 2[a]	31 ± 4[a]		1.4 ± 0.2[a]
	Glyoxylate	L-Alanine	45 ± 2[a]		0.23 ± 0.05[a]	196 ± 4[a]
AGT-Mi[b]	L-Alanine	Glyoxylate	33 ± 5[b]	28 ± 2[b]		1.2 ± 0.2[b]
	Glyoxylate	L-Alanine	37 ± 1[b]		0.22 ± 0.01[b]	168 ± 8[b]
W108R-Mi	L-Alanine	Glyoxylate	0.0013 ± 0.0003	36 ± 3		0.00004 ± 0.00001
	Glyoxylate	L-Alanine	n.d.		n.d.	n.d.
S158L-Ma	L-Alanine	Glyoxylate	0.41 ± 0.03	25 ± 6		0.016 ± 0.001
	Glyoxylate	L-Alanine	0.41 ± 0.04		0.35 ± 0.09	1.2 ± 0.3
G161S-Mi	L-Alanine	Glyoxylate	55 ± 2	70 ± 9		0.8 ± 0.1
	Glyoxylate	L-Alanine	58 ± 2		0.63 ± 0.07	92 ± 2
G161C-Mi	L-Alanine	Glyoxylate	36.1 ± 0.7	103 ± 6		0.35 ± 0.02
	Glyoxylate	L-Alanine	36.6 ± 0.7		0.21 ± 0.02	174 ± 1
D183N-Ma	L-Alanine	Glyoxylate	0.008 ± 0.003	140 ± 17		0.00006 ± 0.00001
	Glyoxylate	L-Alanine	n.d.		n.d.	n.d.
S187F-Ma	L-Alanine	Glyoxylate	0.13 ± 0.01	12 ± 2		0.0108 ± 0.0002
	Glyoxylate	L-Alanine	0.12 ± 0.01		0.13 ± 0.04	0.92 ± 0.09
S218L-Ma	L-Alanine	Glyoxylate	2.7 ± 0.1	29 ± 6		0.09 ± 0.02
	Glyoxylate	L-Alanine	2.95 ± 0.08		0.19 ± 0.02	15 ± 2
P319L-Ma	L-Alanine	Glyoxylate	27.5 ± 0.8	44 ± 5		0.63 ± 0.01
	Glyoxylate	L-Alanine	26.2 ± 0.7		0.11 ± 0.02	238 ± 44
G350D-Mi	L-Alanine	Glyoxylate	15.0 ± 0.7	328 ± 51		0.046 ± 0.007
	Glyoxylate	L-Alanine	15 ± 1		0.29 ± 0.04	52 ± 7

n.d. not determined because the rate of glyoxylate half-transamination is comparable to that of PMP dissociation/PLP association at sub-saturating glyoxylate concentrations.
[a] From Cellini B. et al. [18].
[b] From Cellini B. et al. [22].

experiments [9,11–13,15,16,19,31–35]. These studies led to classify all the known pathogenic mutations according to their effect on the AGT catalytic activity and/or immunoreactivity [7,9,36]. During the last years, however, a more detailed biochemical and bioinformatic characterization of several purified recombinant pathogenic variants in both the holo- and apo-forms allowed identification of their defect (s) at a molecular level [18,20–22]. A more complex scenario of the pathogenic mechanisms responsible for AGT deficiency has emerged, thus highlighting that the heterogeneity of the PH1-causing enzymatic phenotypes could be even wider than previously thought and substantiating the idea that a definition of the defect of the AGT variants at molecular level would be highly desirable.

On these bases, we have explored the structural and functional properties of nine pathogenic variants by using in silico predictions based on the available crystal structure of the protein [17] and by defining some biochemical properties of the variants in their holo- and apo- recombinant purified forms. Each mutation was inserted on the background of either the major or the minor allele on the basis of the genotype of PH1 patients. We report the consequences of each amino acid substitution on: (i) the coenzyme binding mode and affinity and the catalytic activity, which are indicative of the effect of a mutation on the AGT functional properties, and (ii) the quaternary structure and the thermal stability of the protein in the holo- and apo-forms, which together are indicative of the structural effects of a particular mutation and of the possible role of the coenzyme on protein stability.

The first observation that comes from our data concerns the thermostability of AGT-Ma and AGT-Mi in the holo form measured either by the loss of secondary/tertiary structure or by the PLP release. Interestingly, in both of these species (i) the T_{mholo} and T_{mPLP} values are identical, (ii) the rate of PLP release is higher than that of the global unfolding, and (iii) the T_{mholo} is lower than the mid-point transition of the $NaBH_4$-reduced form. Thus, since a conversion from the holo- to the apo-form occurs during the thermal transition, the T_{mholo} values are affected by the sensitivity of the active site to the thermal stress. Nevertheless, our results clearly show that, in agreement with previous studies [21,37], AGT-Ma and AGT-Mi in the apo-form are significantly less stable than the corresponding holo-forms. In addition, while a single transition occurs during the thermal unfolding of the holo-proteins, two transitions with melting temperatures (T_{m1apo} and T_{m2apo}) lower than the corresponding T_{mholo} characterize the thermal unfolding of the apoproteins. Taken together, these data

Table 3
T_{mholo} and T_{mPLP} values of AGT-Ma, AGT-Mi and pathogenic variants.

Enzymatic species	T_{mholo}[a](°C) $CD_{222\ nm}$	T_{mPLP}[a](°C) $CD_{420\ nm}$	T_{mholo}[a](°C) DSF
AGT-Ma	77.5	78	78.6
AGT-Mi	73.6	73.6	74.1
W108R-Mi	54.1	53.4	53.9
S158L-Ma	67	64	64.7
G161S-Mi	62.5	62.8	61.8
G161C-Mi	64	64.2	63.8
D183N-Ma	80.8	79.6	80.1
S187F-Ma	76.7	74.4	73.6
S218L-Ma	57.8	57.9	56
P319L-Ma	77.9	76.3	77.5
G350D-Mi	73.5	73.7	72.6

[a] They represent apparent T_m values and are the mean of two independent experiments. The error is within ±0.3 °C.

Table 4
T_{mapo} values of AGT-Ma, AGT-Mi and pathogenic variants.

Enzymatic species	T_{m1apo}[a](°C) $CD_{222\ nm}$	T_{m2apo}[a] (°C) $CD_{222\ nm}$	T_{m1apo}[a] (°C) DSF	T_{m2apo}[a] (°C) DSF
AGT-Ma	61.1	66.4	61.9	67.3
AGT-Mi	53.1	66	54.2	66.5
W108R-Mi	48.9	54		53.3
S158L-Ma	65.9		64.3	
G161S-Mi	46.8		46.5	
G161C-Mi	51.1		51.3	
D183N-Ma	70.2		70.3	
S187F-Ma	48.2		45.3	
S218L-Ma	50.9	57.8	47.2	55.7
P319L-Ma	61.6		60.1	
G350D-Mi	53.6		52.5	

[a] They represent T_m values and are the mean of two independent experiments. The error is within ±0.3 °C.

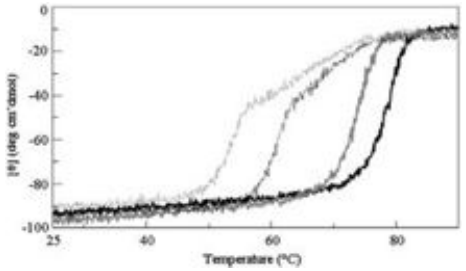

Fig. 3. Far-UV CD-monitored heating scans of AGT-Ma and AGT-Mi. Far-UV CD changes of holoAGT-Ma (black curve, straight line) and holoAGT-Mi (gray curve, straight line) in the presence of 10 μM exogenous PLP, and of apoAGT-Ma (black curve, dotted line) and apoAGT-Mi (gray curve, dotted line). The enzyme concentration was 10 μM, and the buffer was 100 mM potassium phosphate, pH 7.4.

indicate that (i) PLP located at the interface between the two subunits is responsible for the higher stability of holoAGT-Ma and holoAGT-Mi with respect to the corresponding apo-forms, and (ii) the large and small domains unfold in a concerted and cooperative way in the holo-forms, while appear to be differentially stabilized in the apoenzymes. Considering that PLP makes several contacts with the large domain only [17], it can be speculated that in the apoenzymes, but not in the holoenzymes, the large domain could be less stable than the small one. Accordingly, the three state model of thermal denaturation of apoAGT can be described as a process in which a low-temperature transition (T_{m1apo}), that represents the unfolding of the large domain, is followed by a high-temperature transition (T_{m2apo}), that represents the unfolding of the small domain, and by irreversible protein denaturation. This interpretation might explain the reason why the two polymorphic mutations typical of the minor allele induce a ~8 °C reduction only in the T_{m1apo}. Previous evidences have indicated that the reduced stability of AGT-Mi might depend on a distortion of the N-terminal arm of the protein caused by the P11L substitution that, in turn, likely destabilizes the dimeric structure of AGT [21]. Since the N-terminal arm wraps over the surface of the opposite subunit that interacts with the large domain, it follows that the distortion of the N-terminus could specifically destabilize the large domain of AGT.

In Table 5 the major defect(s) of the nine pathogenic variants analyzed on crude lysates and on recombinant purified protein are listed. On the basis of the functional and structural features of the pathogenic variants in the holo-form, it can be inferred that (i) D183N-Ma, G350D-Mi and S187F-Ma display exclusively a functional defect. It is reasonable that Asp183, in analogy with what observed upon replacement of Asp222 with asparagine in *E. coli* aspartate aminotransferase [38], plays a role in stabilizing the positive charge at N(1) of PLP, thus enhancing the electron withdrawing capacity of the coenzyme. Moreover, the functional defect of G350D-Mi, that could be ascribed to as one possible cause of its pathogenicity, might be its high $K_{m\ L\text{-alanine}}$ value. According to the in silico analysis, the substitution of Gly350 with an aspartate residue changes the conformation of the loop 343–357 at the entrance of the AGT active site, thus possibly affecting substrate binding. On the other hand, considering that Ser187 is a residue far from the active site, the features of S187F-Ma in terms of specific activity, PLP binding affinity and mode are unexpected and difficult to explain. (ii) W108R-Mi, S158L-Ma and S218L-Ma are characterized by a functional defect (decreased catalytic activity and PLP binding affinity as well as altered coenzyme binding mode) associated with an increased sensitivity to thermal stress limited to the active site microenvironment. This is not surprising, taking into account that Ser158, Ser218, and Trp108, residues belonging to the large domain, interact directly or indirectly with functional groups of PLP. (iii) HoloGly161 variants show exclusively a structural defect consisting in a decreased thermostability of their active site, and (iv) P319L-Ma in the holo form appears to display neither a functional nor a structural defect. Notably, by looking at the thermal unfolding profiles of these variants in the apo-form, a more detailed and enlightening picture of their molecular defects comes out. Unlike AGT-Ma and AGT-Mi, all the apo forms of the examined variants, except S218L-Ma and W108R-Mi, exhibit a single transition. Based on the T_{mapo} values reported in Table 4, and considering the thermal unfolding model proposed for apoAGT-Ma and apoAGT-Mi, it can be deduced that the large domain D183N and S158L mutations do not decrease AGT stability, being the T_{mapo} values of S158L-Ma and D183N-Ma similar to or higher than the T_{m2apo} of AGT-Ma. On the other hand, the large domain G161S, G161C, S187F, W108R, and S218L mutations cause a destabilizing effect not limited to the large domain but extended to the small domain. In fact, the T_{mapo} values of S187F-Ma and Gly161 variants are lower than the T_{m1apo} of AGT-Ma and AGT-Mi, respectively, and both the T_{m1apo} and the T_{m2apo} of S218L-Ma and W108R-Mi are lower than the

Table 5
Major defect(s) of AGT pathogenic variants analyzed on crude lysates and on recombinant purified proteins.

AGT variants	Analysis on crude lysates		Analysis on purified proteins						
	Specific activity	Expression level	PLP binding affinity	PLP binding mode	Specific activity	T_{mholo} and T_{mPLP}	T_{mapo}	Functional (F) and/or strucural (S) defect	Suggested therapy
W108R-Mi	Decreased[a]	Decreased[a]	Decreased	Altered	Decreased	Decreased	Decreased	F + S	?
S158L-Ma	Decreased[b]	Decreased[b]	Decreased	Altered	Decreased	Decreased	Slightly increased	F + S	?
G161S-Mi	Decreased[b]	Decreased[b]	Slightly decreased	Altered	Sligthy decreased	Decreased	Decreased	S	Pyridoxine + chemical chaperones
G161C-Mi	Decreased[b]	Decreased[b]	Slightly decreased	Altered	Slightly decreased	Decreased	Decreased	S	Pyridoxine + chimica chaperones
D183N-Ma	Decreased[a]	Decreased[a]	Decreased	Slightly altered	Decreased	Slightly increased	Slightly increased	F	?
S187F-Ma	Decreased[a]	Decreased[a]	Increased	Unaltered	Decreased	Unaltered	Decreased	F + S	?
S218L-Ma	Decreased	Decreased	Decreased	Altered	Decreased	Decreased	Decreased	F + S	Chemical chaperones
P319L-Ma	?	?	Slightly increased	Slightly altered	Slightly decreased	Unaltered	Slightly decreased	S	Pyridoxine
G350D-Mi	Decreased[c]	?	Increased	Slightly altered	Decreased[f]	Unaltered	Decreased	F + S	L-Alanine + pyridoxine

[a] From Coultier-Mackie MB et al. [13].
[b] From Williams E. et al. [12].
[c] From von Schnakenburg C. et al. [30].
[f] Mainly due to the high $K_{m\ L\text{-alanine}}$ value.

corresponding of AGT-Ma and AGT-Mi, respectively. While this finding is not easy to explain for W108R-Mi and S218L-Ma, it is consistent with the in silico analysis in the case of Gly161 variants and S187F-Ma. In fact, Gly161 is just located at the interface between the large and small domains, and the bulky hindrance of the side chain of phenylalanine at position 187 could cause a mispositioning of the loop 154–168 involved in interdomain interactions. Finally, the small domain P319L and G350D mutations have essentially a structural effect limited to the small domain, being the T_{mapo} values of the P319L-Ma and G350D-Mi similar to the T_{m1apo} of AGT-Ma and AGT-Mi, respectively.

Overall, with respect to the analysis performed on crude lysates [9–13,15,16,33,34], the data obtained on purified recombinant variants make clear the diversity of the effect(s) caused by each mutation and strength the importance of looking at both holo and apo forms of pathogenic variants. Finally, the new insights into the molecular basis of the defects of the examined AGT pathogenic variants could be instrumental in suggesting possible therapeutic approaches (Table 5). B6 supplementation is expected to be beneficial for those patients carrying the P319L mutation on the major allele. Since the major impact of this mutation is on the thermostability of the apo-form of AGT, the coenzyme is expected to shift the equilibrium toward the holo-form. Patients with G161 mutations on the minor allele could benefit by pyridoxine treatment in association with chemical chaperones because these mutations reduce the thermostability of both the holo and apo-forms of G161 variants. In the case of patients bearing the G350D mutation on the minor allele, a combination of L-alanine and pyridoxine could be suggested to overcome the reduced affinity for the substrate and the reduced thermal stability of the apo form. Again, the administration of molecules acting as chemical chaperones could be effective for patients harboring the S218L mutation on the major allele, considering that the S218L-Ma variant has a reduced thermal stability in both the holo and apo forms and retains a rather significant specific activity. On the other hand, no suggestions can be advanced for a pharmacological treatment of patients carrying the W108R mutation on the minor allele or the S158L, D183N and S187F mutations on the major allele.

5. Conclusions

In conclusion, our characterization of the AGT variants in their recombinant purified form provided evidence for structural and/or functional defects of each enzymatic species. The in vitro approach presented in this study permits to: (i) reassess previous data obtained in crude cellular lysates, (ii) define whether the impact of each mutation is limited to the active site microenvironment or extended to the large and/or the small domain, thus posing itself as a valid instrument to shed light on the molecular defects of other PH1-causing variants and (iii) suggest possible treatments for patients bearing the examined mutations.

Supplementary materials related to this article can be found online at doi:10.1016/j.ymgme.2011.09.033

References

[1] C.J. Danpure, G. Rumsby, Molecular aetiology of primary hyperoxaluria and its implications for clinical management, Expert Rev. Mol. Med. 6 (2004) 1–16.
[2] C.J. Danpure, P.R. Jennings, Peroxisomal alanine:glyoxylate aminotransferase deficiency in primary hyperoxaluria type I, FEBS Lett. 201 (1986) 20–24.
[3] P.E. Purdue, M.J. Lumb, M. Fox, G. Griffo, C. Hamon-Benais, S. Povey, C.J. Danpure, Characterization and chromosomal mapping of a genomic clone encoding human alanine:glyoxylate aminotransferase, Genomics 10 (1991) 34–42.
[4] P.E. Purdue, M.J. Lumb, J. Allsop, C.J. Danpure, An intronic duplication in the alanine: glyoxylate aminotransferase gene facilitates identification of mutations in compound heterozygote patients with primary hyperoxaluria type 1, Hum. Genet. 87 (1991) 394–396.
[5] P.E. Purdue, Y. Takada, C.J. Danpure, Identification of mutations associated with peroxisome-to-mitochondrion mistargeting of alanine/glyoxylate aminotransferase in primary hyperoxaluria type 1, J. Cell Biol. 111 (1990) 2341–2351.
[6] E.L. Williams, C. Acquaviva, A. Amoroso, F. Chevalier, M. Coulter-Mackie, C.G. Monico, D. Giachino, T. Owen, A. Robbiano, E. Salido, H. Waterham, G. Rumsby, Primary hyperoxaluria type 1: update and additional mutation analysis of the AGXT gene, Hum. Mutat. 30 (2009) 910–917.
[7] C.J. Danpure, P.J. Cooper, P.J. Wise, P.R. Jennings, An enzyme trafficking defect in two patients with primary hyperoxaluria type 1: peroxisomal alanine/glyoxylate aminotransferase rerouted to mitochondria, J. Cell Biol. 108 (1989) 1345–1352.
[8] C.J. Danpure, P.R. Jennings, P. Fryer, P.E. Purdue, J. Allsop, Primary hyperoxaluria type 1: genotypic and phenotypic heterogeneity, J. Inherit. Metab. Dis. 17 (1994) 487–499.
[9] M.J. Lumb, C.J. Danpure, Functional synergism between the most common polymorphism in human alanine:glyoxylate aminotransferase and four of the most common disease-causing mutations, J. Biol. Chem. 275 (2000) 36415–36422.
[10] M.B. Coulter-Mackie, Q. Lian, D. Applegarth, J. Toone, The major allele of the alanine: glyoxylate aminotransferase gene: nine novel mutations and polymorphisms associated with primary hyperoxaluria type 1, Mol. Genet. Metab. 86 (2005) 172–178.
[11] P.E. Purdue, M.J. Lumb, J. Allsop, Y. Minatogawa, C.J. Danpure, A glycine-to-glutamate substitution abolishes alanine:glyoxylate aminotransferase catalytic activity in a subset of patients with primary hyperoxaluria type 1, Genomics 13 (1992) 215–218.
[12] E. Williams, G. Rumsby, Selected exonic sequencing of the AGXT gene provides a genetic diagnosis in 50% of patients with primary hyperoxaluria type 1, Clin. Chem. 53 (2007) 1216–1221.
[13] M.B. Coulter-Mackie, Q. Lian, Partial trypsin digestion as an indicator of mis-folding of mutant alanine:glyoxylate aminotransferase and chaperone effects of specific ligands. Study of a spectrum of missense mutants, Mol. Genet. Metab. 94 (2008) 368–374.
[14] O. Basmaison, M.O. Rolland, P. Cochat, D. Bozon, Identification of 5 novel mutations in the AGXT gene, Hum. Mutat. 15 (2000) 577.
[15] Y. Minatogawa, S. Tone, J. Allsop, P.E. Purdue, Y. Takada, C.J. Danpur, R. Kido, A serine-to-phenylalanine substitution leads to loss of alanine:glyoxylate aminotransferase catalytic activity and immunoreactivity in a patient with primary hyperoxaluria type 1, Hum. Mol. Genet. 1 (1992) 643–644.
[16] C.J. Danpure, P.E. Purdue, P. Fryer, S. Griffiths, J. Allsop, M.J. Lumb, K.M. Guttridge, P.R. Jennings, J.I. Scheinman, S.M. Mauer, et al., Enzymological and mutational analysis of a complex primary hyperoxaluria type 1 phenotype involving alanine:glyoxylate aminotransferase peroxisome-to-mitochondrion mistargeting and intraperoxisomal aggregation, Am. J. Hum. Genet. 53 (1993) 417–432.
[17] X. Zhang, S.M. Roe, Y. Hou, M. Bartlam, Z. Rao, L.H. Pearl, C.J. Danpure, Crystal structure of alanine:glyoxylate aminotransferase and the relationship between genotype and enzymatic phenotype in primary hyperoxaluria type 1, J. Mol. Biol. 331 (2003) 643–652.
[18] B. Cellini, M. Bertoldi, R. Montioli, A. Paiardini, C. Borri Voltattorni, Human wild-type alanine:glyoxylate aminotransferase and its naturally occurring G82E variant: functional properties and physiological implications, Biochem. J. 408 (2007) 39–50.
[19] M.B. Coulter-Mackie, Q. Lian, Consequences of missense mutations for dimerization and turnover of alanine:glyoxylate aminotransferase: study of a spectrum of mutations, Mol. Genet. Metab. 89 (2006) 349–359.
[20] B. Cellini, R. Montioli, A. Paiardini, A. Lorenzetto, F. Maset, T. Bellini, E. Oppici, C.B. Voltattorni, Molecular defects of the glycine 41 variants of alanine glyoxylate aminotransferase associated with primary hyperoxaluria type I, Proc. Natl. Acad. Sci. U. S. A. 107 (2010) 2896–2901.
[21] B. Cellini, A. Lorenzetto, R. Montioli, E. Oppici, C.B. Voltattorni, Human liver peroxisomal alanine:glyoxylate aminotransferase: different stability under chemical stress of the major allele, the minor allele, and its pathogenic G170R variant, Biochimie 92 (2010) 1801–1811.
[22] B. Cellini, R. Montioli, A. Paiardini, A. Lorenzetto, C.B. Voltattorni, Molecular insight into the synergism between the minor allele of human liver peroxisomal alanine:glyoxylate aminotransferase and the F152I mutation, J. Biol. Chem. 284 (2009) 8349–8358.
[23] C.G. Monico, J.B. Olson, D.S. Milliner, Implications of genotype and enzyme phenotype in pyridoxine response of patients with type I primary hyperoxaluria, Am. J. Nephrol. 25 (2005) 183–188.
[24] C.G. Monico, S. Rossetti, J.B. Olson, D.S. Milliner, Pyridoxine effect in type I primary hyperoxaluria is associated with the most common mutant allele, Kidney Int. 67 (2005) 1704–1709.
[25] C.S. van Woerden, J.W. Groothoff, F.A. Wijburg, C. Annink, R.J. Wanders, H.R. Waterham, Clinical implications of mutation analysis in primary hyperoxaluria type 1, Kidney Int. 66 (2004) 746–752.
[26] W. De Lano, The pyMol Molecular Graphics System, DeLano Scientifics, San Carlos, CA, 2002.
[27] B. Cellini, M. Bertoldi, C. Borri Voltattorni, Treponema denticola cystalysin catalyzes beta-desulfination of L-cysteine sulfinic acid and beta-decarboxylation of L-aspartate and oxalacetate, FEBS Lett. 554 (2003) 306–310.
[28] C.N. Pace, B.A. Shirley, J.T. Thompson, Measuring the Conformational Stability of a Protein, in: T.E. Creighton (Ed.), Protein Structure, a Pratical Approach, IRL Press, IRL Press, Oxford, England, 1989, pp. 311–330.
[29] F.H. Niesen, H. Berglund, M. Vedadi, The use of differential scanning fluorimetry to detect ligand interactions that promote protein stability, Nat. Protoc. 2 (2007) 2212–2221.
[30] C. von Schnakenburg, G. Rumsby, Identification of new mutations in primary hyperoxaluria type 1 (PH1), J. Nephrol. 11 (Suppl 1) (1998) 15–17.
[31] C.J. Danpure, Molecular etiology of primary hyperoxaluria type 1: new directions for treatment, Am. J. Nephrol. 25 (2005) 303–310.
[32] C.J. Danpure, Primary hyperoxaluria type 1: AGT mistargeting highlights the fundamental differences between the peroxisomal and mitochondrial protein import pathways, Biochim. Biophys. Acta 1763 (2006) 1776–1784.
[33] M.B. Coulter-Mackie, D. Applegarth, J.R. Toone, H. Henderson, The major allele of the alanine:glyoxylate aminotransferase gene: seven novel mutations causing primary hyperoxaluria type 1, Mol. Genet. Metab. 82 (2004) 64–68.

[34] M.B. Coulter-Mackie, Q. Lian, S.G. Wong, Overexpression of human alanine: glyoxylate aminotransferase in *Escherichia coli*: renaturation from guanidine-HCl and affinity for pyridoxal phosphate co-factor, Protein Expr. Purif. 41 (2005) 18–26.
[35] E.C. Salido, X.M. Li, Y. Lu, X. Wang, A. Santana, N. Roy-Chowdhury, A. Torres, L.J. Shapiro, J. Roy-Chowdhury, Alanine–glyoxylate aminotransferase-deficient mice, a model for primary hyperoxaluria that responds to adenoviral gene transfer, Proc. Natl. Acad. Sci. U. S. A. 103 (2006) 18249–18254.
[36] C.J. Danpure, P. Fryer, S. Griffiths, K.M. Guttridge, P.R. Jennings, J. Allsop, A.B. Moser, S. Naidu, H.W. Moser, M. MacCollin, et al., Cytosolic compartmentalization of hepatic alanine:glyoxylate aminotransferase in patients with aberrant peroxisomal biogenesis and its effect on oxalate metabolism, J. Inherit. Metab. Dis. 17 (1994) 27–40.
[37] E.D. Hopper, A.M. Pittman, M.C. Fitzgerald, C.L. Tucker, In vivo and in vitro examination of stability of primary hyperoxaluria-associated human alanine:glyoxylate aminotransferase, J. Biol. Chem. 283 (2008) 30493–30502.
[38] T. Yano, S. Kuramitsu, S. Tanase, Y. Morino, H. Kagamiyama, Role of Asp222 in the catalytic mechanism of *Escherichia coli* aspartate aminotransferase: the amino acid residue which enhances the function of the enzyme-bound coenzyme pyridoxal 5′-phosphate, Biochemistry 31 (1992) 5878–5887.

[Frontiers in Bioscience 17, 621-634, January 1, 2012]

Molecular insights into primary hyperoxaluria type i pathogenesis

Barbara Cellini[1], Elisa Oppici[1], Alessandro Paiardini[2], Riccardo Montioli[1]

[1]Department of Life Sciences and Reproduction, Section of Biological Chemistry, University of Verona, Strada Le Grazie 8 37134 Verona, Italy, [2]Department of Biochemical Sciences, A. Rossi Fanelli, University, La Sapienza, 00185 Roma, Italy

TABLE OF CONTENTS

1. ABSTRACT

Primary hyperoxaluria type 1 (PH1) is a rare autosomal recessive disorder of glyoxylate metabolism caused by the deficiency of liver peroxisomal alanine:glyoxylate aminotransferase (AGT), a pyridoxal 5'-phosphate (PLP)–dependent enzyme. The PH1 pathogenesis is mostly due to single point mutations (more than 150 so far identified) on the *AGXT* gene, and is characterized by a marked heterogeneity in terms of genotype, enzymatic and clinical phenotypes. This article presents an up to date review of selected aspects of the biochemical properties of the two allelic forms of AGT and of some PH1-causing variants. These recent discoveries highlight the effects at the protein level of the pathogenic mutations, and, together with previous cell biology and clinical data, (i) improve the understanding of the molecular basis of PH1 pathogenesis, and (ii) help to delineate perspectives for predicting the response to pyridoxine treatment or for suggesting new strategies for PH1 patients bearing the analyzed mutations.

2. INTRODUCTION

Pyridoxal 5-phosphate (PLP), a vitamer of vitamin B6, is a very versatile coenzyme acting on more than 140 enzyme-catalyzed human reactions involved in the metabolism of amino acids, biogenic amines, amino sugars and tetrapyrrolic compounds (1). In PLP-catalyzed reactions the cofactor is covalently bound to the apoenzyme by a Schiff base linkage with a lysine residue and functions as an electronic sink able to stabilize negatively-charged reaction intermediates thanks to the positive charge of its pyridine nitrogen. The outstanding involvement of PLP in physiological processes is also proven by the variety of inborn errors of metabolism affecting PLP-enzymes among which homocystinuria, caused by the deficiency of cystathionine-β-synthase, and sideroblastic anemia, caused by the deficiency of δ-aminolevulinic acid synthase, are well known examples (2).

3. PRIMARY HYPEROXALURIA TYPE I

Primary Hyperoxaluria Type I (PH1) is a rare autosomal recessive disorder of glyoxylate metabolism

whose prevalence in European population is estimated as 1-3 per million. The disease is caused by the deficiency of liver peroxisomal alanine:glyoxylate aminotransferase (AGT), a PLP-dependent enzyme that catalyzes the conversion of L-alanine and glyoxylate to pyruvate and glycine, respectively. The absence of functional AGT allows glyoxylate to be oxidized to oxalate in liver cytosol. Oxalate is an end-product of metabolism and is removed from the body mainly by renal excretion. In PH1, the increased oxalate concentration in urine leads to the formation and deposition of insoluble calcium oxalate crystals, resulting in nephrocalcinosis and urolithiasis. This could lead to renal failure that in turn allows the progressive calcium oxalate deposition in various body sites, a potentially fatal condition named systemic oxalosis (3) .

AGT is encoded by the *AGXT* gene, located on chromosome 2q37.3, and is present in human populations as two polymorphic variants, the "major allele" (AGT-Ma) and the less common "minor allele" (AGT-Mi) (4-5). The frequency of the minor allele can vary in different populations ranging from a 28% in the Sami North Sweden population to about 2-3% in Japanese people; the average frequency in European and North American populations is about 20%. AGT-Mi differs from AGT-Ma by a 74-bp duplication in intron 1 and by the presence of the mutations 32C→T and 1020A→G leading to the Pro11Leu and Ile340Met amino acid substitutions, respectively (6-7). More than 150 different pathogenic mutations on the *AGXT* gene leading to PH1 have been identified so far, that encompass nonsense, frameshift and missense mutations. While nonsense and frameshifts are null mutations that lead to the complete loss of the gene product, the most common type of *AGXT* mutations are single amino acid substitutions that lead to the synthesis of an aberrant gene product (8). Many PH1-causing mutations, co-segregate and functionally interact with the minor allele polymorphism. In fact, although the presence of the AGT-Mi polymorphism is not pathogenic *per se*, it makes AGT more susceptible to the effect of several missense mutations, which are predicted to be not pathogenic in the absence of the polymorphism (9) (see below).

PH1 is a life-threatening and difficult to treat disease. Classical treatments, aimed to decrease the amounts of oxalate in the body and to prevent kidney failure or to restore kidney functionality, by dialysis or kidney transplantation, are not curative being only directed to the symptoms of the disease . Available treatments for PH1 addressed to the cause of the disease are pyridoxine (Vitamin B6) therapy and liver transplantation (3). Pyridoxine is converted in the body to PLP, the essential cofactor of AGT, but the molecular mechanism of action of this molecule in PH1 patients is nowadays unknown. Moreover, only a minority (10-30%) of patients respond to pyridoxine therapy, and clinical studies seem to indicate that responsiveness is confined to mutations that result in AGT mistargeting (10-11). The only curative approach available for PH1 patients unresponsive to pyridoxine is liver transplantation, which reintroduces most of the body's requirements of AGT but represents a very wasteful intervention because an entire organ is employed to replace only one defective gene.

Notwithstanding the progress made during the last three decades, which has greatly improved the clinical management of PH1 patients, several issues still need to be addressed. One of the most important is the definition of a clear relationship between the genotype, the enzymatic phenotype and the clinical phenotype. In fact PH1 is a disease endowed with a great heterogeneity at both the clinical and the enzymatic phenotype level. The course of the disease can be very different in patients that share the same genotype, thus suggesting a role of genetic or environmental factors, and a large clinical variation can be observed even within the same family (12). Moreover, a great variety of enzymatic phenotypes leading to AGT deficiency can be noticed. On the basis of cell biology analyses, they have been classified in three categories: mutations leading to the loss of both AGT catalytic activity and immunoreactivity, mutations leading to the loss of AGT catalytic activity but not immunoreactivity, mutations leading to the loss of neither AGT catalytic activity nor immunoreactivity (3). It has been demonstrated that in the latter case the disease is due to the aberrant localization of AGT to mitochondria, where the protein is catalytically active but is unable to detoxify the glyoxylate formed inside peroxisomes (13-15). However, the limited number of patients makes difficult to establish any clear correlation between a particular genotype and the effects of the mutation at the enzyme and clinical level (12).

Recently, several efforts have been made to improve the knowledge of the PH1 molecular pathogenesis starting from the detailed study of the biochemical features of AGT as the base to define how a particular amino acid substitution can alter protein's functional and structural properties (Table 1) (16-19). The results obtained have not only shed light on some molecular mechanisms leading to AGT deficiency but have also provided a worthwhile tool to predict the response to pyridoxine therapy and to suggest new treatment strategies for PH1 patients bearing the analyzed mutation.

4. BIOCHEMICAL PROPERTIES OF NORMAL AGT

AGT-Ma is a homodimeric protein each subunit of which, consisting of 392 residues, has a molecular mass of 43 KDa. As shown by the crystal structure of the enzyme in a complex with the competitive inhibitor amino-oxyacetic acid (20), AGT-Ma belongs to the Fold Type I class of PLP-dependent enzymes. Each subunit comprises three structural domains (Figure 1A): an N-terminal extension (residues 1-21) that wraps over the opposite subunit; a large domain (residues 22-282) that has a three layer βαβ architecture and forms a great part of the active site; a C-terminal small domain (residues 283-392) that has a two layer αβ structure and contains the signals for the peroxisomal localization of the protein. Like in all PLP-enzymes, the coenzyme is covalently bound to the apoprotein by a Schiff base linkage with Lys209 (internal aldimine), and its binding at the active site is stabilized by the ring-stacking interaction with the indole ring of Trp108,

Table 1. Summary of AGT variants described in this review

Construct	Sequence mutation	Amino acid sostitution	Major (Ma) or Minor (Mi) haplotipe
AGT-Ma			
AGT-Mi	c.32C>T c.1020A>G	Pro11Leu Ile340Met	
G41R-Mi	c.121G>A	Gly41Arg	Ma/Mi
G41V-Mi	c.122G>T	Gly41Val	Ma
G82E-Ma	c.245G>A	Gly82Glu	Ma
F152I-Mi	c.454T>A	Phe152Ile	Mi
G170R-Mi	c.508G>A	Gly170Arg	Mi

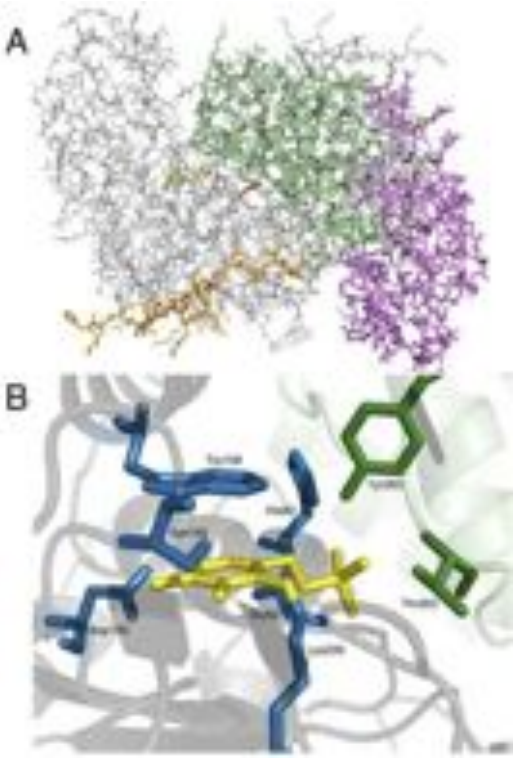

Figure 1. Crystal structure of human AGT-Ma (PDB code 1H0C (20)). A) Stick representation of the AGT dimer. One subunit is coloured white while in the other subunit the N-terminus (residues 1-21) is orange, the large domain (residues 22-282) is coloured green, and the small domain (residues 283-392) is coloured violet. PLP, Gly41 and Gly170 are coloured yellow, red and blue, respectively. B) Ribbon representation of the AGT-Ma active site with one subunit coloured gray and the opposite subunit coloured green. PLP is represented as yellow sticks. Active site residues directly interacting with the coenzyme are labelled and shown as sticks. Blue residues belong to the PLP-binding subunit while green residues belong to the opposite subunit. The figure was rendered using PyMol.

the salt bridge between the protonated pyridine nitrogen and Asp183 and the hydrogen bonds of the hydroxyl O3 of PLP with Ser158 and of the phosphate group of PLP with His83, Gly82, Tyr260* and Thr263* (the * stands for residues from the neighboring subunit) (Figure 1B). AGT-Ma shows a large dimerization interface (~23% of the solvent accessible area) that comprises both interactions between the two large domains and contacts between the N-terminal extension of one subunit and the large domain of the other (20).

A detailed picture of the mechanism of action of AGT-Ma has been given by means of spectroscopic, kinetic and computational methods (16). Figure 2 reports the proposed mechanism of the overall transamination reaction catalyzed by the enzyme. In the first half-reaction, upon L-

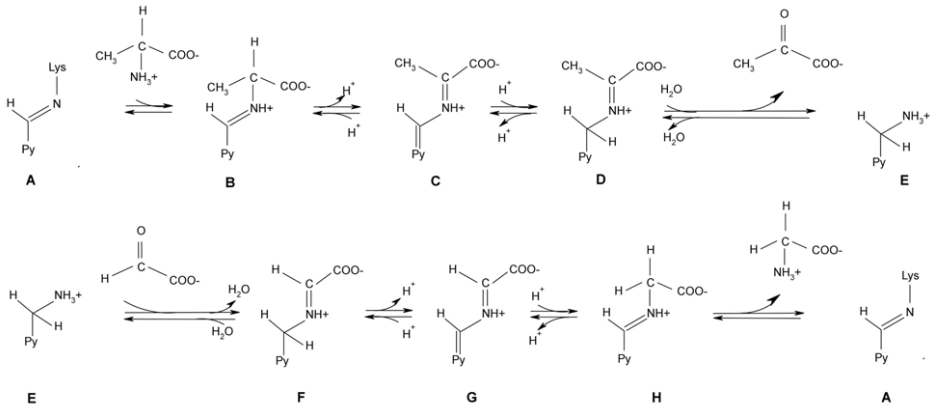

Figure 2. Kinetic mechanism of the overall transamination catalyzed by AGT (16). A: AGT-PLP; B: L-alanine external aldimine; C: alanine-PLP quinonoid intermediate; D: pyruvate ketimine intermediate; E: AGT-PMP; F: glyoxylate ketimine intermediate; G: glycine-PLP quinonoid intermediate; H: glycine external aldimine.

alanine binding, the AGT-PLP internal aldimine (A) is converted into the external aldimine (B). Then, the L-alanine α-proton extraction by a base catalyst generates the resonance-stabilized quinonoid intermediate (C), which is reprotonated at the C4' of the coenzyme to give the ketimine intermediate (D). The latter is then hydrolyzed to give pyruvate and the pyridoxamine 5'-phosphate (PMP) form of the coenzyme (E). In the second half-reaction, the AGT-PMP complex (E) binds glyoxylate and, by the same steps of the first half-reaction but in reverse direction (E→F→G→H→A), it is converted to AGT-PLP and generates glycine. Steady-state and presteady-state kinetic studies indicated that, in analogy with other aminotransferases, the overall transamination catalyzed by AGT-Ma follows a ping-pong kinetic mechanism whose rate-limiting step is the formation of ketimine or its hydrolysis. Moreover, the equilibrium constant of the overall transamination was found to be ~9400, and it was suggested that this value is mainly driven by the glyoxylate↔glycine equilibrium largely shifted toward glycine. These data, along with the finding that the k_{cat} for the pair alanine/glyoxylate (45 s^{-1}) is about 100-fold higher than that for the pair glycine/pyruvate (0.3 s^{-1}) led to the conclusion that AGT is highly specific for the glyoxylate-to-glycine conversion, in agreement with the proposed physiological role of the enzyme in glyoxylate detoxification (16). Like in many PLP-enzymes, the binding of the coenzyme at the AGT-Ma active site gives rise to specific absorbance and dichroic signals. In particular the AGT-PLP complex is characterized by an absorbance band at 420 nm associated with a positive dichroic signal centered at 429 nm, while the AGT-PMP complex is characterized by an absorbance band at 335 nm associated with a positive dichroic signal centered at 320 nm (Figure 3). Fluorescence and circular dichroism studies indicated that AGT has an higher affinity for PMP ($K_{D(PMP)}$ << 100 nM) than for PLP ($K_{D(PLP)}$ = 270 nM) (Table 2) and that PMP remains tightly bound to the enzyme during the transamination reaction. Moreover, basing on bioinformatic analyses, it has been suggested that subtle rearrangements of active site aromatic residues and a tilting of the coenzyme moiety could occur during the AGT-PLP↔AGT-PMP interconversion. These structural changes could be very important to prevent PMP release and allow a more efficient glyoxylate-to-glycine conversion (16).

AGT-Ma is characterized by a wide substrate and reaction specificity. Indeed, besides L-alanine, the enzyme is able to utilize as amino donors several amino acids like L-serine, L-phenylalanine, L-arginine, L-glutamate and L-aspartate, although with different catalytic efficiencies. Moreover, it catalyzes the α,β-elimination of β-chloro-L-alanine, with turnover times measured in seconds, and the β-elimination and half-transamination of L-cysteine, with turnover times measured in minutes (21).

5. EFFECTS OF THE POLYMORPHIC MUTATIONS P11L AND I340M ON THE AGT FUNCTIONAL AND STRUCTURAL PROPERTIES

The product of the minor allelic form of the *AGXT* gene, AGT-Mi, is characterized by the two point mutations P11L and I340M (Table 1). Although these mutations are not known to cause any clinical phenotype, the presence of the minor allele makes AGT more susceptible to the effects of many PH1-associated mutations that are pathogenic only when associated with the minor allele (9). This explains why many investigations have been carried out to understand the differences between the two allelic forms of AGT at a cellular and molecular level.

Studies performed on human hepatocytes (9, 15) expressing the major and the minor allele of AGT indicate

Table2, Steady-state kinetic parameters and equilibrium coenzyme binding constants of AGT-Ma, AGT-Mi and variants

	k_{cat} (s^{-1})	$K_{M\ L\text{-}Ala}$ (mM)	$k_{cat}/K_{m\ L\text{-}alanine}$ ($mM^{-1}s^{-1}$)	$K_{M\ Glyoxylate}$ (mM)	$k_{cat}/K_{m\ Glyoxylate}$ ($mM^{-1}s^{-1}$)	$K_{D\ PLP}$ (μM)	$K_{D\ PMP}$ (μM)
AGT-Ma	45 ± 2[1]	31 ± 4[1]	1.4 ± 0.2	0.23 ± 0.05[1]	196 ± 43	0.27 ± 0.03[1]	< 0.1[1]
AGT-Mi	35 ± 2[2]	28 ± 2[2]	1.2 ± 0.1	0.22 ± 0.01[2]	159 ± 12	0.26 ± 0.02[2]	< 0.1[2]
G41R-Ma	19.5 ±0.5[3]	22 ± 2[3]	0.89 ± 0.08	0.41 ± 0.04[3]	48 ± 5	1.5 ± 0,4[3]	> 5mM[3]
G41R-Mi	10.8 ± 0.4[3]	30 ±5[3]	0.36 ± 0.06	0.32 ± 0.02[3]	34 ± 2	6.1 ± 0.5[3]	> 5mM[3]
G41V-Ma	17.7 ± 0.6[3]	42 ± 4[3]	0.42 ± 0.04	0.13 ±0.02[3]	136 ± 21	0.55 ± 0.01[3]	> 5mM[3]
G82E-Ma	0.07 ± 0.03	15 ± 2[1]	0.0047 ± 0.0021	0.15 ± 0.06[1]	0.47 ± 0.27	198 ± 50[1]	> 5mM[1]
F152I-Mi	37 ± 1	41 ± 1[2]	0.90 ± 0.03	0.25 ± 0.03[2]	148 ± 18	0.085 ± 0.001[2]	19 ± 4[2]
G170R-Mi	34 ± 1	36 ± 2[4]	0.94 ± 0.06	0.4 ± 0.1[4]	85 ± 21	0.4 ± 0.1[4]	N.D.

N.D., not determined, [1]from ref 16, [2]from ref. 19, [3]from ref. 18

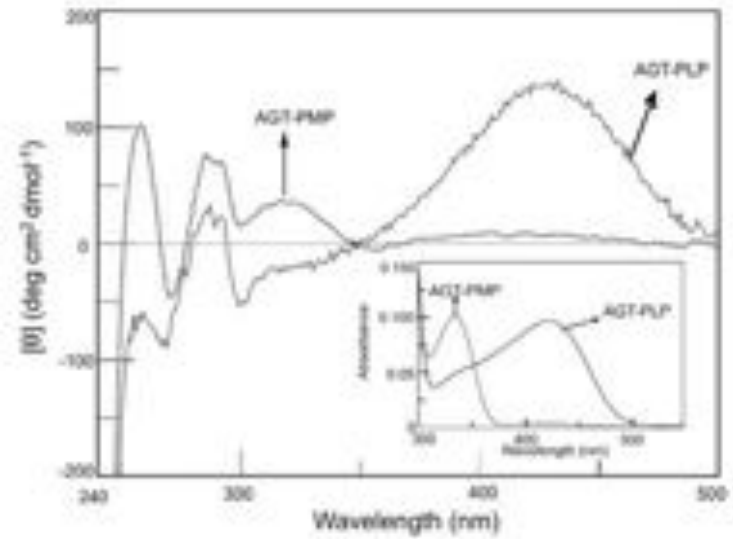

Figure 3. CD and absorbance spectra of AGT-Ma in the PLP and PMP form. UV-visible CD spectra of AGT-PLP (—) and AGT-PMP (▪▪▪▪) in 100 mM potassium phosphate buffer, pH 7.4 (16). Inset: UV-visible absorbance spectra of AGT-PLP (—) and AGT-PMP (▪▪▪▪) in 100 mM potassium phosphate buffer, pH 7.4. Enzyme concentration was 10 μM.

that AGT-Mi is characterized by a catalytic activity slightly lower (about 50-70%) than that of AGT-Ma as well as by an about 5% mistargeting of the protein from peroxisomes to mitochondria, which is due to the P11L substitution that generates a mitochondrial targeting sequence at the N-terminus of AGT. Moreover, it has been reported that AGT-Mi is less stable *in vivo* than AGT-Ma, as revealed by yeast complementation assays (22), and is more susceptible to proteolytic degradation and to aggregation, as revealed by pulse-chase and cross-linking experiments performed on cell-free transcription/translation products (23).

Recently, the biochemical properties distinguishing the two allelic forms of AGT have been thoroughly analyzed *in vitro* with purified recombinant AGT-Ma and AGT-Mi (19). These studies have indicated that the P11L/I340M mutations, typical of the minor allele, i) do not affect either the UV-visible absorbance, dichroic and fluorescence features of AGT or the $K_{D(PLP)}$ value, thus suggesting that no gross conformational changes have occurred and that the two species share a similar active site architecture and ii) these mutations induce a slight decrease (about 30%) of the k_{cat} value for the overall transamination of alanine and glyoxylate (Table 2). This is in agreement with the decreased enzymatic activity observed *in vivo*. Nevertheless, under conditions of chemical and thermal stress, a decreased stability of AGT-Mi with respect to AGT-Ma has been demonstrated. When the urea-induced equilibrium unfolding process of the two proteins was analyzed, both the holo and the apo-form of AGT-Mi were found to undergo dimer dissociation at lower urea concentrations with respect to the corresponding form of AGT-Ma, and that this destabilization is ascribable to the P11L mutation (17). It has been suggested that the substitution of Pro11 with a leucine residue would loosen the interaction of the N-terminal arm of one subunit of AGT with the large domain of the opposite subunit, thus facilitating dimer dissociation. This perturbation could also be transmitted to the AGT active site through a loop (residues 24-32) that contributes to the PLP binding site.

Table 3, Transition midpoint of thermal denaturation (Tm) and inactivation (Ti) of AGT-Ma, AGT-Mi and pathogenic variants

	Tm (°C)				Ti (°C)	
	DSC		CD (222nm)			
	Holo form	Apo form	Holo form	Apo form	Holo form	Apo form
AGT-Ma	77.3[2]	62.4[2]	N.D.	N.D.	77.4[1]	59.1[1]
AGT-Mi	73.2[2]	55.6[2]	73.6[3]	53.1[3] 66[3]	72.6[1]	52.2[1]
G41R-Ma	60.3[2]	57.6[2]	N.D.	N.D.	57.7[2]	53[2]
G41R-Mi	53.7[2]	N.D.	N.D.	N.D.	51.8[2]	46[2]
G41V-Ma	61.0[2]	58.3[2]	N.D.	N.D.	62.3[2]	54.5[2]
F152I-Mi	N.D.	N.D.	N.D.	N.D.	69.9[1]	52.4[1]
G170R-Mi	N.D.	N.D.	72.5[3]	48.2[3] 64[3]	N.D.	N.D.

N.D., not determined, [1]from ref 19, [2]from ref. 18, [3]from ref. 17

This could explain why P11L mutation induces PLP release from holoAGT-Mi at urea concentrations lower than those necessary for holoAGT-Ma. In addition, thermal denaturation of AGT-Ma and AGT-Mi has been performed using different procedures, including differential scanning calorimetry, CD-monitored thermal unfolding and thermal inactivation (Table 3). These experiments provided evidence that the P11L/I340M mutations decrease the thermal stability of both the holo- and the apo-form of AGT and that the decrease is driven by the Pro11-to-Leu substitution, in agreement with the chemical denaturation results (17-19).

Overall these analyses, besides elucidating the differences between AGT-Ma and AGT-Mi, represented the starting point to investigate the effect of pathogenic mutations associated with PH1 and to unravel the defects of the corresponding variants at molecular level.

6. LOSS OF AGT CATALYTIC ACTIVITY: THE G82E VARIANT

A 245G→A mutation on the major allele of the *AGXT* gene leading to the G82E substitution is one of the rarest PH1-causing mutations. Clinical data show that normal levels of correctly targeted AGT and the complete absence of transaminase activity represent the enzymatic phenotype typical of PH1 patients bearing G82E mutation (24). About ten years ago, Lumb et al. (9) reported that the purified G82E variant expressed in *E.coli* is devoid of catalytic activity and is unable to bind PLP. Gly82 is an active site residue whose peptide NH, along with the side-chain of His83, contributes to the binding of the coenzyme through hydrogen-bonding interactions with the phosphate group of PLP (Figure 1B) (20). Thus, it has been argued that the absence of catalytic activity in the variant is strictly related to the inability of the protein to bind PLP as a consequence of steric hindrance by the glutamate side chain. On 2007 (16), the detailed inspection of the biochemical properties of the purified recombinant G82E variant highlighted a more complex scenario. In fact, evidence has been provided that the G82E mutation greatly affects the binding affinity for both coenzymatic forms, as shown by the decrease of the equilibrium dissociation constant value for PLP and PMP in the variant of about 700 and 50000-fold, respectively (Table 2). Moreover, the absorbance and CD (Figure 4) spectral properties of G82E in the presence of exogenous coenzyme show that Gly82 to glutamate mutation significantly changes the microenvironment of the internal aldimine of AGT. These data have been explained by considering that Gly82 is part of a glycine loop that stabilizes the phosphate of PLP (20) and that the side chain of Glu82 in the variant could partially distort the active site thus altering coenzyme binding mode and affinity. Interestingly, the catalytic efficiency of the G82E variant for the alanine/glyoxylate pair measured in the presence of saturating exogenous PLP has been found to be about 0.1% that of AGT-Ma (Table 2). Kinetic analyses of the two half-transamination reactions allowed to infer that i) in contrast with what was observed with AGT-Ma, the rate-limiting step for the L-alanine half-transamination catalyzed by the G82E variant is the external aldimine formation (A→B in Figure 2); ii) the addition of a pre-formed PLP-L-alanine Schiff base could partially improve the half-transamination rate and iii) the glyoxylate half-transamination catalyzed by the apomutant in the presence of PMP occurs with a rate 1800-fold lower than that of AGT-Ma (16).

On the basis of all these data, it was concluded that the molecular defect of the G82E pathogenic variant does not lie in the inability to bind PLP, but rather in a perturbed active site microenvironment that causes a strong reduction of the coenzyme binding affinity and a decrease in the catalytic efficiency due to the slowing down of the amino acids transaldimination step and of the AGT-PMP to AGT-PLP conversion. Thus, the administration of pyridoxine does not seem to represent an ideal therapy to treat PH1 patients bearing G82E mutation, while the administration of a preformed external aldimine PLP-L-alanine could possibly be a better approach by bypassing the transaldimination step.

7. LOSS OF BOTH AGT CATALYTIC ACTIVITY AND IMMUNOREACTIVITY: THE GLY41 VARIANTS

Gly41 variants are three pathogenic forms of AGT characterized by the presence of the G41R point mutation, associated with either the major or the minor allele (G41R-Ma and G41R-Mi), or the G41V mutation associated with the major allele (G41V-Ma) (25-26). While no information are currently available about the *in vivo* enzymatic phenotype of patients bearing the G41R or the G41V mutation associated with the major allele, the analysis of liver biopsies of PH1 patients bearing the G41R mutation associated with the minor allele revealed the nearly complete absence of both AGT catalytic activity and immunoreactivity and the presence of amorphous core-like AGT aggregates inside patient's peroxisomes (25). As shown in Figure 1A, Gly41 is located at the end of the helix 34-42 running at the dimer interface, and the peptide group

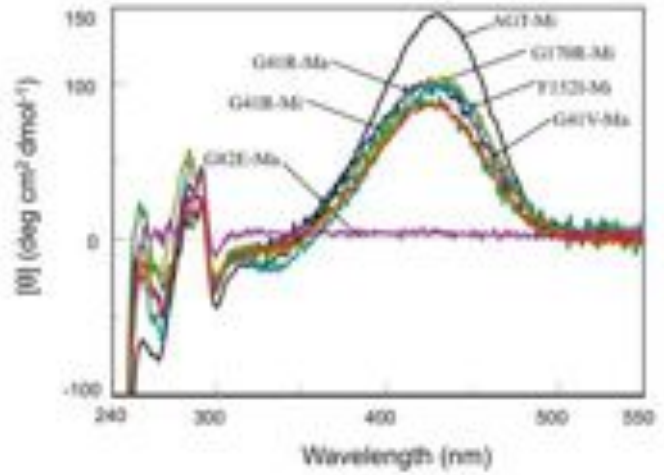

Figure 4. CD spectra of polymorphic and pathogenic variants of AGT in the holo-form (16, 18-19). UV-visible CD spectra of AGT-Mi (black), G82E-Ma (violet), G41R-Ma (blue), G41R-Mi (green), G41V-Ma (orange), G170R-Mi (yellow), F152I-Mi (cyan) in 100 mM potassium phosphate buffer, pH 7.4 at 10 μM enzyme concentration.

connecting Gly41 and Gly42 of one monomer is in van der Waals contact with the equivalent group of the other monomer. On these bases it has been proposed, but not proved, that the pathogenicity of Gly41 variants was linked to a dimer destabilization caused by the arginine or valine side-chains that would lead to a non-functional monomeric protein prone to degradation and aggregation (20). Coulter-Mackie et al. (23) reported that unlike AGT-Ma and AGT-Mi, Gly41 variants are subjected to proteasomal degradation as well as to an ATP-independent intracellular proteolytic activity when expressed by a cell-free transcription/translation system. Moreover, dimerization impairment for G41R-Ma and G41R-Mi was established by these authors on the basis of cross-linking and pulse-chase experiments. Recently, the molecular effect of Gly41 mutation on AGT has been investigated by studying the biochemical properties of purified recombinant Gly41 variants (18). Size-exclusion chromatography experiments did not allow us to detect any effect of the mutations on the dimerization of G41R-Mi, G41R-Ma and G41V-Ma variants in the holo-form, while they revealed an increase from 3 to about 20 fold in the monomer-dimer equilibrium dissociation constant value of the variants in the apo-form with respect to that of apoAGT-Ma or apoAGT-Mi. These results well agree with the proposed effect of the valine or arginine side chains introduced at the AGT interface on dimer stability. However, they also prove that, unlike what expected, Gly41 variants are able to form a dimer. Interestingly, the biochemical analyses showed that G41R-Ma, G41R-Mi and G41V-Ma in the dimeric form differ from AGT-Ma and AGT-Mi under several respects. In fact they display, even to a different extent, a reduced affinity for PLP and PMP, a reduced catalytic activity (Table 2), altered UV-visible absorbance, dichroic (Figure 4) and fluorescence features as well as a reduced thermostability (Table 3). Another striking feature that distinguish Gly41 variants from AGT-Ma and AGT-Mi comes from limited proteolysis experiments. In fact, the three variants are susceptible to both trypsin and proteinase K digestion. It has been shown that trypsin is able to cleave the Arg41-Gly42 or the Arg122-Val123 peptide bonds of G41R-Mi and G41R-Ma and the Arg36-Ile37 peptide bond of G41V-Ma (27). However, being the trypsin digestion performed on a cell-free transcription/translation product, it is not possible to understand whether the proteolytic degradation occurs on the monomeric or the dimeric form of each variant. On the other hand, proteinase K digestion, performed at protein concentrations in which Gly41 variants are in the dimeric form, results in the cleavage of the Met53-Tyr54 peptide bond (18). This suggested that the N-terminal region in Gly41 variants could be flexible and/or exposed to the solvent. In agreement with these results, the comparison between the conformational space sampled by the putative structures of AGT-Mi and G41R-Mi, carried out by high-temperature molecular dynamics simulations, suggested that the Gly41-to-Arg substitution in AGT could cause a marked increase in the fluctuation of the first 44 N-terminal residues (Figure 5) and their exposure to the solvent as well as a partial unwinding of the helix 34-42. On the other hand, no fluctuation of the N-terminal region can be seen for AGT-Mi. Overall, the above reported spectroscopic, kinetic and limited proteolysis data, along with the bioinformatic analysis, led to the conclusion that Gly41 mutation not only destabilizes the dimeric structure of AGT, but also induces some structural changes possibly related to the N-terminus of the protein in the dimeric form.

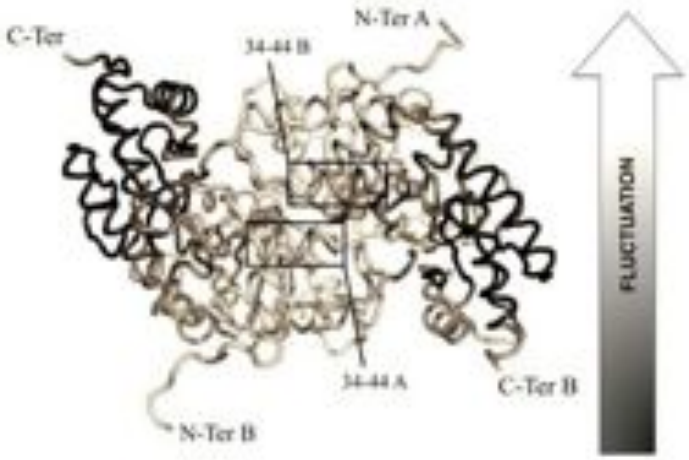

Figure 5. Average putative structure of G41R-Mi (18). The figure shows the protein backbone shaded in tones of gray, black meaning less movement and white meaning more movement, on the basis of the fluctuation observed by molecular dynamics simulations. The position of the helix 34-42 containing the mutated residue is highlighted.

Liver biopsies of patients bearing G41R mutation on the background of the minor allele are characterized by the presence of intra-peroxisomal amorphous core-like structures that stain for AGT but are unreactive against other six peroxisomal enzymes, as shown by immunoelectron microscopy. These data led to the conclusion that G41R mutation is associated with an AGT intra-peroxisomal aggregation (25). Moreover, the authors found that the presence of these cores correlated with the presence of high-molecular weight bands detected by the anti-AGT antibody on western-blot analyses. In order to shed light on the aggregative behaviour of Gly41 variants, the molecular dimensions of the mutants were studied by dynamic light scattering (DLS) under physiological conditions of temperature, ionic strength and pH (18). These studies showed that G41R-Ma, G41R-Mi and G41V-Ma, both in their holo- and apo-forms, are prone to aggregation and that the associative process is driven by inter-molecular electrostatic interactions. In fact, although DLS does not allow to estimate the absolute percentage of high molecular weight aggregates (~5000 Da) in the sample, the rate and the extent of the time-dependent changes in the total count rate increase as the ionic strength decreases.

A model to explain this propensity to aggregate of Gly41 variants has been proposed. Figure 6 compares the possible dimerization pathway of AGT-Ma with that of Gly41 variants. In both cases, the folded monomer M could either bind PLP and then dimerize (route M→ M_{PLP}→ D_{PLP}) or dimerize and then bind PLP (route M→ D → D_{PLP}). In the case of Gly41 variants, electrostatic potential surface calculations have revealed that the fluctuation of the N-terminus caused by Gly41 mutation would uncover several negatively charged residues on both the holo and the apo-form of the AGT dimer. This would convert the positively charged surface of AGT into a surface that displays a dipole segregation of charges. The negative patches could possibly interact with positive patches of neighbouring dimers, thus inducing the electrostatically-driven aggregation of the protein according to the model depicted on panel B of Figure 6 (18). However, the physiological meaning of this proposed mechanism of aggregation is currently unknown. Moreover, it remains to be established if the *in vivo* aggregation is due to electrostatic forces and if the aggregates have a structure similar to those formed *in vitro*.

Altogether, the above described results allow to propose a plausible model that could explain how the Gly41 mutation leads to AGT deficiency. Indeed, they clearly indicate that the enzymatic defect of the Gly41 variants does not only rely on the destabilization of the AGT dimeric structure, but also on a structural change probably related to the N-terminus causing the susceptibility of the variants to proteolytic degradation and their propensity to aggregate under physiological conditions. Although data from Coulter-Mackie et al. (27) suggest that the presence of PLP could decrease the sensitivity of Gly41 variants to trypsin, pyridoxine therapy alone does not seem to be sufficient to treat PH1 patients bearing mutation at Gly41 because the molecular defects of the variants are related to both their holo- and apo-forms. Rather, a promising approach could be the administration of small molecules able to stabilize the native state of the protein. Indeed, some preliminary data indicate that osmolytes, like trimethylamine-N-oxide and betaine, are able to partially reduce the aggregation extent of Gly41 variants (18). Although one should bear in mind that both these molecules are not suitable for clinical use because of

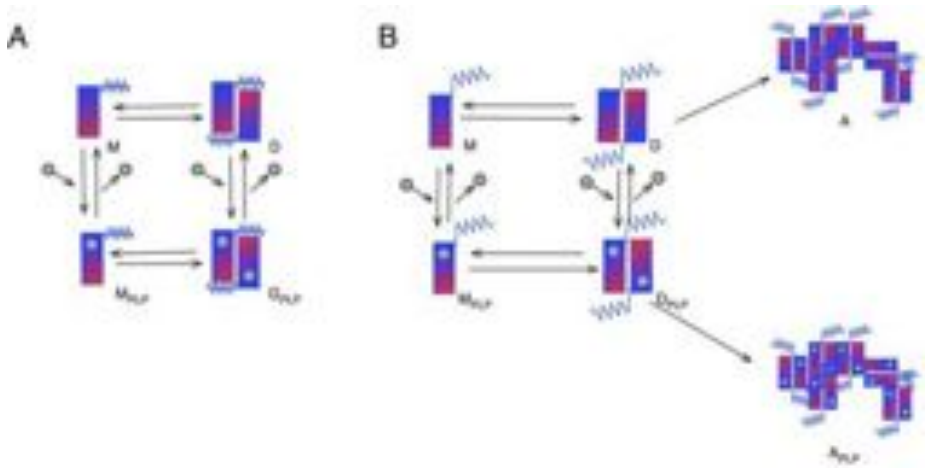

Figure 6. Proposed dimerization pathways of AGT-Ma (A) and of Gly41 variants (B). The blue and red colour in the folded protein subunits represent positively and negatively charged surfaces, respectively. M: folded monomer; M_{PLP}: PLP-bound monomer; D: apodimer; D_{PLP}, holodimer; A: insoluble aggregates; A_{PLP}: insoluble PLP-bound aggregates; ●: PLP

their poor specificity, they provide a good proof-of-principle for the development of a new strategy to counteract the disease. In this regard, it should be mentioned that the second most common mutation causing PH1, the 731T→C nucleotide substitution leading to the I244T amino acid replacement on the minor allele, causes AGT misfolding and aggregate formation that can be at least partially reversed by the use of small osmolytes, particularly betaine (28). However, these studies have been performed in different eukaryotic cell lines stably expressing the I244T-Mi variant and the detailed analysis of the *in vitro* aggregation propensity of the variant in the recombinant purified form is still lacking. Thus, it is not possible to define if the aggregation mechanism is similar to that observed on Gly41 variants.

8. MISTARGETING OF AGT: THE F152I-MI AND THE G170R-MI VARIANTS.

A large subclass of PH1 patients, corresponding to about one third of the total, displays an enzymatic phenotype in which neither the loss of AGT catalytic activity, nor the loss of immunoreactivity can be noticed. The point mutations on the *AGXT* gene associated with this phenotype are G170R, the most common PH1-causing mutation, and F152I. Both mutations cosegregate with the minor allele polymorphism and are supposed to be innocuous when associated with the major allele (15, 25, 29-31).

The enzymatic phenotype of the G170R-Mi variant has been widely studied during the last twenty years. The analysis of AGT subcellular localization on liver biopsies of patients bearing G170R mutation on the minor allele as well as on COS cells transiently expressing the G170R-Mi variant led to the conclusion that the molecular defect associated with this mutation is the mislocalization of the protein (32). The G170R-Mi variant, instead to be correctly targeted to peroxisomes, localizes to mitochondria where it is unable to fulfill its physiological role of glyoxylate detoxification. Cell biology investigations have proved the combined effect of the P11L polymorphic mutation and the G170R pathogenic mutation on the abnormal mitochondrial targeting of the protein. The P11L substitution allows the N-terminus of AGT to adopt a conformation of an amphiphilic α-helix able to act as a mitochondrial targeting sequence (4), while the G170R substitution is supposed to delay AGT folding and dimerization enough to make the protein compatible with the mitochondrial import machinery. In fact, while peroxisomes import fully-folded proteins, mitochondria can only import partly folded monomeric proteins (33). Lumb et al. described how non-specific factors known to increase protein stability are able to correct the enzyme trafficking defect of the G170R-Mi variant, while treatments known to decrease protein stability exacerbate the mistargeting (34). In order to shed light on the mechanistic bases of AGT mistargeting, the crystal structure of the G170R-Ma variant has been solved at a resolution of 2.6 Å (35). It showed that the pathogenic mutation does not significantly change the overall structure of AGT, but induces local perturbations leading to the loss of the hydrogen-bonding interaction between Arg197 of one monomer and Lys5 of the other (Figure 7). Although these results did not allow these scientists to evaluate the combined effect of the P11L and G170R mutations, they provided a possible explanation to the suggested reduction in dimer stability induced by the pathogenic mutation. Recently, the effect of the G170R mutation on AGT-Mi has been studied by elucidating both the biochemical features and the stability under urea stress

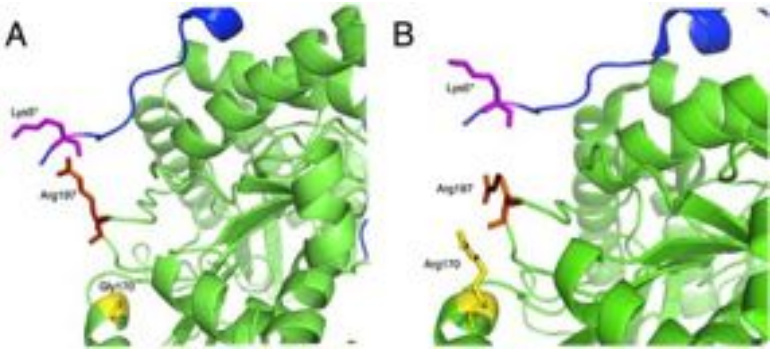

Figure 7. Localized effect of the G170R mutation on AGT (35). (A) Ribbon diagram of the AGT structure (PDB code 1H0C) showing the region in which Gly170 is located; (B) Ribbon diagram of the structure of the G170R-Ma variant (PDB code 1j04) showing the position of Arg170. The subunit comprising residue 170 is coloured green while the opposite subunit is coloured blue. Residues at position 5, 170 and 197 are labelled and coloured as purple, yellow and orange sticks, respectively. The * means that the residue comes from the other subunit.

of the two species (17). The results obtained indicated that the variant in the holo-form displays spectroscopic and kinetic features as well as PLP binding affinity analogous to those of AGT-Mi, thus confirming previous studies showing that the molecular defect of the variant does not consist in a loss of AGT functional activity. However, when the sensitivity to both urea and thermal stress of the variant was investigated, it was found that while holoG170R-Mi is indistinguishable from holoAGT-Mi, apoG170R-Mi shows a stability of the dimeric structure lower than that of apoAGT-Mi. In fact, monomerization occurs with a Cm of ~1.1 M urea for apoAGT-Mi and of ~1.4 M urea for apoG170R-Mi. Moreover, while the Tm of holoG170R-Mi is equal, within the limits of experimental error, to that of holoAGT-Mi, the Tm of the first transition of apoG170R-Mi is about 5°C lower than the corresponding value of apoAGT-Mi (Table 3). Thus, the enzymatic defect of the G170R-Mi variant is related to a lower stability of the dimeric structure of the apoenzymatic form of the protein. In agreement with these results, Pey et al. (36) reported that although holoG170R-Mi does not display gross conformational changes as compared with AGT-Mi, the apo-form of the variant shows an about 1000-fold increase in the thermal unfolding rate with respect to apoAGT-Mi. Moreover, when expressed in a mammalian cell-free system at neutral pH, the variant shows an higher tendency to interact with the Hsp70 and Hsp90 chaperones, thus suggesting that the reduced stability could be associated with a kinetic trapping of the variant in a partly-folded state. On these bases, it has been also suggested that this interaction with molecular chaperones in the cytosol could be responsible for the mistargeting of the G170R-Mi variant by facilitating the delivery of the protein to the mitochondrial import machinery.

Only few reports have been published describing the enzymatic phenotype associated with F152I mutation on the minor allele. A mistargeting defect similar to that observed for the G170R-Mi variant has been suggested for the F152I-Mi variant by studying liver biopsies of patients heterozygous for the F152I and G41R mutations on the minor allele background as well as patients homozygous for the F152I mutation (25). *In vitro* studies upon expression in *E.coli* have shown that the F152I-Mi mutant: (i) is prone to aggregation (9), thus suggesting that in the patients the variant could be unstable and rapidly degraded; (ii) has a catalytic activity of about 14% compared to that of AGT-Mi (27), and (iii) shows a low sensitivity to trypsin cleavage (27), thus suggesting that the protein should be largely in the folded state. In order to provide insights into the molecular defect of the F152I-Mi variant, as well as into the molecular synergism between the F152I mutation and the minor allele polymorphism, the effect of the mutation on the biochemical properties of the major and minor AGT allele has been investigated (19). The data obtained provided evidence that the Phe152 mutation does not significantly change neither the spectroscopic (Figure 4) and kinetic features of AGT, nor the PLP binding affinity (Table 2). It causes instead a strong reduction of the PMP binding affinity (Table 2), which leads to the progressive conversion of the variant from the holo- to the apo-form during the overall transamination reaction in the absence of exogenous PLP. In addition, the determination of the half-inactivation temperatures (Ti) of F152I-Mi and AGT-Mi, in both the holo and the apo-forms (Table 3) showed that the F152I-Mi variant in the apo-form has a 6°C reduction in the Ti with respect to apoAGT-Mi. Moreover, unlike apoAGT-Mi, apoF152I-Mi undergoes a time-dependent loss of enzymatic activity when incubated at 37°C, which is associated with a loss of the peak area on size-exclusion chromatography and is indicative of an aggregation event (Figure 8). The finding that the loss of activity and the aggregation extent increase at low protein concentrations led to the conclusion that both phenomena are due to protein monomerization. From these results it appears that the enzymatic defect of the F152I-Mi variant

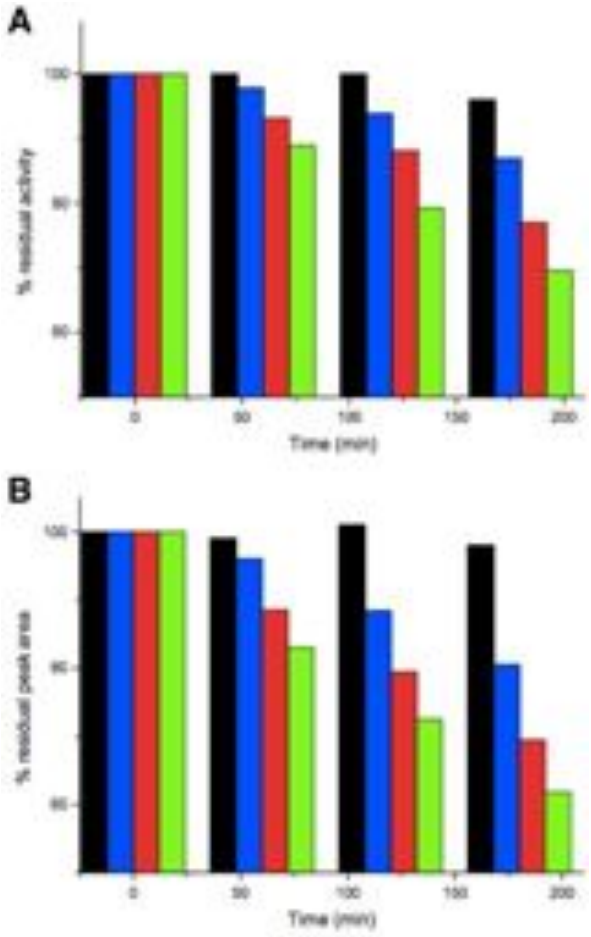

Figure 8. Histograms showing the time course of the loss of peak area on size-exclusion chromatography (A) and loss of transaminase activity (B) of apoF152I-Mi upon incubation at 37°C (19). ApoF152I-Mi was incubated at 37°C in 100 mM potassium phosphate buffer pH 7.4 at 1 μM (blue bars), 0.5 μM (red bars) or 0.25 μM (green bars) enzyme concentration. Aliquots were withdrawn at the indicated times and they were either assayed for transaminase activity or subjected to size-exclusion chromatography. Black bars represent the time course of transaminase activity and peak area for apoAGT-Mi at 0.25 μM enzyme concentration upon incubation at 37°C in 100 mM potassium phosphate buffer pH 7.4.

not only consists in the propensity of the variant to be converted into the apo-form during the overall transamination in the absence of added coenzyme, but also in the intrinsic instability of the apo-form at physiological temperature, due to protein monomerization.

Overall, the characterization of the G170R-Mi and F152I-Mi variants at a molecular level, along with previous evidence coming from cell biology and biochemical analyses, allows to propose a model that explains the pathogenic mechanism of the mutations and their synergism with the minor allele polymorphism. Figure 9 represents the possible routes that AGT could follow during its folding in the cytosol. Considering that vitamin B6 concentration in the whole blood is about 2 μM (23) and that monomeric species have probably a lower affinity for the coenzyme with respect to the dimeric ones, it can be postulated that the route $M^* \rightarrow M \rightarrow D \rightarrow D_{PLP}$ should be

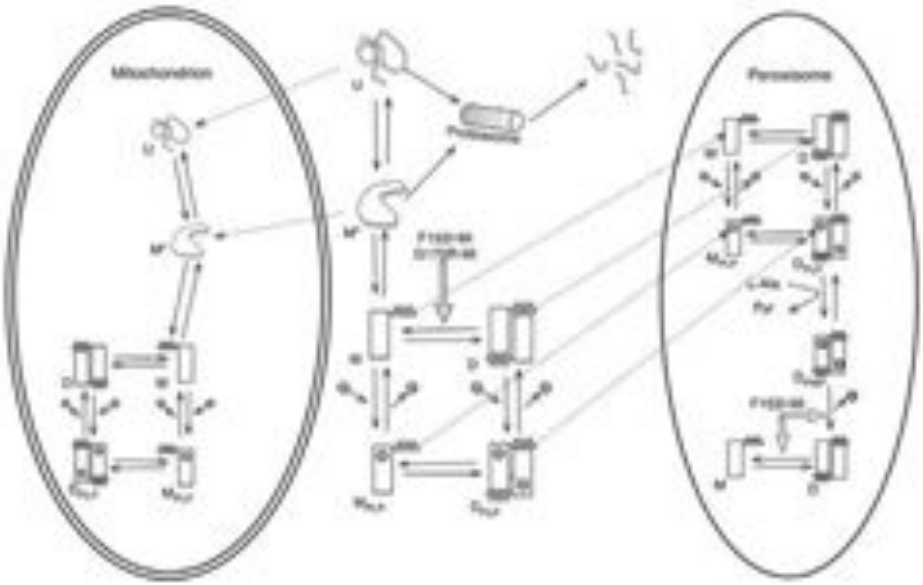

Figure 9. Proposed folding and targeting pathway of AGT. U: unfolded monomer; M*: partly folded monomer: M: folded monomer; M_{PLP}: PLP-bound monomer; D: apodimer; D_{PLP}, holodimer in the PLP form; D_{PMP}, holodimer in the PMP form; ●: PLP; ○: PMP. Gray arrows indicate the step (s) possibly affected by the G170R and/or F152I mutation.

preferred by AGT with respect to the $M^* \rightarrow M \rightarrow M_{PLP} \rightarrow D_{PLP}$ route. U and M* are compatible with the mitochondrial import machinery, which recognizes N-terminal targeting sequences and acts on partly-folded monomeric species. On the other hand, M, M_{PLP}, D, and D_{PLP} are only compatible with the peroxisomal import machinery, that recognizes C-terminal targeting sequences and acts on folded species (32), even in the dimeric form. Nevertheless, it cannot be excluded that M* could be imported into peroxisomes. In the case of G170R-Mi, data indicate that the holoenzyme of the variant does not significantly differ from AGT-Mi, while the apoenzyme displays a lower stability of the dimeric structure. This implies that the step affected by the mutation should be the conversion of M* or M to D. The consequent accumulation of the M* or M species would synergize with the presence of the N-terminal putative MTS of the minor allele thus allowing more protein to be imported to mitochondria. For F152I-Mi, two defective aspects can be pointed out: i) the propensity of the apovariant to monomerize would lead to the accumulation of M* or M, in analogy to what proposed for the G170R-Mi variant, and ii) the low affinity of the variant for PMP would allow the protein to be converted into the apo-form inside peroxisomes, thus leading to inactivation.

On the basis of clinical reports published to date, the responsiveness to pyridoxine therapy has been demonstrated for patients bearing the G170R mutation on the minor allele, and suggested for patients bearing the F152I mutation on the minor allele (12, 31). Although it is known that pyridoxine can be converted to PLP in the human body, the molecular mechanism underlining the effectiveness of the treatment is unknown. Based on the proposed model for the pathogenicity of the G170R-Mi and F152I-Mi variants, it is possible to speculate that the increased levels of PLP in the cytosol could have: (i) a prosthetic role, by shifting the equilibrium from the apo- to the holo-form of the variants. For the F152I-Mi variant, this would also prevent apoenzyme formation during the overall transamination and (ii) a conformational role, by possibly binding to the monomeric species M* and M, and promoting the formation of D_{PLP} through the route $M^* \rightarrow M \rightarrow M_{PLP} \rightarrow D_{PLP}$. In each case, the final result would be the stabilization of the dimeric form of the protein, which is incompatible with the mitochondrial import but compatible with the peroxisomal import.

9. ACKNOWLEDGEMENTS

The financial support of the Hyperoxaluria and Oxalosis Foundation is kindly acknowledged.

10. REFERENCES

1. R. Percudani and A. Peracchi: A genomic overview of pyridoxal-phosphate-dependent enzymes. *EMBO Rep*, 4(9), 850-4 (2003)

2. A. C. Eliot and J. F. Kirsch: Pyridoxal phosphate enzymes: mechanistic, structural, and evolutionary considerations. *Annu Rev Biochem*, 73, 383-415 (2004)

3. C. J. Danpure: Molecular etiology of primary hyperoxaluria type 1: new directions for treatment. *Am J Nephrol*, 25(3), 303-10 (2005)

4. P. E. Purdue, J. Allsop, G. Isaya, L. E. Rosenberg and C. J. Danpure: Mistargeting of peroxisomal L-alanine:glyoxylate aminotransferase to mitochondria in primary hyperoxaluria patients depends upon activation of a cryptic mitochondrial targeting sequence by a point mutation. *Proc Natl Acad Sci U S A*, 88(23), 10900-4 (1991)

5. P. E. Purdue, M. J. Lumb, M. Fox, G. Griffo, C. Hamon-Benais, S. Povey and C. J. Danpure: Characterization and chromosomal mapping of a genomic clone encoding human alanine:glyoxylate aminotransferase. *Genomics*, 10(1), 34-42 (1991)

6. E. F. Caldwell, L. R. Mayor, M. G. Thomas and C. J. Danpure: Diet and the frequency of the alanine:glyoxylate aminotransferase Pro11Leu polymorphism in different human populations. *Hum Genet*, 115(6), 504-9 (2004)

7. C. J. Danpure, G. M. Birdsey, G. Rumsby, M. J. Lumb, P. E. Purdue and J. Allsop: Molecular characterization and clinical use of a polymorphic tandem repeat in an intron of the human alanine:glyoxylate aminotransferase gene. *Hum Genet*, 94(1), 55-64 (1994)

8. E. L. Williams, C. Acquaviva, A. Amoroso, F. Chevalier, M. Coulter-Mackie, C. G. Monico, D. Giachino, T. Owen, A. Robbiano, E. Salido, H. Waterham and G. Rumsby: Primary hyperoxaluria type 1: update and additional mutation analysis of the AGXT gene. *Hum Mutat*, 30(6), 910-7 (2009)

9. M. J. Lumb and C. J. Danpure: Functional synergism between the most common polymorphism in human alanine:glyoxylate aminotransferase and four of the most common disease-causing mutations. *J Biol Chem*, 275(46), 36415-22 (2000)

10. C. G. Monico, J. B. Olson and D. S. Milliner: Implications of genotype and enzyme phenotype in pyridoxine response of patients with type I primary hyperoxaluria. *Am J Nephrol*, 25(2), 183-8 (2005)

11. C. G. Monico, S. Rossetti, J. B. Olson and D. S. Milliner: Pyridoxine effect in type I primary hyperoxaluria is associated with the most common mutant allele. *Kidney Int*, 67(5), 1704-9 (2005)

12. J. Harambat, S. Fargue, C. Acquaviva, M. F. Gagnadoux, F. Janssen, A. Liutkus, C. Mourani, M. A. Macher, D. Abramowicz, C. Legendre, A. Durrbach, M. Tsimaratos, H. Nivet, E. Girardin, A. M. Schott, M. O. Rolland and P. Cochat: Genotype-phenotype correlation in primary hyperoxaluria type 1: the p.Gly170Arg AGXT mutation is associated with a better outcome. *Kidney Int*, 77(5), 443-9 (2010)

13. C. J. Danpure, P. J. Cooper, P. J. Wise and P. R. Jennings: An enzyme trafficking defect in two patients with primary hyperoxaluria type 1: peroxisomal alanine/glyoxylate aminotransferase rerouted to mitochondria. *J Cell Biol*, 108(4), 1345-52 (1989)

14. P. E. Purdue, M. J. Lumb, J. Allsop and C. J. Danpure: An intronic duplication in the alanine: glyoxylate aminotransferase gene facilitates identification of mutations in compound heterozygote patients with primary hyperoxaluria type 1. *Hum Genet*, 87(4), 394-6 (1991)

15. P. E. Purdue, Y. Takada and C. J. Danpure: Identification of mutations associated with peroxisome-to-mitochondrion mistargeting of alanine/glyoxylate aminotransferase in primary hyperoxaluria type 1. *J Cell Biol*, 111(6 Pt 1), 2341-51 (1990)

16. B. Cellini, M. Bertoldi, R. Montioli, A. Paiardini and C. Borri Voltattorni: Human wild-type alanine:glyoxylate aminotransferase and its naturally occurring G82E variant: functional properties and physiological implications. *Biochem J*, 408(1), 39-50 (2007)

17. B. Cellini, A. Lorenzetto, R. Montioli, E. Oppici and C. B. Voltattorni: Human liver peroxisomal alanine:glyoxylate aminotransferase: Different stability under chemical stress of the major allele, the minor allele, and its pathogenic G170R variant. *Biochimie*, 92(12), 1801-11 (2010)

18. B. Cellini, R. Montioli, A. Paiardini, A. Lorenzetto, F. Maset, T. Bellini, E. Oppici and C. B. Voltattorni: Molecular defects of the glycine 41 variants of alanine glyoxylate aminotransferase associated with primary hyperoxaluria type I. *Proc Natl Acad Sci U S A*, 107(7), 2896-901 (2010)

19. B. Cellini, R. Montioli, A. Paiardini, A. Lorenzetto and C. B. Voltattorni: Molecular Insight into the Synergism between the Minor Allele of Human Liver Peroxisomal Alanine:Glyoxylate Aminotransferase and the F152I Mutation. *J Biol Chem*, 284(13), 8349-58 (2009)

20. X. Zhang, S. M. Roe, Y. Hou, M. Bartlam, Z. Rao, L. H. Pearl and C. J. Danpure: Crystal structure of alanine:glyoxylate aminotransferase and the relationship between genotype and enzymatic phenotype in primary hyperoxaluria type 1. *J Mol Biol*, 331(3), 643-52 (2003)

21. M. Bertoldi, B. Cellini, A. Paiardini, R. Montioli and C. Borri Voltattorni: Reactions of human liver peroxisomal alanine:glyoxylate aminotransferase with beta-chloro-L-alanine and L-cysteine: spectroscopic and kinetic analysis. *Biochim Biophys Acta*, 1784(9), 1356-62 (2008)

22. E. D. Hopper, A. M. Pittman, M. C. Fitzgerald and C. L. Tucker: In Vivo and in Vitro Examination of Stability of

Primary Hyperoxaluria-associated Human Alanine:Glyoxylate Aminotransferase. *J Biol Chem*, 283(45), 30493-502 (2008)

23. M. B. Coulter-Mackie and Q. Lian: Consequences of missense mutations for dimerization and turnover of alanine:glyoxylate aminotransferase: study of a spectrum of mutations. *Mol Genet Metab*, 89(4), 349-59 (2006)

24. P. E. Purdue, M. J. Lumb, J. Allsop, Y. Minatogawa and C. J. Danpure: A glycine-to-glutamate substitution abolishes alanine:glyoxylate aminotransferase catalytic activity in a subset of patients with primary hyperoxaluria type 1. *Genomics*, 13(1), 215-8 (1992)

25. C. J. Danpure, P. E. Purdue, P. Fryer, S. Griffiths, J. Allsop, M. J. Lumb, K. M. Guttridge, P. R. Jennings, J. I. Scheinman, S. M. Mauer and et al.: Enzymological and mutational analysis of a complex primary hyperoxaluria type 1 phenotype involving alanine:glyoxylate aminotransferase peroxisome-to-mitochondrion mistargeting and intraperoxisomal aggregation. *Am J Hum Genet*, 53(2), 417-32 (1993)

26. D. Pirulli, D. Puzzer, L. Ferri, S. Crovella, A. Amoroso, C. Ferrettini, M. Marangella, G. Mazzola and F. Florian: Molecular analysis of hyperoxaluria type 1 in Italian patients reveals eight new mutations in the alanine: glyoxylate aminotransferase gene. *Hum Genet*, 104(6), 523-5 (1999)

27. M. B. Coulter-Mackie and Q. Lian: Partial trypsin digestion as an indicator of mis-folding of mutant alanine:glyoxylate aminotransferase and chaperone effects of specific ligands. Study of a spectrum of missense mutants. *Mol Genet Metab*, 94(3), 368-74 (2008)

28. A. Santana, E. Salido, A. Torres and L. J. Shapiro: Primary hyperoxaluria type 1 in the Canary Islands: a conformational disease due to I244T mutation in the P11L-containing alanine:glyoxylate aminotransferase. *Proc Natl Acad Sci U S A*, 100(12), 7277-82 (2003)

29. A. Amoroso, D. Pirulli, F. Florian, D. Puzzer, M. Boniotto, S. Crovella, S. Zezlina, A. Spano, G. Mazzola, S. Savoldi, C. Ferrettini, S. Berutti, M. Petrarulo and M. Marangella: AGXT gene mutations and their influence on clinical heterogeneity of type 1 primary hyperoxaluria. *J Am Soc Nephrol*, 12(10), 2072-9 (2001)

30. M. B. Coulter-Mackie, G. Rumsby, D. A. Applegarth and J. R. Toone: Three novel deletions in the alanine:glyoxylate aminotransferase gene of three patients with type 1 hyperoxaluria. *Mol Genet Metab*, 74(3), 314-21 (2001)

31. C. S. van Woerden, J. W. Groothoff, F. A. Wijburg, C. Annink, R. J. Wanders and H. R. Waterham: Clinical implications of mutation analysis in primary hyperoxaluria type 1. *Kidney Int*, 66(2), 746-52 (2004)

32. C. J. Danpure: Primary hyperoxaluria type 1: AGT mistargeting highlights the fundamental differences between the peroxisomal and mitochondrial protein import pathways. *Biochim Biophys Acta*, 1763(12), 1776-84 (2006)

33. J. M. Leiper, P. B. Oatey and C. J. Danpure: Inhibition of alanine:glyoxylate aminotransferase 1 dimerization is a prerequisite for its peroxisome-to-mitochondrion mistargeting in primary hyperoxaluria type 1. *J Cell Biol*, 135(4), 939-51 (1996)

34. M. J. Lumb, G. M. Birdsey and C. J. Danpure: Correction of an enzyme trafficking defect in hereditary kidney stone disease in vitro. *Biochem J*, 374(Pt 1), 79-87 (2003)

35. S. Djordjevic, X. Zhang, M. Bartlam, S. Ye, Z. Rao and C. J. Danpure: Structural implications of a G170R mutation of alanine:glyoxylate aminotransferase that is associated with peroxisome-to-mitochondrion mistargeting. *Acta Crystallogr Sect F Struct Biol Cryst Commun*, 66(Pt 3), 233-6 (2010)

36. A. L. Pey, E. Salido and J. M. Sanchez-Ruiz: Role of low native state kinetic stability and interaction of partially unfolded states with molecular chaperones in the mitochondrial protein mistargeting associated with primary hyperoxaluria. *Amino Acids* (2010)

Abbreviations: AGT, alanine:glyoxylate aminotransferase; PH1, Primary Hyperoxaluria Type I; PLP, pyridoxal 5'-phosphate; PMP, pyridoxamine 5'-phosphate.

Key words: Alanine, Glyoxylate Aminotransferase, Pyridoxal 5'-Phosphate, Pathogenic Variant, Molecular Defect,Review

Send correspondence to: Barbara Cellini, Department of Life Sciences and Reproduction, Section of Biological Chemistry, University of Verona, Strada Le Grazie 8, 37134 Verona, Italy. Tel: 39-045-8027293, Fax: 39-045-8027170, E-mail: barbara.cellini@univr.it

http://www.bioscience.org/current/vol17.htm

Int J Pept Res Ther
DOI 10.1007/s10989-012-9333-9

TAT-Mediated Delivery of Human Alanine:Glyoxylate Aminotransferase in a Cellular Model of Primary Hyperoxaluria Type I

Alessandro Roncador · Elisa Oppici · Riccardo Montioli · Fabio Maset · Barbara Cellini

Accepted: 13 October 2012

Abstract Defects in liver peroxisomal alanine:glyoxylate aminotransferase (AGT), as a consequence of inherited mutations on the *AGXT* gene, lead to primary hyperoxaluria type I (PH1), a rare metabolic disorder characterized by the formation of calcium oxalate stones at first in the urinary tract and then in the whole body. The curative treatments currently available for PH1 are pyridoxine therapy, effective in only 10–30 % of the patients, and liver transplantation, an invasive procedure with potentially serious complications. A valid therapeutic option for PH1 patients would be the development of an enzyme administration therapy. However, the exogenous administration of the missing AGT would require the crossing of the plasma membrane to deliver the protein to liver peroxisomes. In this study, we constructed, purified and characterized the fusion protein of AGT with the membrane-penetrating Tat peptide (Tat-AGT). Although Tat-AGT shows subtle active site conformational changes as compared with untagged AGT, it retains a significant transaminase activity. Western-blot analyses, enzymatic assays and immunofluorescence studies show that active Tat-AGT can be successfully delivered to a mammalian cellular model of PH1 consisting of chinese hamster ovary cells expressing glycolate oxidase (CHO-GO), whereas untagged AGT cannot. Moreover, the intracellular transduced Tat-AGT makes CHO-GO cells able to detoxify endogenously produced glyoxylate to an extent similar to that of CHO-GO cells stably expressing AGT. Altogether, these results show that the Tat peptide is capable of delivering a functional AGT to mammalian cells, thus paving the way for the possibility to use Tat-AGT as an enzyme replacement therapy to counteract PH1.

Keywords Primary hyperoxaluria type I · Rare disease · Pyridoxal 5′-phosphate · Tat peptide · Enzyme administration therapy · Protein delivery

Abbreviations

PH1	Primary hyperoxaluria type I
AGT	Alanine:glyoxylate aminotransferase
PLP	Pyridoxal 5′-phosphate
CD	Circular dichroism
DLS	Dynamic light scattering
GO	Glycolate oxidase
CHO-GO	Chinese hamster ovary cells expressing glycolate oxidase
CHO-GO-AGT	Chinese hamster ovary cells expressing glycolate oxidase and AGT

Introduction

Primary hyperoxaluria type I (PH1) (OMIM 259900) is a rare disorder of metabolism characterized by the overproduction and excretion of oxalate resulting in recurrent urolithiasis and nephrocalcinosis, a condition leading to systemic oxalosis with calcium oxalate precipitation in several body areas (Danpure 2005). The disease is caused by

Electronic supplementary material The online version of this article (doi:10.1007/s10989-012-9333-9) contains supplementary material, which is available to authorized users.

A. Roncador · E. Oppici · R. Montioli · B. Cellini (✉)
Section of Biological Chemistry,
Department of Life Sciences and Reproduction, University of Verona, Strada Le Grazie 8, 37134 Verona, Italy
e-mail: barbara.cellini@univr.it

F. Maset
Department of Pharmaceutical Sciences,
University of Padova, Via F. Marzolo 5, 35131 Padua, Italy

Published online: 02 November 2012

mutations in the *AGXT* gene encoding liver peroxisomal alanine:glyoxylate aminotransferase (AGT), a pyridoxal 5′-phosphate (PLP)-dependent enzyme that catalyses the conversion of alanine and glyoxylate to pyruvate and glycine (Danpure and Jennings 1986). The loss of functional AGT in PH1 leads to the oxidation of increased amounts of glyoxylate to oxalate by lactate dehydrogenase, thus causing the formation and deposition of calcium oxalate crystals.

PH1 is a very heterogeneous disease. Genetic analyses have identified more than 150 different pathogenic mutations on the *AGXT* gene including nonsense, frameshift and the most common missense mutations (Williams et al. 2009). Moreover, missense mutations can cause AGT deficiency by a number of different mechanisms spanning from functional (loss of catalytic activity or reduced affinity for the PLP cofactor) to structural effects (loss of immunoreactivity, reduced stability, aggregation propensity, aberrant intracellular localization) (Cellini et al. 2007, 2009, 2010a, b; Coulter-Mackie and Lian 2006, 2008; Coulter-Mackie et al. 2008; Danpure et al. 1989, 1994; Hopper et al. 2008; Lumb and Danpure 2000; Pittman et al. 2012).

A variety of therapeutic approaches for PH1 have been developed. Classical treatments are aimed at increasing the solubility of the urinary calcium oxalate, removing the stones once formed, and dealing with renal failure by dialysis and kidney transplantation (Danpure 2005). All of these approaches, however, are symptomatic and do not address the cause of the disease. Another current therapeutic approach is the administration of pharmacological doses of pyridoxine (Vitamin B6), a precursor of the essential cofactor of AGT, but only a minority (10–30 %) of patients is responsive to this therapy (Monico et al. 2005). The only curative approach available for PH1 patients unresponsive to pyridoxine is liver transplantation, which reintroduces most of the body's requirements of active AGT. However, it represents a very invasive and wasteful intervention because an entire organ is used to replace only one defective gene (Cochat et al. 2012). Therefore, a novel pharmacological treatment for PH1 addressing the causes of the disease, but with limited side-effects, is urgently required. Since the disease is caused by the deficit of a single gene, an enzyme administration therapy could be a valid therapeutic option.

AGT is dimeric and belongs to the Fold Type I family of PLP-dependent enzymes. Each subunit is made up of (i) a large domain, comprising most of the active site and the dimerization interface, (ii) an N-terminal extension that wraps over the surface of the neighbouring subunit and is important for the preservation of the correct conformation and activity (Montioli et al. 2012), and (iii) a small domain, containing regions that mediate the peroxisomal import of the protein (Fodor et al. 2012; Zhang et al. 2003). Although AGT can be easily purified both in its histidine-tagged and untagged forms and is highly resistant to thermal and chemical denaturation (Cellini et al. 2007, 2008), a major obstacle for the development of an enzyme administration therapy is the passage through the hepatocyte plasma membrane required for the localization to liver peroxisomes, where AGT should be efficiently directed once released into the cytosol via its C-terminal targeting signal.

During the last years, it has been shown that the 11-residues domain rich in basic amino acids of the HIV-1 Tat protein, along with similar domains found in VP22 from the herpes simplex virus and Antennapedia from *Drosophila*, possesses the ability to traverse biological membranes in a process termed protein transduction (van den Berg and Dowdy 2011; Fittipaldi and Giacca 2005; Schwarze et al. 1999). Although the exact transduction mechanism is controversial, it is clear that the internalization does not occur through a receptor-, transporter-, or endosome-mediated fashion. The Tat basic peptide has been employed as a carrier to direct the uptake of various heterologous proteins into living cells, including for therapeutic applications (Vyas et al. 2012; Rapoport et al. 2011; Toro and Grunebaum 2006; Toro et al. 2006). In this study, we have generated, purified from *Escherichia coli* and characterized a fusion protein made up of the HIV-1 Tat protein transduction domain and AGT (Tat-AGT). Tat-AGT internalized into mammalian cells retains catalytic activity and prevents glyoxylate accumulation in a cellular model of PH1. These data suggest that AGT delivery through the Tat peptide is feasible and could represent an important step toward a new therapeutic approach for the disease.

Materials and Methods

Plasmid Construction

The pTrcTat-AGT plasmid containing the Tat-AGT coding sequence has been constructed by means of PCR amplification adding the Tat derived cell penetrating peptide (CPP) coding sequence (amino acids 49–57) at the 5′ end of the native AGT cDNA. For cloning purposes, consensus sequences of *Nco*I/*Hind*III restriction enzymes were added to the 5′ and 3′ ends respectively. The native AGT start codon was deleted and replaced by an ATG sequence in the 3′ *Nco*I consensus sequence. Four subsequent PCR amplifications were required to generate the appropriate sequence. The first PCR was performed by using the AGT cDNA as template, the forward primer Fw1 (5′ CGT CGC GGT GCC TCT CAC AAG CTG CTG 3′) and the reverse primer Rw1 (5′ GGTCTGG AAG CT TCA CAG CTT CTT CTT GGGGC 3′). The succeeding PCR runs have been performed with the same reverse primer of the first reaction and with the following forward primers: Fw2 (5′ CGG CAA CGC CGT

CGC GGT GCC T CT C 3′), Fw3 (5′ CGC AAG AAA CGT CGG CAA CGC CGT CGC 3′), Fw4 (5′ GAT ACC ATG GGC CGC AAG AAA CGT CGG CAA C 3′). In each run, the purified PCR product of the previous amplification round has been used as template. The final PCR product has been digested with *Nco*I and *Hind*III restriction enzymes (Fermentas) and cloned into the pTrcHis2 expression vector.

Protein Expression and Purification

Escherichia coli JM109 cells transformed with the plasmid pTrcTat-AGT were grown in 4.5 l of Luria broth at 37 °C to a turbidity of 0.4–0.6 at 600 nm as previously described (Cellini et al. 2008). Briefly, expression was induced with 0.1 mM isopropyl-D-thiogalactopyranoside for 15 h at 30 °C. Cells were harvested and resuspended in 10 mM sodium phosphate buffer pH 7.2 containing 2 mM EDTA, 0.1 mM dithiothreitol and 0.1 mM PLP. Lysozyme was added to a concentration of 0.2 mg/ml and the culture was incubated for 15 min at room temperature. After a freeze–thaw, leupeptin (0.5 g/ml) and pepstatin (0.7 g/ml) were added and the suspension was centrifuged at 30,000×*g* for 30 min at 4 °C. The cleared lysate was diluted to about 20 mg/ml, adjusted to pH 7.2 and then loaded on a DEAE Sepharose FF 26/20 column (GE Healthcare) equilibrated with 10 mM sodium phosphate buffer pH 7.2 and washed with the same buffer. A linear gradient (600 ml) from 10 to 200 mM sodium phosphate buffer, pH 7.2, was then applied. Under these conditions, Tat-AGT elutes between 100 and 130 mM sodium phosphate. Active fractions were pooled and concentrated using an Amicon Ultra 15 unit (Millipore) to around 50 ml and extensively dialysed versus 1 M potassium phosphate pH 7.4. The protein solution was loaded into a Phenyl-Sepharose column previously equilibrated with 1 M potassium phosphate pH 7.4. Tat-AGT was eluted with a linear gradient from 1 to 0.05 M potassium phosphate pH 7.4. Active fractions elute between 0.25 and 0.2 M potassium phosphate. The apoenzyme of Tat-AGT was prepared as previously described (Cellini et al. 2007).

Spectroscopic Measurements

Absorption measurements were made with a Jasco V-550 spectrophotometer with 1 cm path-length quartz cuvettes at a protein concentration of 5 μM. Visible and far-UV circular dichroism (CD) spectra were recorded on a Jasco J-710 spectropolarimeter equipped with a thermostatically controlled compartment at 25 °C, by using 1 cm path-length quartz cuvettes. The enzyme concentration was 5 μM. Routinely, three spectra were recorded at a scan speed of 50 nm/min with a bandwidth of 2 nm and averaged automatically. Dynamic light scattering (DLS) analyses were performed as previously described (Oppici et al. 2012). Intrinsic fluorescence emission spectra were recorded on a Jasco FP-750 spectrofluorometer equipped with a thermostatically controlled cell holder. The equilibrium dissociation constant for PLP ($K_{D(PLP)}$) of Tat-AGT was determined by measuring the quenching of the intrinsic fluorescence of the apoenzyme at 0.1 μM concentration in the presence of PLP at a concentration range of 0.03–5 μM as previously described (Daidone et al. 2012).

Cell Culture, Transduction and Lysis

Chinese hamster ovary cells stably expressing glycolate oxidase (CHO-GO) and double stable clones expressing both AGT and GO (CHO-GO-AGT) (kindly provided by Prof. C.J. Danpure, University College London) were cultured at 37 °C under O_2/CO_2 (19:1) in Ham's F12 Glutamax medium (Invitrogen) supplemented with 10 % (v/v) fetal calf serum, 100 units/ml penicillin and 100 μg/ml streptomycin. CHO-GO cells were cultured in the presence of 400 μg/ml zeocin, while CHO-GO-AGT cells were cultured in the presence of 400 μg/ml zeocin and 1 mg/ml G-418, as previously reported (Behnam et al. 2006; Montioli et al. 2012). CHO-GO cells were seeded in a 6-well plate at 2.5×10^5 cells/well. After 24 h the medium was replaced with fresh Ham's F12 medium containing Tat-AGT at a concentration range of 1.5–15 μM. After 24 h cells were extensively rinsed with PBS, trypsinized and lysed according to (Montioli et al. 2012). Protein concentration of the cell lysate was determined with a modified Lowry Assay protein determination kit (Biorad).

Activity Assays

The AGT enzymatic activity of *E. coli* and CHO-GO lysates and of purified Tat-AGT was determined by measuring pyruvate production using a spectrophotometric assay coupled with lactate dehydrogenase as previously described (Behnam et al. 2006; Cellini et al. 2007). The kinetic parameters for the overall transamination reaction for the pair alanine/glyoxylate of 0.1 μM Tat-AGT were determined in the presence of 100 μM exogenous PLP by varying the substrate concentration at a fixed saturating co-substrate concentration. Data of initial velocity as a function of substrate concentration were fitted to the Michaelis–Menten equation.

Western-Blot Analyses

5 μg of the CHO-GO cell lysate were loaded into each lane of a polyacrylamide gel. Upon transfer on an ImmobilonP membrane (Millipore), the filter was incubated with the purified antiAGT IgG from rabbit serum (kindly provided by Prof. C.J. Danpure, University College London) at a dilution

1:2,000. After extensive washing, the filter was incubated with a peroxidase-conjugated anti rabbit secondary antibody (GE Healthcare) at a 1:2,000 dilution and the signal was detected using a chemiluminescent detection system (ECL, Millipore). Blotted proteins were detected using the Chem-iDoc XRS Imaging System (BioRad, Hercules, CA) and quantified by the Quantity One software.

Immunofluorescence Studies

CHO-GO cells on glass coverslip were fixed in 4 % (w/v) paraformaldehyde, permeabilized with 0.3 % Triton X-100 in PBS plus 3 % bovine serum albumin followed by immunolabelling. Rabbit polyclonal anti-human glycolate oxidase (GO) (kindly provided by Dr. G. Rumsby, University College Hospital, London) and guinea-pig polyclonal anti-AGT human (kindly provided by Prof. C.J. Danpure, University College London) were used as primary antibodies (Behnam et al. 2006), followed by Alexa Fluor-conjugated antibodies (Life Technologies). The images were captured using a Leica SP5 confocal laser-scanning fluorescence microscope (Leica Microsystem, Manheim, Germany) at 63× magnification and processed using Image J (Rasband, W.S., ImageJ, U.S. NIH, Bethesda, Maryland, USA) and Adobe Photoshop softwares.

Glycolate Toxicity Assay

Cells were plated at 7,000 cells/well in a 96 wells plate. The day after cells were treated with Tat-AGT as explained above. Upon 1 h incubation, glyoxylate production was induced by the addition of Hepes buffered glycolate pH 7.0 at final concentration of 1 mM. Cell viability was evaluated after 24 h incubation using the crystal violet staining (Sigma). Cells were rinsed with PBS, incubated at room temperature for 5 min with 4 % formaldehyde + 0.5 % Crystal Violet solution to perform fixing and staining. The cells were then extensively washed with distilled water to remove the excess of dye. Cells were finally lysed with 1 % SDS in PBS to allow for crystal violet solubilization and quantification. The absorbance at 595 nm, which is proportional to the number of viable cells, has been measured with a TECAN plate reader. Six replicates were performed for each assay condition. Statistic analysis was performed with GraphPad Prism Version 5.0 (GraphPad software, San Diego, CA, USA).

Results

Construction, Expression and Purification of the Tat-AGT Fusion Protein

As a first step to produce a cell-permeable AGT, we constructed the pTrcTat-AGT expression vector, which contains the HIV-1 Tat basic domain ($Tat_{49–57}$) at the 5′ end of the cDNA sequence encoding AGT. A nucleotide triplet encoding a glycine residue was inserted between the sequence of the Tat peptide and that encoding AGT to minimize any possible effect of the N-terminal Tat peptide on the folding and the conformational stability of the protein (Montioli et al. 2012).

Recombinant Tat-AGT overexpressed in *E. coli* was purified from the soluble fraction of the bacterial lysate as detailed in Table 1. This method yields about 4 mg of pure protein per litre of bacterial culture and gives a 62-fold purification with 57 % recovery of the initial enzyme units. As expected, purified Tat-AGT migrates as a single band on SDS-PAGE with an apparent molecular mass slightly higher than untagged AGT (Supplementary Fig. 1). Unfortunately, we didn't succeed in the determination of the molecular mass of Tat-AGT because the protein aggregates at the almost null saline concentration required for the analysis. Considering that perturbations of the N-terminus make AGT prone to an electrostatically-driven aggregation (Cellini et al. 2010b; Montioli et al. 2012), the behaviour of Tat-AGT could be due to subtle conformational changes of the N-terminal arm induced by the presence of the Tat peptide (see below).

Spectroscopic and Kinetic Properties of Tat-AGT

All the spectroscopic and kinetic experiments are performed in 0.1 M potassium phosphate buffer pH 7.4. The CD spectrum of purified recombinant Tat-AGT in the far-UV region, reflecting the secondary structure composition of the protein, is identical to that of untagged AGT. Moreover, DLS analyses indicate that the protein has a hydrodynamic diameter of about 10 nm, as previously found for untagged AGT (Cellini et al. 2010b). Thus, the addition of the Tat peptide at the N-terminus does not alter the gross conformation and the dimeric structure of AGT.

Table 1 Summary of the purification of the Tat-AGT fusion protein expressed in *E. coli*

	Volume (ml)	Protein (mg)	Total activity (units)	Specific activity (units/mg)	Yield (%)	Purification (fold)
Cleared lysate	160	1,936	500,800	259	–	–
DEAE-FF	180	133	367,000	2,759	73	11
Phenyl Sepharose	91	17.8	284,000	15,955	57	62

As in all PLP-dependent enzymes, AGT binds the cofactor via a Shiff base linkage between the carbonyl group of the coenzyme and an active site lysine residue (Lys209 in AGT) forming a complex called internal aldimine (Zhang et al. 2003). Purified Tat-AGT binds two molecules of PLP per dimer. The absorbance and visible CD spectra of the protein were compared with those of untagged AGT (Fig. 1 and inset). Tat-AGT displays two absorbance maxima at 419 and 331 nm, attributable to the ketoenamine and enolimine tautomers of the internal aldimine, respectively, whose relative intensity is different from untagged AGT. Moreover, although the CD spectra of the two proteins are qualitatively similar, the magnitude of the positive band at 430 nm is lower in Tat-AGT with respect to the untagged protein. Tat-AGT in the apo-form does not show any absorbance and CD signal in the visible region. The intrinsic fluorescence emission spectrum of apoTat-AGT shows an about 2.5-fold higher intensity with respect to the holo-form. The difference is due to the quenching of a substantial fraction of the tryptophan emission fluorescence by the bound coenzyme. Titration of apoTat-AGT with PLP and analysis of the quenching of intrinsic fluorescence as a function of coenzyme concentration (Supplementary Fig. 2) yields a $K_{D(PLP)}$ value for the PLP-Tat-AGT complex equal to 243 ± 7 nM, a value comparable to that of untagged AGT (Cellini et al. 2008). Altogether, these results indicate that, although the presence of the Tat peptide could induce some small structural changes at the active site of the protein affecting the coenzyme binding mode, it does not alter the affinity of AGT for the PLP coenzyme.

The steady-state kinetic parameters for the overall transamination reaction of the alanine/glyoxylate pair catalyzed by Tat-AGT have been measured and compared with those of untagged AGT. As reported in Table 2, although Tat-AGT displays a k_{cat} value equal to ~40 % compared to untagged AGT and a 2-fold higher K_m for the two substrates, it retains a significant catalytic activity.

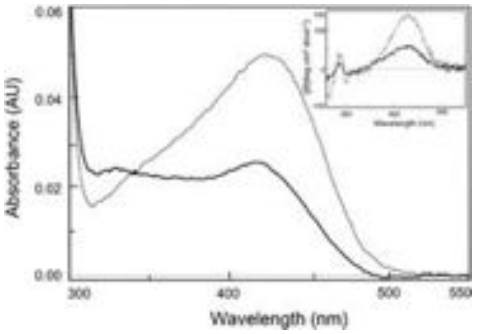

Fig. 1 Spectral properties of untagged AGT and Tat-AGT. Absorption and CD spectra (*inset*) of 5 μM untagged AGT (*dotted line*) and Tat-AGT (*dark line*). In each case the buffer was 0.1 M potassium phosphate pH 7.4

Table 2 Steady-state kinetic parameters of Tat-AGT and untagged AGT in 0.1 M potassium phosphate buffer pH 7.4 at 25 °C

	Substrate	Cosubstrate	k_{cat} (s^{-1})	K_m (mM)
Untagged AGT	Alanine	Glyoxylate	50 ± 5[a]	35 ± 4[a]
	Glyoxylate	Alanine	42 ± 4[a]	0.11 ± 0.02[a]
Tat-AGT	Alanine	Glyoxylate	17 ± 1	74 ± 9
	Glyoxylate	Alanine	16.1 ± 0.4	0.26 ± 0.03

[a] From Cellini et al. (2007)

Transduction of Tat-AGT into Mammalian Cells

In order to test the ability of Tat-AGT to be internalized into mammalian cells, we used a cellular model of PH1 consisting of CHO cells stably transfected with GO (CHO-GO). When these cells are treated with glycolate, a physiological precursor of peroxisomal glyoxylate, the activity of GO converts it to glyoxylate. In the absence of AGT, the accumulating and highly reactive glyoxylate cannot be detoxified to glycine and becomes toxic for CHO-GO cells (Behnam et al. 2006). Thus, the ability of CHO-GO cells to survive when treated with glycolate is an indirect measure of the presence of functional AGT inside the cells.

As a first step, we evaluated the transduction ability of Tat-AGT by adding the fusion protein to the culture medium of CHO-GO cells and determining the level of transduced AGT into the cells by western-blot analysis after 24 h. Neither Tat-AGT nor untagged AGT at 60 μM concentration were toxic for CHO-GO cells. As shown in Fig. 2, Tat-AGT is successfully delivered to CHO-GO cells whereas untagged AGT is not. The extent of the transduction of Tat-AGT into cultured cells is linear in the range 0.1–3 μM, reaches it's maximum at 7.5 μM and does not increase further by increasing the concentration of the fusion protein. In this regard, it should be noticed that the plateau seen between 7.5 and 60 μM is not due to a saturation of the chemiluminescence signal, as we checked by loading the gel with two different amounts of protein. Moreover, it can be observed that the levels of intracellular AGT in CHO-GO cells treated with 7.5–15 μM Tat-AGT are very similar to those present on CHO-GO cells stably transfected with AGT (CHO-GO-AGT).

The restoration of the catalytic activity of the transduced protein in cells is a key issue in the application of the protein transduction technology for therapeutic use. Therefore, we determined the transaminase activity of

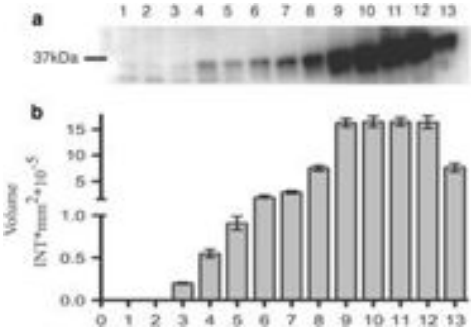

Fig. 2 Analyses of AGT expression in CHO-GO cells treated with Tat-AGT. AGT expression of CHO-GO cells after 24 h treatment with Tat-AGT at different concentrations. 5 µg of whole cell lysates were subjected to SDS/PAGE electrophoresis and immunoblotted against anti-AGT as described under the Materials and Methods section. The total AGT expression of CHO-GO-AGT cells is shown for comparison. **a** Immunoblot, **b** *Histogram* representative of the immunoblot *bands* volume. The immunoblot *lanes* and the *histogram* are coded as follow: *1* CHO-GO, *2* CHO-GO treated with 60 µM untagged AGT, *3* CHO-GO treated with 0.1 µM Tat-AGT, *4* CHO-GO treated with 0,2 µM Tat-AGT, *5* CHO-GO treated with 0.5 µM Tat-AGT, *6* CHO-GO treated with 1 µM Tat-AGT, *7* CHO-GO treated with 1.5 µM Tat-AGT, *8* CHO-GO treated with 3 µM Tat-AGT, *9* CHO-GO treated with 7,5 µM Tat-AGT, *10* CHO-GO treated with 15 µM Tat-AGT, *11* CHO-GO treated with 30 µM Tat-AGT, *12* CHO-GO treated with 60 µM Tat-AGT, *13* CHO-GO-AGT. Data come from the mean of three different experiments

AGT in CHO-GO cells treated with Tat-AGT. Cells treated with untagged AGT as well as CHO-GO-AGT cells were used as negative and positive control, respectively. While untransduced CHO-GO cells and CHO-GO cells treated with untagged AGT do not show any detectable AGT transaminase activity, CHO-GO cells transduced with 1.5 µM Tat-AGT for 24 h display a transaminase activity of 19 ± 1 nmol pyruvate/min/mg protein and CHO-GO-AGT cells display a transaminase activity of 42 ± 2 nmol pyruvate/min/mg proteins. This result indicates that the Tat peptide has a specific effect on protein internalization and that the transaminase activity is not due to residual AGT from the culture medium non-specifically bound to the cell. Thus, these data demonstrate that Tat-AGT is efficiently transduced into mammalian cells and that the delivered protein maintains its catalytic activity.

To determine the cellular localization of the transduced fusion protein, CHO-GO cells treated with Tat-AGT were analysed by immunofluorescence staining and compared with CHO-GO-AGT cells. As expected, no AGT fluorescence signal was present in CHO-GO cells treated with untagged AGT and, as shown in Fig. 3a and b, AGT co-localizes with the peroxisomal marker GO in CHO-GO-AGT cells. The analysis of cells treated with Tat-AGT indicates that the fusion protein is able to cross the plasma membrane, thus confirming the efficacy of the transduction process. However, as shown in Fig. 3c and d, the AGT fluorescence is localized into discrete compartments in the cytoplasm and does not superimposes with the GO fluorescence. Although this result suggests that Tat-AGT is retained in intracellular vesicles, it cannot be excluded that a very small fraction of the protein could be soluble in the cytoplasm or correctly imported into peroxisomes but the signal is too low to be detected by the microscope.

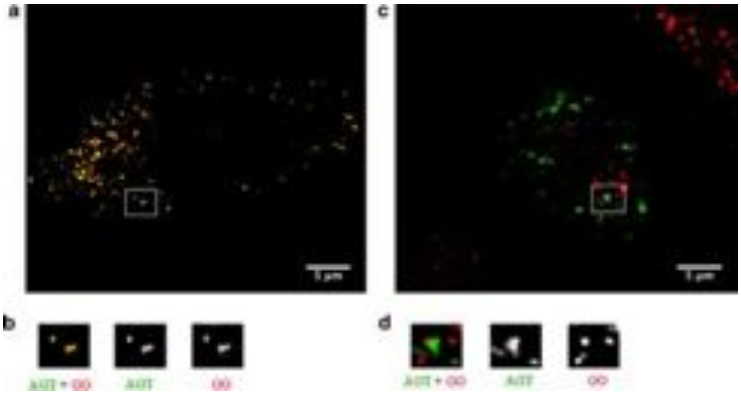

Fig. 3 Immunofluorescence analysis of CHO-GO-AGT cells (**a, b**) and CHO-GO cells transduced with Tat-AGT (**c, d**). CHO-GO-AGT cells and CHO-GO cells after 24 h incubation with 1.5 µM Tat-AGT were fixed on glass coverslips, permeabilized and stained as described in the Materials and Methods section. Polyclonal antibodies were used to detect AGT (*green*) and GO (*red*). The *small rectangles in* panels **a** and **c** indicate the areas shown in close-up in panels **b** and **d**, respectively. In panels **b** and **d** the original image and the individual split channels are shown (Color figure online)

Effect of Transduced Tat-AGT on Cell Viability Upon Glycolate Treatment

We then evaluated whether transduced Tat-AGT protects CHO-GO cells from glycolate-induced toxicity, as an indication that transduced Tat-AGT is functionally active inside the cell. As a first step we determined that the addition of either Tat-AGT or untagged AGT to the culture medium of CHO-GO cells does not have any effect on cell viability. Then, CHO-GO cells pretreated with Tat-AGT or untagged AGT were exposed to 1 mM glycolate and their viability was compared with that of CHO-GO cells stably expressing AGT under identical experimental conditions. As shown in Fig. 4, in the presence of glycolate the viability of the cells pretreated with Tat-AGT significantly increases in a dose-dependent manner, while untagged AGT fails to rescue the cells from the toxic effect of glyoxylate, thus indicating that Tat-AGT has a specific effect on glyoxylate detoxification. Notably, the transduction of CHO-GO cells with 15 μM Tat-AGT gives a protection similar to that provided by the stable expression of AGT. This could suggest that once transduced inside the cell, Tat-AGT is able to detoxify glyoxylate to an extent similar to that of the endogenously produced protein.

Discussion

A wide range of disorders are known that involve PLP-dependent enzymes spanning from metabolic (Cellini et al. 2012; Ferreira 1993; Zhu et al. 2008), neurologic (di Salvo et al. 2012; Giardina et al. 2011; Montioli et al. 2011), and infectious diseases (Bertoldi et al. 2002; Muller et al. 2009). While in many cases enzyme inhibitors are likely therapeutic options (Daidone et al. 2012; Pegg et al. 1995; Wu et al. 2011), in some cases, when the disease is caused by inherited mutations of a gene leading to an enzymatic deficit, the rescue of the catalytic activity of the lacking enzyme is necessary. To this aim, several strategies are currently being developed, including enzyme enhancement therapies (Ringe and Petsko 2009), effective for mutations that affect protein folding, and gene therapy (Humbert et al. 2012), whose safety is questioned by the use of viral vectors. An alternative approach is represented by the enzyme administration therapy. Although the potential immunogenicity of the administered protein should not be underestimated (Deegan 2012), the reversibility of the treatment and the control over the levels of protein in the cell should guarantee lower side effects. PH1 is a very good candidate for the development of an enzyme administration therapy because it is a single gene disorder caused by the deficit of AGT that is almost only expressed in liver peroxisomes (Motley et al. 1995). However, one of the limiting factors of an efficient protein administration is the crossing of the plasma membrane for the intracellular delivery (Fittipaldi and Giacca 2005; van den Berg and Dowdy 2011). During the last years, the discovery of protein transduction domains, small cationic peptides able to penetrate the cellular membrane, has opened the door to the possibility to deliver macromolecular drug conjugates for a variety of diseases including cancer, ischemia and neurodegenerative disorders (van den Berg and Dowdy 2011). Although an enzyme replacement therapy based on the use of Tat-fusion proteins has been recently exploited for the treatment of inherited metabolic diseases (Rapoport et al. 2011; Toro et al. 2006; Vyas et al. 2012), this approach has not been attempted until now for PH1.

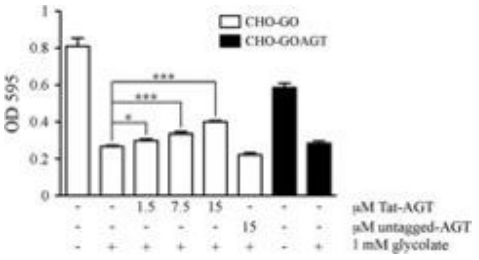

Fig. 4 Glycolate cytotoxicity assay of CHO-GO cells transduced with Tat-AGT. The *histogram* is representative of the cell viability after 24 h treatment with 1 mM glycolate measured by the crystal violet colorimetric assay and expressed as absorbance at 595 nm. Data are representative of three different experiments. *Bar graphs* represent the mean ± SEM $*P < 0.05$; $***P < 0.001$

In this study, we describe for the first time a protein transduction approach to deliver recombinant AGT to mammalian cells. The gene encoding AGT was fused with a gene fragment encoding the Tat protein basic domain in a bacterial expression vector to produce the Tat-AGT fusion protein. Moreover, a protocol has been developed to obtain in a short time a significant amount of pure protein.

The biochemical characterization of Tat-AGT reveals that the protein has no gross conformational differences with respect to untagged AGT and is able to catalyse the overall transamination reaction. This is a relevant finding because represents a promising starting point for the use of Tat-AGT for an enzyme replacement therapy for PH1. However, it should be noted that Tat-AGT is endowed with a lower catalytic activity and a slightly different coenzyme binding mode with respect to untagged AGT. A recent study has demonstrated that the N-terminus plays an essential role for the maintenance of the AGT functionality, probably as a consequence of the presence of the loop 24–32 that faces the active site of the enzyme (Montioli et al. 2012). It is possible to hypothesize that

the presence of the Tat tag at the N-terminus could slightly change the conformation of this loop, thus inducing small conformational changes at the AGT active site that could account for the observed effects on activity and coenzyme binding mode. In this regard, a future optimization of Tat-AGT should involve the insertion of a linker between the Tat peptide and the N-terminus of AGT in order to minimize the effects of the tag on the active site integrity.

In our study we showed that the administration of Tat-AGT to CHO-GO cells, which represent a cellular model of PH1, is not toxic for the cells and results in the presence of intracellular catalytically active AGT. It should be noted that CHO-GO cells transduced with 1.5 μM Tat-AGT and CHO-GO-AGT cells display a transaminase activity of 19 ± 1 and 42 ± 2 nmol pyruvate/min/mg proteins, respectively. Considering that the k_{cat} of purified Tat-AGT is about 40 % that of untagged AGT, this result would indicate that the amount of AGT present in CHO-GO cells transduced with 1.5 μM Tat-AGT is similar to that of CHO-GO-AGT cells. This is apparently in contrast with the results shown in Fig. 2, where the amount of total AGT of CHO-GO cells transduced with 1.5 μM Tat-AGT is about 50 % that of CHO-GO-AGT cells. This can be explained by considering that while activity assay only measures the amount of active protein, western-blot analyses are performed under denaturing conditions and measure the total amount of protein including aggregated and misfolded species. Thus, it is possible to speculate that about 50 % of AGT in CHO-GO-AGT cells, being endogenously produced and not exogenously transduced, could be in a misfolded and/or inactive conformation.

We found that transduced Tat-AGT is able to catalyse peroxisomal glyoxylate detoxification similar to stably expressed untagged AGT. Since glycolate treatment of CHO-GO cells induces the production of glyoxylate in peroxisomes by peroxisomal GO, the protective effect of Tat-AGT would suggest that the delivered protein is correctly localized to peroxisomes. However, our immunofluorescence studies indicate that AGT appears localized in discrete cytosolic vesicles that do not overlap with peroxisomes. A similar localization has been reported for other Tat-fusion proteins (Caron et al. 2004; Gump and Dowdy 2007; Sloots and Wels 2005; Fittipaldi et al. 2003) and might be related to the Tat peptide-mediated protein transduction. Although the exact mechanism has been a matter of debate and is still not completely clarified, many studies indicate that the internalization does not occur through clatrin-mediated endocytosis followed by fusion with lysosomes (Fittipaldi and Giacca 2005). Indeed, the transduction appears to be a multi-step process that involves the binding of the TAT peptide to the cell surface, the uptake of the cargo by macropinocytosis and the release of the cargo into the cytoplasm. The latter step seems to be stimulated by the decrease of pH inside the vesicle or by a membrane perturbation induced by the Tat peptide. Although a similar transduction mechanism might operate for AGT internalization into CHO-GO cells, the question of how the protein is able to detoxify peroxisomal glyoxylate remains. A first possibility is that a very small percentage of the protein is imported into peroxisomes and is sufficient to catalyse glyoxylate detoxification but is not detected due to the low signal. This would be possible because the peroxisomal targeting machinery act on the protein once folded and the targeting information is located at the C-terminus of AGT (Motley et al. 1995; Rucktaschel et al. 2011). A second possibility is that glyoxylate detoxification is performed by cytosolic AGT, even though inside vesicles. Indeed, it is known that in the absence of AGT, glyoxylate escapes peroxisomes and can be metabolized to either oxalate or glycolate by the cytosolic enzymes lactate dehydrogenase (LDH) and glyoxylate reductase (GRHPR). On the basis of the kinetic properties of the enzymes involved in glyoxylate metabolism, it has been proposed that the fate of glyoxylate depends on the ambient conditions within the cell, including the relative abundance of enzymes and substrates (Mdluli et al. 2005). Considering that the catalytic efficiency of Tat-AGT is similar to that of LDH and GRHPR, it is possible to speculate that in CHO-GO cells transduced with Tat-AGT a significant amount of glyoxylate could be converted to glycine in the cytosol, thus accounting for the higher survival of the cells in the presence of glyoxylate.

In conclusion, our results not only demonstrate that the AGT delivery to mammalian cells through the Tat peptide is feasible, but also suggest that this approach could allow to rescue for the enzymatic deficit of PH1. Many reports have been published in the last years describing the application of protein transduction approaches to various diseases and the Tat-fusion delivered proteins have been tested both in animal and in cellular disease systems (Rapoport et al. 2011; Toro and Grunebaum 2006; van den Berg and Dowdy 2011; Vyas et al. 2012). Further studies will be necessary to establish the efficacy and potential use of Tat-AGT as therapeutic strategy for PH1. In particular, we plan to deeply investigate the fate of Tat-AGT inside the cell as well as its possible effects in an animal model of PH1 previously described (Salido et al. 2006) or in hepatic cell lines derived from PH1 patients once they will be available.

Acknowledgments This work was supported by the Telethon Foundation (Grant No. GGP 10092).

Conflict of interest The authors declare that they have no conflict of interest.

References

Behnam JT, Williams EL, Brink S, Rumsby G, Danpure CJ (2006) Reconstruction of human hepatocyte glyoxylate metabolic pathways in stably transformed Chinese-hamster ovary cells. Biochem J 394(Pt 2):409–416

Bertoldi M, Cellini B, Clausen T, Voltattorni CB (2002) Spectroscopic and kinetic analyses reveal the pyridoxal 5′-phosphate binding mode and the catalytic features of Treponema denticola cystalysin. Biochemistry 41(29):9153–9164

Caron NJ, Quenneville SP, Tremblay JP (2004) Endosome disruption enhances the functional nuclear delivery of Tat-fusion proteins. Biochem Biophys Res Commun 319(1):12–20. doi:10.1016/j.bbrc.2004.04.180

Cellini B, Bertoldi M, Montioli R, Paiardini A, Borri Voltattorni C (2007) Human wild-type alanine: glyoxylate aminotransferase and its naturally occurring G82E variant: functional properties and physiological implications. Biochem J 408(1):39–50. doi:10.1042/BJ20070637

Cellini B, Montioli R, Bianconi S, Lopez-Alonso JP, Voltattorni CB (2008) Construction, purification and characterization of untagged human liver alanine-glyoxylate aminotransferase expressed in *Escherichia coli*. Protein Pept Lett 15(2):153–159

Cellini B, Montioli R, Paiardini A, Lorenzetto A, Voltattorni CB (2009) Molecular insight into the synergism between the minor allele of human liver peroxisomal alanine:glyoxylate aminotransferase and the F152I mutation. J Biol Chem 284(13):8349–8358. doi:10.1074/jbc.M808965200

Cellini B, Lorenzetto A, Montioli R, Oppici E, Voltattorni CB (2010a) Human liver peroxisomal alanine:glyoxylate aminotransferase: different stability under chemical stress of the major allele, the minor allele, and its pathogenic G170R variant. Biochimie 92(12):1801–1811. doi:10.1016/j.biochi.2010.08.005

Cellini B, Montioli R, Paiardini A, Lorenzetto A, Maset F, Bellini T, Oppici E, Voltattorni CB (2010b) Molecular defects of the glycine 41 variants of alanine glyoxylate aminotransferase associated with primary hyperoxaluria type I. Proc Natl Acad Sci USA 107(7):2896–2901. doi:10.1073/pnas.0908565107

Cellini B, Oppici E, Paiardini A, Montioli R (2012) Molecular insights into primary hyperoxaluria type 1 pathogenesis. Front Biosci 17:621–634

Cochat P, Hulton SA, Acquaviva C, Danpure CJ, Daudon M, De Marchi M, Fargue S, Groothoff J, Harambat J, Hoppe B, Jamieson NV, Kemper MJ, Mandrile G, Marangella M, Picca S, Rumsby G, Salido E, Straub M, van Woerden CS, OxalEurope (2012) Primary hyperoxaluria Type 1: indications for screening and guidance for diagnosis and treatment. Nephrol Dial Transplant 27(5):1729–1736. doi:10.1093/ndt/gfs078

Coulter-Mackie MB, Lian Q (2006) Consequences of missense mutations for dimerization and turnover of alanine:glyoxylate aminotransferase: study of a spectrum of mutations. Mol Genet Metab 89(4):349–359

Coulter-Mackie MB, Lian Q (2008) Partial trypsin digestion as an indicator of mis-folding of mutant alanine:glyoxylate aminotransferase and chaperone effects of specific ligands. Study of a spectrum of missense mutants. Mol Genet Metab 94(3):368–374

Coulter-Mackie MB, Lian Q, Applegarth DA, Toone J, Waters PJ, Vallance H (2008) Mutation-based diagnostic testing for primary hyperoxaluria type 1: survey of results. Clin Biochem 41(7–8):598–602. doi:10.1016/j.clinbiochem.2008.01.018

Daidone F, Montioli R, Paiardini A, Cellini B, Macchiarulo A, Giardina G, Bossa F, Borri Voltattorni C (2012) Identification by virtual screening and in vitro testing of human DOPA decarboxylase inhibitors. PLoS One 7(2):e31610. doi:10.1371/journal.pone.0031610

Danpure CJ (2005) Molecular etiology of primary hyperoxaluria type 1: new directions for treatment. Am J Nephrol 25(3):303–310

Danpure CJ, Jennings PR (1986) Peroxisomal alanine:glyoxylate aminotransferase deficiency in primary hyperoxaluria type I. FEBS Lett 201(1):20–24

Danpure CJ, Cooper PJ, Wise PJ, Jennings PR (1989) An enzyme trafficking defect in two patients with primary hyperoxaluria type 1: peroxisomal alanine/glyoxylate aminotransferase rerouted to mitochondria. J Cell Biol 108(4):1345–1352

Danpure CJ, Jennings PR, Fryer P, Purdue PE, Allsop J (1994) Primary hyperoxaluria type 1: genotypic and phenotypic heterogeneity. J Inherit Metab Dis 17(4):487–499

Deegan PB (2012) Fabry disease, enzyme replacement therapy and the significance of antibody responses. J Inherit Metab Dis 35(2):227–243. doi:10.1007/s10545-011-9400-y

di Salvo ML, Safo MK, Contestabile R (2012) Biomedical aspects of pyridoxal 5′-phosphate availability. Front Biosci (Elite Ed) 4:897–913

Ferreira GC (1993) Erythroid 5-aminolevulinate synthase and X-linked sideroblastic anemia. J Fla Med Assoc 80(7):481–483

Fittipaldi A, Giacca M (2005) Transcellular protein transduction using the Tat protein of HIV-1. Adv Drug Deliv Rev 57(4):597–608. doi:10.1016/j.addr.2004.10.011

Fittipaldi A, Ferrari A, Zoppe M, Arcangeli C, Pellegrini V, Beltram F, Giacca M (2003) Cell membrane lipid rafts mediate caveolar endocytosis of HIV-1 Tat fusion proteins. J Biol Chem 278(36):34141–34149. doi:10.1074/jbc.M303045200

Fodor K, Wolf J, Erdmann R, Schliebs W, Wilmanns M (2012) Molecular requirements for peroxisomal targeting of alanine-glyoxylate aminotransferase as an essential determinant in primary hyperoxaluria type 1. PLoS Biol 10(4):e1001309. doi:10.1371/journal.pbio.1001309

Giardina G, Montioli R, Gianni S, Cellini B, Paiardini A, Voltattorni CB, Cutruzzola F (2011) Open conformation of human DOPA decarboxylase reveals the mechanism of PLP addition to Group II decarboxylases. Proc Natl Acad Sci USA 108(51):20514–20519. doi:10.1073/pnas.1111456108

Gump JM, Dowdy SF (2007) TAT transduction: the molecular mechanism and therapeutic prospects. Trends Mol Med 13(10):443–448. doi:10.1016/j.molmed.2007.08.002

Hopper ED, Pittman AM, Fitzgerald MC, Tucker CL (2008) In vivo and in vitro examination of stability of primary hyperoxaluria-associated human alanine:glyoxylate aminotransferase. J Biol Chem 283(45):30493–30502

Humbert O, Davis L, Maizels N (2012) Targeted gene therapies: tools, applications, optimization. Crit Rev Biochem Mol Biol 47(3):264–281. doi:10.3109/10409238.2012.658112

Lumb MJ, Danpure CJ (2000) Functional synergism between the most common polymorphism in human alanine:glyoxylate aminotransferase and four of the most common disease-causing mutations. J Biol Chem 275(46):36415–36422

Mdluli K, Booth MP, Brady RL, Rumsby G (2005) A preliminary account of the properties of recombinant human glyoxylate reductase (GRHPR), LDHA and LDHB with glyoxylate, and their potential roles in its metabolism. Biochim Biophys Acta 1753(2):209–216. doi:10.1016/j.bbapap.2005.08.004

Monico CG, Olson JB, Milliner DS (2005) Implications of genotype and enzyme phenotype in pyridoxine response of patients with type I primary hyperoxaluria. Am J Nephrol 25(2):183–188

Montioli R, Cellini B, Borri Voltattorni C (2011) Molecular insights into the pathogenicity of variants associated with the aromatic amino acid decarboxylase deficiency. J Inherit Metab Dis 34(6):1213–1224. doi:10.1007/s10545-011-9340-6

Montioli R, Fargue S, Lewin J, Zamparelli C, Danpure CJ, Borri Voltattorni C, Cellini B (2012) The N-terminal extension is

essential for the formation of the active dimeric structure of liver peroxisomal alanine:glyoxylate aminotransferase. Int J Biochem Cell Biol 44(3):536–546. doi:10.1016/j.biocel.2011.12.007

Motley A, Lumb MJ, Oatey PB, Jennings PR, De Zoysa PA, Wanders RJ, Tabak HF, Danpure CJ (1995) Mammalian alanine/glyoxylate aminotransferase 1 is imported into peroxisomes via the PTS1 translocation pathway. Increased degeneracy and context specificity of the mammalian PTS1 motif and implications for the peroxisome-to-mitochondrion mistargeting of AGT in primary hyperoxaluria type 1. J Cell Biol 131(1):95–109

Muller IB, Wu F, Bergmann B, Knockel J, Walter RD, Gehring H, Wrenger C (2009) Poisoning pyridoxal 5-phosphate-dependent enzymes: a new strategy to target the malaria parasite Plasmodium falciparum. PLoS One 4(2):e4406. doi:10.1371/journal.pone.0004406

Oppici E, Montioli R, Lorenzetto A, Bianconi S, Borri Voltattorni C, Cellini B (2012) Biochemical analyses are instrumental in identifying the impact of mutations on holo and/or apo-forms and on the region(s) of alanine:glyoxylate aminotransferase variants associated with primary hyperoxaluria type I. Mol Genet Metab 105(1):132–140. doi:10.1016/j.ymgme.2011.09.033

Pegg AE, Shantz LM, Coleman CS (1995) Ornithine decarboxylase as a target for chemoprevention. J Cell Biochem Suppl 22:132–138

Pittman AM, Lage MD, Poltoratsky V, Vrana JD, Paiardini A, Roncador A, Cellini B, Hughes RM, Tucker CL (2012) Rapid profiling of disease alleles using a tunable reporter of protein misfolding. Genetics. doi:10.1534/genetics.112.143750

Rapoport M, Salman L, Sabag O, Patel MS, Lorberboum-Galski H (2011) Successful TAT-mediated enzyme replacement therapy in a mouse model of mitochondrial E3 deficiency. J Mol Med (Berl) 89(2):161–170. doi:10.1007/s00109-010-0693-3

Ringe D, Petsko GA (2009) What are pharmacological chaperones and why are they interesting? J Biol 8(9):80

Rucktaschel R, Girzalsky W, Erdmann R (2011) Protein import machineries of peroxisomes. Biochim Biophys Acta 1808(3):892–900. doi:10.1016/j.bbamem.2010.07.020

Salido EC, Li XM, Lu Y, Wang X, Santana A, Roy-Chowdhury N, Torres A, Shapiro LJ, Roy-Chowdhury J (2006) Alanine-glyoxylate aminotransferase-deficient mice, a model for primary hyperoxaluria that responds to adenoviral gene transfer. Proc Natl Acad Sci USA 103(48):18249–18254

Schwarze SR, Ho A, Vocero-Akbani A, Dowdy SF (1999) In vivo protein transduction: delivery of a biologically active protein into the mouse. Science 285(5433):1569–1572

Sloots A, Wels WS (2005) Recombinant derivatives of the human high-mobility group protein HMGB2 mediate efficient nonviral gene delivery. FEBS J 272(16):4221–4236. doi:10.1111/j.1742-4658.2005.04834.x

Toro A, Grunebaum E (2006) TAT-mediated intracellular delivery of purine nucleoside phosphorylase corrects its deficiency in mice. J Clin Invest 116(10):2717–2726. doi:10.1172/JCI25052

Toro A, Paiva M, Ackerley C, Grunebaum E (2006) Intracellular delivery of purine nucleoside phosphorylase (PNP) fused to protein transduction domain corrects PNP deficiency in vitro. Cell Immunol 240(2):107–115. doi:10.1016/j.cellimm.2006.07.003

van den Berg A, Dowdy SF (2011) Protein transduction domain delivery of therapeutic macromolecules. Curr Opin Biotechnol 22(6):888–893. doi:10.1016/j.copbio.2011.03.008

Vyas PM, Tomamichel WJ, Pride PM, Babbey CM, Wang Q, Mercier J, Martin EM, Payne RM (2012) A TAT-frataxin fusion protein increases lifespan and cardiac function in a conditional Friedreich's ataxia mouse model. Hum Mol Genet 21(6):1230–1247. doi:10.1093/hmg/ddr554

Williams EL, Acquaviva C, Amoroso A, Chevalier F, Coulter-Mackie M, Monico CG, Giachino D, Owen T, Robbiano A, Salido E, Waterham H, Rumsby G (2009) Primary hyperoxaluria type 1: update and additional mutation analysis of the AGXT gene. Hum Mutat 30:910–917

Wu F, Christen P, Gehring H (2011) A novel approach to inhibit intracellular vitamin B6-dependent enzymes: proof of principle with human and plasmodium ornithine decarboxylase and human histidine decarboxylase. FASEB J 25(7):2109–2122. doi:10.1096/fj.10-174383

Zhang X, Roe SM, Hou Y, Bartlam M, Rao Z, Pearl LH, Danpure CJ (2003) Crystal structure of alanine:glyoxylate aminotransferase and the relationship between genotype and enzymatic phenotype in primary hyperoxaluria type 1. J Mol Biol 331(3):643–652

Zhu W, Lin A, Banerjee R (2008) Kinetic properties of polymorphic variants and pathogenic mutants in human cystathionine gamma-lyase. Biochemistry 47(23):6226–6232. doi:10.1021/bi800351a

Send Orders of Reprints at reprints@benthamscience.org

The Open Biochemistry Journal, 2012, *6*, 116-130 1

Open Access

Biochemical and Computational Approaches to Improve the Clinical Treatment of Dopa Decarboxylase-Related Diseases: An Overview

Barbara Cellini*, Riccardo Montioli, Elisa Oppici, and Carla Borri Voltattorni*

Department of Life Sciences and Reproduction, Section of Biological Chemistry, University of Verona, Italy

Abstract: Dopa decarboxylase (DDC) is a pyridoxal 5'-phosphate (PLP)-dependent enzyme that by catalyzing the decarboxylation of L-Dopa and L-5-hydroxytryptophan produces the neurotransmitters dopamine and serotonin. The functional properties of pig kidney and human DDC enzymes have been extensively characterized, and the crystal structure of the enzyme in the holo- and apo-forms has been elucidated. DDC is a clinically relevant enzyme since it is involved in Parkinson's disease (PD) and in aromatic amino acid decarboxylase (AADC) deficiency. PD, a chronic progressive neurological disorder characterized by tremor, bradykinesia, rigidity and postural instability, results from the degeneration of dopamine-producing cells in the *substantia nigra* of the brain. On the other hand, AADC deficiency is a rare debilitating recessive genetic disorder due to mutations in *AADC* gene leading to the inability to synthesize dopamine and serotonin. Development delay, abnormal movements, oculogyric crises and vegetative symptoms characterize this severe neurometabolic disease. This article is an up to date review of the therapies currently used in the treatment of PD and AADC deficiency as well as of the recent findings that, on one hand provide precious guidelines for the drug development process necessary to PD therapy, and, on the other, suggest an aimed therapeutic approach based on the elucidation of the molecular defects of each variant associated with AADC deficiency.

Key words: Dopa decarboxylase, Parkinson's disease, AADC deficiency, pyridoxal 5'-phosphate.

INTRODUCTION

Pyridoxal 5'-phosphate (PLP)-dependent enzymes, except glycogen phosphorylase, synthesize, degrade and interconvert amino acids. They catalyze a wide variety of reactions including racemisation [1], transamination [2], decarboxylation [3], α-elimination [4], β-replacement [5] and γ-replacement [6]. They play indispensable roles in the primary metabolism of cells as well as in secondary metabolism, synthesizing important signaling molecules. Consistent with these metabolic roles, inhibitors of many PLP-enzymes have been and/or are used against certain types of neurological affections [7, 8], infectious diseases [9-11], and cancer [12]. The main hindrance in designing a PLP-enzyme inhibitor is the common chemistry of this family leading to low specificity and broad action. B6 enzyme inhibitors in medicinal use are substrate analogs but they follow different mechanisms for inhibiting their target enzymes. In fact, vigabatrin, difluoromethylornithine and D-cycloserine act as suicide inhibitors of human γ-aminotransferase [11], ornithine decarboxylase [12] and alanine racemase [11], respectively, while pregablin competitively inhibits human γ-aminotransferase [8], and benserazide and carbidopa irreversibly bind Dopa decarboxylase (DDC), thus blocking its active site. Recently, a general procedure for designing phosphopyridoxyl- substrate-conjugate inhibitors of PLP-enzymes modified to make them membrane-permeable has been described [7]. Favorable targets for this approach appear to be enzymes that have relatively low PLP affinity or undergo transamination as a significant side reaction with their amino acid substrate, thus forming the non covalently, less firmly bound pyridoxamine 5'-phosphate form of the cofactor.

Moreover, some PLP-enzymes are pharmacotherapeutic targets since their deficit is responsible for rare diseases, a heterogeneous group of disorders that encompass more than 14 distinct metabolic diseases. The incidence as a group is about 1:10000, but, taken individually, each disease is very rare and many have an incidence of less than 1:1000000. The list of these rare disorders along with the symptoms and the enzyme involved is reported in Table **1**. The molecular basis of many of these diseases has been analyzed by comparing the characteristics of the normal enzyme with those of the pathogenic variants either in their recombinant purified form [13-17] or expressed in cellular systems [18, 19]. A particular emphasis has been addressed to pathogenic variants of human peroxisomal liver alanine:glyoxylate aminotransferase [20-26] and cysthathionine- β-synthase [27-29]. It should be also mentioned that several neurological pathologies such as autism, schizophrenia, Alzheimer's disease, epilepsy and Down's syndrome can be caused by the deficiency of PLP, often determined by a reduced activity of PLP salvage pathway enzymes including pyridoxal kinase and pyridoxine 5'-phosphate oxidase [30-32].

Dopa decarboxylase (DDC), a PLP-enzyme responsible for the synthesis of the neurotransmitters dopamine and sero-

*Address correspondence to this author at the Department of Life Sciences and Reproduction, Section of Biological Chemistry, University of Verona, Italy; Tel:+390458027175; Fax: +390458027170;
E-mails:carla.borrivoltattorni@univr.it; barbara.cellini@univr.it

1874-091X/12

Table 1. Rare Diseases Involving PLP-enzymes

Rare Disease	Involved Enzyme	Main Symptoms
Aromatic L-amino acid decarboxylase deficiency [61]	DOPA decarboxylase	delay in development, abnormal movements, oculogyric crisies, vegetative symptoms
Cystathioninuria [69]	Cystathionine-γ-lyase	abnormal urinary excretion of cystathionine, fibrotic liver
GABA-transaminase deficiency [70]	γ-aminobutyric acid-transaminase	hyperreflexia, hypotonia, lethargia, macrosomia, mental retardation, and siezures
Gilles de la tourette syndrome [71]	Histidine decarboxylase	arm thrusting, eye blinking, repeated throat clearing or sniffing, shoulder shrugging
Glycine encephalopathy [72]	P protein (a pyridoxal phosphate-dependent glycine decarboxylase)	mental retardation, hypotonia, seizures, brain malformations, ataxia
Hereditary sensory and autonomic neuropathy Type I [73]	Serine palmitoyltransferase	sensory deficit in the distal portion of the lower extremities, chronic perforating ulcerations of the feet and progressive destruction of underlying bones, sweating
Homocystinuria [74]	Cystathionina-β-syntase	high level of homocysteine, endothelial injury, isk of other artery or vein diseases
Ornithine aminotransferase deficiency (Gyrate atrophy) [75]	Ornithine aminotransferase	poor vision at night or in dim light, peripheral vision loss
Primary hyperoxaluria Type I [76]	Alanine:glyoxylate aminotransferase	oxalosis, nephrocalcinosis urolithiasis, nephrolithiasis, kidney stones
Smith-Magenis syndrome [77]	Serine hydroxymethyltransferase	square-shaped face with deep-set eyes, engaging personalities, short stature, scoliosis, reduced sensitivity to pain and temperature, and a hoarse voice
Stiff-Man Syndrome [78]	Glutamic Acid Decarboxylase	muscle rigidity that waxes and wanes with concurrent spasms, encephalomyelitis, epilepsy, cerebral palsy, or cerebellar deficits
Type II Tyrosinemia (Richner-Hanhart syndrome) [79]	Tyrosine aminotransferase	excessive tearing, photophobia, eye pain and redness, and painful skin lesions on the palms and soles, mental retardation
Xanthurenic aciduria [80]	L-Kynurenine hydrolase	vomiting, jaundice, high excretion of Xanthurenic acid
"X-linked" sideroblastic anemia [81]	δ-aminolevulinate synthase	microcytic red blood cells hypochromic an abnormal accumulation of iron in red blood cells

tonin, represents a double-face therapeutic target because it is involved both in Parkinson's disease (PD) and in a rare neurometabolic disorder named aromatic amino acid decarboxylase (AADC) deficiency. In this review the attention is focused on the structural elements and functional features of DDC, on the current DDC-directed therapies for PD and AADC deficiency as well as on recent findings providing important guidelines for the future management of patients affected by these diseases.

DDC: STRUCTURAL AND FUNCTIONAL PROPERTIES

DDC, a PLP-dependent homodimeric enzyme, is an α-decarboxylase that catalyzes the conversion of L-aromatic amino acids into their corresponding amines. DDC, abundant in the nervous system and kidney, is central in the synthesis of dopamine and serotonin. Thus, its essential function is to provide the organism with these biogenic amines. Pig kidney, rat liver and human DDC enzymes have been cloned, expressed in *E. coli* and purified [16, 33, 34]. Our group has been involved for long time in the characterization of the pig kidney enzyme [10, 35-42], and recently in that of human DDC [16]. Pig kidney DDC and human DDC display similar spectroscopic features, kinetic parameters, susceptibility to proteolysis and thermostability [16]. The resolution of the three-dimensional structure of holoDDC in its ligand-free form and in complex with the anti-Parkinson drug carbidopa has allowed to point out that the structure is a tightly associated dimer in which the active site is located

near the monomer-monomer interface, although being mainly composed of residues from one monomer. Moreover, thanks to solved structures, we were able to identify the residues involved in the binding of the coenzyme, to evidence the antiparkinsonian drug binding mode, and to suggest which amino acid residues may be involved in catalysis [43]. Each of the two monomers is composed of three distinct domains. The large domain contains the PLP binding site and includes a core formed by a seven-stranded mixed β-sheet surrounded by eight α-helices in a typical α/β fold. The C-terminal small domain comprises a four-stranded antiparallel β-sheet with three helices packed against the face opposite to the large domain. The N-terminal domain, composed of two parallel helices linked by an extended strand, lies like a flap over the top of the second subunit. Until now, only few studies have been published that describe the functional role of the N-terminus of PLP-enzymes [44-46]. For human DDC, the recent resolution of the crystal structure of the enzyme in its apo form has provided evidence for an unexpected open bivalve conformation (as compared with the holoenzyme) with the interface between the N-terminal domains functioning as the hinge [47], thus suggesting a role for the N-terminus in the formation of the closed dimeric conformation of the holoenzyme.

PD

PD is a neurodegenerative disorder characterized by tremor, bradykinesia, rigidity, and postural instability. These symptoms are caused by the reduced levels of dopamine, consequent to the progressive degeneration of dopamine-producing cells in the *substantia nigra* of the brain [48]. Dopamine itself cannot pass the blood-brain barrier and, therefore, cannot be used as a drug in the PD treatment. Thus, one of the most effective clinical treatments of the disease is to routinely administer L-Dopa, in combination with a DDC inhibitor. The rational of this treatment is that since L-Dopa is rapidly converted to dopamine in the blood stream, only a small percentage of a given dose of Dopa, when administered as a drug, can reach the nervous system (Scheme **1A**). By adding a DDC inhibitor, greater amounts of L-Dopa can reach the brain (Scheme **1B**), where the level of dopamine will result to be substantially increased. The most commonly DDC inhibitors used in the treatment of PD are carbidopa ((2*S*)-3-(3,4-dihydroxyphenyl)-2-hydrazino-2-methylpropanoic acid; MK485) and benserazide ((*RS*)-2-amino-3-hydroxy-*N*′-(2,3,4-trihydroxybenzyl)propanehydrazide; Ro-4-4602). In animals and humans benserazide is completely metabolized to serine and trihydroxybenzylhydrazine (Ro-4-5127) before it reaches the arterial blood [49]. Thus, it is likely that trihydroxybenzylhydrazine represents the actual DDC inhibitor. Indeed, while benserazide is not a powerful DDC inhibitor [50], carbidopa and trihydroxybenzylhydrazine, both substrate analogs endowed with a substituted hydrazine function, have been found to bind pig kidney DDC by forming a hydrazone linkage with PLP, and work as powerful irreversible DDC inhibitors [50, 51]. However, several side effects (nausea, hypotension, arrhythmias, gastrointestinal bleeding and serious psychiatric symptoms) ensue from co-administration of L-Dopa with carbidopa or benserazide [52, 53], which are possibly related to the following findings: (i) carbidopa and trihydroxybenzylhydrazine react non-enzymatically with free PLP [52-54], (ii) the condensation products formed between PLP and hydrazine derivatives are the most potent inhibitors of pyridoxal kinase, an enzyme involved in PLP biosynthesis [55, 56], and (iii) high levels of homocysteine inversely correlate with PLP concentrations in the treated patients [57-59]. Thus, the current protocol seems to alter the PLP metabolism. Recently, a promising step forward in the drug development for PD has been accomplished. A virtual screening protocol, integrating pharmacofore search and molecular docking, has been developed starting from the atomic structure of the DDC-carbidopa complex [43]. The combination of these comupational methods with enzymatic assays and spectroscopic analyses has provided

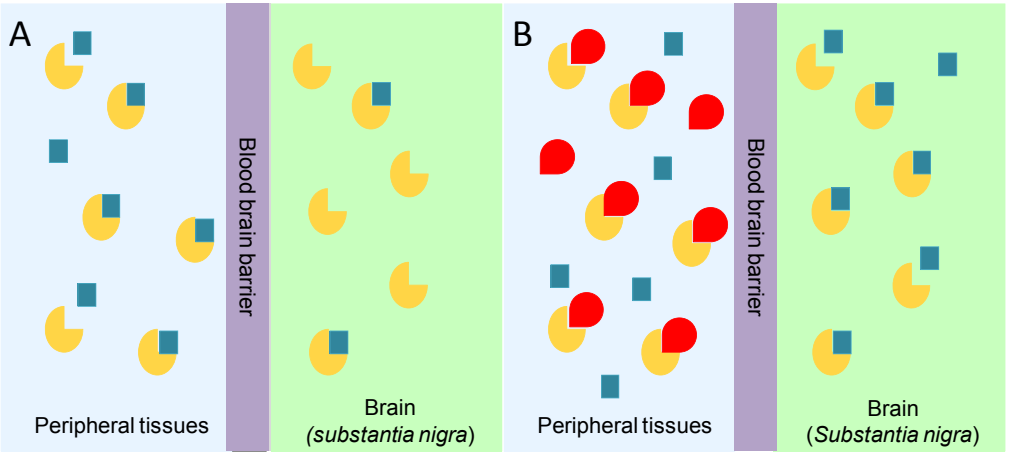

Scheme (1). Availability of administrated L-Dopa in the *substantia nigra* of brain in the absence (A) or in the presence (B) of an inhibitor of peripheral DDC. The yellow and the red symbols represent DDC and DDC inhibitor, respectively; the blue squares represent L-Dopa.

ten compounds identified as competitive inhibitors with K_i values in the low micromolar range and predicted to not cross the blood-brain barrier [60]. This approach, the first reported in the field of DDC inhibitors discovery, has represented an excellent staring point to further hit-to-lead development. In fact, it is relevant that these molecules, unlike carbidopa and trihydroxybenzylhydrazine, are devoid of an hydrazinic group, do not bind free PLP and act as good reversible inhibitors. Compounds endowed with such chemical features are more selective than the drugs commonly used in the treatment of PD. Thus, when improved and developed as drugs, they could reduce the very undesirable side effects of the current therapeutic strategy. On the basis of the above considerations and results, the drug development for the PD therapy seems to be a promising endeavor.

AADC DEFICIENCY

Recessive inherited deficiency of DDC (OMIM#608643) results in a severe neurometabolic disorder with developmental delay, abnormal movements, oculogyric crises and vegetative symptoms. Since the first report in 1990 [61], about 50 cases of DDC deficiency have been reported [62]. Patients display a typical pattern characterized by a distinct reduction of the stable degradation products of dopamine and serotonin, homovanillic acid and 5-hydroxyindolacetic acid, accompanied by the increase of the level of the precursors of dopamine and serotonin, L-Dopa and 5-hydroxytryptophan, respectively. Additionally, the levels of 3-ortho-methyldopa, resulting from methylation of accumulating L-Dopa, are clearly increased [63]. The diagnosis is confirmed by measuring the enzyme activity of DDC in plasma or cells [64]. Although about 30 mutations on the AADC gene have been identified and much is known about the clinical phenotype of the patients, the enzymatic phenotypes are so far largely unknown as well as of course the molecular mechanisms by which each mutation leads to the deficiency of DDC. While the effect of nonsense and frameshift mutations that lead to the complete loss of the gene product is straightforward, single amino acid substitutions leading to the synthesis of an aberrant gene product can in principle affect the enzymatic activity, the binding of the coenzyme, the protein stability and /or folding, the enzyme half-life inside the cell, etc. Moreover, it should be emphasized that many patients affected by DDC deficiency are compound heterozygous and their enzymatic phenotype depends on the combination of the effect of one mutation on a monomer and a different mutation on the other monomer. The core treatments for AADC deficiency are pyridoxine, MAO-B inhibitors, and dopamine agonists. Administered pyridoxine is phosphorylated by pyridoxal kinase and then subsequently converted to PLP by pyridoxal oxidase. The aim of this treatment is to provide an excess of PLP, which may in turn bolster or enhance residual DDC activity. MAO-B inhibitors (tranylcypromine, selegiline, moclobemide) are given to prevent the breakdown of the limited amounts of dopamine and serotonin produced by AADC deficient patients. Dopamine agonists (bromocriptine, pergolide, pramipexole and ropinirole) are administered in AADC deficiency in an attempt to stimulate dopamine receptors and consequently replace dopamine neurotransmission (Scheme **2**) [65]. It should be mentioned that in the last years a gene therapy approach has been explored, and good indications have been provided for the potential success of this technique for AADC deficiency [65, 66]. The response to the therapies in clinical use has been variable, but the overall outcome remains poor, probably reflecting the allelic heterogeneity. Moreover, since drugs were almost always given in combination, the response is hard to be ascribed to a single drug. Again, these classic treatments tend to address the more distal aspects of the disease process, i.e. symptoms rather than causes. A very important issue for the diagnosis and the therapy of diseases correlated to protein malfunction is the understanding of the multiple mechanisms that relate the specific mutants with the pathology. In fact, the knowledge of the enzymatic phenotype associated with each mutation represents the basis for predicting the response of patients to the available therapies as well as to project new therapeutic strategies. The structural and/or func-

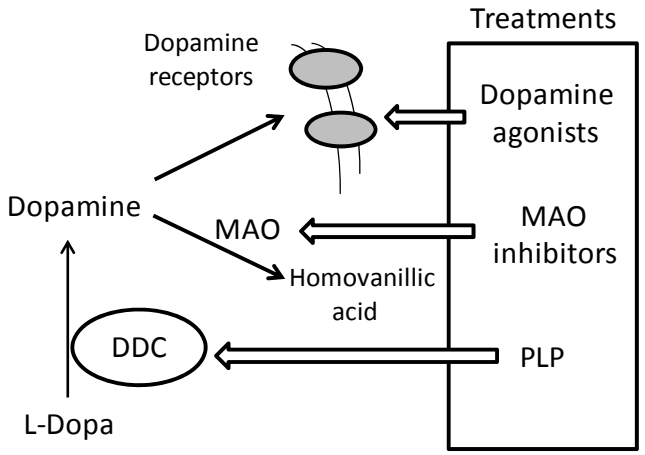

Scheme 2. Current clinical management of AADC deficiency.

tional effect(s) that amino acid substitutions produce on DDC has been recently investigated. A first approach in this direction is the analysis of the crystal structure of the enzyme to rationalize and interpret the impact of some disease-specific mutations in terms of their likely effects on enzyme's tertiary and quaternary structure. Fig. (**1**) represents an overview of DDC pathogenic mutation sites. Visual inspection of the three-dimensional structure of DDC in its holo-form suggests that, despite the variability in the space distribution, some physico-chemical effects shared by the disease-associated mutations might lead to similar enzymatic phenotypes. In particular, some point mutations (S147R, G102S, F309L, A275T, and R347Q) may affect the integrity of the active site, some (L38P and A110Q) might affect the stability of the dimer interface, while some (P47H and L38P) are expected to mostly compromise the stability of the monomeric form of the enzyme. For a number of mutants (R358H, V460G, G123G, S250F, R285W) the substitution is expected to perturb important hydrophobic patches within the structure, which might lead to misfolding or protein aggregation in cases where the perturbation occurs in solvent-exposed areas. Three mutants (L408I, R412W, R447H) are located in the small C-terminal domain in sites neither involved in the dimerization, nor in the catalytic areas. Such a "hot spot" in a well-defined domain might have functional consequences, which are currently unknown. Finally, the resolution of the structure of apoDDC [47] has highlighted that some pathogenic mutations (such as Y79C, H70T, H72Y and T69M) (Fig. **2**) involve residues important for the conformational changes occurring upon PLP binding, thus possibly affecting the apo-to-holo transition.

Recently, biochemical and bioinformatic investigations of several pathogenic DDC variants in the recombinant puri-

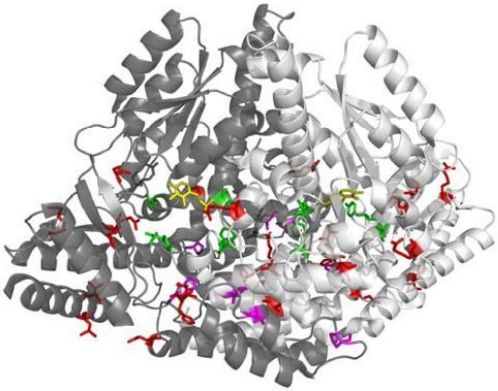

Fig. (1). Overview of DDC pathogenic mutation sites.

3D representation of the dimeric DDC molecule in which the two chains are represented as white and grey ribbon respectively. Sites of mutation are sorted in: mutations near the active site (green sticks), mutations at the dimer interface (magenta sticks), and mutations in the peripheral regions (red sticks). PLP molecules are also highlighted as yellow sticks.

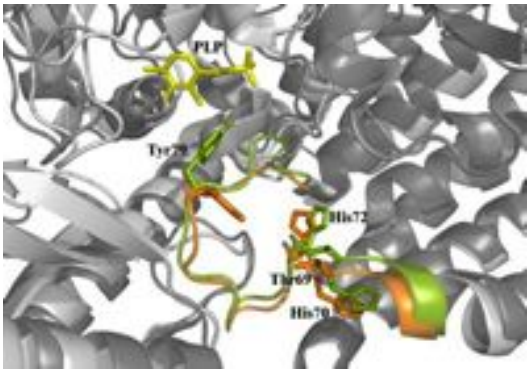

Fig. (2). Pathogenic mutation sites belonging to the loop 66-84.

Structural superposition of the apo (green) and holo (orange) DDC active site. Thr69, His70, His72 and Tyr79 residues are represented as stick. PLP molecule is represented as yellow stick.

fied form have been instrumental to uncover their molecular defects and to suggest an appropriate therapeutic strategy for AADC deficiency patients. The G102S, F309L, S147R and A275T variants associated with AADC deficiency, in which mutations concern amino acid residues interacting directly or indirectly with PLP and/or its microenvironment, have been constructed, expressed and purified [16]. These mutations cause, even if to different extents, a reduced PLP binding affinity (in the range 1.4-170-fold), an altered PLP binding mode, and, except for the S147R mutation, an increased K_m value for L-Dopa (in the range 3-35-fold). Moreover, all the variants display a reduced k_{cat} value, which appears to be correlated to a mispositioning of the external aldimine at the active site. In fact, in comparison with wild-type DDC, the external aldimines formed by the variants with L-aromatic amino acids exhibit different absorbance and dichroic features, do no protect against tryptic limited proteolysis, and, with time, in addition to aromatic amines production, lead to a decrease in the original PLP content and a concomitant increase in cyclic-PLP-substrate adducts. On these bases, it has been suggested that the examined pathogenic mutations are responsible for an active site perturbation, and, consequently substrate binding does not permit to completely reach a conformation where the catalytic groups are in correct proximity and orientation to allow a high level of reaction specificity, i.e., a conformation productive for decarboxylation. Such a conformation is, instead, achieved in wild-type DDC upon substrate-induced conformational change [67].

These data have allowed not only to understand the molecular defects of the examined DDC pathogenic variants, but also to give some suggestions for the treatment strategy of AADC deficiency patients bearing these mutations. In particular, a therapy consistent in pyridoxine plus L-Dopa and L-Dopa alone has been proposed for patients carrying F309L and G102S mutations, respectively. It is interesting that Chang Y. T. *et al* [68] have observed the effectiveness of L-Dopa administration to three siblings with the G102S mutation. Although up to date, no patients with homozygous genotype harboring S147R or A275T mutations have been identified, but only compound heterozygous patients [68], it has been proposed that pyridoxine treatment could effectively counteract the effects of the A275T mutation. No similar conclusion can be drawn for the S147R variant whose catalytic activity is 840-fold lower than that that of the wild-type, even in the presence of saturating PLP concentration.

Therefore, it appears highly desirable to extend this approach at the protein level to as many as possible other mutations associated with AADC deficiency in order to (i) understand the molecular basis of the pathogenicity of each mutation associated with the disease, (ii) advance proposals for the different drugs to overcome the disease, and (iii) help in listing patients in different therapeutic categories depending on the molecular defect(s) of each mutation. Advances in the understanding of the molecular etiology of AADC deficiency shift the attention towards the more proximal aspects of the disease process, i.e. the causes rather than the symptoms. This approach at the protein level could open new possibilities to (i) rationalize the choice of pharmacological agents to counteract the adverse effects of these mutations and (ii) prevent loss of time and unsuitable treatment regimens biochemically futile the use of biochemically futile.

CONCLUSIONS

DDC, a PLP-dependent enzyme, plays a key role in supplying the organisms with the neurotransmitters dopamine and serotonin. The enzyme is a pharmacotherapeutic target since it is involved in PD, a neurodegenerative disorder, and in AADC deficiency, an inherited rare neurometabolic disease. In this review, we point out how biochemical and computational findings could be instrumental for improving the current treatments of these pathologies.

CONFLICT OF INTEREST

None declared

REFERENCES

[1] Contestabile, R.; Paiardini, A.; Pascarella, S.; di Salvo, M.L.; D'Aguanno, S.; Bossa, F. l-Threonine aldolase, serine hydroxymethyltransferase and fungal alanine racemase. A subgroup of strictly related enzymes specialized for different functions. *Eur. J. Biochem.,* **2001,** *268*(24), 6508-6525.

[2] Christen P.; Metzler D.E. *Transaminases;* Wiley: New York, **1985**.

[3] Keller, J.W.; Baurick, K.B.; Rutt, G.C.; O'Malley, M.V.; Sonafrank, N.L.; Reynolds, R.A.; Ebbesson, L.O.; Vajdos, F.F. Pseudomonas cepacia 2,2-dialkylglycine decarboxylase. Sequence and expression in Escherichia coli of structural and repressor genes. *J. Biol. Chem.,* **1990,** *265*(10), 5531-5539.

[4] Kaiser, J.T.; Bruno, S.; Clausen, T.; Huber, R.; Schiaretti, F.; Mozzarelli, A.; Kessler, D. Snapshots of the cystine lyase C-DES during catalysis. Studies in solution and in the crystalline state. *J. Biol. Chem.,* **2003,** *278*(1), 357-365.

[5] Miles, E.W. Tryptophan synthase: a multienzyme complex with an intramolecular tunnel. *Chem. Rec.,* **2001,** *1*(2), 140-151.

[6] Brzovic, P.; Holbrook, E.L.; Greene, R.C.; Dunn, M.F. Reaction mechanism of Escherichia coli cystathionine gamma-synthase: direct evidence for a pyridoxamine derivative of vinylglyoxylate as a key intermediate in pyridoxal phosphate dependent gamma-elimination and gamma-replacement reactions. *Biochemistry,* **1990,** *29*(2), 442-451.

[7] Amadasi, A.; Bertoldi, M.; Contestabile, R.; Bettati, S.; Cellini, B.; di Salvo, M.L.; Borri-Voltattorni, C.; Bossa, F.; Mozzarelli, A. Pyridoxal 5'-phosphate enzymes as targets for therapeutic agents. *Curr. Med. Chem.,* **2007,** *14*(12), 1291-1324.

[8] Silverman, R.B. From basic science to blockbuster drug: the discovery of Lyrica. *Angew. Chem. Int. Ed. Engl.,* **2008,** *47*(19), 3500-3504.

[9] Chu, L.; Holt, S.C. Purification and characterization of a 45 kDa hemolysin from Treponema denticola ATCC 35404. *Microb. Pathog.,* **1994,** *16*(3), 197-212.

[10] Bertoldi, M.; Gonsalvi, M.; Contestabile, R.; Voltattorni, C.B. Mutation of tyrosine 332 to phenylalanine converts dopa decarboxylase into a decarboxylation-dependent oxidative deaminase. *J. Biol. Chem.,* **2002,** *277*(39), 36357-36362.

[11] Fenn, T.D.; Stamper, G.F.; Morollo, A.A.; Ringe, D. A side reaction of alanine racemase: transamination of cycloserine. *Biochemistry,* **2003,** *42*(19), 5775-5783.

[12] Seiler, N. Thirty years of polyamine-related approaches to cancer therapy. Retrospect and prospect. Part 1. Selective enzyme inhibitors. *Curr. Drug. Targ.,* **2003,** *4*(7), 537-564.

[13] Cotter, P.D.; Baumann, M.; Bishop, D.F. Enzymatic defect in "X-linked" sideroblastic anemia: molecular evidence for erythroid delta-aminolevulinate synthase deficiency. *Proc. Natl. Acad. Sci. USA.,* **1992,** *89*(9), 4028-4032.

[14] Medina-Kauwe, L.K.; Tobin, A.J.; De Meirleir, L.; Jaeken, J.; Jakobs, C.; Nyhan, W.L.; Gibson, K.M. 4-Aminobutyrate aminotransferase (GABA-transaminase) deficiency. *J. Inherit. Metab. Dis.,* **1999,** *22*(4), 414-4127.

[15] Zhu, W.; Lin, A.; Banerjee, R. Kinetic properties of polymorphic variants and pathogenic mutants in human cystathionine gamma-lyase. *Biochemistry,* **2008,** *47*(23), 6226-6232.

[16] Montioli, R.; Cellini, B.; Borri Voltattorni, C. Molecular insights into the pathogenicity of variants associated with the aromatic

amino acid decarboxylase deficiency. *J. Inherit. Metab. Dis.,* **2011,** *34*(6), 1213-1224.

[17] Cellini, B.; Oppici, E.; Paiardini, A.; Montioli, R. Molecular insights into primary hyperoxaluria type 1 pathogenesis. *Front. Biosci.,* **2012,** *17*, 621-634.

[18] Brody, L.C.; Mitchell, G.A.; Obie, C.; Michaud, J.; Steel, G.; Fontaine, G.; Robert, M.F.; Sipila, I.; Kaiser-Kupfer, M.; Valle, D. Ornithine delta-aminotransferase mutations in gyrate atrophy. Allelic heterogeneity and functional consequences. *J. Biol. Chem.,* **1992,** *267*(5), 3302-3307.

[19] Pittman, A.M.; Lage, M.D.; Poltoratsky, V.; Vrana, J.D.; Paiardini, A.; Roncador, A.; Cellini, B.; Hughes, R.M.; Tucker, C.L. Rapid Profiling of Disease Alleles Using a Tunable Reporter of Protein Misfolding. *Genetics,* **2012**.

[20] Cellini, B.; Bertoldi, M.; Montioli, R.; Paiardini, A.; Borri Voltattorni, C. Human wild-type alanine:glyoxylate aminotransferase and its naturally occurring G82E variant: functional properties and physiological implications. *Biochem. J.,* **2007,** *408*(1), 39-50.

[21] Cellini, B.; Montioli, R.; Bianconi, S.; Lopez-Alonso, J.P.; Voltattorni, C.B. Construction, purification and characterization of untagged human liver alanine-glyoxylate aminotransferase expressed in Escherichia coli. *Protein. Pept. Lett.,* **2008,** *15*(2), 153-159.

[22] Cellini, B.; Montioli, R.; Paiardini, A.; Lorenzetto, A.; Voltattorni, C.B. Molecular Insight into the Synergism between the Minor Allele of Human Liver Peroxisomal Alanine:Glyoxylate Aminotransferase and the F152I Mutation. *J. Biol. Chem.,* **2009,** *284*(13), 8349-8358.

[23] Cellini, B.; Montioli, R.; Paiardini, A.; Lorenzetto, A.; Maset, F.; Bellini, T.; Oppici, E.; Voltattorni, C.B. Molecular defects of the glycine 41 variants of alanine glyoxylate aminotransferase associated with primary hyperoxaluria type I. *Proc. Natl. Acad. Sci. USA.,* **2010,** *107*(7), 2896-2901.

[24] Cellini, B.; Lorenzetto, A.; Montioli, R.; Oppici, E.; Voltattorni, C.B. Human liver peroxisomal alanine:glyoxylate aminotransferase: Different stability under chemical stress of the major allele, the minor allele, and its pathogenic G170R variant. *Biochimie.,* **2010,** *92*(12), 1801-1811.

[25] Cellini, B.; Montioli, R.; Voltattorni, C.B. Human liver peroxisomal alanine:glyoxylate aminotransferase: characterization of the two allelic forms and their pathogenic variants. *Biochim. Biophys. Acta.,* **2011,** *1814*(11), 1577-1584.

[26] Oppici, E.; Montioli, R.; Lorenzetto, A.; Bianconi, S.; Borri Voltattorni, C.; Cellini, B. Biochemical analyses are instrumental in identifying the impact of mutations on holo and/or apo-forms and on the region(s) of alanine:glyoxylate aminotransferase variants associated with primary hyperoxaluria type I. *Mol. Genet. Metab.,* **2012,** *105*(1), 132-140.

[27] Sen, S.; Banerjee, R. A pathogenic linked mutation in the catalytic core of human cystathionine beta-synthase disrupts allosteric regulation and allows kinetic characterization of a full-length dimer. *Biochemistry,* **2007,** *46*(13), 4110-4116.

[28] Singh, S.; Madzelan, P.; Stasser, J.; Weeks, C.L.; Becker, D.; Spiro, T.G.; Penner-Hahn, J.; Banerjee, R. Modulation of the heme electronic structure and cystathionine beta-synthase activity by second coordination sphere ligands: The role of heme ligand switching in redox regulation. *J. Inorg. Biochem.,* **2009,** *103*(5), 689-697.

[29] Kozich, V.; Sokolova, J.; Klatovska, V.; Krijt, J.; Janosik, M.; Jelinek, K.; Kraus, J.P. Cystathionine beta-synthase mutations: effect of mutation topology on folding and activity. *Hum. Mutat.,* **2010,** *31*(7), 809-819.

[30] di Salvo, M.L.; Contestabile, R.; Safo, M.K. Vitamin B(6) salvage enzymes: mechanism, structure and regulation. *Biochim. Biophys. Acta.,* **2011,** *1814*(11), 1597-1608.

[31] di Salvo, M.L.; Safo, M.K.; Contestabile, R. Biomedical aspects of pyridoxal 5'-phosphate availability. *Front. Biosci. (Elite Ed.),* **2012,** *4*, 897-913.

[32] Gandhi, A.K.; Desai, J.V.; Ghatge, M.S.; di Salvo, M.L.; Di Biase, S.; Danso-Danquah, R.; Musayev, F.N.; Contestabile, R.; Schirch, V.; Safo, M.K. Crystal structures of human pyridoxal kinase in complex with the neurotoxins, ginkgotoxin and theophylline: insights into pyridoxal kinase inhibition. *PLoS. One.,* **2012,** *7*(7), e40954.

[33] Hayashi, H.; Mizuguchi, H.; Kagamiyama, H. Rat liver aromatic L-amino acid decarboxylase: spectroscopic and kinetic analysis of the coenzyme and reaction intermediates. *Biochemistry,* **1993,** *32*(3), 812-818.

[34] Moore, P.S.; Dominici, P.; Borri Voltattorni, C. Cloning and expression of pig kidney dopa decarboxylase: comparison of the naturally occurring and recombinant enzymes. *Biochem. J.,* **1996,** *315(Pt 1)*, 249-256.

[35] Voltattorni, C.B.; Minelli, A.; Turano, C. Spectral properties of the coenzyme bound to DOPA decarboxylase from pig kidney. *FEBS. Lett.,* **1971,** *17*(2), 231-235.

[36] Voltattorni, C.B.; Minelli, A.; Dominici, P. Interaction of aromatic amino acids in D and L forms with 3,4-dihydroxyphenylalanine decarboxylase from pig kidney. *Biochemistry,* **1983,** *22*(9), 2249-2254.

[37] Dominici, P.; Tancini, B.; Borri Voltattorni, C. Chemical modification of pig kidney 3,4-dihydroxyphenylalanine decarboxylase with diethyl pyrocarbonate. Evidence for an essential histidyl residue. *J. Biol. Chem.,* **1985,** *260*(19), 10583-10589.

[38] Tancini, B.;Dominici, P.;Simmaco, M.;Schinina, M. E.;Barra, D.;Voltattorni, C. B., Limited tryptic proteolysis of pig kidney 3,4-dihydroxyphenylalanine decarboxylase. *Arch Biochem Biophys* **1988,** *260* (2), 569-76.

[39] Maras, B.; Dominici, P.; Barra, D.; Bossa, F.; Voltattorni, C.B. Pig kidney 3,4-dihydroxyphenylalanine (dopa) decarboxylase. Primary structure and relationships to other amino acid decarboxylases. *Eur. J. Biochem.,* **1991,** *201*(2), 385-391.

[40] Bertoldi, M.; Moore, P.S.; Maras, B.; Dominici, P.; Voltattorni, C.B. Mechanism-based inactivation of dopa decarboxylase by serotonin. *J. Biol. Chem.,* **1996,** *271*(39), 23954-23959.

[41] Bertoldi, M.; Dominici, P.; Moore, P.S.; Maras, B.; Voltattorni, C.B. Reaction of dopa decarboxylase with alpha-methyldopa leads to an oxidative deamination producing 3,4-dihydroxyphenylacetone, an active site directed affinity label. *Biochemistry,* **1998,** *37*(18), 6552-6561.

[42] Bertoldi, M.; Voltattorni, C.B. Multiple roles of the active site lysine of Dopa decarboxylase. *Arch. Biochem. Biophys.,* **2009,** *488*(2), 130-139.

[43] Burkhard, P.; Dominici, P.; Borri-Voltattorni, C.; Jansonius, J.N.; Malashkevich, V.N. Structural insight into Parkinson's disease treatment from drug-inhibited DOPA decarboxylase. *Nat. Struct. Biol.,* **2001,** *8*(11), 963-967.

[44] Fukumoto, Y.; Tanase, S.; Nagashima, F.; Ueda, S.; Ikegami, K.; Morino, Y. Structural and functional role of the amino-terminal region of porcine cytosolic aspartate aminotransferase. Catalytic and structural properties of enzyme derivatives truncated on the amino-terminal side. *J. Biol. Chem.,* **1991,** *266*(7), 4187-4193.

[45] Kravchuk, Z.; Tsybovsky, Y.; Koivulehto, M.; Vlasov, A.; Chumanevich, A.; Battchikova, N.; Martsev, S.; Korpela, T. Truncated aspartate aminotransferase from alkalophilic Bacillus circulans with deletion of N-terminal 32 amino acids is a non-functional monomer in a partially structured state. *Protein. Eng.,* **2001,** *14*(4), 279-285.

[46] Montioli, R.; Fargue, S.; Lewin, J.; Zamparelli, C.; Danpure, C.J.; Borri Voltattorni, C.; Cellini, B. The N-terminal extension is essential for the formation of the active dimeric structure of liver peroxisomal alanine:glyoxylate aminotransferase. *Int. J. Biochem. Cell. Biol.,* **2012,** *44*(3), 536-546.

[47] Giardina, G.; Montioli, R.; Gianni, S.; Cellini, B.; Paiardini, A.; Voltattorni, C.B.; Cutruzzola, F. Open conformation of human DOPA decarboxylase reveals the mechanism of PLP addition to Group II decarboxylases. *Proc. Natl. Acad. Sci. USA.,* **2011,** *108*(51), 20514-20519.

[48] Hauser, R.A. Levodopa: past, present, and future. *Eur. Neurol.,* **2009,** *62*(1), 1-8.

[49] Schwartz, D.E.; Brandt, R. Pharmacokinetic and metabolic studies of the decarboxylase inhibitor benserazide in animals and man. *Arzneimittelforschung,* **1978,** *28*(2), 302-307.

[50] Borri-Voltattorni, C.; Minelli, A.; Borri, P. Interaction of N-(DL-seryl)N'-(2,3,4-trihydroxybenzyl)-hydrazine with L-dopa decarboxylase from pig kidney. *Experientia,* **1977,** *33*(2), 158-160.

[51] Borri Voltattorni, C.; Minelli, A.; Borri, P. The interaction of 2,3,4-trihydroxybenzylhydrazine with DOPA decarboxylase from pig kidney. *Life. Sci.,* **1981,** *28*(1), 103-108.

[52] Bender, D.A.; Earl, C.J.; Lees, A.J. Niacin depletion in Parkinsonian patients treated with L-dopa, benserazide and carbidopa. *Clin. Sci. (Lond.),* **1979,** *56*(1), 89-93.

[53] Bender, D.A. Effects of benserazide, carbidopa and isoniazid administration on tryptophan-nicotinamide nucleotide metabolism in the rat. *Biochem. Pharmacol.,* **1980,** *29*(15), 2099-2104.

[54] Bender, D.A. Inhibition *in vitro* of the enzymes of the oxidative pathway of tryptophan metabolism and of nicotinamide nucleotide synthesis by benserazide, carbidopa and isoniazid. *Biochem. Pharmacol.,* **1980,** *29*(5), 707-712.

[55] McCormick, D.B.; Gregory, M.E.; Snell, E.E. Pyridoxal phosphokinases. I. Assay, distribution, I. Assay, distribution, purification, and properties. *J. Biol. Chem.,* **1961,** *236*, 2076-2084.

[56] Ebadi, M.S.; Russell, R.L.; McCoy, E.E. The inverse relationship between the activity of pyridoxal kinase and the level of biogenic amines in rabbit brain. *J. Neurochem.,* **1968,** *15*(7), 659-665.

[57] Allain, P.; Le Bouil, A.; Cordillet, E.; Le Quay, L.; Bagheri, H.; Montastruc, J.L. Sulfate and cysteine levels in the plasma of patients with Parkinson's disease. *Neurotoxicology,* **1995,** *16*(3), 527-529.

[58] Kuhn, W.; Roebroek, R.; Blom, H.; van Oppenraaij, D.; Muller, T. Hyperhomocysteinaemia in Parkinson's disease. *J. Neurol.,* **1998,** *245*(12), 811-812.

[59] Miller, J.W.; Selhub, J.; Nadeau, M.R.; Thomas, C.A.; Feldman, R.G.; Wolf, P.A. Effect of L-dopa on plasma homocysteine in PD patients: relationship to B-vitamin status. *Neurology,* **2003,** *60*(7), 1125-1129.

[60] Daidone, F.; Montioli, R.; Paiardini, A.; Cellini, B.; Macchiarulo, A.; Giardina, G.; Bossa, F.; Borri Voltattorni, C. Identification by virtual screening and *in vitro* testing of human DOPA decarboxylase inhibitors. *PLoS. One.,* **2012,** *7*(2), e31610.

[61] Hyland, K.; Clayton, P.T. Aromatic amino acid decarboxylase deficiency in twins. *J. Inherit. Metab. Dis.,* **1990,** *13*(3), 301-304.

[62] Brun, L.; Ngu, L.H.; Keng, W.T.; Ch'ng, G.S.; Choy, Y.S.; Hwu, W.L.; Lee, W.T.; Willemsen, M.A.; Verbeek, M.M.; Wassenberg, T.; Regal, L.; Orcesi, S.; Tonduti, D.; Accorsi, P.; Testard, H.; Abdenur, J.E.; Tay, S.; Allen, G.F.; Heales, S.; Kern, I.; Kato, M.; Burlina, A.; Manegold, C.; Hoffmann, G.F.; Blau, N. Clinical and biochemical features of aromatic L-amino acid decarboxylase deficiency. *Neurology,* **2010,** *75*(1), 64-71.

[63] Hyland, K.; Surtees, R.A.; Rodeck, C.; Clayton, P.T. Aromatic L-amino acid decarboxylase deficiency: clinical features, diagnosis, and treatment of a new inborn error of neurotransmitter amine synthesis. *Neurology,* **1992,** *42*(10), 1980-1988.

[64] Hyland, K.; Clayton, P.T. Aromatic L-amino acid decarboxylase deficiency: diagnostic methodology. *Clin. Chem.,* **1992,** *38*(12), 2405-2410.

[65] Allen, G.F.; Land, J.M.; Heales, S.J. A new perspective on the treatment of aromatic L-amino acid decarboxylase deficiency. *Mol. Genet. Metab.,* **2009,** *97*(1), 6-14.

[66] Hwu, W.L.; Muramatsu, S.; Tseng, S.H.; Tzen, K.Y.; Lee, N.C.; Chien, Y.H.; Snyder, R.O.; Byrne, B.J.; Tai, C.H.; Wu, R.M. Gene therapy for aromatic L-amino acid decarboxylase deficiency. *Sci. Transl. Med.,* **2012,** *4*(134), 134ra61.

[67] Bertoldi, M.; Frigeri, P.; Paci, M.; Voltattorni, C.B. Reaction specificity of native and nicked 3,4-dihydroxyphenylalanine decarboxylase. *J. Biol. Chem.,* **1999,** *274*(9), 5514-5521.

[68] Chang, Y.T.; Mues G.; Mcpherson J.; Bedell J.L. Mutations in the human aromatic L-aminoacid decarboxylase gene. *J. Inherit. Metab. Dis.,* **1998**.

[69] Wang, J.; Hegele, R.A. Genomic basis of cystathioninuria (MIM 219500) revealed by multiple mutations in cystathionine gamma-lyase (CTH). *Hum. Genet.,* **2003,** *112*(4), 404-408.

[70] Jaeken, J.; Casaer, P.; de Cock, P.; Corbeel, L.; Eeckels, R.; Eggermont, E.; Schechter, P.J.; Brucher, J.M. Gamma-aminobutyric acid-transaminase deficiency: a newly recognized inborn error of neurotransmitter metabolism. *Neuropediatrics,* **1984,** *15*(3), 165-169.

[71] Ercan-Sencicek, A.G.; Stillman, A.A.; Ghosh, A.K.; Bilguvar, K.; O'Roak, B.J.; Mason, C.E.; Abbott, T.; Gupta, A.; King, R.A.; Pauls, D.L.; Tischfield, J.A.; Heiman, G.A.; Singer, H.S.; Gilbert, D.L.; Hoekstra, P.J.; Morgan, T.M.; Loring, E.; Yasuno, K.; Fernandez, T.; Sanders, S.; Louvi, A.; Cho, J.H.; Mane, S.; Colangelo, C.M.; Biederer, T.; Lifton, R.P.; Gunel, M.; State, M.W. L-histidine decarboxylase and Tourette's syndrome. *N. Engl. J. Med.,* **2010,** *362*(20), 1901-1908.

[72] Tada, K.; Kure, S. Non-ketotic hyperglycinaemia: molecular lesion, diagnosis and pathophysiology. *J. Inherit. Metab. Dis.,* **1993,** *16*(4), 691-703.

[73] Dawkins, J.L.; Hulme, D.J.; Brahmbhatt, S.B.; Auer-Grumbach, M.; Nicholson, G.A. Mutations in SPTLC1, encoding serine palmitoyltransferase, long chain base subunit-1, cause hereditary sensory neuropathy type I. *Nat. Genet.,* **2001,** *27*(3), 309-312.

[74] Finkelstein, J. D.; Mudd, S.H.; Irreverre, F.; Laster, L. Homocystinuria Due to Cystathionine Synthetase Deficiency: The Mode of Inheritance. *Science,* **1964,** *146*(3645), 785-787.

[75] Shih, V.E.; Berson, E.L.; Mandell, R.; Schmidt, S.Y. Ornithine ketoacid transaminase deficiency in gyrate atrophy of the choroid and retina. *Am. J. Hum. Genet.,* **1978,** *30*(2), 174-179.

[76] Danpure, C.J.; Jennings, P.R. Peroxisomal alanine:glyoxylate aminotransferase deficiency in primary hyperoxaluria type I. *FEBS. Lett.,* **1986,** *201*(1), 20-24.

[77] Elsea, S. H.; Juyal, R.C.; Jiralerspong, S.; Finucane, B.M.; Pandolfo, M.; Greenberg, F.; Baldini, A.; Stover, P.; Patel, P.I. Haploinsufficiency of cytosolic serine hydroxymethyltransferase in the Smith-Magenis syndrome. *Am. J. Hum. Genet.,* **1995,** *57*(6), 1342-1350.

[78] Daw k.; Ujihara N.; Atkinson M.; A.C.; A. P. Glutamic Acid Decarboxylase Autoantibodies in Stiff-Man Syndrome and Insulin-Dependent Diabetes Mellitus Exhibit SimilaritiesandDifferences in EpitopeRecognition. *J. Immunol.* **1996,** (156), 818-825.

[79] Natt, E.; Kida, K.; Odievre, M.; Di Rocco, M.; Scherer, G. Point mutations in the tyrosine aminotransferase gene in tyrosinemia type II. *Proc. Natl. Acad. Sci. USA.,* **1992,** *89*(19), 9297-9301.

[80] Tada, K.; Yokoyama, Y.; Nakagawa, H.; Yoshida, T.; Arakawa, T. Vitamin B6 dependent xanthurenic aciduria. *Tohoku. J. Exp. Med.,* **1967,** *93*(2), 115-124.

[81] Takaku, F.; Nakao, K. Delta-aminolevulinic acid synthetase activity in erythroblasts of patients with sideroblastic anemia. *Life. Sci. II.,* **1971,** *10*(13), 721-726.

Received: September 10, 2012 Revised: October 12, 2012 Accepted: October 23, 2012

HMG Advance Access published January 30, 2013

Human Molecular Genetics, 2013 ***1–10***
doi:10.1093/hmg/ddt011

S250F variant associated with aromatic amino acid decarboxylase deficiency: molecular defects and intracellular rescue by pyridoxine

Riccardo Montioli†, Elisa Oppici†, Barbara Cellini, Alessandro Roncador, Mirco Dindo and Carla Borri Voltattorni*

Department of Life Sciences and Reproduction, University of Verona, Verona, Italy

Received December 4, 2012; Revised and Accepted January 10, 2013

Dopa or aromatic amino acid decarboxylase (DDC, AADC) is a pyridoxal 5′-phosphate-dependent enzyme that catalyses the production of the neurotransmitters dopamine and serotonin. Among the so far identified mutations associated with AADC deficiency, an inherited rare neurometabolic disease, the S250F mutation is the most frequent one. Here, for the first time, the molecular basis of the deficit of the S250F variant was investigated both *in vitro* and in cellular systems. Ser250 is not essential for the catalytic activity of the enzyme. However, its mutation to Phe causes a ∼7-fold reduction of catalytic efficiency and a conformational change in the proximity of the mutated residue that is transmitted to the active site. In cellular extracts of *E. coli* and mammalian cells, both the specific activity and the protein level of the variant decrease with respect to the wild-type. The results with mammalian cells indicate that the mutation does not affect intracellular mRNA levels, and are consistent with a model where S250F undergoes a degradation process via the proteasome, possibly through an ubiquitination process occurring faster than in the wild-type. Overall, biochemical and cell biology experiments show that loss of function of S250F occurs by two distinct but not exclusive mechanisms affecting activity and folding. Importantly, 4-phenylbutirric acid (4-PBA) or, to a major extent, pyridoxine increase the expression level and, in a dose-dependent manner, the decarboxylase specific activity of mutant-expressing cells. This strongly suggests that 4-PBA and/or pyridoxine administration may be of important value in therapy of patients bearing the S250F mutation.

INTRODUCTION

Aromatic amino acid decarboxylase (AADC) deficiency, a rare neurometabolic disorder, is a loss-of-function disease whose symptoms are directly related to the absence of functional dopa decarboxylase (DDC), a pyridoxal 5′-phosphate (PLP)-dependent enzyme responsible for the production of the neurotransmitters dopamine and serotonin. More than 50 patients with DDC deficiency have been tabulated on the BIOMDB database (http://www.biopku.org/biomdb/biomdb_start.asp), and 23 missense pathogenic mutations have been identified, half of which in homozygous patients. Although the clinical phenotype associated with the disease has been widely investigated (1,2), the molecular effect(s) that any mutation induces on DDC is almost unknown. Nonsense and frameshifts mutations lead to the complete loss of the gene product, while missense point mutations cause the synthesis of an aberrant gene product which can be characterized by defects of enzymatic activity, PLP binding, protein stability and/or folding, protein half-life, etc. Current treatments for AADC deficiency are the administration of pyridoxine or PLP to increase the residual DDC activity, or MAO-B inhibitors to minimize the dopamine degradation or dopamine agonists to mime the action of the neurotransmitter (3). The response to these therapies is variable, but the overall outcome is rather poor, probably reflecting the allelic heterogeneity. Moreover, since drugs are almost always given in combination, response is hardly ascribable to a single drug. In diseases related to protein malfunction, it is diagnostically and therapeutically essential to understand the

*To whom correspondence should be addressed at: Department of Life Sciences and Reproduction (Section of Biological Chemistry), University of Verona (Italy) Strada Le Grazie, 8, 37134 Verona, Italy. Tel: +39 0458027175; Fax: +39 0458027179; Email: carla.borrivoltattorni@univr.it
†The authors wish it to be known that, in their opinion, the first two authors should be regarded as joint First Authors.

multiple mechanisms that relate the specific mutants with the pathology. Therefore, the knowledge of the structural and/or functional effect(s) that each amino acid substitution produces on DDC would be highly desirable. A first example of this approach is a recent study in which, by means of biochemical and bioinformatic analyses, the molecular defects of four recombinant purified pathogenic variants whose mutations concern residues located at or near the active site have been identified. On these bases, a therapeutic treatment has also been proposed (4). In the present work, we tried to understand the structural and/or functional defects of the S250F variant, the most common one associated with AADC deficiency (1,5–7). A combination of biochemical analyses on the purified recombinant protein paired with expression studies using a well-characterized mammalian tissue culture cell line [Chinese hamster ovary (CHO) cells] has been used. From our investigations, it can be deduced that the S250F mutation causes both catalytic and folding defects consisting in a reduction in catalytic activity and an enhanced susceptibility to degradation mediated by the proteasome pathway. Importantly, 4-phenylbutirric acid (4-PBA) and, to a major extent, pyridoxine partially rescue the functionality of the variant. This suggests that these molecules may be of value in therapy of patients bearing the S250F mutation.

RESULTS

Expression studies of S250F variant in *E. coli*

Decarboxylase assays and western blotting analyses of crude cellular extracts of *E. coli* reveal that the specific activity and the immunoreactivity of the S250F variant are 14 and 66%, respectively, of the corresponding ones of the wild-type (Table 1). Although these data confirm the pathogenicity of S250F mutation, they do not allow the identification of the mechanism(s) producing the enzyme malfunction. In fact, the low specific activity appears to be due not only to the drop of the expression yield, but also to the decrease in the catalytic activity of the mutant. Since the expression in *E. coli* offers the possibility to produce and purify sufficient quantities of the S250F variant for detailed structural and functional analyses, we followed this approach in order to elucidate the molecular basis of the deficit of the S250F variant.

Biochemical studies of recombinant purified S250F

The purified S250F variant is homogeneous as indicated by a single band on SDS PAGE with a mobility identical to that of wild-type human DDC. The equilibrium dissociation constant value for PLP, [$K_{D(PLP)}$] of the variant (62 ± 24 nM) does not significantly change when compared with that of the wild-type [43 ± 12 nM (4)]. This is consistent with the fact that Ser250, belonging to the large domain of DDC, is located at 12 Å from PLP. However, several lines of evidence indicate that substitution of Ser by Phe at position 250 alters the PLP binding mode and microenvironment. First, while wild-type human DDC displays two absorbance bands centred at 420 and 335 nm with a ratio A_{335nm}/A_{420nm} of 2 (4), these bands in the S250F variant show a lower intensity and a 3-nm blue shift with a ratio A_{417nm}/A_{332nm} of 1.5 (Fig. 1). Second,

Table 1. Specific activity (nmol/min/mg/) of crude extracts in *E. coli* and CHO cells

Enzyme	*E. coli*	CHO cells
Wild-type	124 ± 3	35 ± 1
S250F	16.8 ± 0.3	5.4 ± 0.4

although the absorbance bands of both wild-type and mutant are associated with positive dichroic bands, the magnitudes of the 420 nm dichroic signal of wild-type and variant are identical, while that of the 332 nm band of the variant is about half with respect to that of the wild-type (inset of Fig. 1). Thus, the wild-type and S250F enzymes display optical activity (mdeg/absorbance unit) values of 54 and 32 mdeg/A_{420} and of 102 and 59 mdeg/A_{335}, respectively. Third, upon excitation at 335 nm, the $NaBH_4$-reduced S250F mutant exhibits a decreased emission fluorescence intensity at 390 nm with respect to wild-type DDC (Fig. 2). Again, as shown in the inset of Figure 2, the reduced variant, when excited at 280 nm, displays a decreased energy transfer efficiency between tryptophan residues(s) and the reduced coenzyme. Phenylalanine at position 250 might perturb the active site directly through unfavourable electrostatic or steric interactions with PLP or indirectly by inducing conformational changes in the vicinity of the mutation site. The latter possibility may be favoured on the basis of the following data of the mutant compared with the corresponding ones of the wild-type: (i) a consistent decrease in the 280-nm optically active band (inset of Fig. 1), (ii) a reduction in the intrinsic fluorescence emission intensity accompanied by a 2-nm blue shift of the emission maximum (Fig. 3A) and (iii) an increase in aniline-1-naphtalenelsulphonic acid (ANS) fluorescence emission intensity and a shift of the emission maximum from 479 to 475 nm (Fig. 3B). However, circular dichroism (CD) spectra taken in the far-UV region were practically superimposable for wild-type and S250F variant, indicating no gross alterations in the secondary structure (data not shown). Moreover, the profile and the kinetics of limited proteolysis of the variant were identical to those of wild-type DDC (data not shown). Finally, dynamic light scattering (DLS) measurements indicate that S250F has a hydrodynamic diameter of ~10 nm, identical to that of the wild-type. This value is consistent with either that derived from the crystal structure of pig kidney DDC (9.5 nm) (8) or that calculated by an appropriate empirical equation (7 ± 2 nm) (9).

The steady-state turnover and apparent K_m values of L-dopa for the wild-type and S250F mutant enzymes have been compared (Table 2). At pH 7.4 and 25°C, the k_{cat} value of the variant drops by a factor of ~3.5, while the K_m value increases by a 2-fold factor, resulting in a ~7-fold reduction of the catalytic efficiency. Thus, taking into account the k_{cat} value of the variant in comparison with that of the wild-type, it could be deduced that the true specific activity of the S250F variant in the crude cellular extracts of *E. coli* is ~ 49% that of the wild-type.

Like the apo wild-type, the apo variant does not display absorbance and CD bands in the visible region. However, in comparison with the apo wild-type, a modest reduction in the magnitude of the dichroic signal in the near UV region, in the intensity of the intrinsic fluorescence emission and

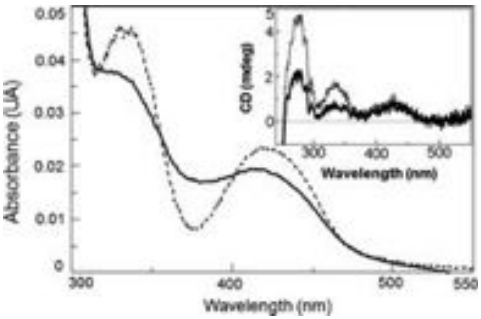

Figure 1. Absorbance and CD spectra of wild-type and S250F variant. Absorbance spectra of DDC wild-type (- - -) and S250F variant (-) in 100 mM potassium phosphate buffer, pH 7.4, at an enzyme concentration of 5 μM. (inset): CD spectra, same as absorption.

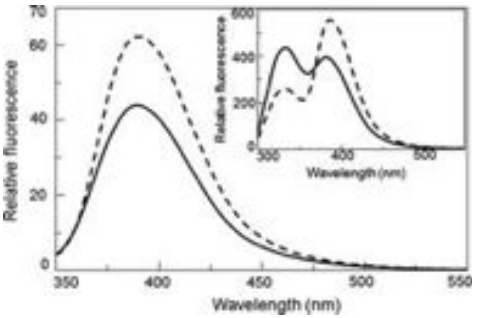

Figure 2. Intrinsic and coenzyme fluorescence emission spectra of $NaBH_4$ reduced wild-type and S250F variant. The excitation wavelength was at 280 nm (inset): excitation wavelength was at 330 nm. For all spectra, the protein concentration was 1 μM in 100 mM potassium phosphate buffer, pH 7.4. Symbols as in Figure 1.

in the ANS emission intensity can be detected in the apo variant (data not shown).

To understand if the S250F mutation has an impact on the thermostability of the holo and/or apo forms of the variant, their thermal inactivation kinetics has been examined at 37°C over a period of 3 h and compared with that of the wild-type (Fig. 4). No loss of decarboxylase activity of the holo forms of both wild-type and variant has been observed. In contrast, we detected a time-dependent apoS250F-inactivation more consistent than that of the apo wild-type. This would indicate that the apoS250F at physiological temperature is more susceptible to inactivation than the apo-wild-type.

Molecular modelling

To rationalize how Ser250 replacement with Phe could affect the DDC structure, we performed a molecular modelling study based on the crystal structure of pig kidney holo DDC (8). This structure might be a good model, being the overall degree of identity with human DDC equal to 88.7%. Ser250 belongs to the loop 243–252 with the stretch 243–246 facing the active site and the stretch 247–252 facing the surface of the molecule. The Oγ of Ser250 is in a proper position to form an H-bond interaction with the Oγ of Thr245. Figure 5 shows the superimposition of the active site of the solved DDC structure with the putative one of the S250F variant obtained by energy minimization means. In the variant the Phe250 side chain is predicted to be oriented toward the protein surface and to possibly make an hydrophobic interaction with Phe215. Thus, the Ser-to-Phe substitution could not only destabilize the conformation of the loop 243–252, as a consequence of the loss of the H-bond between Ser250 and Thr245, but also alter the chemical features of the DDC surface that is predicted to become more hydrophobic.

S250F variant: cell biology analyses in a cellular system

To ascertain whether the replacement of Ser250 with Phe affects the functional features of DDC in a mammalian cellular system, wild-type and variant were transiently expressed in CHO cells. The specific activity and the expression level of the S250F mutant were 14 and 30% (Fig. 6), respectively, of those of wild-type DDC (Table 1). Considering that the S250F mutation causes an ∼70% reduction in the k_{cat} value of the purified recombinant enzyme, the decreased specific activity in CHO cells can be ascribed partly to the reduced catalytic activity and partly to the low expression level of the variant.

As a first step, we checked if the difference in the protein expression levels between wild-type DDC and the S250F variant was due to a varied transfection efficiency or to a different mRNA intracellular stability. No differences in the levels of mRNA for wild-type DDC and the S250F variant were observed, as revealed by the amount of the encoding transcripts quantified by real-time PCR (data not shown). Therefore, the low mutant expression appears to be due to a failure at the protein level rather than at the transcriptional level, thus suggesting that the S250F mutation could affect the folding process and/or the susceptibility of DDC to intracellular degradation. Nevertheless, the finding that the relative amounts of soluble and insoluble protein recovered from lysates of CHO cells expressing wild-type and mutant DDC are similar indicates that the mutation does not make DDC prone to intracellular aggregation, which is consistent with the data obtained with the purified protein. Thereafter, we measured the half-life of wild-type and mutant DDC by cycloheximide chase assays. As shown in Figure 7A–C, the S250F mutation decreases the DDC half-life in CHO cells from 19 ± 1 to 11 ± 1 h, thus suggesting that the variant could be more susceptible than wild-type DDC to intracellular degradation. To have insights about the mechanism of degradation, cycloheximide chase assays have been carried out in the presence of the lysosome inhibitor, chloroquine, or the proteasome inhibitor, MG132. Chloroquine does not change the half-life of the two enzymatic species, while MG132 partly slows down protein degradation. However, this effect is higher for the variant than for the wild-type

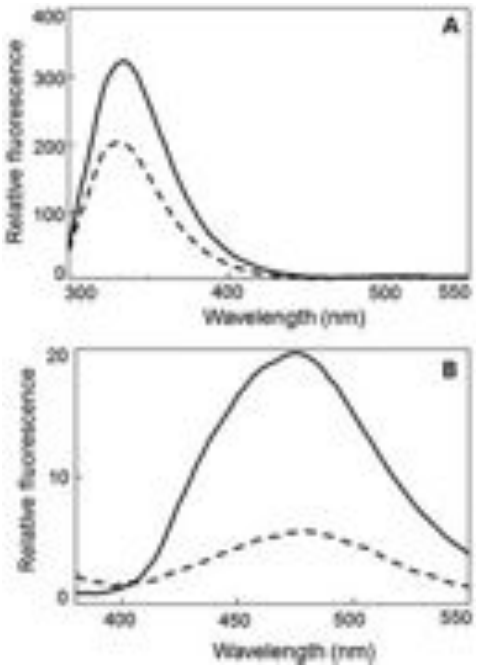

Figure 3. Intrinsic and ANS fluorescence emission spectra of wild-type and S250F variant. (**A**) Intrinsic fluorescence emission spectra (exc. at 280 nm); (**B**) Fluorescence emission spectra (exc. at 365 nm) in the presence of 15 μM ANS. For all spectra, the protein concentration was 1 μM in 100 mM potassium phosphate buffer, pH 7.4. Symbols as in Figure 1.

(Fig. 7A–C). These data mean that (i) the DDC turnover inside the cell is partly mediated by the proteasome instead of the lysosome pathway, and (ii) the mutation makes DDC more susceptible to proteasomal degradation. On these bases, since poly-ubiquitination is an important process for targeting proteins to proteasome, we investigated whether S250F is more susceptible than wild-type DDC to ubiquitination. CHO cells transiently expressing wild-type DDC or the S250F variant were immunoprecipitated with antibodies against ubiquitin and subsequently immunoblotted with the anti-DDC antibody. The results shown in Supplementary Material, Fig. S1A and B, show that while no signal is detected, as expected, in CHO cells transfected with the empty vector, a broad smear pattern typical of the poly-ubiquitin-conjugated DDC is observed in cells expressing wild-type and mutant. It should be noticed that, even if the smear pattern prevents a precise densitometric analysis, the signal relative to the mutant is higher than that relative to wild-type DDC. These data indicate that DDC is conjugated to ubiquitin prior to proteasomal degradation and corroborate the idea that the S250F variant is more prone to degradation upon poly-ubiquitination.

Table 2. Kinetic parameters for wild-type and S250F variant DDCs

Enzyme	k_{cat} (s^{-1})	K_m (mM)	k_{cat}/K_m mM^{-1}/s^{-1}
Wild-type[a]	7.6 ± 0.1	0.11 ± 0.01	70.6 ± 8.4
S250F	2.1 ± 0.1	0.22 ± 0.04	9.3 ± 1.7

[a]From ref. (4).

Following these results, we investigated the effects of pyridoxine, a precursor of PLP used in the clinical practice for patients with inherited diseases associated with deficit of PLP enzymes, and of some compounds (betaine and 4-PBA) known to act as small-molecule chaperones on the expression level and the specific activity of wild-type and mutant DDC transiently expressed in CHO cells. As shown in Figure 8A, while betaine does not affect the expression of wild-type and mutant DDC, either pyridoxine or 4-PBA increase the expression level of both enzymatic species. Accordingly, the results reported in Figure 8B indicate that: (i) pyridoxine increases the specific activity measured in CHO cells expressing wild-type or S250F variant, but the change is statistically significant only in the case of the variant, (ii) pyridoxine plus betaine or 4-PBA significantly increase the specific activity detected in cells expressing wild-type, and, to a major extent, that of cells expressing the pathogenic variant, (iii) pyridoxine plus betaine has an effect on the specific activity of CHO cells expressing wild-type and mutant, which is not significantly different from that of pyridoxine alone, which is consistent with the null effect of betaine. The increase in the specific activity of the S250F variant is dependent on vitamin B6 or 4-PBA concentration, reaching its maximum at 10 μM pyridoxine and 1 mM 4-PBA (Fig. 8B)

Taken together, the results obtained in the CHO cellular model system allow us to conclude that (i) the S250F mutation causes a structural defect in DDC that makes the protein more susceptible to intracellular degradation and (ii) pyridoxine or 4-PBA are able to rescue for the effect of the mutation by increasing the expression level and specific activity of the variant.

DISCUSSION

Several diseases mainly of neurological and metabolic origin are associated with inherited mutations of genes encoding PLP-enzymes (10–12). AADC deficiency is a rare neurometabolic disorder whose molecular bases are poorly understood. Since the S250F mutation is the most frequent one being present in one-tenth of all reported cases of patients with AADC deficiency, we decided to investigate the molecular basis of this mutation both *in vitro* and in cellular systems.

Steady-state kinetic parameters of the purified recombinant S250F variant show that the mutation does not involve a residue essential for catalytic activity, since it only causes a ∼ 7-fold reduction of the catalytic efficiency. Although the far-UV and DLS data exclude any gross alteration in the conformation of the S250F variant, the finding that the variant has an intrinsic fluorescence emission spectrum, a CD spectrum in

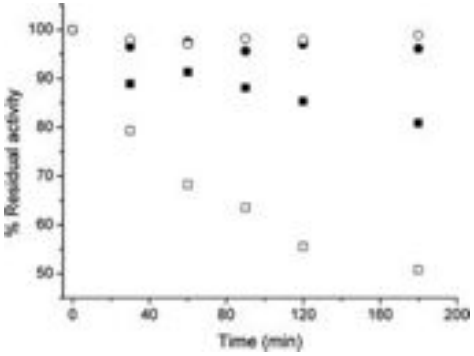

Figure 4. Time-dependent loss of decarboxylase activity of the holo and apo forms of DDC wild-type and S250F upon incubation at 37°C. Holo (closed circle) or apo (closed square) DDC wild-type at 0.2 μM concentration, holo (open circle) or apo (open square) S250F variant at 0.5 μM were incubated at 37°C. Aliquots were withdrawn at the indicated times and assayed for decarboxylase activity, as reported under the 'Materials and Methods' section.

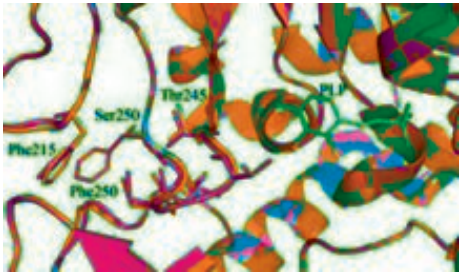

Figure 5. Comparison of the 3D structure of wild-type DDC and S250F variant. Overlapping of the crystal structure of wild-type DDC (orange) with the averaged structure of the S250F mutant (purple) obtained by molecular modelling analysis. The amino acids belongings to the loop 243–252 are represented as sticks. Ser 250 and Phe250 side chains are highlighted in cyan and red, respectively. The position of Thr245 and Phe215 are indicated. PLP is represented as green stick. The image was constructed by means of PyMol software (Delano Scientific).

the near-UV region and ANS binding properties different from the corresponding ones of the wild-type suggests that it has a slightly altered tertiary structure. Moreover, S250F has a perturbed active site, as can be inferred from the altered absorbance and CD bands of the bound PLP and the decreased intensity of the coenzyme emission of the $NaBH_4$-reduced protein. An explanation for all these data is that the mutation at position 250 of Ser to Phe possibly induces a conformational change in the proximity of the mutation site that is transmitted to the active site. According to the computational analysis, substitution to Phe predictably (i) breaks a hydrogen bond between Ser250 and Thr245, an interaction which could be important to stabilize the loop 243–252, (ii) causes an altered mobility of this loop due to the bulky side chain of Phe and (iii) enhances the hydrophobic surface of the enzyme. Although the information derived from the molecular modelling of the S250F variant is of course not an experimental evidence, it is not in contrast with the *in vitro* data.

Based on these results, one can consider S250F a catalytic mutation. However, DDC assays and western immunoblot analyses of the crude cellular extracts of *E. coli* and of CHO cells transiently expressing wild-type or S250F variant indicate, in addition to a reduced specific activity, a decreased amount of immunoreactive S250F protein with respect to wild-type. This implies that the molecular defect of the S250F variant does not only rely on the decreased catalytic activity of the protein compared with wild-type DDC, but also on a decreased expression level that exacerbates the molecular defect responsible for the decreased specific activity of the variant. It should be noted that the reduced protein level caused by the mutation in the mammalian cellular milieu is (i) not produced by differences at the level of transcription since the intracellular mRNA levels are not decreased, and (ii) not ascribable to intracellular protein aggregation because the relative amounts of soluble and insoluble S250F are comparable with those of the wild-type. The latter finding is in agreement with the fact that DLS measurements do not reveal any aggregation propensity of recombinant S250F. Instead, considering that the half-life drops from 19 h for the wild-type to 11 h for the S250F, it is reasonable to suggest that the variant is expressed in cells but is degraded faster than the wild-type. We have also shown that the degradation of wild-type and mutant depends, at least in part, on the activity of the proteasome instead of the lysosome pathway. Indeed, MG132 does not completely block protein degradation, thus suggesting that other proteolytic pathways could contribute to DDC turnover, as already proposed for other proteins (13). Remarkably, MG132 preserves from the degradation process more efficiently the S250F variant than the wild-type, and ubiquitination is more pronounced in the S250F variant than in the wild-type. Ubiquitination is often driven by conformational changes and/or order–disorder transition since unstructured region or newly exposed surface of the target protein is recognized by ubiquitin ligase. Indeed, the S250F mutation generates a conformational change that possibly leads to a more hydrophobic surface (as indicated by ANS experiments, and predicted by molecular modelling). Altogether, these data reinforce the view that the reduction in the S250F protein level might be ascribable to its degradation by the proteasomal pathway, and allow us to advance that the mutation might affect the folding pathway leading to accumulation of denatured and/or partially denatured forms of the variant prone to proteolytic degradation. It has been already reported that mis- or unfolded proteins are usually processed by cellular degradation pathways (14).

For this reason, small-molecule chaperones, which could help to improve the folding of S250F variant, have been tested. Exposure of mutant-expressing CHO cells to betaine

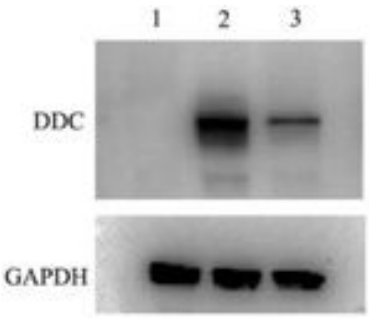

Figure 6. Analyses of DDC expression in CHO cells expressing DDC wild-type or the S250F variant. CHO cells, 24 h after transfection, were harvested and lysed; 15 μg of cell lysate was subjected to SDS PAGE, immunoblotted with anti-DDC from goat (1:250) and detected by chemiluminescence; GAPDH was used as loading control. The immunoblot lanes are coded as follow: 1. untransfected CHO cells, 2. CHO cells expressing wild-type DDC, 3. CHO cells expressing S250F variant.

does not affect the specific activity and immunoreactivity of the variant. In contrast, 4-PBA at 1 mM concentration raises the specific activity of the variant to ∼34% of wild-type, a good improvement over the specific activity (15%) of this mutant under non-treated cells. Notably, 4-PBA is of clinical use in the treatment of patients affected by cystic fibrosis bearing the ΔF508 responsible for a folding defect (15). Quite intriguing is the effect of pyridoxine, a PLP precursor, which results to be more effective than 4-PBA since at 10 μM concentration increases the specific activity to ∼60% of wild-type. The effect of pyridoxine and/or PLP, even if at a variable degree of responsiveness, has already been demonstrated for some inborn errors associated with PLP-dependent enzymes: 90% in δ-aminolevulinate synthase deficiency, 50% in cystathionine β-synthase deficiency, 10–30% in alanine glyoxylate aminotransferase and 5% in ornithine δ-aminotransferase deficiency (10,16). For some patients, the obvious explanation could be that they carry mutations that impair the PLP binding to the enzyme. However, since the mutation site in some pyridoxine-responsive patients makes this explanation unlike (10,17), it has already been proposed that PLP could assist protein folding, thus reducing the likelihood of degradation of misfolded proteins (18–20). This appears to be the case for the S250F variant associated with AADC deficiency. A question remains to be elucidated: is the chaperoning activity of pyridoxine exerted on the apo or the holo form of the variant? Some conclusions can be drawn from our data and literature. Cell biology studies provided evidence that the apo form of rat liver DDC is degraded in PC12 cells faster than the holo form (21). The structural basis of this behaviour has been recently related to the striking difference between the crystal structure of apo- (22) and holo-DDC (8). At physiological temperature, while the S250F mutation does not affect the kinetic stability of the holo form of the variant, it causes a time-dependent more significant inactivation of the apo variant compared with that of the apo wild-type. The inactivation, not dependent on the protein concentration and not accompanied by generation of aggregates, presumably originates from an enhanced amount of denatured and/or misfolded forms of the apovariant in comparison with the apowild-type. Based on these *in vitro* results, the hypothesis could be advanced that *in vivo* the coenzyme plays a prosthetic role shifting from the less stable apo to the more stable holo form, thus preventing the degradation process. However, several lines of evidence argue against this view. First, since, on the basis of the medium composition, the pyridoxine concentration in CHO cells is ∼0.3 μM, and both the apo forms of wild-type and variant exhibit a $K_{D(PLP)}$ value of ∼50 nM, both these enzymatic species should be mainly in the holo form. Second, the effect of pyridoxine on the variant is not limited to an increase in the specific activity but also in the expression level. Third, the effect of pyridoxine observed in CHO cells is dose-dependent, reaching its maximum at a concentration ∼ 200-fold higher than the $K_{D(PLP)}$.

On these bases, it can be proposed that pyridoxine could act as a pharmacological chaperone on the holo form of the S250F variant. Such a role has been already raised for tyrosine aminotransferase (18) and alanine glyoxylate aminotransferase folding (19,20). For both these enzymes, a degradation via a proteasome pathway has been reported (18,23).

This is the first study in which the molecular basis of the AADC deficiency has been elucidated by a combination of biochemical and cell biology analyses. This approach allowed us to highlight that the S250F mutation results in catalytic and folding effects, thus confirming its pathological involvement and paving the way for the implementation of a useful tailored treatment. The yet undescribed chaperoning effect of pyridoxine on the S250F variant may be useful in patients bearing this mutation as well as other mutations associated with AADC deficiency giving rise to structural defects.

MATERIALS AND METHODS

Materials

PLP, L-dopa, 2,4,6-trinitrobenzene-1-sulfonic acid, isopropyl-β-D-thiogalactopyranoside, protease inhibitor cocktail, betaine, pyridoxine hydrochloride and 4-PBA were purchased from Sigma. ANS was purchased from Molecular Probes. The polyclonal goat anti-DDC (C-16), the anti-ubiquitin antibody and the anti-glyceraldehyde 3′-phosphate dehydrogenase (GAPDH) antibody were purchased from Santa Cruz Biotechnology, from AbCam and from Millipore, respectively. All other chemicals were of the highest purity available.

Expression constructs

The full-length cDNA coding for human DDC cloned on a pCMV-XL5 vector (pCMV-DDC) was purchased from Origine Technologies and cloned on a pTrcHis2A vector to give the construct pDDChis as previously described (4). The S250F mutation was inserted into the pDDChis and pCMV-DDC expression vectors by the QuikChange II site-directed mutagenesis kit (Stratagene) using the

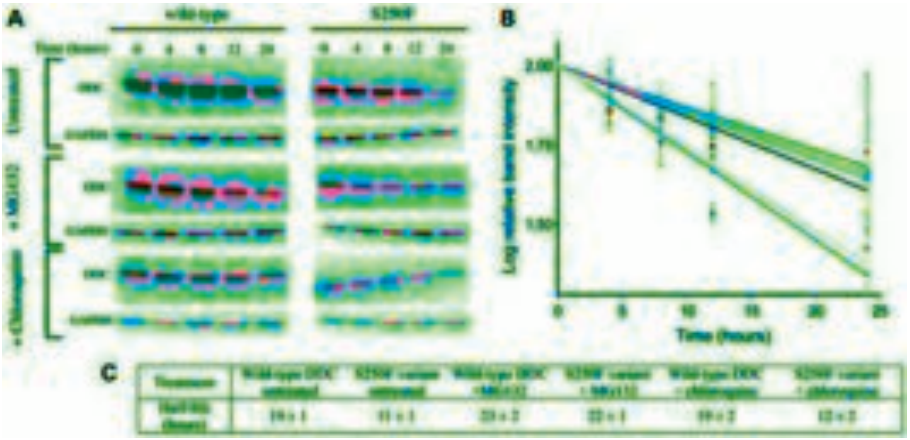

Figure 7. Measurement of protein half-lives by cycloheximide chase assays. CHO cells, 24 h after transfection, were treated with cycloheximide (final concentration 10 μg/ml) for the indicated times. Where indicated 10 μM MG132 or 100 μM chloroquine was added 1 h before cycloheximide treatment. GAPDH was used as loading control. (**A**) Immunoblot (**B**) quantification of results in (A) by the QuantityOne software. The colour code is black (wild-type DDC), blue (wild-typeDDC plus MG132), magenta (wild-type DDC plus chloroquine), red (S250F variant), green (S250F variant plus MG132) and cyan (S250F variant plus chloroquine). The lines represent a linear regression fit of the data. (**C**) Table showing the half-life values derived from data in (B). Data come from the mean of three different experiments.

oligonucleotide 5′ GGACCACAACATGCTGCTTCTTTGACAATCTCTTAGAAG 3′ and its complement (the mutated codon is underlined). The mutation was confirmed by DNA sequencing.

Protein purification and determination of the coenzyme equilibrium dissociation constant

Purification of his-tagged wild-type DDC and of the S250F variant was performed following the procedure previously described (4). Protein concentration was determined using the $\varepsilon_M = 142\,000\ M^{-1}cm^{-1}$ at 280 nm. The PLP content of the S250F variant was determined by releasing the coenzyme in 0.1 M NaOH and by using $\varepsilon_M = 6600\ M^{-1}cm^{-1}$ at 388 nm. For the apoenzyme preparation, the S250F variant was incubated with 5 mM hydroxylamine in 0.5 M potassium phosphate buffer, pH 6.9 at 25°C for 3 h and the mixture was loaded on a desalting 26/10 column (GE Healtcare) pre-equilibrated with the same buffer without hydroxylamine (24).

The equilibrium dissociation constant for PLP, $K_{D(PLP)}$, from the S250F variant was determined by measuring the quenching of the intrinsic fluorescence of the apoenzyme (0.1 μM) in the presence of PLP at a concentration range of 0.01–10 μM in 100 mM potassium phosphate buffer, pH 7.4 and by fitting the data to the following equation:

$$Y = Y_{\max}\,\frac{[E]_t + [PLP]_t + K_{D(PLP)} - \sqrt{([E]_t + [PLP]_t + K_{D(PLP)})^2 - 4[E]_t[PLP]_t}}{2[E]_t},$$

where $[E]_t$ and $[PLP]_t$ represent the total concentrations of the enzyme and PLP, respectively, Y refers to the intrinsic quenching changes at a PLP concentration, [PLP], and Y_{max} refers to the aforementioned changes when all enzyme molecules are complexed with coenzyme.

Enzyme activity assays

The decarboxylase activity toward L-dopa of wild-type DDC and the S250F variant in the purified form was measured by the spectrophotometric assay described by Sherald *et al.* (25), and modified by Charteris and John (26). Measurements were performed in the presence of 100 μM PLP in 100 mM potassium phosphate buffer, pH 7.4. Data of enzymatic activity as a function of substrate concentration were fitted to the Michaelis–Menten equation. The effect of PLP on thermostability of the apo form of wild-type and mutant was measured as follows: wild-type (0.2 μM) or S250F (0.5 μM) either in the holo or apo form was incubated in 100 mM phosphate buffer, pH 7.4, at 37°C. Aliquots were withdrawn at various times, and, after incubation with 10 μM PLP for 10 min, assayed as above described.

The DDC decarboxylase activity toward L-dopa in the soluble fraction of cellular lysates of CHO cells was determined through HPLC analysis (27). Thirty micrograms of

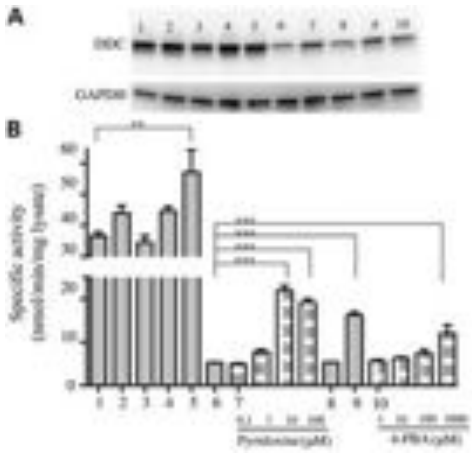

Figure 8. Effect of betaine, 4-PBA and pyridoxine on expression level and specific activity of DDC wild-type and S250F variant. CHO cells, 4 h after transfection, were treated with these compounds, and, 24 h after transfection, were harvested and lysed. (**A**) Fifteen micrograms of cell lysate were subjected to SDS PAGE, immunoblotted with anti-DDC from goat (1: 250) and detected by chemiluminescence. GAPDH was used as loading control. (**B**) Thirty micrograms of cell lysate were incubated with 2 mM L-dopa, and the amount of dopamine produced after 30 min was determined by HPLC as described under the 'Materials and Methods' section. The immunoblot lanes and histogram bars are coded as follow: CHO cells expressing wild-type DDC, 1. untreated, 2. treated with 100 μM pyridoxine, 3. treated with 15 mM betaine, 4. treated with 100 μM pyridoxine plus 15 mM betaine, 5. treated with 1 mM 4-PBA; CHO cells expressing the S250F variant, 6 untreated, 7. treated with pyridoxine at the indicated concentrations, 8. treated with 15 mM betaine, 9. treated with 100 μM pyridoxine plus 15 mM betaine and 10. treated with 4-PBA at the indicated concentrations. Data are representative of three different experiments. Bar graphs represent the mean ± SEM $^{**}P < 0.01$; $^{***}P < 0.001$.

cell lysate were incubated in 100 mM potassium phosphate buffer pH 7.4 at 25°C in the presence of 2 mM L-dopa and 10 μM PLP. After 30 min (a time within which a linear product formation is observed) the reaction was stopped by adding trichloracetic acid to a final concentration of 10% (v/v). After centrifugation to remove precipitated proteins, the supernatants were analysed using a Supelcosyl C18 (250 × 4.6 mM) (Supelco) column connected to a Jasco PU-2080 Plus HPLC control system. The eluent was 50 mM potassium phosphate buffer, pH 2.35, at flow rate of 1 ml/min. A Jasco UV-2075 Plus detector set at 280 nm was employed for dopamine detection. Peaks corresponding to dopamine eluting at 9 min were integrated with Jasco Borwin software. A standard curve of peak area as function of dopamine concentration was prepared using commercially available dopamine.

Spectroscopic measurements

Absorption measurements were performed with a Jasco V-550 spectrophotometer at a protein concentration of 5 μM. Fluorescence spectra were recorded with a FP750 Jasco spectrofluorimeter using 5 nm excitation and emission bandwidths at a protein concentration of 0.1–1 μM. CD measurements were made with a Jasco J-710 spectropolarimeter at a protein concentration of 5 μM. All the spectroscopic measurements were carried out in 100 mM potassium phosphate buffer, pH 7.4, at 25°C.

DLS analyses were performed on a ZetasizerNano S instrument (Malvern Instruments) by using disposable 12.5 × 45-mm cells with stopper (20). Wild-type DDC and S250F variant were diluted to 4 μM concentration in 60 mM potassium phosphate buffer, pH 7.4 in the presence of 20 μM PLP. The temperature was kept at 37 ± 0.1°C during the measurements by a Peltier temperature controller.

Limited proteolysis

DDC wild-type and S250F variant at 10 μM enzyme concentration were treated with proteinase K at a 1/50 (w/w) protease to enzyme ratio in 100 mM potassium phosphate buffer, pH 7.4, at 25°C in the presence of 20 μM PLP. At various times, 15 μl aliquots were withdrawn and the reaction was stopped by addition of PMSF to a final concentration of 2 mM. Samples were analysed by SDS PAGE. After staining with Coomassie brilliant blue, the band intensities were visualized and analysed using ImageJ software (Wajne Rasband).

Molecular modelling analysis

The structural model of the S250F mutant was generated starting from the pig kidney crystal structure of DDC in complex with PLP (pdb file 1JS6). Protonation state assignment and local energy minimization were performed setting a protein and solvent dielectric constant of 2.0 and 80.0, respectively, a pH value of 7.4, a ionic strength of 150 mM, and a temperature of 37°C. For all calculation, the force field adopted was AMBER99. The analysis was performed using the Molecular Operating Environment software (CCG group).

Cell culture, transfection and lysis

CHO cells were cultured at 37°C under O_2/CO_2 (19:1) atmosphere in Ham's F12 Glutamax medium (Invitrogen) supplemented with foetal bovine serum (10%,v/v), penicillin (100 units/ml) and streptomycin (100 μg/ml), as previously described (28). Cell transfection was performed using the Turbofect^{TM} Transfection Reagent (Fermentas) according to the manufacturer's instructions. After 4 h the medium containing the DNA–lyposome complex was replaced with fresh complete Ham's F12 medium. Cells were harvested after 24 h and pellets were stored at −80°C until lysis. The effect of pyridoxine, betaine, and 4-PBA was tested by adding each of the compounds or their combination to the medium 4 h after transfection.

Cells were lysed in phosphate-buffered saline (PBS) plus protease inhibitor cocktail (Complete Mini, Roche) and subjected to five freeze-thaw cycles. Samples were treated with DNAse (10 *U*) at 37°C for 45 min. The whole cell extract was separated by centrifugation (28 400*g*, 10 min, 4°C) to obtain the soluble fraction. The pellet was then resuspended

in an equal volume of denaturing gel loading buffer to obtain the insoluble fraction. The total protein concentration of the soluble fraction was measured using the Bio-Rad DC™ protein assay according to the manufacturer's instructions.

Transcript expression analysis

CHO cells were grown in a 6-well plate and transfected using Turbofect (Fermentas) as described above. Cells were harvested, washed with PBS, and RNA was extracted using the RNeasy mini kit (Qiagen). The cDNA was synthetized from 1 μg of mRNA using the Supersctipt VILO cDNA synthesis kit (Invitrogen, Carlsbad, CA) according to manufacturer's instructions. Real-time PCR was performed using 3 μl of a 1:10 cDNA dilution in a 25 μl reaction volume using SYBR Premix Ex Taq master mix (TaKaRa) on a Corbett RotorGene 6000 thermocycler. The reaction conditions included initial denaturation at 95°C for 15 min followed by 45 cycles of PCR which included 15 s melting at 95°C, 30 s annealing at 55°C and 30 s extension at 72°C. The samples were examined for the expression of human DDC using the forward primer 5′-GAAGGAGAGGGAAGGAGATGG-3′ and the reverse primer 5′-GGAAGTAGGCGAAGAAGTAGG-3′. The amount of the wild-type and S250F hDDC mRNA was calculated in relation to the GAPDH mRNA in the same sample. Quantitation of individual transcripts was performed using the 'Comparative Quantitation' software supplied by Corbett Research for the RotorGene. The mean efficiency of a group of cycling curves is calculated at the point that the cycling curves take off and used to calculate a fold change according to the formula: fold change = efficiency Ct1−Ct2, where Ct1 and Ct2 are the take-off values of the cycling curves being compared. All reactions were performed in duplicate.

Western blotting

Fifteen micrograms of lysate were loaded per lane on a Mini Protean TGX™ pre-cast gel (Biorad) along with Precision plus protein Kaleidoscope™ (Bio-Rad) as molecular mass markers. Following transfer on a nitrocellulose membrane by the iBlot device (Invitrogen) the membrane was blocked in 5% bovine serum albumin for 1 h at 37°C. For DDC detection, the membrane was incubated with polyclonal goat anti-DDC (C-16) (Santa Cruz Biotechnology) (dilution 1:250) and peroxidase-conjugated donkey-anti-goat IgG (dilution 1:2000) as primary and secondary antibody, respectively. Blotted proteins were detected and quantified with ECL® (Millipore), using the ChemiDoc XRS Imaging System (Bio-Rad, Hercules, CA). As a gel loading control, the amount of GAPDH was determined using the mouse monoclonal antibody anti GAPDH (Millipore) (dilution 1:1000).

Pulse-chase experiments and DDC immunoprecipitation

The half-life of DDC in the wild-type and S250F mutant form was determined by treating transfected CHO cells with cycloheximide (10 μg/ml) 24 h post-transfection. After 4, 8, 12 and 24 h of cycloheximide treatment, cells were lysed and DDC levels were quantified by immunoblotting as described above. Where indicated, cells were treated with the proteasomal inhibitor, MG132 (10 μM), or the lysosome inhibitor, chloroquine (100 μM), 1 h before the addition of cycloheximide. To assess the increase in total ubiquitinated proteins, which confirms the proteasome inhibition in the presence of 10 μM MG132, CHO cell lysates were immunoblotted with the rabbit anti-ubiquitin antibody (AbCam).

To check the ubiquitination level of wild-type and S250F DDC, the soluble fraction of each cell lysate (100 μg) was incubated over night with 2 μg of rabbit anti-ubiquitin antibody (AbCam) on a rotator at 4°C. Thereafter, the immunoprecipitation reaction was performed at room temperature by adding 30 μl of agarose-protein A (GE, Healthcare) to the mixture and by incubating the solution for 1 h on a rotator. The immunoprecipitated complex was collected by centrifuging at 29 200 *g* at 4°C for 5 min, washed three times with IP wash/lysis buffer (Thermo Scientific), and resuspended in 20 μl of denaturing gel loading buffer. Proteins were separated on SDS PAGE and DDC was detected by immunoblotting as described above. Untransfected and non-immunoprecipitated DDC-transfected CHO cell lysates were used as negative and positive control, respectively.

Statistical analysis

The two-way ANOVA algorithm for repeated measures was used for data analysis. Differences with $P < 0.05$ were considered significant.

SUPPLEMENTARY MATERIAL

Supplementary Material is available at *HMG* online.

ACKNOWLEDGEMENTS

We thank the AADC research trust (UK) for its interest in our research. This paper is dedicated to the memory of Prof. Hisanori Suzuki.

Conflict of interest statement. None declared.

FUNDING

This work was supported by grants from M.I.U.R. to C.B.V. and B.C.

REFERENCES

1. Pons, R., Ford, B., Chiriboga, C.A., Clayton, P.T., Hinton, V., Hyland, K., Sharma, R. and De Vivo, D.C. (2004) Aromatic L-amino acid decarboxylase deficiency: clinical features, treatment, and prognosis. *Neurology*, **62**, 1058–1065.
2. Manegold, C., Hoffmann, G.F., Degen, I., Ikonomidou, H., Knust, A., Laass, M.W., Pritsch, M., Wilichowski, E. and Horster, F. (2009) Aromatic L-amino acid decarboxylase deficiency: clinical features, drug therapy and follow-up. *J Inherit Metab Dis*, **32**, 371–380.
3. Allen, G.F., Land, J.M. and Heales, S.J. (2009) A new perspective on the treatment of aromatic L-amino acid decarboxylase deficiency. *Mol Genet Metab*, **97**, 6–14.
4. Montioli, R., Cellini, B. and Borri Voltattorni, C. (2011) Molecular insights into the pathogenicity of variants associated with the aromatic amino acid decarboxylase deficiency. *J Inherit Metab Dis*, **34**, 1213–1224.

5. Hyland, K., Surtees, R.A., Rodeck, C. and Clayton, P.T. (1992) Aromatic L-amino acid decarboxylase deficiency: clinical features, diagnosis, and treatment of a new inborn error of neurotransmitter amine synthesis. *Neurology*, **42**, 1980–1988.
6. Fiumara, A., Brautigam, C., Hyland, K., Sharma, R., Lagae, L., Stoltenborg, B., Hoffmann, G.F., Jaeken, J. and Wevers, R.A. (2002) Aromatic L-amino acid decarboxylase deficiency with hyperdopaminuria. Clinical and laboratory findings in response to different therapies. *Neuropediatrics*, **33**, 203–208.
7. Verbeek, M.M., Geurtz, P.B., Willemsen, M.A. and Wevers, R.A. (2007) Aromatic L-amino acid decarboxylase enzyme activity in deficient patients and heterozygotes. *Mol Genet Metab*, **90**, 363–369.
8. Burkhard, P., Dominici, P., Borri-Voltattorni, C., Jansonius, J.N. and Malashkevich, V.N. (2001) Structural insight into Parkinson's disease treatment from drug-inhibited DOPA decarboxylase. *Nat Struct Biol*, **8**, 963–967.
9. Wilkins, D.K., Grimshaw, S.B., Receveur, V., Dobson, C.M., Jones, J.A. and Smith, L.J. (1999) Hydrodynamic radii of native and denatured proteins measured by pulse field gradient NMR techniques. *Biochemistry*, **38**, 16424–16431.
10. Clayton, P.T. (2006) B6-responsive disorders: a model of vitamin dependency. *J Inherit Metab Dis*, **29**, 317–326.
11. Cellini, B., Oppici, E., Paiardini, A. and Montioli, R. (2012) Molecular insights into primary hyperoxaluria type 1 pathogenesis. *Front Biosci*, **17**, 621–634.
12. Cellini, B., Montioli, R., Oppici, E. and Voltattorni, C.B. (2012) Biochemical and computational approaches to improve the clinical treatment of dopa decarboxylase-related diseases: an overview. *Open Biochem J*, **6**, 116–130.
13. Fuertes, G., Villarroya, A. and Knecht, E. (2003) Role of proteasomes in the degradation of short-lived proteins in human fibroblasts under various growth conditions. *Int J Biochem Cell Biol*, **35**, 651–664.
14. Knecht, E., Aguado, C., Carcel, J., Esteban, I., Esteve, J.M., Ghislat, G., Moruno, J.F., Vidal, J.M. and Saez, R. (2009) Intracellular protein degradation in mammalian cells: recent developments. *Cell Mol Life Sci*, **66**, 2427–2443.
15. Rubenstein, R.C. and Zeitlin, P.L. (1998) A pilot clinical trial of oral sodium 4-phenylbutyrate (Buphenyl) in deltaF508-homozygous cystic fibrosis patients: partial restoration of nasal epithelial CFTR function. *Am J Respir Crit Care Med*, **157**, 484–490.
16. Cochat, P., Hulton, S.A., Acquaviva, C., Danpure, C.J., Daudon, M., De Marchi, M., Fargue, S., Groothoff, J., Harambat, J., Hoppe, B. *et al.* (2012) Primary hyperoxaluria Type 1: indications for screening and guidance for diagnosis and treatment. *Nephrol Dial Transplant*, **27**, 1729–1736.
17. Cellini, B., Montioli, R. and Voltattorni, C.B. (2011) Human liver peroxisomal alanine:glyoxylate aminotransferase: characterization of the two allelic forms and their pathogenic variants. *Biochim Biophys Acta*, **1814**, 1577–1584.
18. Gross-Mesilaty, S., Hargrove, J.L. and Ciechanover, A. (1997) Degradation of tyrosine aminotransferase (TAT) via the ubiquitin-proteasome pathway. *FEBS Lett*, **405**, 175–180.
19. Coulter-Mackie, M.B., Lian, Q. and Wong, S.G. (2005) Overexpression of human alanine:glyoxylate aminotransferase in Escherichia coli: renaturation from guanidine-HCl and affinity for pyridoxal phosphate co-factor. *Protein Expr Purif*, **41**, 18–26.
20. Cellini, B., Lorenzetto, A., Montioli, R., Oppici, E. and Voltattorni, C.B. (2010) Human liver peroxisomal alanine:glyoxylate aminotransferase: different stability under chemical stress of the major allele, the minor allele, and its pathogenic G170R variant. *Biochimie*, **92**, 1801–1811.
21. Matsuda, N., Hayashi, H., Miyatake, S., Kuroiwa, T. and Kagamiyama, H. (2004) Instability of the apo form of aromatic L-amino acid decarboxylase in vivo and in vitro: implications for the involvement of the flexible loop that covers the active site. *J Biochem*, **135**, 33–42.
22. Giardina, G., Montioli, R., Gianni, S., Cellini, B., Paiardini, A., Voltattorni, C.B. and Cutruzzola, F. (2011) Open conformation of human DOPA decarboxylase reveals the mechanism of PLP addition to Group II decarboxylases. *Proc Natl Acad Sci USA*, **108**, 20514–20519.
23. Coulter-Mackie, M.B. and Lian, Q. (2006) Consequences of missense mutations for dimerization and turnover of alanine:glyoxylate aminotransferase: study of a spectrum of mutations. *Mol Genet Metab*, **89**, 349–359.
24. Daidone, F., Montioli, R., Paiardini, A., Cellini, B., Macchiarulo, A., Giardina, G., Bossa, F. and Borri Voltattorni, C. (2012) Identification by virtual screening and in vitro testing of human DOPA decarboxylase inhibitors. *PLoS One*, **7**, e31610.
25. Sherald, A.F., Sparrow, J.C. and Wright, T.R. (1973) A spectrophotometric assay for Drosophila dopa decarboxylase. *Anal Biochem*, **56**, 300–305.
26. Charteris, A. and John, R. (1975) An investigation of the assay of dopamine using trinitrobenzensulphonic acid. *Anal Biochem*, **66**, 365–371.
27. Bertoldi, M. and Voltattorni, C.B. (2009) Multiple roles of the active site lysine of Dopa decarboxylase. *Arch Biochem Biophys*, **488**, 130–139.
28. Montioli, R., Fargue, S., Lewin, J., Zamparelli, C., Danpure, C.J., Borri Voltattorni, C. and Cellini, B. (2012) The N-terminal extension is essential for the formation of the active dimeric structure of liver peroxisomal alanine:glyoxylate aminotransferase. *Int J Biochem Cell Biol*, **44**, 536–546.